# Inducing and detecting neuroplasticity: insights from TMS-EEG and RS-EEG

**Inaugural-Dissertation**

**zur Erlangung des Doktorgrades**

**der Mathematisch-Naturwissenschaftlichen Fakultät**

**der Universität zu Köln**

**vorgelegt von**


**Maximilian Hommelsen**

aus Heidelberg


Köln 2021

Diese Dissertation wurde von der Mathematisch-Naturwissenschaftlichen Fakultät der Universitat zu Köln im Oktober 2021 angenommen.

| | |
|---|---|
| **Berichterstatter (Gutachter):** | Prof. Dr. Silvia Daun |
| | Prof. Dr. Martin Nawrot |
| **Tag der mündlichen Prüfung:** | 27.10.2021 |

# Contents

# Abstract

Damage to the brain, such as stroke, can lead to severe cognitive and motor disabilities in the affected individuals. Neuroplasticity refers to the intrinsic capacities of the brain to reorganize cortical networks at different spatial and temporal scales, potentially resulting in spontaneous recovery of function after such damage. A better understanding about the measurement and the support of those neuroplastic processes is an important prerequisite to improve therapeutic interventions and ultimately the outcome of the recovery process. This thesis comprises the results of two studies that investigated the ability to induce neuroplasticity using repetitive transcranial magnetic stimulation (TMS) and the ability to measure neuroplasticity using a combination of TMS and electroencephalography (EEG) or resting state (RS)-EEG measurements in cohorts of young and healthy individuals.

The first study utilized continuous theta burst stimulation (cTBS) to induce neuroplasticity targeting the primary motor cortex. After-effects on cortical and corticospinal excitability were quantified in terms of TMS-evoked potentials (TEP) and motor-evoked potentials. The study demonstrated that cTBS-induced neuroplasticity leads to significant local and remote changes in cortical excitability that were measurable with TMS-EEG. The modulation of the N45 peak of the TEP suggests that the neuroplastic effects of cTBS are mediated by changes in gamma-aminobutyric acid $(GABA)_A$-mediated cortical inhibition.

The second study investigated the suitability of RS-EEG for individualized longitudinal tracking of neuroplastic processes. In this scenario, it is important to distinguish whether observed changes in activity between measurements are attributable to incidental variations in cognitive state or truly related to processes of neuroplastic reorganization. A classification algorithm was adopted to extract individual-specific signatures from EEG oscillations at rest. These signatures were very robust across multiple days and detectable across different cognitive states, indicating a close relationship to the underlying neuro-

physiology. Using these individual activity pattern, it was possible to distinguish inter-day variations in cognitive state from simulated changes in the neurophysiological organization of the brain with very high accuracy.

The current thesis therefore provides important support for the usability of TMS-EEG and RS-EEG as methodological approaches to measure neuroplasticity within healthy and young individuals. Furthermore, cTBS may be used as a strategy to interact with abnormally elevated or reduced levels of $GABA_A$-mediated cortical inhibition. Further studies are required to validate the significance of the current findings and to test whether they can be translated into clinical practice, especially into the realms of stroke recovery.

# Nomenclature

| | |
|---|---|
| cTBS | continuous theta burst stimulation |
| DLPFC | dorsolateral prefrontal cortex |
| EEG | electroencephalography |
| EMG | electromyography |
| FDI | first dorsal interosseus |
| FFT | fast fourier transform |
| fMRI | functional magnetic resonance imaging |
| FTT | finger tapping task |
| GABA | gamma-aminobutyric acid |
| ICA | independent component analysis |
| iTBS | intermittent theta burst stimulation |
| MEP | motor-evoked potential |
| MSO | maximum stimulator output |
| MSO | maximum stimulator output |
| M1 | primary motor cortex |
| RMT | resting motor threshold |
| rTMS | reptitive transcranial magnetic stimulation |
| TBS | theta burst stimulation |
| TEP | TMS-evoked potential |
| TMS | transcranial magnetic stimulation |

# 1 Introduction

The brain corresponds to the central part of the human nervous system and represents the neural basis of our cognitive abilities. It acts as an important control hub for a wide range of body functions that are remotely monitored and regulated, even in the complete absence of our awareness. The realization of these complicated demands require a fast integration and processing of large amounts of information in parallel, which is implemented through a complex and densely connected network of nerve cells. It is estimated that the brain contains approximately 86 billion neurons and as many non-neuronal cells (Herculano-Houzel, 2012). The communication of neurons within these networks is achieved through a combination of chemical as well as electrical signal transmission (Lovinger, 2008).

Neuroplasticity refers to the capacities of these neural networks to grow and change in a process of adaptation, either by forming completely new connections or by recalibrating the transmission efficacy within already existing connections of the networks (Dayan & Cohen, 2011). Structural and functional changes in network properties are one of the core mechanisms by which humans can learn new behaviors and adapt to changing environments (Galván, 2010). Such reorganization can take place in various spatial scales within the peripheral and central nervous system, affecting efficiency of synaptic transmission in circuits with only a small number of neurons, up to larger scale reorganization of brain networks, e.g. in the process of cortical remapping (Kolb & Whishaw, 1998; Münte et al., 2002; Pascual-Leone et al., 1996; Pascual-Leone et al., 2005).

The interplay of these different neuroplastic processes is especially relevant for the recovery of function following severe lesions of the brain. For example, a stroke can damage or completely destroy existing pathways within the brain, leaving the affected individuals with severe impairment or even a complete loss of certain cognitive or motor functions (Noble & Schenk, 2014). This is furthermore often associated with significant reductions in quality of life (Carod-Artal & Egido, 2009; King, 1996) and concomitant neuropsychiatric disorders (Robinson, 1997). Motor impairments are among the most frequent consequences of stroke and around 80% of patients suffer from such deficits (Langhorne et al., 2009). Usually, the largest improvements in functional recovery are observed within the first weeks up to a three month post stroke (Cramer, 2008; Verheyden et al., 2008). Neuroplastic reorganization of cortical networks represents an intrinsic mechanism of the brain to compensate dysfunctional activity within a damaged region or network, thereby mediating spontaneous recovery of function after such lesions (H. Chen et al., 2010; Hosp & Luft, 2011; Murphy & Corbett, 2009). However, the exact patterns of cortical reorganization that ultimately lead to recovery of function are complex and depend on the interplay of many different factors (Cramer, 2008; Hallett, 2001). For example, recovery can result from repair of damage in the affected networks, usage of alternative but already existing pathways or the development of new neuronal connections (Talelli et al. 2006). Importantly, depending on the time and location of occurrence as well as interaction with other ongoing recovery processes, neuroplastic changes can even be maladaptive and exert detrimental effects on the process of recovery (Quartarone et al., 2006; Takeuchi & Izumi, 2012).

Repetitive transcranial magnetic stimulation (rTMS) is a noninvasive brain stimulation (NIBS) technique that can initiate and induce neuroplastic processes in the human cerebral cortex, transiently altering excitability within a targeted region (R. Chen et al., 1997; Pascual-Leone et al., 1994). In particular, rTMS can inhibit or increase cortical excitability depending on the exact stimulation parameters. This can provide a way to externally "guide" the induction of neuroplastic processes, promoting changes that contribute pos-

itively to recovery of function while inhibiting adaptions that might be harmful. There are already some promising studies targeting the human motor system with rTMS, suggesting that this strategy can improve recovery of motor function after stroke (Dafotakis et al., 2008; Du et al., 2019; Lefaucheur, 2006; Mansur et al., 2005; Talelli et al., 2007). However, there is often still a considerable variability in study outcomes and a reliable improvement of recovery processes by inducing plasticity using rTMS is still challenging (Sebastianelli et al. 2017). In part, this variability is likely caused by the high interindividual variability in induced plasticity that has also been observed when applying rTMS protocols within healthy individuals (Hamada et al., 2013; Maeda et al., 2000; Nettekoven et al., 2015). While some individuals show modulations of cortical activity in the expected manner, others might show an opposite change in cortical excitability. Such paradox responses are of course highly problematic, as e.g. a further reduction of activity within the affected hemisphere might potentially worsen the functional recovery after stroke rather than improving it.

Another contributor to variability in stroke are the complex temporal and individual dynamics of cortical reorganization after stroke itself. Studies in mice have shown that after stroke, there is a critical period of increased neuroplasticity. For instance, intrinsic neuroplastic mechanisms are upregulated within hours after stroke, increasing within the first one or two weeks and disappear again after approximately four weeks (Coleman et al., 2017). In humans, this critical period is usually longer, as spontaneous functional recovery can usually appear within weeks to month post stroke (Cortes et al., 2017; Duncan & Sue Min Lai, 1997; Heller et al., 1987; Kwakkel et al., 2006). The potential benefits of rTMS-induced cortical plasticity therefore dependent on the temporal dynamics and pattern of cortical reorganization within a particular individual. Thus, timing, targeted region and direction of induced plasticity (i.e. excitation or inhibition) are crucial parameters to determine if rTMS can actually aid in reorganization of cortical networks and support the recovery of function rather than worsen it.

Cross-sectional and longitudinal neuroimaging studies using functional magnetic resonance imaging (fMRI) have provided important insights into how the brain activity changes during the critical period of cortical reorganization at different temporal stages after stroke (Golestani et al., 2013; Park et al., 2011; Rehme et al., 2011; Ward et al., 2003). Longitudinal tracking of cortical plasticity on an individual basis would allow to optimize timing and type of therapeutic intervention to specifically support ongoing beneficial neuroplastic processes and inhibit those that potentially have negative effects on functional recovery. However, precise temporal tracking would require repeated measurements of brain activity at very short time scales, potentially within hours or days. This is unfeasible when fMRI is used to perform frequent measurements, due to the high maintenance cost of the brain scanners and their lack of availability. In contrast, the measurement of resting state (RS) activity using electroencephalography (EEG) has many desirable properties for the realization of longitudinal and frequent tracking of brain activity. The method itself is comparably easy to perform, there are no exclusion criteria, it is suitable for bedside testing, it does not require active participation of the subject, and the purchase and maintenance costs are relatively low compared to other neuroimaging modalities. In addition, there are many studies demonstrating that various properties of the oscillatory dynamics during rest can be used as indicators of brain network integrity and organization in different clinical populations and age groups (Hata et al., 2016; Scally et al., 2018; Stam et al., 2005). Thus, RS-EEG provides a promising experimental environment for potential tracking of individual trajectories of cortical plasticity following stroke.

In summary, there are currently two major difficulties that significantly weaken the impact of rTMS to support functional recovery after stroke. First, there is a lack of understanding about how exactly rTMS induces plasticity and modulates brain activity within the target region and the other nodes of the network. A better understanding of this could facilitate targeted induction of cortical plasticity and potentially help to reduce undesired response characteristics. Second, it is necessary to establish strategies to measure and characterize

the ongoing neuroplastic processes that drive the dynamics of cortical reorganization in the early stages after stroke on an individual basis. This is an important prerequisite to ensure, e.g. that rTMS is applied over the correct region of a network, or that rTMS and rehabilitative physiotherapy will be delivered at an appropriate time to support and not interfere with the ongoing intrinsic processes of neuroplastic reorganization. Due to these important challenges in clinical practice, there is considerable interest in further investigating methodological approaches that could help to address these problems, by providing additional insights into their mode of action or by testing their suitability to fulfill these demands.

This thesis comprises the results of a study combining rTMS and TMS-EEG and a RS-EEG study that were performed within cohorts of young and healthy individuals. Even though the studies were not conducted with stroke patients, their design was inspired by the challenges that emerge in the clinical practice after stroke, including the induction of neuroplasticity via rTMS and the tracking of neuroplastic processes within individuals. The goal of this thesis is therefore to improve the understanding about the modulation and measurement of intrinsic and induced neuroplastic processes based on these different methodological approaches (rTMS, TMS-EEG, RS-EEG).

The first study was entitled "Modulation of cortical excitability by continuous theta burst stimulation over the primary motor cortex: a TMS-EEG study" and will be referred to as "Study 1" throughout this thesis. Study 1 was designed to investigate the effects of a modulation of cortical excitability caused by rTMS-induced neuroplasticity and whether those effects can be measured and quantified using TMS-EEG. For that purpose, 29 young and healthy individuals received three doses of rTMS over the primary motor cortex (M1) to induce neuroplasticity (in a dose dependent manner). The excitability of M1 was measured repeatedly throughout the experiment, using the TMS-evoked potential (TEP) as an index to measure local and remote changes in cortical excitability. Cortical responses were furthermore investigated with respect to the direction of the induced plasticity within individuals, which was inferred based on changes in amplitude of the

motor-evoked potential (MEP).

The second study was entitled "Robustness of individualized inferences from longitudinal resting state dynamics" (referred to as "Study 2") and was designed to investigate the suitability of RS-EEG for longitudinal tracking of neuroplastic changes within individuals. Longitudinal tracking of RS activity can be confounded by involuntary variations of the person's cognitive state between the measurements. Being able to distinguish whether differences in RS activity between two measurements are caused by an incidental change in cognitive state rather than a real change in the person's neurophysiological organization is an important prerequisite for the suitability of RS-EEG to track individual trajectories of neuroplastic reorganization. In order to test if RS-EEG can fulfill these demands, EEG was acquired longitudinally on five subsequent days from 27 young and healthy individuals. A classification approach was adopted to extract individual-specific brain activation pattern from RS activity. Using interindividual differences as proxy for changes in neurophysiological organization, it was specifically tested if those changes would actually be distinguishable from changes in cognitive state as they might appear in the framework of repeated measurements.

In this way, the current thesis can hopefully contribute to a better understanding of the possibility to accurately induce and measure neuroplastic processes in the human brain, ultimately promoting the usability of these methodological approaches in the clinical setting, e.g. when trying to improve functional recovery after stroke. In short, Study 1 aims to improve the understanding of rTMS to induce local and remote neuroplastic changes and the ability to measure those changes at the cortical level using TMS-EEG. Study 2 investigates the usage of a novel RS-EEG framework for the longitudinal tracking of individual trajectories of cortical plasticity. The following sections will provide some additional basic information about the methods and concepts that were used in the studies of this thesis.

## 1.1 Electroencephalography (EEG)

EEG is a non-invasive neuroimaging technique which can measure the electrical activity generated by the brain through electrodes that are placed on a person's scalp. Depending on the EEG system that is used, up to 256 electrodes are placed on the scalp to measure the activity of the underlying brain regions. However, most conventional systems use fewer electrodes (16 to 64) as this already provides a sufficient spatial resolution for most applications. The electrodes are often placed according to the 10-20 system introduced by Jasper (1958), which uses anatomical landmarks (nasion and inion) to arrange the electrodes in a standardized grid above the different cortical lobes.
The measured electrical activity of the EEG arises primarily as consequence of the firing of large pyramidal neurons, spatially organized in columns across the different layers of the cerebral cortex (Kirschstein & Köhling, 2009). Activity of single neurons cannot be detected using EEG, but if large neuronal populations are firing in synchrony, their activity can sum up and become large enough to produce measurable voltage changes at the scalp's surface (Jackson & Bolger, 2014; Kirschstein & Köhling, 2009). EEG captures these potential changes at a macroscopic scale, representing the activity of nerve cells within several square centimeters of cortical tissue below the recording electrode (Buzsáki et al., 2012).

These large-scale voltage fluctuations usually appear with a certain rhythmicity at the cortical surface, revealing dynamic oscillatory activity that varies in frequency and amplitude. These brain waves constitute one of the core component of the EEG activity and are partly visible with the naked eye when inspecting the recorded signals. The properties of these oscillations depend in part on the cortical region from which they are recorded (Buzsáki, 2006; Srinivasan et al., 2006), but they are also specifically modulated in many different scenarios, e.g. as the brain processes sensory information (Ergenoglu et al., 2004), when performing cognitive tasks (Fitzgibbon et al., 2004; Ward et al., 2003), during memory retrieval (Jacobs et al., 2006), during movement execution (Pfurtscheller &

Lopes da Silva, 1999), during processes involving selective attention (Foxe & Snyder, 2011) or in relation to vigilance and fatigue (Aeschbach & Borbély, 1993; Kubicki et al., 1979).

Quantifying the spatiotemporal dynamics of these oscillations can therefore reveal important information about the prevalent brain state and even the integrity of the cerebral cortex (Rabiller et al., 2015; Stpień et al., 2011; Van Putten & Tavy, 2004). It is common practice to subdivide these different oscillations into five frequency bands, namely the $\delta$-band (1–4 Hz), the $\theta$-band (4–7 Hz), $\alpha$-band (8–13 Hz), $\beta$-band (14–30 Hz) and the $\gamma$-band (>30 Hz). However, there is also no uniform definition for the exact range of these frequency bands and they will often show slight variations regarding their boundaries between studies.

The modulation of these bands has been linked to the execution of specific cognitive or motor processes, or the presence of a particular brain state. For example, the power of the $\delta$-band is heavily increased during deep sleep (Davis et al., 2011) and the $\theta$-band is often associated with cognitive and memory processing or processes of attention (Klimesch, 1999; Schacter, 1977). The $\alpha$-waves appear predominantly around the occipital cortex and have been initially described by Hans Berger, in the earliest days of EEG research (Berger, 1929). They are heavily suppressed during visual processing and increase in size when eyes are closed and visual input is absent (Barry et al., 2007). The $\beta$-band is often associated with sensorimotor processing and its modulation by voluntary movements (Engel & Fries, 2010; Pfurtscheller & Lopes da Silva, 1999). The $\gamma$-band is probably the least well studied EEG frequency band, but it has been suggested that it plays a role in higher cognitive processing, such as feature binding (Başar-Eroglu et al., 1996).

A lion's share about the functional relevance of these frequency bands and the brain regions that generate them was derived from experiments in which participants were instructed to perform specific tasks. For example, if participants are instructed to move their right hand or arm, the power in the $\beta$-band will be reduced around the contralateral sensorimotor cortex. If participants are instructed to open and close their eyes every few

seconds, power in $\alpha$-band will be reduced and increased around the visual cortex in the same period. In order to investigate and probe the function of multiple brain networks in this way, a battery of sometimes complex experimental tasks would be required. This might be challenging for some clinical populations, such as children, the elderly or patients with brain damage who may be unable to perform complex tasks conveniently to probe the underlying network function.

RS measurements refer to the acquisition of brain activity during a state of rest, in the absence of any particular task. In a famous study by Biswal et al. (1995), they observed that the fMRI signal intensity of blood oxygenation showed high temporal correlations in the very low frequency range between several motor-related brain regions, even though participants were not instructed to perform a motor tasks. This discovery of RS functional connectivity in fMRI indicated that even during such a state of rest, brain activity is highly structured and carries rich information about the function and integrity of large-scale brain networks, such as the default mode network (Raichle, 2015) or the motor network (Pool et al., 2015). Importantly, those RS networks have been shown to appear consistently across individuals (Damoiseaux et al., 2006) and seem to contain noticeable predictive value about individual behavioral and cognitive functions (Lin et al., 2018; Pool et al., 2015; Reineberg et al., 2015) or may serve as indicator for the presence of diseases (de Vos et al., 2018). In addition, RS measurements can usually be obtained within a few minutes and do not require active participation of the subject.

Although RS networks are less well characterized in EEG compared to their fMRI counterparts, it is evident that EEG measurements at rest can enable similar inferences about individual behavior and cognition based on the integrity and functionality of brain networks (Erickson et al., 2018; Sugata et al., 2020; Wu et al., 2014). This predictive potential is not limited to EEG-based measures of connectivity but also encompasses general properties of the oscillatory dynamics, i.e. modulation of amplitude and frequency of oscillations across the whole brain. The capacities for individual predictions of oscillatory power at rest are also supported by many studies that show a very high individual speci-

ficity of these oscillations (Di et al., 2019; La Rocca et al., 2012; Näpflin et al., 2007; Pathania et al., 2021). This close connection to the individual neurophysiological organization of the brain contains a large potential to identify biomarkers related to onset or presence of disease based on RS-EEG measurements.

## 1.2 Transcranial magnetic stimulation (TMS)

Transcranial magnetic stimulation is a NIBS technique that was developed and first applied by Barker et al. (1985). TMS utilizes the principle of electromagnetic induction to deliver small electrical currents to the brain. It enables a relatively well-tolerated and safe stimulation of cortical neurons through the intact skull Rossi et al. (2009). A TMS system consists of a large capacitor or a series of capacitors that can discharge a high-current, high-voltage pulse through a wire coil. This electrical pulse leads to the generation of a very strong but brief magnetic field (up to 2.5T and lasting around 30µs up to 1000µs) generated perpendicular to the current flow in the stimulation coil (Groppa et al., 2012; Hallett, 2007; Hannah et al., 2016; Siebner et al., 2009). This rapidly changing magnetic field then induces a secondary intracranial current, in parallel to the current flow in the wire coil, but in opposite direction.

The focality and strength of the induced electrical field will finally determine the spatial extend to which the underlying cortical tissue will be activated by the pulse. This depends on many different parameters, including coil orientation (Laakso et al., 2013), coil geometry (Deng et al., 2013), stimulation intensity, pulse configuration (Pisoni et al., 2018) and individual anatomy (e.g. head shape and gyral folding (Bijsterbosch et al., 2012)). However, when using commercially available coils and stimulation intensities that are within the TMS safety guidelines, it is unlikely that the stimulation depth exceeds 2–3 cm (Deng et al., 2014). Depending on the stimulation intensity, pyramidal neurons in cortical lamina V are either activated directly, or indirectly through a complex interplay of excitatory and inhibitory circuits in lamina II that have lower thresholds and will activate the lamina

V pyramidal neurons transynaptically (Di Lazzaro & Ziemann, 2013; Diana et al., 2017; Klomjai et al., 2015).

Single or paired pulse paradigms are frequently used in research and clinical practice to investigate and assess the integrity, excitability and connectivity of central as well as peripheral components of the human motor system (Daskalakis et al., 2002; Ferbert et al., 1992; Hummel et al., 2009; Klomjai et al., 2015; Rothwell, 1997). One of the most prominent examples is the assessment of corticospinal excitability, in which a single magnetic pulse is applied to the primary motor cortex region that controls a specific hand muscle (often the first dorsal interosseous (FDI) or abductor pollicis brevis (Rossi et al., 2009)). If the induced electrical field is strong enough to activate cortical motor neurons (suprathreshold pulse), a descending volley will travel down the corticospinal tract to the periphery. This will produce a compound muscle action potential in the corresponding hand muscle (Bestmann & Krakauer, 2015), which is usually referred to as MEP.

The latency and amplitude of this MEP can be quantified using surface electromyography (EMG) electrodes. The MEP represents a sum of cortical, subcortical and spinal contributions to the measured amplitude in the target muscle (Duque et al., 2017) and is used to index corticospinal excitability. Other parameters of important clinical value that can be inferred from MEP measurements include the stimulation threshold or central conduction time (Magistris et al., 1998). A voluntary pre-activation of the cortical region corresponding to the target muscle, either by imagination of movements (Kasai et al., 1997) or actual contractions will lead to an increased excitability and result in larger amplitudes of the MEPs. In contrast, during periods of cortical inhibition, e.g. if a movement has to be stopped abruptly, participants are instructed to resist a movement or a movement of the contralateral hand has to be suppressed, corticospinal excitability will be largely reduced when probed with TMS (Bonnard et al., 2009; Bonnard et al., 2003; Duque et al., 2017).

RTMS refers to a collection of specific TMS stimulation protocols that have been demonstrated to induce cortical plasticity. During rTMS, a large number of pulses (up to several

thousands), are applied with a specific frequency and within a fixed timeframe to a cortical region. This can lead to temporary changes of cortical excitability that can outlast the actual stimulation period. If pulses are applied to the cortex with a low frequency (< 1 Hz), the effects resemble long-term depression (LTD)-like effects, reducing corticospinal excitability (R. Chen et al., 1997). In contrast, frequencies above 5 Hz produce long-term potentiation (LTP)-like effects and increase corticospinal excitability (Jennum et al., 1995). As consequence, rTMS has been established as therapeutic intervention in the clinical environment, in the attempt to normalize dysfunctional cortical activity in patients suffering from a variety of neurological and psychiatric conditions (George et al., 2013; Kleinjung et al., 2005; Nowak et al., 2009; Ridding & Rothwell, 2007).

Theta burst stimulation (TBS) corresponds to a modified rTMS protocol that utilizes high frequency bursts of pulses to induce cortical plasticity (Huang et al., 2005). TBS was described as a faster, more robust and reliable stimulation protocol to modulate corticospinal excitability. In contrast to high and low frequency rTMS, TBS consists of high frequency bursts of pulses (three pulses at 50Hz) that are applied repeatedly at a frequency of 5 Hz, corresponding to the frequency of human theta rhythm. Continuous TBS (cTBS) is usually applied as a series of 300 or 600 pulses in 20s or 40s, respectively. During intermittent TBS (iTBS), the same total number of pulses are applied to the brain but after 2s of stimulation, there is a break of 8s. Due to the high frequency of pulse application, TBS only requires a fraction of time to complete compared to conventional rTMS protocols. When following safety guidelines and using subthreshold stimulation intensities, TBS imposes low risk of severe side effects and is generally considered very safe (Oberman et al., 2011).

## 1.3 TMS-evoked potential (TEP)

The combination of TMS and EEG (TMS-EEG) allows the measurement of cortical responses to the application of TMS pulses. TMS-evoked potential (TEP) refers to the spatiotemporal profile of electrical activity that can be measured across the whole scalp using EEG, after a single pulse of TMS is applied to a certain cortical region (Ilmoniemi et al., 1997). The TEP belongs to a larger group of electrophysiological responses called evoked potentials. These potentials are usually defined by a series of characteristic peaks which are quantified in terms of latency and amplitude. The peaks reflect a distinct sequence of activations within a particular pathway of the nervous system and can therefore provide information about the functional integrity of this pathway. As consequence, evoked potentials are of high relevance in clinical practice (Tandon, 1998; Walsh et al., 2005). For example, if a person is presented with a flash of light, a visually evoked potential (VEP) is elicited and can be recorded from electrodes placed on the occipital region around the visual system. The peaks and throughs of the VEP can then inform about the electrical transmission of the stimulus along the visual pathway, including the retina, optic nerves, the lateral geniculate nucleus, the optic radiation and the primary visual cortex (Creel, 2019). In case of neuronal damage along the pathway, the potential will be altered in terms of latency and amplitude, depending on where the damage is localized (Walsh et al., 2005).

In case of the TEP, the potentials are not evoked by the presentation of a sensory stimulus, but directly caused through electrical stimulation of the neural pathways with TMS. The induced activity spreads within milliseconds from the stimulated region through cortico-cortical connections to adjacent and distant brain regions. The recorded potential is usually largest below the site of stimulation and decreases in amplitude as it spreads to other cortical regions (Ilmoniemi & Kičić, 2010). For a single pulse stimulation of M1, several positive and negative peaks occur within the following 300-400 ms after the pulse. The exact latencies and amplitudes of the TEP peaks can vary, depending on the coil type, coil

orientation, stimulation intensity, stimulated region and due to interindividual differences (Casarotto et al., 2010; Ilmoniemi & Kičić, 2010; Roos et al., 2021). Nevertheless, the propagation of the activity relies on the functional integrity of connections from the stimulation site to other regions. Thus, an investigation of the distinct TEP peaks can provide important insights into the different stages of signal transduction as the pulse propagates from the stimulation site to the connected regions of the cerebral cortex.

Pharmacological studies have furthermore demonstrated that some of the TEP peaks reflect the recruitment of specific excitatory (e.g. glutamatergic) and inhibitory (e.g. gamma-aminobutyric acid (GABA)) circuits within the brain (Belardinelli et al., 2021; Premoli et al., 2014). Thus, the TEP can provide valuable information about the integrity, excitability and connectivity of the cerebral cortex (Komssi et al., 2002; Rogasch & Fitzgerald, 2013) and it has a high potential to serve as biomarker for cortical integrity and connectivity in healthy and diseased populations (Hordacre et al., 2019; Tscherpel et al., 2020).

In addition, assessing neural pathways by means of the TEP opens the possibilities to probe connectivity of different cortical regions that would be inaccessible through simple sensory stimulation with conventional evoked potentials.

# 2 Study 1: Modulation of cortical excitability by continuous theta burst stimulation over the primary motor cortex: a TMS-EEG study

Author Contributions

Conceived the research

**Caroline Tscherpel, Christian Grefkes**

Performed the experiments

**Maximilian Hommelsen**

Data Preprocessing

**Maximilian Hommelsen**

Data analysis

**Maximilian Hommelsen**

Wrote the manuscript

**Maximilian Hommelsen, Silvia Daun**

UNPUBLISHED MANUSCRIPT

# Modulation of cortical excitability by continuous theta burst stimulation over the primary motor cortex: a TMS-EEG study

Maximilian Hommelsen[1], Caroline Tscherpel[1,3], Christian Grefkes[1,3], and Silvia Daun[1,2]

[1]*Cognitive Neuroscience, Institute of Neuroscience and Medicine (INM-3), Forschungszentrum Jülich, Jülich, Germany*

[2]*Institute of Zoology, University of Cologne, Cologne, Germany*

[3]*Department of Neurology, University Hospital Cologne, Cologne, Germany*

---

**Abstract:**

Continuous theta burst stimulation (cTBS) is a transcranial magnetic stimulation (TMS) protocol that can induce neuroplasticity and transiently alter excitability when applied over the primary motor cortex (M1). The TMS-evoked potential (TEP) provides a way to measure excitability of M1 and connected regions directly from the scalp, using a combination of TMS and electroencephalography (EEG). In this sham-controlled study, three doses of cTBS were applied over M1 of young and healthy individuals. Motor-evoked potentials (MEP) and TEPs were measured prior and after application of each dose of cTBS. The goal of this study was to characterize the cTBS-induced plasticity directly on the level of the cortex, using the TEP as

index for cortical excitability. Application of cTBS revealed prominent modulations of the N45 component of the TEP, a marker of $GABA_A$-mediated inhibition, after each dose. Changes in cortical excitability were not restricted to M1 but also appeared in connected regions, especially around the parietal cortex and the contralateral hemisphere. Investigation of cTBS responder subgroups revealed that MEPs, but not the N100 component of the TEP, are modulated by cTBS in a dose-dependent manner. MEPs and TEPs might reflect separate but not necessarily independent measures of cTBS-induced cortical plasticity. The current results demonstrate that TMS-EEG is a suitable approach to measure cTBS-induced cortical plasticity in healthy individuals and may complement the conventional measurement of corticospinal excitability based on MEP amplitude. Moreover, cTBS may be a suitable tool to regulate $GABA_A$-mediated cortical inhibition.

**Keywords:** EEG; Continuous theta burst stimulation; Transcranial magnetic stimulation; Motor cortex; TMS-evoked potential; Motor-evoked potential; Neuroplasticity

# 1 Introduction

Transcranial magnetic stimulation (TMS) is a non-invasive brain stimulation (NIBS) technique that allows to directly stimulate the superficial layers of the brain tissue in proximity to the scalp's surface through the intact skull (Hallett, 2007). Theta burst stimulation (TBS) corresponds to a specific repetitive TMS (rTMS) protocol, in which hundreds of TMS pulses are applied in quick succession, usually within several minutes or less. Such repeated and extrinsic activation of cortical circuits can mimic the brain's intrinsic neural firing pattern, and has been shown to induce transient neuroplasticity in the human motor cortex, potentially exhibiting long-lasting after-effects on corticospinal excitability (Huang et al., 2005). These neuroplastic effects are likely mediated by changes in synaptic transmission and resemble the long-term potentiation (LTP) and long-term depression (LTD) - like effects that were observed in in vitro experiments using rat hippocampal slices (Larson et al., 1986; Larson & Lynch, 1989). Early studies suggested that the effects of such rTMS protocols are bidirectional and the direction of after-effects primarily depends on the stimulation pattern and frequency that is used to apply the pulses (Pascual-Leone et al., 1994; Jennum et al., 1995; Chen et al., 1997; Chen & Seitz, 2001). In the case of TBS, Huang et al. (2005) reported a dichotomous result, namely that continuous TBS (cTBS) has inhibitory after-effects on corticospinal excitability, whereas intermittent TBS (iTBS) was described to facilitate corticospinal excitability. These after-effects have been described in numerous studies targeting different cortical regions, revealing that the stimulation could lead to meaningful increases and decreases in electrophysiological or behavioral performance measures (Cazzoli et al., 2009; Cho et al., 2010; Verbruggen et al., 2010; Meehan et al., 2011; Teo et al., 2011; Hoy et al., 2016).

However, this simple relationship between stimulation pattern and directional induction of plasticity has been questioned by diverging results. Several studies observed a substantial degree of interindividual variability regarding the direction and strength of induced plasticity, resulting in inconclusive or even contradictory results on the group-level (Martin et al., 2006; Hamada

et al., 2013; Lakhani et al., 2014; López-Alonso et al., 2014; Hordacre et al., 2021). There is a growing body of evidence indicating that a multitude of factors may play an important role in how TBS can modify cortical plasticity beyond the pattern of the stimulation. This includes age, attention, certain genetic variants, interactions with (pharmacologically) elevated or reduced neurotransmitter levels as well as synaptic history, i.e. alterations in neural plasticity following priming stimulation or physical exercise (Martin et al., 2006; Ridding & Ziemann, 2010; Hamada et al., 2013; Katagiri et al., 2020). Nevertheless, it is poorly understood how all of these factors interact and providing accurate predictions about an individual's response to TBS is still challenging. However, understanding the mechanisms behind individual cortical responses to neuromodulatory protocols and TBS after-effects are absolutely crucial for clinical applications, as unexpected or opposite after-effects might have a detrimental impact on the outcome of a therapy.

A majority of evidence about TBS after-effects is derived from studies targeting the primary motor cortex (M1) (see Chung et al. (2016) for a review). This is attributable to the fact that motor-evoked potentials (MEP) currently represent the most convenient method to assess size and direction of TBS after-effects. However, this peripheral readout of corticospinal excitability has several limitations. First, MEPs can only be acquired from M1 and cannot be used to study excitability in non-motor regions, as they are unable to evoke muscle activity in the periphery. Second, MEPs represent a combined measure of the cortical excitability as well as excitability of the spinal pathways (Di Lazzaro et al., 2008; Groppa et al., 2012), making it difficult to isolte the cortical contributions to the potential after-effects. Last, TMS pulses also propagate through intracortical pathways, indirectly activating distant but interconnected brain regions from the stimulation site (Daskalakis et al., 2002). Thus, TBS after-effects might lead to excitability changes in remote regions, where excitability cannot be probed through MEPs.

The combination of TMS and EEG (TMS-EEG) provides an alternative physiological read-out to assess changes in cortical excitability and connectivity (Rogasch & Fitzgerald, 2013). The TMS-evoked potential (TEP) corresponds to the cortical response that can be recorded from the scalp using EEG after a single TMS pulse is applied to a target region (Ilmoniemi et al., 1997; Komssi et al., 2002). TEPs are characterized by a series of positive and negative deflections, which are usually labeled regarding their polarity (P = positive, N = negative) and time of appearance (in ms after the pulse). These peaks are thought to reflect activity of specific excitatory and inhibitory circuits, as the TMS pulse propagates through intracortical pathways from the stimulation site to connected brain regions (Komssi et al., 2002; Nikulin et al., 2003; Premoli, Castellanos, et al., 2014).

The TEP bypasses some of the inherent problems associated with the indirect measurement of cortical excitability using MEPs. First, the TEP can be recorded from any region of the cerebral cortex, as the EEG can measure the spread of activity from the target site to neighboring and distant regions. Second, it represents changes in cortical excitability without additional modulations of spinal motor neurons and peripheral nerves. Third, several studies have investigated the reliability and reproducibility of TEPs within individuals, suggesting that the cortical responses are highly stable within individuals within days (ter Braack et al., 2019) or between days (Lioumis et al., 2009; Casarotto et al., 2010; Kerwin et al., 2018). Thus, the TEP has many desirable features as a potential marker to track changes of TBS-induced neuroplasticity. One potential marker for this tracking might be the N100 component of the TEP, which appears as pronounced negativity bilateral around the central electrodes following around 100 ms after a pulse is applied to M1. Early TMS-EEG studies already suggested that the N100 component reflects inhibitory processing mediated by the activity of inhibitory interneurons (Nikulin et al., 2003; Bender et al., 2005). For example Paus et al. (2001) reported a significant correlation between the amplitude of the MEPs and the amplitude of the N100 component. Nikulin et al. (2003) observed that MEP amplitude and N100 component had an inverse relationship in a pre-

movement period and an increases in MEP amplitude were associated with decreases in size of the N100 component. In addition, Bonnard et al. (2009) investigated the relationship of the N100 component at different stages of a movement process. They found that in periods of high cortical excitability, i.e. during the preparation of movement, the N100 amplitude was reduced, whereas the intention to resist a movement was associated with a higher N100 amplitude around the central motor areas. The inhibitory character of the component is also supported by pharmacological studies, which were able to provide direct evidence that the N100 component is linked to late $GABA_B$-mediated inhibitory neurotransmission within the primary motor cortex (Premoli, Castellanos, et al., 2014).

There are only few studies who investigated TBS after-effects directly on the level of the cortex, using TEPs and MEPs as variables of interest (Vernet et al., 2013; Gedankien et al., 2017; Ozdemir et al., 2021). As a consequence, it is not well understood how cTBS modulates cortical excitability beyond the area of M1. It is also unclear whether TEPs and MEPs represent TBS-induced modulation of cortical excitability in a similar fashion, or whether they index separate mechanisms of cortical plasticity. Last, it is unknown how the TEP is modulated within responder subgroups, i.e. individuals that show either an inhibitory or facilitatory cTBS response at the corticospinal level.

The current study utilized a single-blinded sham controlled design in which three doses of cTBS were applied over the M1 and the resulting after effects were subsequently tracked by repeated measurements of MEPs and TEPs. This experimental design is inspired by a study from Nettekoven et al. (2014), who used a similar multi-dose approach to investigate iTBS induced cortical plasticity and the associated changes in functional magnetic resonance imaging (fMRI)-based motor-network connectivity. Based on this repeated modulation and measurement approach, the current study aims to explore the (dose-dependent) cTBS after-effects on cortical and corticospinal excitability indexed through the TEP and MEP, respectively.

# 2 Material and Methods

## 2.1 Participants

The study was conducted with 29 healthy volunteers (15 female, age (mean ± SD): 26.2 ± 3.0 years, range: 20-32 years) recruited from the campus of the Juelich Research Centre. All participants gave their information consent prior to participation and received a monetary compensation of 15 € per hour. Participants had no self-reported history of neurological conditions and had no metallic implants. Participants were right handed, which was assessed through the Edinburgh Handedness Inventory (Oldfield, 1971). The study received approval by the ethics committee of the Faculty of Medicine, University of Cologne (Zeichen: 17-244). The results of this study are based on 21 out of 29 participants that could be included in the final analysis after preprocessing.

## 2.2 Data acquisition

### 2.2.1 Electromyography (EMG)

MEPs were recorded from the first dorsal interosseous (FDI) muscle of the right hand using adhesive Ag/AgCl surface electrodes (H124SG, Covidien, Dublin, Ireland). The electrodes were placed in a belly-tendon montage with the active electrode placed on the belly of the muscle, the reference electrode placed on the metacarpophalangeal joint of the index finger and the ground electrode was placed proximally over the tendons to the muscle. The EMG signals were digitized with a 10 kHz using a PowerLab 26T and the LabChart 8 software package, epoched from -5 ms to 75 ms around the TMS pulse and stored for later analysis (ADInstruments, New Zealand). Participants were instructed to relax their hand during the experiment if visual inspection of the EMG activity suggested a pre-activation of the FDI.

### 2.2.2 Electroencephalography (EEG)

TEPs were recorded with a TMS-compatible EEG system (Easy Cap, Brain Products, Germany), consisting of 61 Ag/AgCl C-slit electrodes positioned according to the standard 10-20 System on the subject's scalp. Two additional electrodes (FT9, FT10) were used to record electrooculographic activity evoked by vertical and horizontal eye movements by placing them below the left eye and another close the lateral canthi of the right eye, respectively. The ground electrode was placed on the AFz position and the reference electrode was placed on position FCz. Electrode wires on the EEG cap were arranged perpendicular to the current flow induced by the TMS coil in order to minimize the impact of TMS-induced measurement artifacts (Sekiguchi et al., 2011) prior to the experimental session.

After the cap was positioned on the participant's head, the skin below the electrodes was cleaned and disinfected with alcohol using a cotton swap and then scraped and filled with Abralyt HiCl Electrolyte Gel (EASYCAP GmBH, Germany). Skin-electrode impedance was checked to be below 5 kΩ before start of the measurement. A thin plastic layer was wrapped around the EEG cap to avoid a direct contact of the TMS coil with EEG electrodes. The EEG signals were recorded and amplified by a BrainAmp DC MR+ amplifier (BrainProducts GmbH, Germany) at a sampling rate of 5 kHz and stored on a computer for further analysis. Earplugs were provided to the subjects to reduce the contamination of TEPs with auditory evoked potentials caused by clicking noise from discharging the TMS coil (Ilmoniemi & Kičić, 2010; ter Braack et al., 2015).

### 2.2.3 Transcranial magnetic stimulation (TMS)

The application of single magnetic pulses was performed with a figure-of-eight Double 70mm Alpha Coil (Magstim Company Ltd., UK), connected to a monophasic Magstim Bistim2 stimulator (Magstim Company Ltd., UK). The hotspot of the FDI muscle was determined by localizing the point on the scalp above left M1 that produced the strongest and most reliable peripheral EMG response in the right hand. The center of the stimulation coil was placed tangentially to

the skull, with the coil handle pointing posterior and tilted approximately 45 degrees away from the sagittal plane. In this orientation, the induced current in the brain flows in posterior-anterior direction, and recruits the corticospinal pathways primarily transsynaptically through excitatory interneurons (Kaneko et al., 1996; Hallett, 2007; Klomjai et al., 2015).

This FDI hotspot was registered within a BrainSight neuronavigation system (Rogue Research Inc, Canada) on a MNI template brain and used as a reference point to monitor accurate coil positioning throughout and between experimental session. The resting motor threshold (RMT) is defined as the intensity that generates a MEP with at least 50 μV peak-to-peak amplitude in at least 5 out of 10 consecutive trials (Rossini et al., 1994). In this study, the RMT was determined using a maximum-likelihood estimation as implemented in the TMS Motor Threshold Assessment Tool (MTAT; http://www.clinicalresearcher.org/software.htm), which has shown to be an efficient method to determine RMTs (Ah Sen et al., 2017). The RMTs were always defined based on the maximum stimulator output (MSO). The stimulation intensities for the different experimental blocks were then always selected relative to the RMT of the particular individual and are therefore reported as percentage of the individual RMT. For example, if the RMT of an individual is 36% of the MSO, 90% of the individual RMT will correspond to a stimulation intensity of ((36 * 90%) / 100) = 32.4% MSO. Localization of the FDI hotspot and the determination of the RMT were performed after the EEG cap was placed on the subject's head, as the EEG cap increases the distance between the TMS coil and the brain and therefore requires higher stimulation intensities.

Three different stimulation intensities were used when probing corticospinal and cortical excitability. Single-pulses were applied with 90% or 110% RMT during the measurement of MEPs and with 80% RMT during measurement of TEPs (Figure 1A). Importantly, stimulation intensities always refer to the intensity of the single pulses that were used to measure cortical or corticospinal excitability and not the stimulation intensity of the cTBS. The low intensity

during measurement of the TEP was specifically chosen to avoid peripheral activation of the target muscle, as recurrent somatosensory feedback might affect the resulting TEP response (Petrichella et al., 2017; Conde et al., 2019). Furthermore, lower stimulation intensities reduce the size of TMS-induced artifacts in the EEG recording (Mutanen et al., 2013).

Application of cTBS was performed with a figure of eight 70mm Double Air Film Coil (Magstim Company Ltd., UK) connected to a biphasic Magstim Rapid2 stimulator (Magstim Company Ltd., UK). The RMT was determined for this stimulator and stimulation coil independently from the setup used for single pulse stimulation. The application of cTBS was performed as originally described by Huang et al. (2005) and applied over FDI hotspot of M1. Each application consisted of 600 pulses, applied in bursts of three pulses at a frequency of 50 Hz, repeated each 200 ms for a total duration of 40 s in total. The stimulation was performed with an intensity of 70% of the individual RMT.

In the sham session, a parieto-occipital vertex sham stimulation was performed, comparable to the sham stimulation performed by Nettekoven et al. (2014). The stimulation coil was placed around the POz electrode along the vertex, with the coil handle pointing downwards towards the ground. The coil handle was then tilted away in posterior direction so that the center of coil was at least a few centimeters away from the head and not tangential to the surface of the skull or the underlying cortex. In this position, participants can still perceive the vibration of the coil during stimulation and hear the clicking noise, but the induced electric field cannot excite cortical neurons.

## 2.3 Experimental Design

The study was conducted as a single-blinded cross-over study designed to investigate the dose dependent effects of cTBS on corticospinal excitability (assessed through MEPs) and cortical excitability (assessed through the TEP). The experiment was performed in two separate ses-

sions that either included three repetitions of a real cTBS or a sham stimulation instead. The order of sessions was pseudo-randomized and sessions were performed at least 1 week apart (mean ± SD: 15.9 ± 13.6 days) to avoid possible carry-over effects from the cTBS to the sham sessions. If possible, sessions were always performed at the same time of the day, to minimize intra-individual variability and avoid possible confounds (ter Braack et al., 2019). Each session took approximately three hours to complete (90 minutes of preparation and 90 minutes of measurement time). In the following sections, the procedures will be described in detail using a cTBS session as example, since both sessions (cTBS and sham) were performed exactly in the fashion anyway.

### 2.3.1 Motor tasks

The motor performance of the participants was assessed with two different tasks that were performed before and after the TMS-EEG recordings (see next section). First, participants performed the Purdue Pegboard Test (PPT) (Tiffin & Asher, 1948), which tests manipulative dexterity and requires the participants to insert small metal pegs into a series of holes as quickly as possible. Due its resemblance to actions performed real life situations, improvements in PPT performance are more likely to indicate clinically relevant changes in behavior than improvements in simple reaction time tasks. Participants performed three repetitions of the PPT with each hand (alternating) and each run took 30 s to complete. The PPT performance for each hand was evaluated based on the average number of pegs correctly placed across the three runs. Afterwards, participants performed a simple bimanual finger tapping task (FTT), which is a common method to index basal properties of motor performance, such as tapping frequency, reaction time or amplitude of the finger movement in ageing or in clinical populations (Shammi et al., 1998; Sommervoll et al., 2011). The task was implemented using the Presentation software (Neurobehehavioral Systems, Inc.). Left and right CTRL key on the keyboard were used as response keys. During the task, participants were presented with a pseudo-random sequence of arrows pointing to the left or to the right (20 trials in total). Arrows were always presented

for 2 s on the screen and the inter-trial interval between presentation of arrows was 1.5 s with an additional jitter of 0-2 s. Subjects were instructed to repeatedly tap the left or the right CTRL key on the keyboard with their left or right index finger respectively, depending on the direction of the arrow direction was displayed on the screen. They were instructed to press the keys as quickly as possible without causing discomfort and stop immediately when the arrow disappeared again. The frequency of key presses as well as reaction times (i.e. time of first button press after presentation of the arrow) were used as index for possible behavioral effects induced by cTBS.

### 2.3.2 TMS-EEG protocol

Participants were seated in a comfortable Brainsight TMS chair with their elbows supported by the chair's armrest and their forearms relaxing on a pillow to minimize muscle activity from involuntary movements. Participants were also specifically instructed to avoid any unnecessary movements for the duration of electrophysiological measurements as this might potentially alter the after-effects of cTBS (Iezzi et al., 2008). The heads of the participants were fixed with a chinrest and an additional articulated arm was used support the head on the right hemisphere (opposite to the stimulation coil) against potential lateral movements of the head. Once the FDI hotspot was located and the RMT determined, the coil was fixed to the coil holder of the TMS chair to avoid unnecessary movement of the coil during the experiment. If the coil position deviated due to subject movement (indicated by the neuronavigation), the coil was readjusted by the experimenter during an inter stimulus interval (ISI). Participants were also instructed to keep their eyes open and focus on a white dot displayed on the computer screen in front of them.

Each of two experimental sessions consisted of four blocks of electrophysiological recordings (Figure 1B). Block 0 represented a pre-interventional assessment and was performed to acquire a baseline of corticospinal excitability (MEP) and cortical excitability (TEP) prior to any modulation through cTBS. At the beginning of the other three blocks, cTBS was applied over left

M1 to modulate excitability. Afterwards, changes in excitability were quantified by measuring MEPs, TEPs and MEPs again. MEPs were measured by applying 15 single pulses with 90% RMT and 15 single pulses with 110% RMT to the FDI hotspot of the left hemisphere (Figure 1A), using an ISI of 6.5s. For the measurement of TEPs, 100 single pulses were applied with an intensity of 80% RMT and an ISI of 6.5 - 9s (plus a random jitter of 0 - 0.5 s).

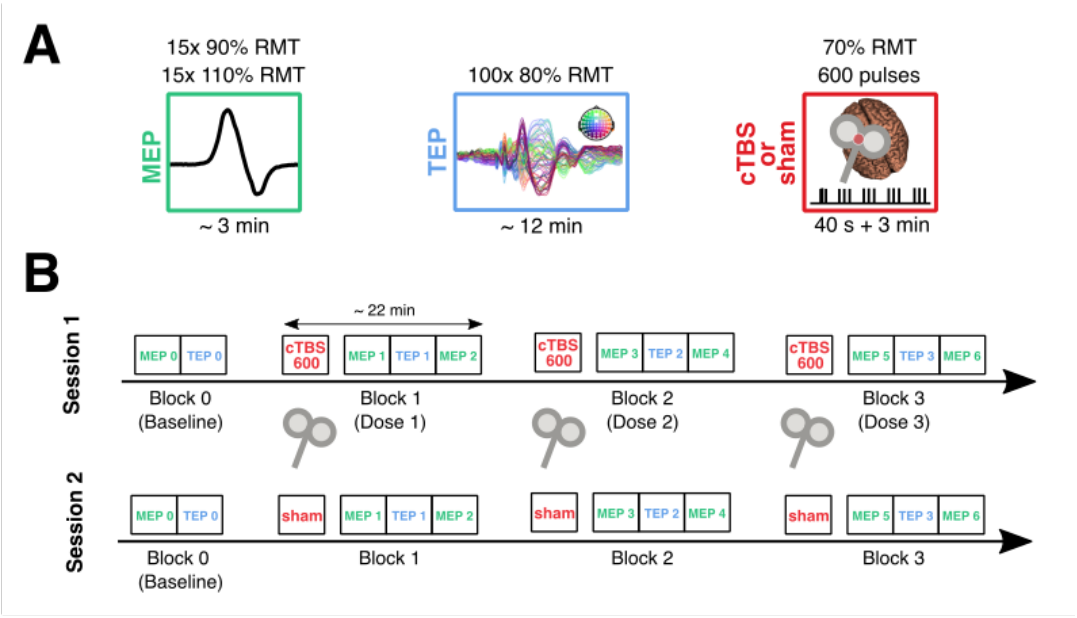


**Figure 1: Visual summary of the experimental protocol.** **(A)** Summary of stimulation parameters and approximate duration of the intervention, acquisition of motor-evoked potentials (MEP) and TMS-evoked potentials (TEP). **(B)** Sequence of stimulation blocks within the experiment. Block 0 represents a baseline measurement of MEPs and TEPs. Remaining blocks start by inducing neuroplasticity via cTBS and measure the dose-dependent changes in MEPs and TEPs afterwards.

After the baseline assessment of MEPs and TEPs, the first dose of cTBS (600 pulses) was applied to the left M1 (FDI hotspot) at the beginning of block 1. A waiting period of three minutes was included after the application of cTBS, as earlier studies suggested that the neuroplastic effects of TBS require some time to develop (Huang et al., 2005; Hamada et al., 2013). Following this waiting period, MEPs were measured (MEP 1 in Figure 1B) to quantify the early impact of

cTBS on corticospinal excitability approximately 5 minutes after the modulation. Then, TEPs were acquired (TEP 1 in Figure 1B) over a period of around 12 minutes. Approximately 18 minutes after the application of the cTBS, MEPs were measured a second time to quantify the late effect of cTBS on corticospinal excitability (MEP 2 in Figure 1B). This procedure of modulating M1 excitability with cTBS (600 pulses), measuring MEPs shortly after cTBS, measuring TEPs and measuring MEPs again was performed two additional times (block 2 and 3), until three doses of cTBS (a total of 1800 pulses) were applied to the subject's FDI hotspot. After the last acquisition of MEPs (MEP 6), the RMT was determined and the subjects completed the PPT and the FTT again.

## 2.4 Data preprocessing

### 2.4.1 EMG signals

Raw EMG signals were detrended, demeaned and MEP amplitudes were extracted by measuring the peak-to-peak voltage in a time window of 15–50 ms after the TMS pulse using custom made scripts written in MATLAB (R2016b, Mathworks, Inc., Natick, MA). All trials were visually inspected to exclude MEPs contaminated by a pre-activation of the target muscle or high levels background activity or noise in the EMG signals. MEP amplitudes were averaged within each measurement block and normalized to the baseline measurement (MEP 0) of each session (mean amplitude at block X / mean amplitude at baseline) * 100). Thus, changes in MEP amplitude are reported as percentage of the baseline measurement if not explicitly stated otherwise.

Since differences in motor cortical excitability prior to the intervention might potentially influence the susceptibility to the cTBS-induced plasticity, absolute MEP amplitudes at baseline were statistically compared between both sessions using a two sample t-test. Participants showing significant differences in MEP amplitude at baseline between the two sessions ($p < 0.01$) were excluded from the analysis, as this suggested that either the RMT was not appropriately measured, the stimulation hotspot was not well defined, or the participant did not relax their

muscles appropriately during the baseline measurement. This criterion was only applied to MEPs acquired with 110% RMT, as the MEP amplitude evoked by subthreshold intensities (90% RMT) are not as consistent as suprathreshold intensities and might have led to an erroneous rejection of participants based on differences in EMG noise levels between the sessions. There were significant differences ($p < 0.01$) in MEP amplitudes at baseline in 6 out of 29 participants, which were excluded from further analysis. An average of 14.2 ± 1.5 (mean ± SD) MEPs were included in the calculation of the MEP block average. The minimum number of MEPs within a block were 8 out of 15, which is still in the range of number of MEPs required to allow an appropriate estimation of the corticospinal excitability (Groppa et al., 2012).

### 2.4.2 EEG Signals

The preprocessing of EEG data was performed using MATLAB and a combination of the EEGLAB toolbox (version 14.1.1) (Delorme & Makeig, 2004), the TMS-EEG signal analyser (TESA) extension (Rogasch et al., 2017) and additional custom made scripts. Due to the complex interaction of TMS-induced artifacts, appropriate preprocessing of TMS-EEG signals is a crucial step to obtain valid measurements of cortical excitability. EEG preprocessing steps were performed independently for each subject, session and measurement block.

First, the four blocks TMS-EEG blocks, containing 100 TEPs each, were extracted from the continuous EEG recording. High amplitude TMS pulse artifacts were removed between -2 to 10 ms relative to the trigger of the associated pulse and interpolated using a smoothed segment directly preceding the removed interval (-14 to -2 ms). Afterwards, a DC detrend was applied to the recording. An initial rejection of corrupted channels was performed, primarily to remove channels that were unambiguously disconnected or otherwise defective and not recording EEG activity. Channels that showed high levels of background noise (e.g. due to power-line interferences or high impedances) were still maintained in the recording at this stage. A 60 Hz low-pass filter was applied, followed by 1 Hz high-pass filter and a notch-filter between 49–51

Hz. Last, EEG signals were epoched from -1000 to 1000 ms around the TMS pulses and down-sampled from 5 kHZ to a sampling frequency of 625 Hz. A first visual inspection of epochs was performed to remove epochs that were contaminated by high amplitude artifacts or flat lining thereby corrupting the whole epoch (due to bad connection of ground or reference electrode, or bursts of EMG activity caused by head movements or facial muscles).

A second round of channel rejections was performed to remove remaining channels containing high levels of noise or unsystematic high amplitude artifacts, as they might otherwise interfere with the independent component analysis (ICA). Missing channels were then interpolated using the superfast spherical spline interpolation implemented in the eeg_interp() function of EEGLAB. A baseline correction was applied, using the whole pre-stimulus period from -1000 ms to -2 ms as baseline. EEG channels were then re-referenced to the common average reference. The ICA was then performed on this pre-cleaned dataset, using the logistic infomax algorithm (Bell & Sejnowski, 1997), implemented in the binica() function of EEGLAB. Afterwards, a second round of epoch rejection was performed in the component space. This step was required to exclude epochs that were contaminated by high amplitude artifacts in the component space that might have remained unnoticed in the channel space. If epochs were removed during the inspection of the component space, the ICA was repeated again without these epochs. These ICs were then visually inspected to remove the remains of the TMS pulse artifacts, electrooculographic activity caused by eye movements and eye blinks, TMS-evoked muscle activity and electrode noise, using the component classifications from TESA to make informed decisions about the origin of the components (i.e. either neural or artificial).

2 out of 29 subjects had to be excluded from analysis as insufficient EEG data quality did not permit a systematic removal of TMS-induced artifacts. In the final dataset (N = 21, after EMG and EEG preprocessing), an average of 93.4 ± 4.0 (mean ± SD) trials were included for the generation of the TEPs in each block. The minimum number of TEPs across all these measurements were 78, which is still above the minimum number of trials required to obtain a reliable TEP,

according to a study from (Kerwin et al., 2018). An average of 2.8 ± 1.9 (mean ± SD) channels were removed per measurement block, but not more than 6. Following ICA, 18.2 ± 4.6 (mean ± SD) components were removed on average, but not more than 31.

## 2.5 Data analysis

### 2.5.1 Analysis of motor tasks

Differences in motor task performance between cTBS and sham session was assessed based on three variables of interest. This includes the number of pins placed during PPT, as well as the tapping frequency and reaction time in the FTT. These variables were analyzed separately for both hands (and not as a compound measure), as there are indications that cTBS modulation can lead to opposite after-effects on cortical excitability in the contralateral hemisphere (Suppa et al., 2008).

### 2.5.2 Analysis of motor-evoked potentials (MEP)

Differences in MEP amplitude between cTBS and sham were analyzed in several different ways and separately for MEPs acquired with 90% RMT and 110% RMT. The main focus was on MEPs acquired with 110% RMT, as intensities below 100% RMT are considered sub-threshold and only elicit MEPs sporadically. Furthermore, it has been shown that the strongest cTBS-induced MEP suppressions can be observed when MEPs are probed with higher stimulation intensities (Vallence et al., 2015; Goldsworthy et al., 2016). The general effect of interventions on MEP amplitude was established by testing whether cTBS or sham produced significant deviations from baseline at any measurement point. The general relationship between time (MEP 1, ... MEP 6) and interventions (cTBS, sham) and their influence on MEP amplitude were also assessed. A direct comparison of normalized MEP amplitudes between cTBS and sham was performed to test if cTBS resulted in significant changes in corticospinal excitability between interventions.

### 2.5.3 Definition of responder subgroups

Prior studies have demonstrated a large inter-individual variability regarding the strength and direction of TBS after-effects on cortical excitability (Hamada et al., 2013). Hence, individuals were categorized into responder subgroups based on their change in MEP amplitude in the cTBS session. Subgroups were defined based on the average change in normalized MEP amplitude (110% RMT) averaged across all timepoints after the first application of cTBS (MEP 1 to MEP 6). Subjects were categorized as cTBS faciliatory if the averaged MEP amplitude showed a net decrease and as cTBS inhibitory if their MEP amplitude showed an overall increase. Differences between responder subgroups were always investigated based on the average TEP at baseline from both sessions.

### 2.5.4 Analysis of TMS-evoked potentials (TEP)

Analysis of EEG activity was focused around the TEP, which was used as a measure of cortical excitability (Rogasch & Fitzgerald, 2013). Differences between TEPs were investigated by directly comparing the cortical responses between cTBS and sham session, either within the whole group of 21 individuals or within the responder subgroups. An additional analysis directly compared the cortical responses between the two responder subgroups. TEPs were investigated with a particular focus on three channels of interest, covering ipsilateral (C3) and contralateral M1 (C4) as well as the region in between, over the vertex (Cz). Channel C3 was located directly below the stimulation site and therefore captures the cortical response immediately after the TMS pulse activates M1. Differences in cortical excitability between cTBS and sham session were assessed through a direct comparison of the TEPs in the temporal domain, using a cluster based permutation test for statistical analysis (see section 2.6.2). An equivalent analysis was also performed for the global mean field power (GMFP). The GMFP corresponds to the standard deviation of all EEG channels across time and represents a general measure of cortical activity (Lehmann & Skrandies, 1980).

The latency of TEP peaks can exhibit considerable interindividual variability (ter Braack et al., 2019). In order to account for these interindividual differences, peak amplitudes were extracted at individual latencies for each subject, session and measurement block. Peak amplitudes were obtained from predefined time windows corresponding to the temporal extent of the commonly observed TEP peaks, i.e. P30 (20–40 ms), N45 (40–55 ms), P60 (55–85 ms), N100 (85–135 ms) and P200 (160–240 ms). Comparable time windows were also utilized in previous TMS-EEG studies (Casula et al., 2014; Premoli, Castellanos, et al., 2014; Opie et al., 2017; Chung et al., 2018).

Channel C3 was used as a reference channel to determine the peak latencies of the TEP peaks for all other channels. This means that the scalp topography of e.g. peak N45 shows the voltage of all channels at the same latency, i.e. the time in the interval of 40–55 ms at which the activity of channel C3 showed the most negative amplitude. In addition, peak components were computed by averaging the EEG signal ±5 ms centered around the peak latency to reduce the variability of the estimated peak amplitude. Reductions or increases of peak amplitudes are always described with respect to the polarity of the component. For example, an amplitude increase of the N45 component (N = negative) will indicate that the negative peak became more negative, whereas an increase in amplitude of the P30 component (P = positive) will mean that the voltage of the peak increased.

### 2.5.5 Dose effect of cTBS on MEP amplitude and N100 component of the TEP

One hypothesis of the current study was that a repeated application of cTBS may lead to accumulating facilitatory or inhibitory effects on corticospinal and cortical excitability as the experiment progresses. These dose effects of cTBS were investigated using MEP amplitude as well as the N100 component of the TEP as variable of interest. In order to test whether time within the session allowed a general prediction about the size of the MEP amplitude as more doses of cTBS were applied, a linear regression was performed on the individual trajectories of normalized MEP changes (using the MEP amplitude from MEP 0 to MEP 6 to fit the regression line

within each individual). If cTBS leads to a dose-dependent increase or decrease of corticospinal excitability, the slopes should be significantly greater or smaller than zero on a group-level (i.e. within whole group and subgroups). In contrast, slopes obtained from the sham session should not be significant from zero at group-level, as no dose-dependent modulation was expected in this case. Based on this assumption, it was tested whether the collections of individuals slopes were significantly different from zero for any of the groups or interventions. The same procedure was also utilized to investigate dose-dependent effects at the cortical level, using the normalized N100 peak of the TEP (i.e. each peak is represented as percentage of baseline) as variable of interest. In this case, only four data points were used to fit the regression line within individuals, since the TEP was only acquired four times throughout the experiment. The analysis was repeated for the three channels of interest (C3, Cz, and C4).

### 2.5.6 Correlation between MEP and TEP

Another goal of this study was to investigate whether cTBS-induced changes in cortical excitability (TEP) are related to the changes in corticospinal excitability (MEP). For this purpose, the change in N100 amplitude was correlated with the early and late MEP responses (110% RMT) that were acquired before and after the TEP within in the same block. Both measures were represented as voltage difference from baseline, i.e. $\Delta$ MEP and $\Delta$ TEP. Correlations were calculated between early MEPs and the TEPs, as well as late MEPs and the TEPs for all 61 EEG channels.

## 2.6 Statistical Analysis

### 2.6.1 General statistics

Statistical analyses were performed in Python (version 3.6.10) using the pingouin package (version 0.3.2), the scipy package (version 1.3.1) and the mne-python package (0.21.0). General relationships between time and interventions for behavioral performance variables, RMT and MEPs were assessed through a two-way repeated measures analysis of variance (rmANOVA)

using the rm_anova() function of the pingouin package. T-tests were performed using the implementation of the pingouin package. Differences from baseline were assessed using one-sample t-tests for normalized MEPs. Differences in MEPs between experimental conditions were assessed with paired t-tests. Dose-effects were assessed through linear regressions, implemented in the scipy package. Correlation between MEPs and TEPs were based on the Spearman's rank correlation coefficient, also implemented in the scipy package. For cluster based permutation testing (section 2.6.2), the permutation_cluster_test() implementation of the mne-python package (version 0.21.0) was utilized. Error bars or shaded regions in the figures indicate the standard deviation (SD), the standard error of the mean (SEM) or the within-subject standard error (SE) (O'Brien & Cousineau, 2014). The exact meaning will be specifically declared in the figure caption. Thresholds for statistical significance were set to $p < 0.05$ if not stated otherwise.

Correction for multiple comparisons was performed using the Bonferroni method. In case of MEPs, correction for multiple comparisons was performed at the level of MEP blocks (N = 6, excluding baseline). Statistical results will always be reported using the uncorrected p-values. However, the null hypothesis was only rejected if the p-value was smaller than the Bonferroni-adjusted $\alpha$ = 0.00833 (0.05/6). Regarding the relationship between MEPs and TEPs (section 2.5.5), a sequential approach was used for correction of multiple comparisons. Channel C3, Cz and C4 were assessed first, only correcting for three channels and the two MEP blocks using a Bonferroni-adjusted -level of 0.0833 (0.05/6). Correlations of the remaining 58 EEG channels were considered explorative, and therefore corrected using a Bonferroni-adjusted $\alpha$ = 0.0008 (0.05/58).

### 2.6.2 Cluster based permutation tests

Differences in the TEP between the two experimental conditions (cTBS vs. sham) or responder subgroups (inhibitory vs. faciliatory group) were statistically assessed using a non-parametric cluster based permutation test. These statistics belong to the family of non parametric permu-

tation tests. They are particularly useful if the variables of interest are spatially or temporally correlated, as they do not require an explicit adjustment to deal with the problem of multiple comparisons. Therefore, they are highly recommended for statistical comparisons in EEG or MEG data (Maris & Oostenveld, 2007).

In cluster based permutation testing, a test statistic (e.g. t-test or F-test) is computed for all samples of interest (e.g. channels, time points, frequencies or a combination of those) between two groups or experimental conditions. The obtained test statistics are then compared to a predefined threshold corresponding to a desired $\alpha$-level to establish significance of samples (e.g. a p-value < 0.05). Samples below the critical threshold are then clustered based on their adjacency to neighboring or directly connected samples by aggregating their test statistics together (through a sum). Here, clusters are either formed on a series of consecutive timepoints or on electrodes localized next to each other on the scalp (e.g. during analysis of TEP peaks).
The size of the aggregated test statistic of a particular cluster in the real dataset is then compared against the largest cluster of a reference distribution of random clusters that were obtained from permuting the original data n times (Monte Carlo permutation tests). The count of random clusters that are smaller than the cluster obtained from the real measurement then corresponds to the p-value of that cluster. For example, if n = 100 permutations were performed and the real cluster is larger than the test statistic of 95% of the permutations, the cluster would be considered significant if the threshold for significance was set to $p < 0.05$ at the level of clusters.
A paired t-test was used as a test statistic whenever cTBS and sham were directly compared within the whole or within subgroups. An independent t-test was used as test statistic if responder subgroups (faciliatory and inhibitory) were statistically compared against each other. During the formation of clusters, the minimum size of a cluster was defined as n  2, only including directly neighboring samples. The reference distribution of test statistics was always obtained from n = 5000 permutations. Direct comparison of the TEPs in the temporal domain were also realized using cluster based permutation statistics. Tests were performed separately

for each channel of interest (C3, Cz, C4, and the GMFP) and each block. Clustering was performed within each channel along the temporal dimension. TEPs from 0-500 ms post stimulus were compared. For the formation of clusters, only samples with a $p < 0.05$ were considered. The corrected threshold for significance at the level of clusters was set to $p < 0.01$.

Differences in TEP peak amplitude between cTBS and sham were assessed for each peak (P30, N45, P60, N100, P200) and measurement (TEP 0 - 3) using a spatial cluster based permutation test. Similar approaches have been used before in other studies to investigate differences in the TEP between two experimental conditions or between groups (Premoli, Castellanos, et al., 2014; Chung et al., 2018). Clusters were formed using adjacent channels on the scalp topography using a cluster-forming threshold of $p < 0.025$. This slightly lower threshold was selected to improve the spatial sensitivity of the formed clusters, as the initial analysis with a less strict threshold resulted in spatially diffuse clusters. The threshold for significance at the level of clusters was set to $p < 0.05$.

# 3 Results

## 3.1 Effects of cTBS on RMT

A comparison of RMTs revealed a significant main effect of Intervention, but no interaction of Time and Intervention [rmANOVA, Intervention {cTBS, sham} x Time {pre, post}, Intervention*Time: $F_{1, 20} = 0.878$, $p = 0.360$; Intervention: $F_{1, 20} = 9.252$, $p = 0.006$; Time: $F_{1, 20} = 0.547$, $p = 0.468$]. The RMT between cTBS and sham prior to the intervention revealed no significant difference (pre-cTBS: 40.9 ± 4.2%, pre-sham: 40.2 ± 3.9%; $t_{20} = 1.404$, $p = 0.17559$). However, this difference was significant at the second assessment of the RMT after the completion of the experimental protocol between post-cTBS (41.4 ± 4.3%) and post-sham (40.2 ± 4.0%, $t_{20} = 3.477$, $p = 0.00238$).

### 3.2 Effects of cTBS on motor taks performance

Group-level performance during the PPT for the left and right hand is summarized in Figure 2 before and after application of three doses of cTBS or sham. There was no significant interaction between the factors Intervention and Time, as well as no significant main effect of Intervention or Time on PPT performance in the left hand [rmANOVA, Intervention {cTBS, Sham} x Time {pre, post}, Intervention*Time: $F_{1, 20} = 0.659$, $p = 0.427$; Intervention: $F_{1, 20} = 0.206$, $p = 0.655$; Time: $F_{1, 20} = 1.454$, $p = 0.242$]. For the right hand, the rmANOVA revealed again no significant interaction between the factors Intervention and Time ($F_{1, 20} = 0.069$, $p = 0.796$) and no significant effect of the factor Intervention ($F_{1, 20} = 0.149$, $p = 0.704$). However, there was a significant effect of factor Time ($F_{1, 20} = 11.635$, $p = 0.003$) on the subjects' performance in the test.

Regarding the tapping frequency in the FTT, the rmANOVA did not indicate a significance for the interaction between the factors Intervention and Time ($F$, $= 0.856$, $p = 0.366$) or the factor Intervention ($F_{1, 20} = 1.029$, $p = 0.322$) for the left hand. However, there was a significant main effect of factor Time on the subjects' tapping frequency ($F_{1, 20} = 34.853$, $p < 0.00001$). This was also the case for the right hand, revealing only a significant main effect of Time [Intervention {cTBS, Sham} x Time {pre, post}, Intervention*Time: $F_{1, 20} = 0.548$, $p = 0.468$; Condition: $F_{1, 20} = 0.809$, $p = 0.379$; Time: $F_{1, 20} = 73.864$, $p < 0.00001$].

The analysis of reaction times during the FTT did not reveal a significant interaction or significant main effects of any of the two factors for the left hand [rmANOVA, Intervention {cTBS, sham} x Time {pre, post}, Intervention *Time: $F_{1, 20} = 0.671$, $p = 0.422$; Condition: $F_{1, 20} = 0.207$, $p = 0.654$; Time: $F_{1, 20} = 2.681$, $p = 0.117$]. For the right hand, only the main effect for the factor Time was statistically significant [rmANOVA , Intervention {cTBS, sham} x Time {pre, post}, Intervention*Time: $F_{1, 20} = 1.925$, $p = 0.181$; Condition: $F_{1, 20} = 0.392$, $p = 0.539$; Time: $F_{1, 20} = 8.015$, $p = 0.010$].

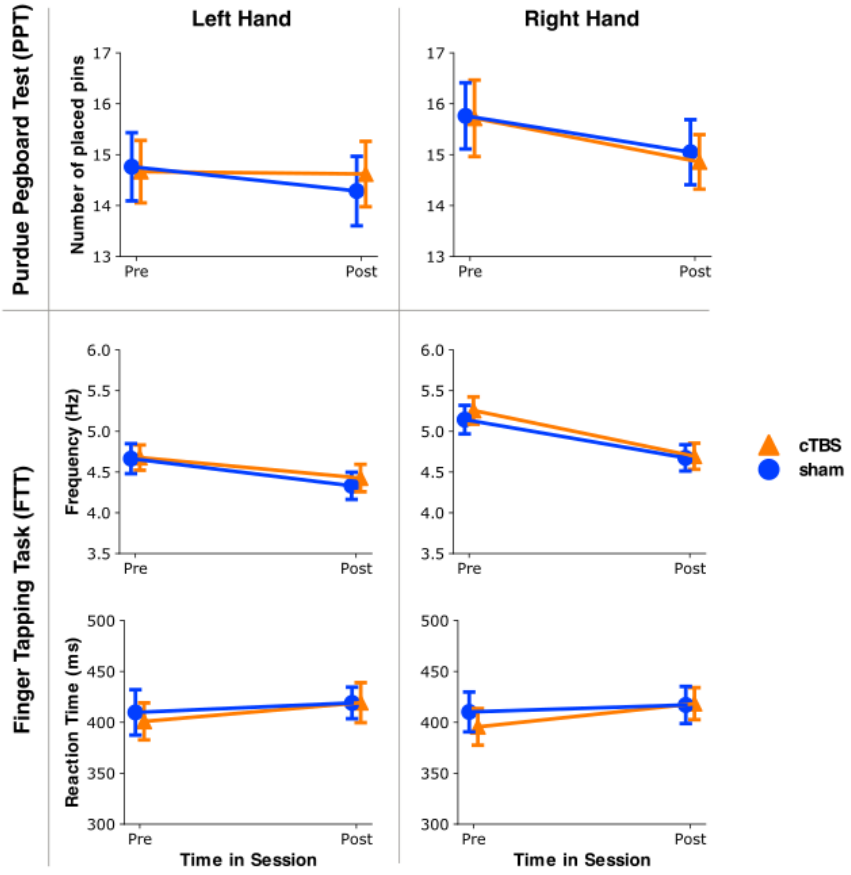


**Figure 2: Changes in behavioral performance at the group-level.** Performance during the PPT and FTT at pre- and post-interventional time points for the left and right hand. Each graph represents the change in motor task performance following three doses of cTBS or three doses of sham. Errorbars indicate the SE.

### 3.3 Effects of cTBS on MEPs

In this sample of 21 individuals, cTBS was associated with an overall increase MEP amplitudes for both stimulation intensities (Figure 3). For MEPs acquired with 90% RMT, none of the normalized MEP amplitudes were significantly different from baseline after correction for multiple comparisons (adjusted $\alpha$ = 0.00833 (0.05/6)). Prior to Bonferroni correction, normalized MEP amplitudes were significantly different at MEP 2 ($t_{20}$ = 2.636, p = 0.01584), MEP 4 ($t_{20}$

= 2.902, p = 0.00881), MEP 5 ($t_{20}$ = 2.314, p = 0.03140) and MEP 6 (t = 2.376, p = 0.02759) following cTBS. In contrast, MEP amplitudes were only different from baseline at MEP 2 ($t_{20}$ = 2.758, p = 0.01213) after sham intervention. There were also no significant differences in normalized MEP amplitude from baseline when probed with 110% RMT. However, prior to Bonferroni correction, MEP amplitudes at MEP 2 ($t_{20}$ = 2.555, p = 0.01887) and MEP 4 ($t_{20}$ = 2.422, p = 0.02506) were indicating an increase in corticospinal excitability following cTBS.

When measured with 90% RMT, MEP amplitudes steadily increased after the first dose (Figure 3A). In contrast, MEP amplitudes were reduced immediately after the second and the third dose (MEP 3, MEP 5), but increased again when measured later in time (MEP 4, MEP 6). Statistical analysis revealed that there was no significant main effect of Intervention at 90% RMT but only for the factor of Time [rmANOVA, Time {MEP 1, . . . , MEP 6} x Intervention {cTBS, Sham}, Time*Intervention: $F_{5,100}$ = 1.074, p = 0.379; Time: $F_{5,100}$ = 4.827, p = 0.001; Intervention: $F_{1,20}$ = 2.990, p = 0.099].

For MEPs assessed with 110% RMT, statistical analysis revealed no significant main effects of Time or Intervention [rmANOVA, Time {MEP 1, . . . , MEP 6} x Intervention {cTBS, Sham}, Time* Intervention: $F_{5,100}$ = 1.438, p = 0.217; Time: $F_{5,100}$ = 1.623, p = 0.161; Condition: $F_{1,20}$ = 3.804, p = 0.065]. Even though the main effect of Intervention was not significant in any of the two stimulation intensities, both stimulation intensities indicated a trend ($p < 0.1$), suggesting the existence of an effect of cTBS-induced plasticity on MEP amplitudes. Furthermore, MEP amplitudes at 110% RMT increased after the first and second dose of cTBS, but decreased after the third application. A visual comparison of normalized MEP amplitudes measured with 90% and 110% RMT revealed a qualitatively dissimilar pattern. While MEPs acquired with 110% RMT showed a trend of increasing corticospinal excitability until MEP 4 and a decrease afterwards, MEPs acquired with 90% RMT revealed a more variable pattern, characterized by a high corticospinal excitability at MEP 2 and MEP 6.

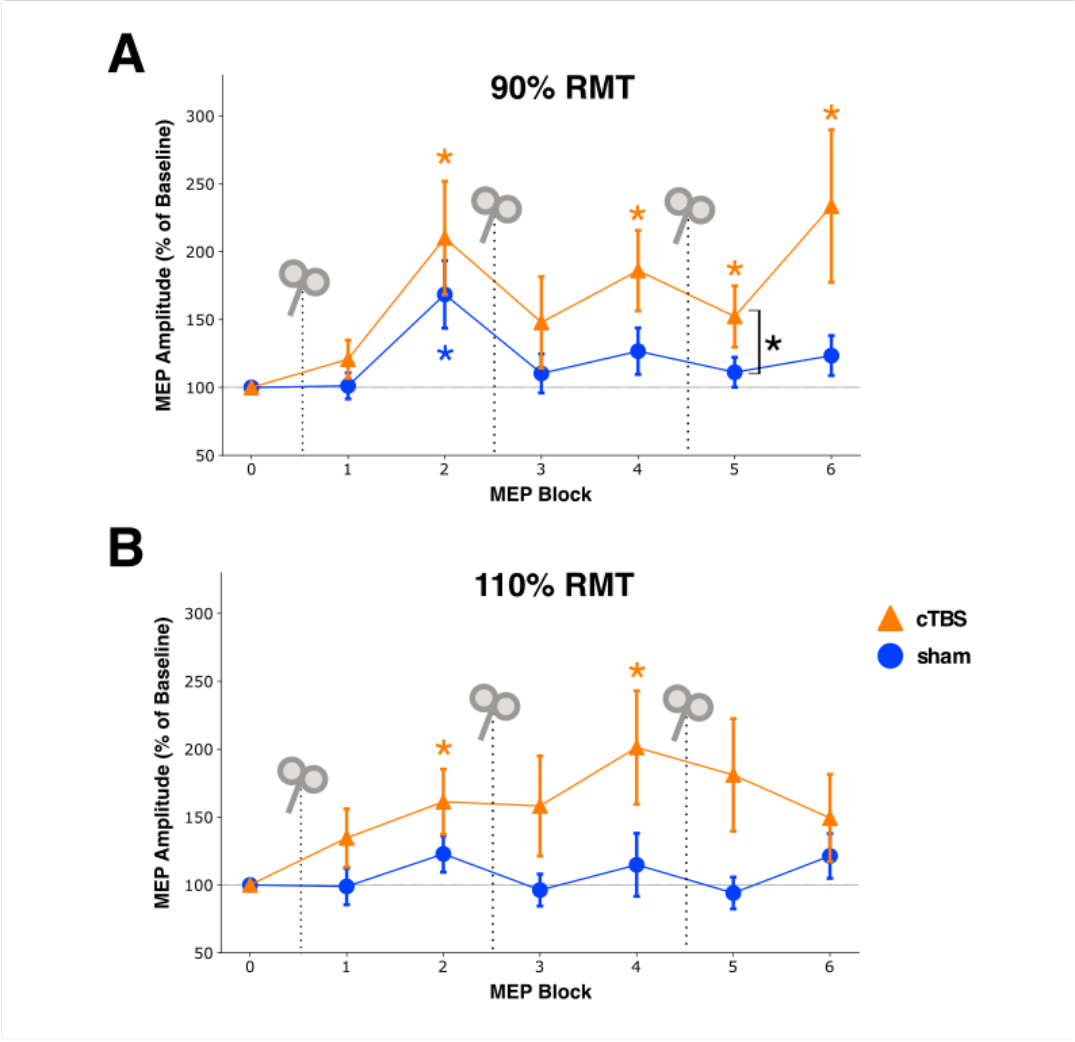


**Figure 3: Modulation of corticospinal excitability at the group-level.** MEP amplitude at the different MEP blocks throughout the experiment, normalized to the baseline measurement (MEP 0) and probed with **(A)** 90% RMT or **(B)** 110% RMT. Approximate timing of each of the intervention (cTBS or sham) is indicated by the TMS coils. Asterisks directly above and below errorbars indicate statistical differences from baseline. Errorbars indicate the SEM (* = $p < 0.05$, uncorrected; ** = $p < 0.05/6$, Bonferroni correction).

Since both stimulation intensities indicated a trend for the main effect of Intervention, a direct comparison between cTBS and sham (paired t-test) was performed at the different MEP blocks to find out at what time after the intervention the differences in corticospinal excitability were most distinct. However, there were no significant differences between cTBS and sham at any

of the six MEP blocks for MEPs acquired with 90% RMT or 110% RMT after Bonferroni correction ($\alpha$ = 0.00833). Prior to correction, the statistical analysis indicated a difference in MEP amplitude between cTBS and sham at MEP 5 ($t_{20}$ = 2.097, p = 0.04892) at a stimulation intensity of 90% of RMT. Differences at MEP 4 ($t_{20}$ = 1.745, p = 0.09630) and MEP 6 ($t_{20}$ = 1.846, p = 0.07969) indicated a statistical trend. For MEPs acquired with 110% RMT, MEP 4 ($t_{20}$ = 1.843, p = 0.08019) and MEP 5 ($t_{20}$ = 2.050, p = 0.05373) indicated a trend.

### 3.4 Effects of cTBS on MEPs within responder subgroups

The cTBS-induced effects on corticospinal excitability revealed a high degree of interindividual and intraindividual variability across the session (Figure 4A). 12 out of 21 individuals were categorized as cTBS facilitatory, as they showed a net increase in MEP amplitude across the post-interventional MEP blocks (1-6). In contrast, 9 out of 21 individuals were characterized by an average decrease in MEP amplitude and were categorized as cTBS inhibitory accordingly. Whole group will always refer to the complete study sample consisting of 21 individuals, whereas the inhibitory subgroup refers to the 9 individuals with an overall inhibitory response and facilitatory subgroup refers to the 12 individuals with an overall faciliatory response to cTBS.

For the inhibitory subgroup, MEP 3 ($t_8$ = -4.305, p = 0.00260), MEP 5 ($t_8$ = -7.157, p = 0.00010) and MEP 6 ($t_8$ = -8.356, p = 0.00003) were significantly different from baseline following cTBS (one-sample t-tests). In the facilitatory subgroup, only MEP 2 was significantly increased compared to baseline ($t_{11}$ = 3.384, p = 0.00610). However, amplitudes at MEP 1 ($t_{11}$ = 2.483, p = 0.03042), MEP 3 ($t_{11}$ = 2.267, p = 0.04451), MEP 4 ($t_{11}$ = 3.126, p = 0.00964), MEP 5 ($t_{11}$ = 3.207, p = 0.00836) and MEP 6 ($t_{11}$ = 3.076, p = 0.01055) were all statistically different prior to the Bonferroni correction. However, it should be noted that the p-values of MEP 4 and MEP 5 were only marginally above the threshold for statistical significance and therefore still indicate a statistical trend after the correction (Bonferroni-adjusted $\alpha$ = 0.00833).

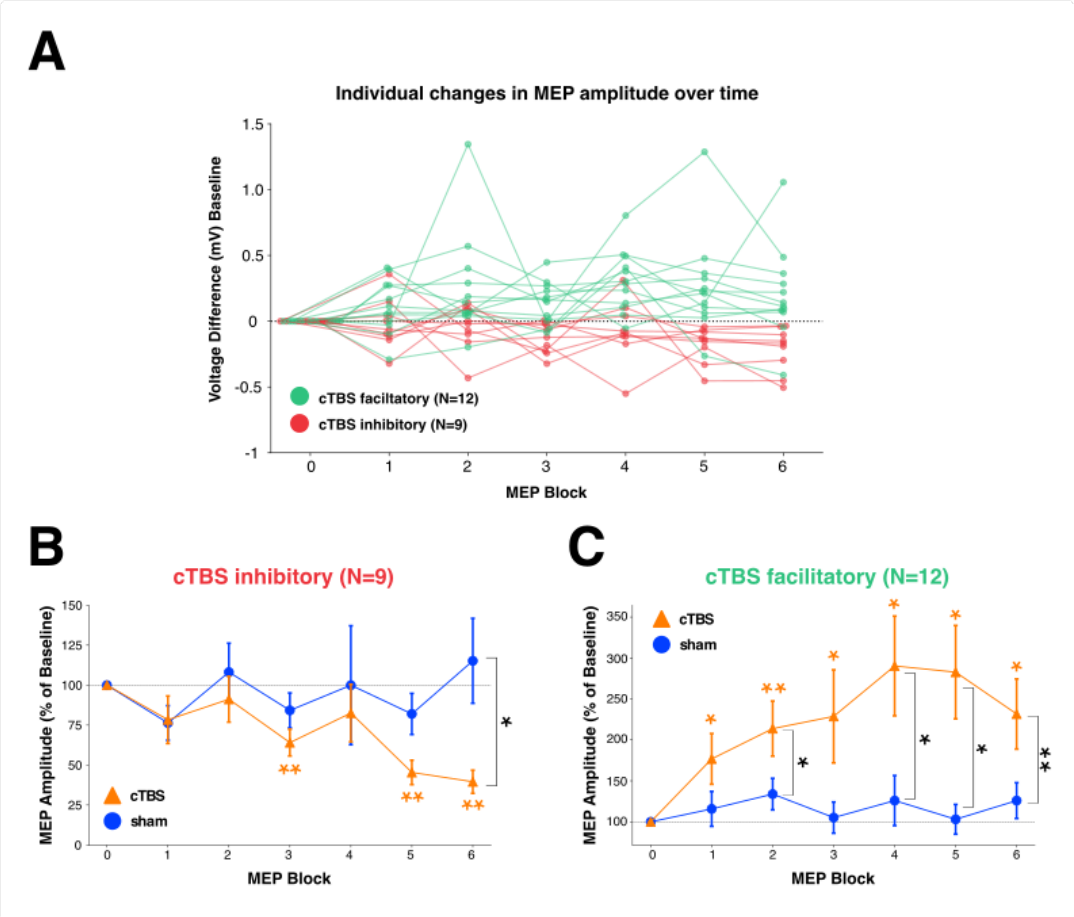


**Figure 4: Modulation of corticospinal excitability within responder subgroups.** **(A)** Individual changes in MEP amplitude (depicted as voltage difference from baseline) measured in the cTBS session with 110% RMT. **(B)** Group-level changes in MEP amplitude within inhibitory subgroup. **(C)** Group-level changes in MEP amplitude within the facilitatory subgroup. Asterisks directly above and below errorbars indicate statistical differences from baseline. Error bars indicate the SEM (* = $p < 0.05$, uncorrected; ** = $p < 0.05/6$, Bonferroni correction).

In the sham condition, none of the post-interventional MEPs were significantly different from baseline in both of the subgroups.

The analysis of normalized MEP amplitudes within the two subgroups (Figure 4B & C) revealed that cTBS-induced changes in corticospinal excitability were not significantly decreased compared to sham within the inhibitory subgroup [rmANOVA, Time {MEP 1, ... , MEP 6} x

Intervention {cTBS, sham}, Time* Intervention: $F_{5, 40}$ = 1.775, p = 0.14; Time: $F_{5, 40}$ = 1.324, p = 0.274; Intervention: $F_{1, 8}$ = 2.683, p = 0.14]. This was different for the facilitatory subgroup (Figure 4C), where corticospinal excitability was significantly increased following cTBS compared to sham as indicated by a significant main effect of Intervention [rmANOVA, Time {MEP 1, ... , MEP 6} x Intervention {cTBS, sham}, Time*Intervention: $F_{5, 55}$ = 1.860, p = 0.116; Time: $F_{5, 55}$ = 1.557, p = 0.188; Intervention: F, = 8.554, p = 0.014]. A post-hoc comparison of MEP amplitudes between cTBS and sham at the different MEP blocks revealed a significant difference between MEP 6 in the facilitatory subgroup ($t_{11}$ = 3.292, p = 0.00718). The differences at MEP 2 ($t_{11}$ = 2.222, p = 0.04819), MEP 4 (t = 2.408, p = 0.03474) and MEP 5 ($t_{11}$ = 2.944, p = 0.01335) were only significant prior to correction for multiple comparisons. The post-hoc comparisons within the inhibitory subgroup revealed a difference between cTBS and sham at MEP 6 that was not statistically significant following Bonferroni correction ($t_8$ = -2.562, p = 0.03353).

A direct comparison of cTBS-induced plasticity (average of normalized change from baseline across all post-interventional MEP blocks) within both subgroups revealed a significant larger variance in the facilitatory compared to the inhibitory subgroup (Levene's Test, $F_{1, 19}$ = 11.12, p = 0.00349), as well as a significantly larger induced cortical plasticity (Welch's t-test, $t_{16}$ = -4.30, p = 0.00119). These differences in size of cTBS-induced plasticity, as well as the larger number of individuals showing a facilitatory response explain why the overall effect of intervention was not statistically significant at the whole group for any of the post-interventional MEP blocks after the Bonferroni correction.

### 3.5 Effects of cTBS on TEPs

The TEP was characterized by a several peaks (P30, N45, P60, N100, P200) that were clearly identifiable on a group-level (Figure 5). The N100 component was associated with a characteristic negativity spatially located in the central regions between the left and right primary motor

cortices around the channel Cz. It should be noted that for visual representation, peaks were detected on the grand average TEP and not within each subject in Figure 5. As consequence, the topographical maps in Figure 5 are not consistent with the topographical maps in Figure 8, where peak amplitudes were first extracted from each individual and then averaged.

A direct comparison of the TEPs in the time domain around the motor related channels (Figure 6) revealed that the cortical response was most differentiated below the stimulation site at the ipsilateral cortex (C3) and became less complex with increasing distance (Cz and C4). Especially the early components (< 100 ms) were only weakly present around the contralateral hemisphere. The TEP around the vertex (Cz) still recorded some of the earlier TEP components (P30, N45 and P60), but was mainly characterized by a large positive peak around 200 ms (P200). Statistical analysis revealed that the TEP was significantly decreased after the third dose of cTBS (TEP 3) approximately 120 to 190ms after the TMS pulse ($p = 0.0056$) around left M1 (C3). In contrast there were no significant differences between the measured controls following cTBS and sham in any of the four blocks in channel Cz, C4 or the GMFP (all clusters with $p > 0.01$).

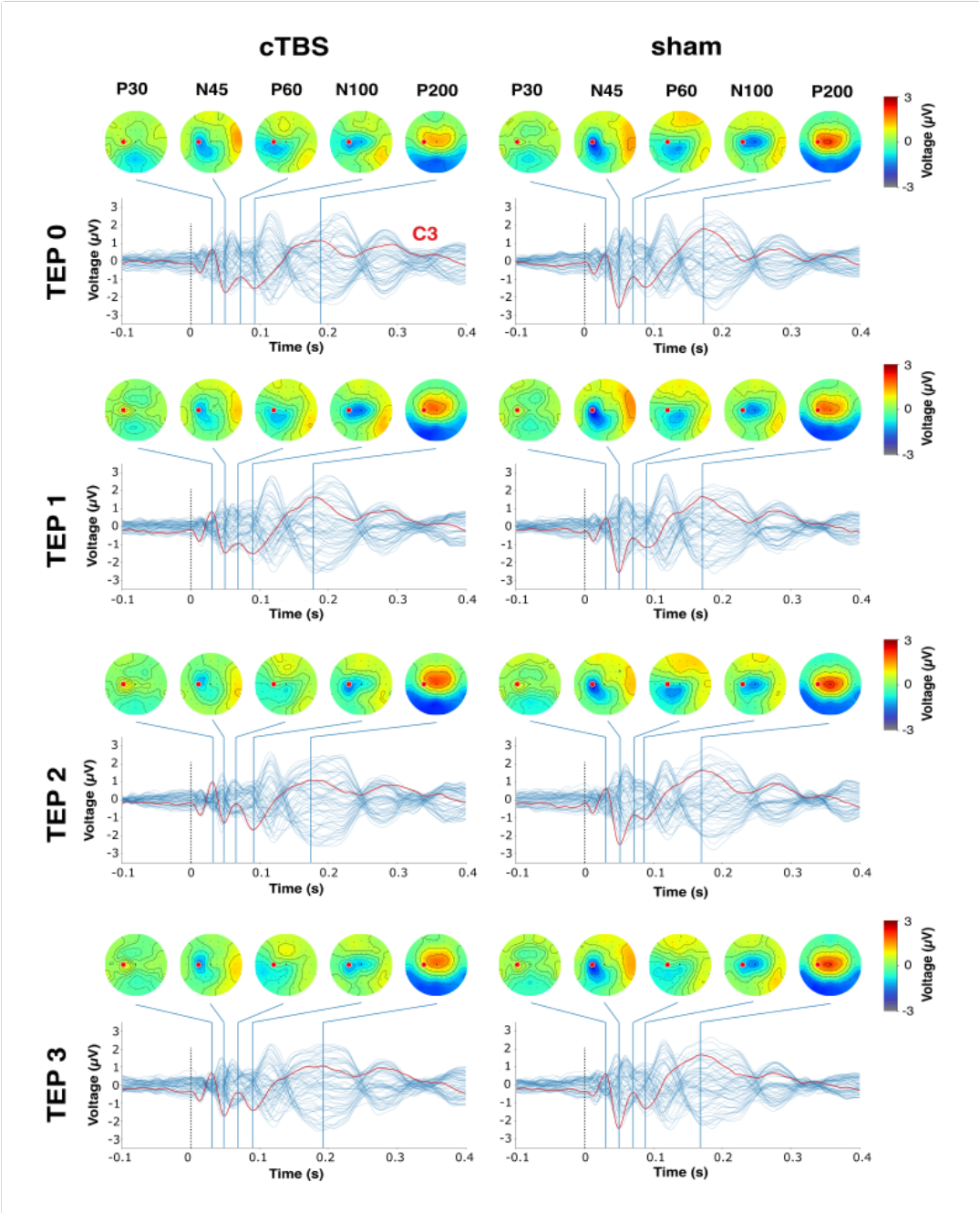


**Figure 5: Grand average of the TMS-evoked potential.** Butterfly plots and topographical scalp maps of the TEP recorded from 61 EEG channels and averaged across 21 subjects. Dotted line at t = 0 indicates the application of the TMS pulse. The channel above the stimulation site (C3) is shown in red. Topographical maps show the electrical potential across the scalp at characteristic time points that correspond to the peak components of the TEP at channel C3.

The comparison of TEP responses in the temporal domain between cTBS and sham within the inhibitory and facilitatory subgroups (Figure 7) revealed very comparable cortical responses compared to the whole group (Figure 6). Again, the TEP was most pronounced around the stimulation site becoming weaker with increasing distance from the stimulation site. Early TEP components showed a similar reduction in the contralateral hemisphere within both subgroups and conditions as observed in the whole group. This was also the case for the response around 200ms over the vertex, showing large interindividual variability within both of the subgroups.

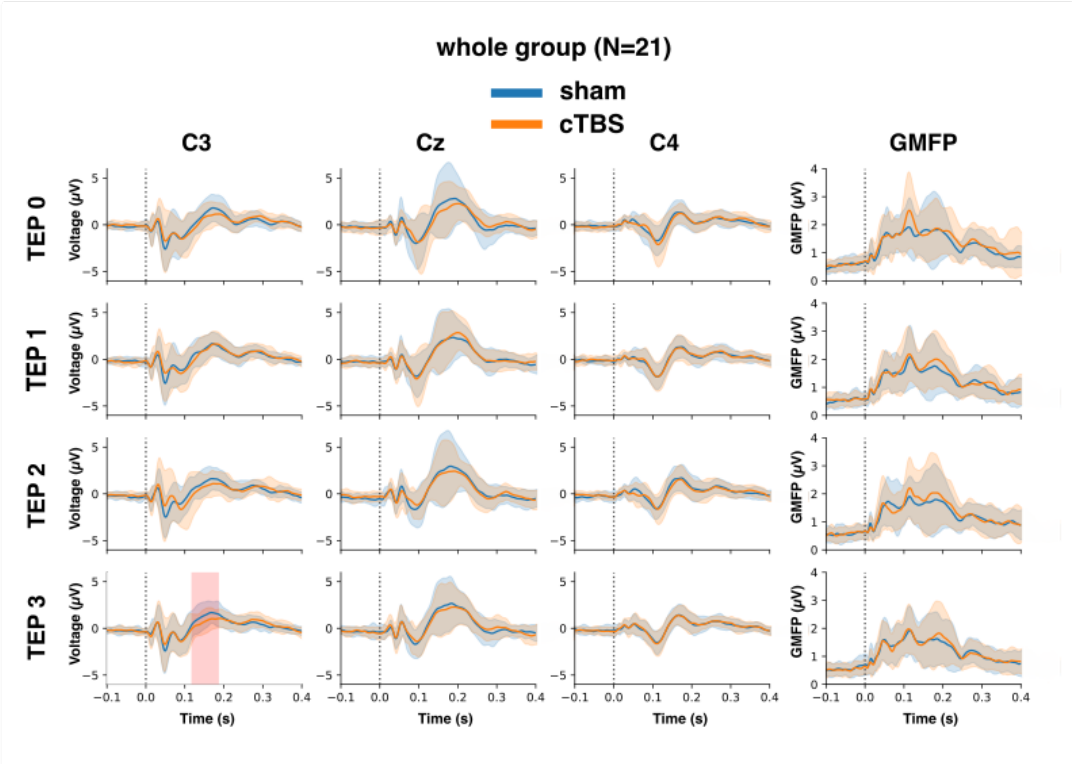


**Figure 6: Comparison of the TEP within the whole group (N=21)** Dotted line at t = 0 indicates the application of the TMS pulse. Shaded areas around the potentials indicate the SD. Red shaded rectangles indicate clusters that were significantly different between both interventions ($p > 0.01$).

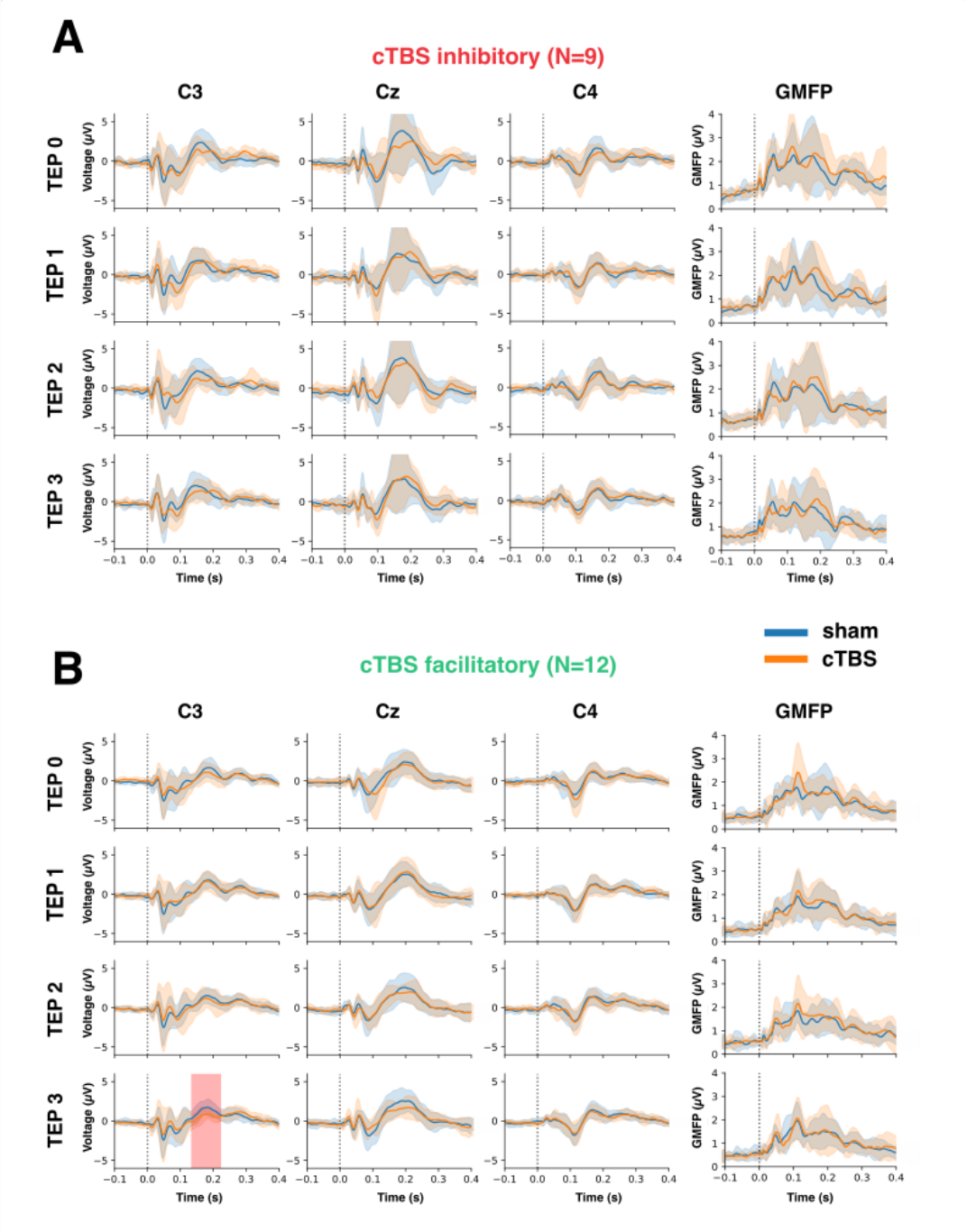


**Figure 7: Comparison of the TEP within the two responder subgroups.** The dotted line at t = 0 indicates the application of the TMS pulse. **(A)** TEP responses and GMFP within the cTBS inhibitory subgroup and **(B)** within the cTBS facilitatory subgroup. Shaded areas around the potentials indicate the SD. Red shaded rectangles indicate clusters that were significantly different between both interventions ($p > 0.01$).

There were no significant differences between cTBS and sham within the inhibitory subgroup (all clusters with $p > 0.01$). Within the facilitatory subgroup, there was a significant cluster of differences after the third dose of cTBS (TEP 3) around C3 ($p = 0.0016$). This cluster was characterized by a reduction of cortical response following cTBS, similar to the difference observed at the group-level, but appearing slightly delayed and with a larger temporal extent. There were no significant differences between the GMFP in any of the four blocks between the two sessions for the whole group or within the two subgroups (all clusters with $p > 0.01$).

### 3.6 Effects of cTBS on TEP peaks

Scalp topographies revealed a general concordance between TEP peaks in cTBS and sham session across all four acquisition time points (Figure 8). The P30 component was characterized by a focal increase in amplitude around the stimulation site (C3) and a weak negativity around the frontal and occipital regions. The topography of the N45 component consisted of a spatially distributed negativity around the stimulation site with a spread towards centro-parietal regions and the vertex. The P60 component was characterized by only weak and sporadic potential differences across the scalp, including an increase in amplitude around the stimulation site as well as a decrease in amplitude at occipital regions. The N100 component showed a commonly observed bilateral negativity around the central somatosensory regions, with a dominance around the ipsilateral hemisphere, which became more pronounced at the later stages of the experiment following cTBS. The P200 component was characterized by a large positivity over fronto-central channels, as well as a large negativity around the occipital regions.

Regarding the baseline measurement (TEP 0), cluster based permutation tests did not detect any clusters of activity that were significantly different between the two interventions. At TEP 1, a significant reduction of amplitude was detected at the N45 component ($p = 0.032$) in the cTBS session. These differences were spatially localized around central and centro-parietal channels (C3, CP1, CP3, CPz, P1, P2, P3, Pz, PO3), with a dominance of channels around the left hemi-

sphere. Another significant cluster with a comparable spatial configuration and reduction of N45 component in the cTBS session was also present in TEP 2 ($p = 0.0344$), with a slightly weaker involvement of channels above the midline, but a stronger lateralization within the left hemisphere (C3, CP1, CP3, CP5, P1, P3, P5, Pz, PO3, POz). There was also a significant increase in the P30 component at TEP 3 following cTBS, primarily involving bilateral parietal and occipital channels (P1, P2, P3, P4, P5, Pz, PO3, PO4, POz, $p = 0.025$).

Statistical comparison of the N100 component at TEP 2 revealed two distinct significant clusters. The first cluster was characterized by an increase of the N100 amplitude following cTBS, comprising channels in the temporal and lateralized central regions with some involvement of frontal channels within the left hemisphere ($p = 0.022$, F5, F7, FC5, FT7, C3, C5, CP3, T7, TP7, TP9). The second cluster consisted of channels localized around the contralateral motor cortex and adjacent centro-parietal and parietal channels ($p = 0.0204$; C4, CP2, CP4, CP6, CPz, P2, P4, P6, Pz, PO4). In this cluster, the amplitude of the N100 component was decreased following cTBS. A visual comparison of the scalp maps also revealed that these clusters were driven by a more focal negativity of the N100 component during the cTBS and a reduced spread towards the contralateral hemisphere, which was still observed after the first dose. This reduction of the N100 component at the contralateral hemisphere was also still visible after the third dose of cTBS, even though cluster based permutation testing did not reveal any significant differences. After the third dose of cTBS at TEP 3, two significant clusters were detected at the N45 component. One cluster involved a spatially distributed set of bilateral centro-parietal and parietal channels ($p = 0.0106$; C1, CP1, CP2, CP3, CP4, CPz, P1, P2, P3, P4, P5, Pz, PO3), revealing a reduction in peak amplitude of the N45 component (i.e. becomes more positive during cTBS). The second cluster indicated an increase of the N45 amplitude following cTBS, involving fronto-lateral channels of the left hemisphere ($p = 0.031$; Fp1, FPz, AF3, AF7, F3, F5, F7, FT7).

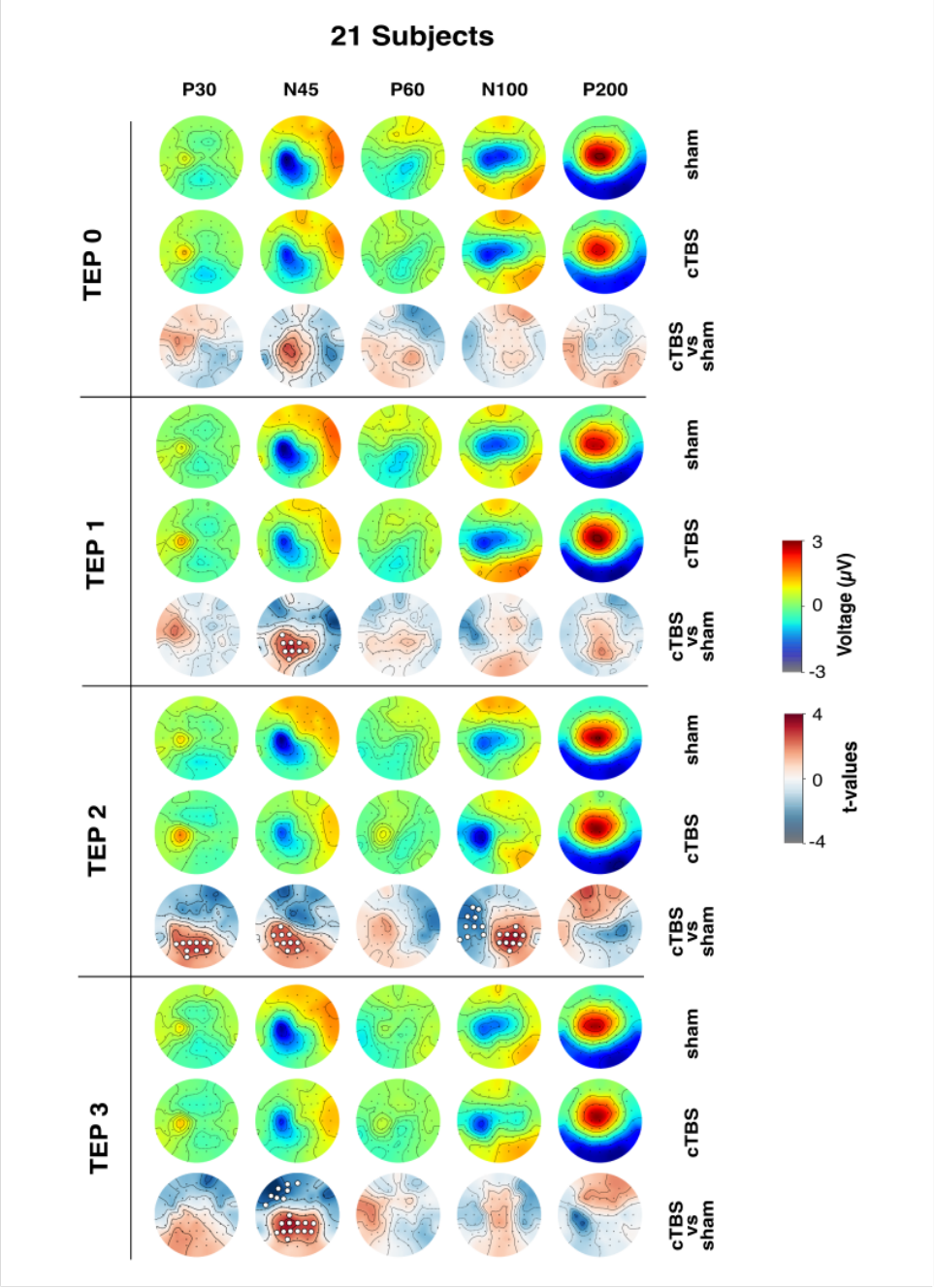


**Figure 8: Group-level differences of TEP peaks between cTBS and sham.** Topographical maps showing the five TEP peaks for cTBS and sham session averaged across 21 individuals. Third row within each cell depicts the t-values obtained from a spatial cluster based permutation test comparing the amplitudes of all 61 channels between cTBS and sham. White circles indicate channels belonging to clusters that were significantly different between the two interventions ($p < 0.05$).

The comparison of scalp topographies between cTBS and sham within the two responder subgroups revealed a considerable resemblance to the activity pattern observed in the whole group (Figure 9). The characteristic features of the different TEP peaks were also in part replicated within both of the subgroups. For example, the positive peak around the stimulation site associated with the P30 component appeared a comparable fashion with both subgroups. Likewise, the N45 component revealed a similar negativity around the stimulation site with a spread towards centro-parietal region of the ipsilateral hemisphere and the vertex. The N100 component also shared large similarities with the group-level observations, showing a bilateral coverage of the central motor regions with a reduced spread towards the contralateral hemisphere at the later stages of the experiment following cTBS. This reduction of spread towards the contralateral hemisphere was especially evident after the second and third dose of cTBS, but more pronounced within in the facilitatory compared to the inhibitory subgroup. The spatial activity pattern of the P200 component did also not reveal any major differences to the pattern observed at the group-level.

The statistical comparison of peak amplitudes within subgroups revealed three clusters of differences within the inhibitory subgroup and two clusters within the facilitatory subgroup (Figure 9). The three clusters within the inhibitory subgroup were characterized by a similar spatial configuration and time of appearance as the significant clusters observed at the group-level (N = 21), even though group-level changes in corticospinal excitability were dominated by the effects of the facilitatory subgroup. One cluster indicated a significant increase in N100 amplitude following the second dose of cTBS ($p = 0.0478$), extending from fronto-central to parietal regions in the contralateral hemisphere (FC6, C6, CP4, CP6, PO4, P2, P4, P6). The other two clusters significant clusters appeared after the third dose of cTBS at the N45 component. Specifically, N45 amplitude was significantly decreased in bilateral centro-parietal to parietal regions (CP1, CP2, CP3, CPz, PO4, P1, P2, P3, P4, P6, Pz; $p = 0.0142$) and increased in ipsilateral frontal regions following the third dose of cTBS (Fp1, AF3, AF7, F3, F5, F7, Fz; $p = 0.0492$).

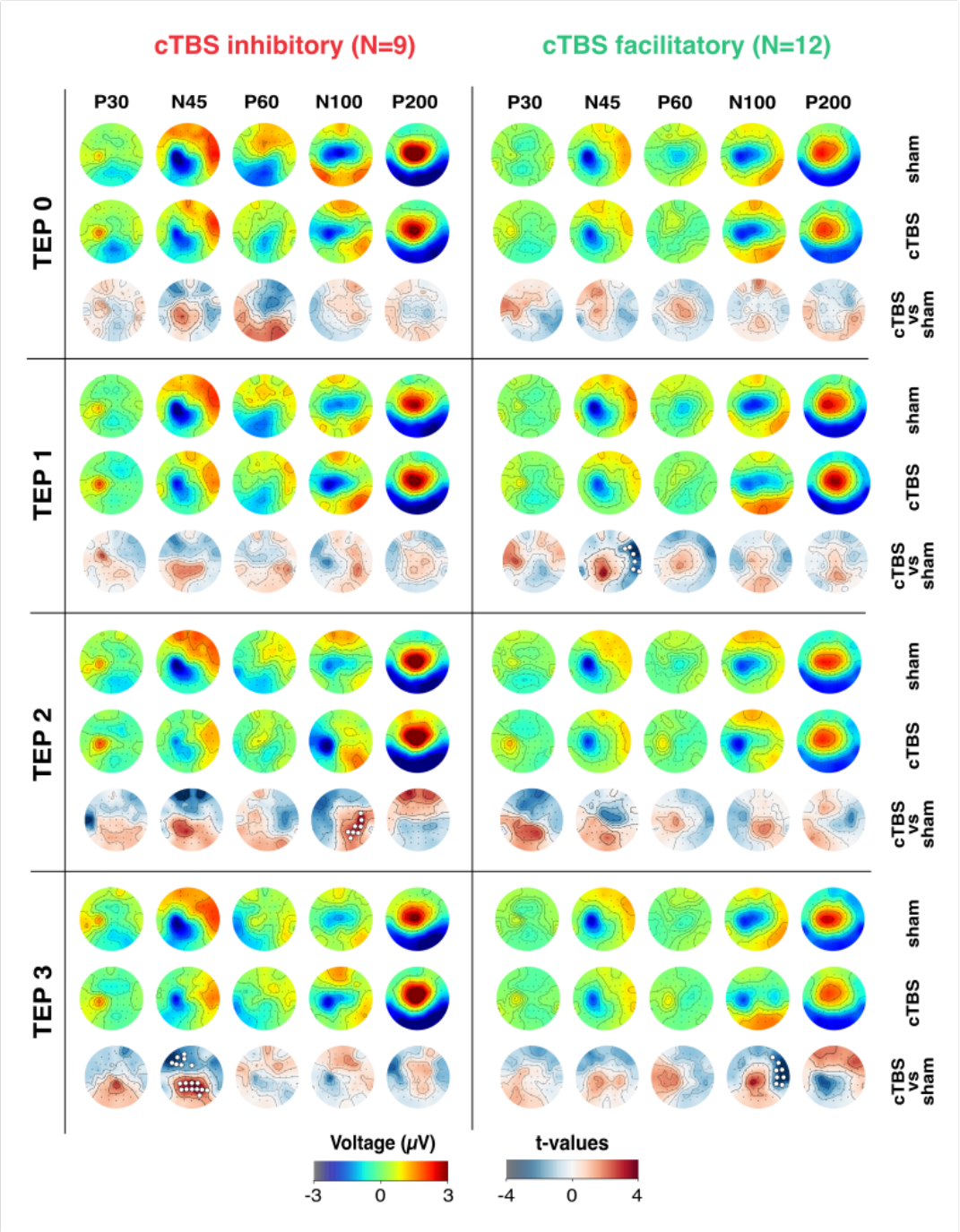


**Figure 9: Differences of TEP peak components between cTBS and sham in responder subgroups.** Topographical maps displaying the five TEP peaks for cTBS and sham session within the two responder subgroups. Third row within each cell depicts the t-values obtained from a spatial cluster based permutation test comparing the amplitudes of all 61 channels between cTBS and sham. White circles indicate channels belonging to clusters that were significantly different between the two interventions ($p < 0.05$).

In contrast, the statistical differences between interventions within the facilitatory group did not resemble any of the differences that were observed at the level of the whole group. Instead, there was a significant increase in the N45 component in the temporal region of the contralateral hemisphere after a single dose of cTBS (F6, F8, FT8, T8, TP8, TP10; p = 0.0478). The other significant cluster appeared in a similar spatial configuration and revealed a significant increase of the N100 component after three doses of cTBS (AF8, FC6, F8, C6, CP6, FT8, T8, TP8; p = 0.0318).

### 3.7 Dose effects of cTBS

Regarding MEPs, the group-level analysis of slopes from individual regression lines were not significantly different from zero within the sham condition for the whole group ($t_{20}$ = 0.60, p = 0.55485), the inhibitory subgroup ($t_8$ = 0.39, p = 0.70935) or the facilitatory subgroup ($t_{11}$ = 0.44, p = 0.6686). In contrast, the slopes were significantly different from zero for the inhibitory subgroup ($t_8$ = -6.62, p = 0.00017) and the facilitatory subgroup ($t_{11}$ = 2.79, p = 0.01743) but not the whole group ($t_{20}$ = -1.63, p = 0.11971) in the cTBS session. Thus, cTBS significantly increased corticospinal excitability over time within the facilitatory subgroup whereas it decreased corticospinal excitability within the inhibitory subgroup as more doses were applied. These relationships could not be replicated on the cortical level, using the N100 component of the TEP from the motor related channel as variable of interest (Table 1). The N100 component did not reveal any dose-related increases or decreases within any of the three channels within the whole group (all p > 0.05). This was also the case within the inhibitory and facilitatory subgroup. Interestingly, slopes on a group-level were frequently characterized by a distinct interindividual differences, as the SD was often considerably larger than the mean. This suggests that a dose-dependent effect might have been present within some individuals, even though cTBS did not lead to a dose dependent increase or cortical excitability in any of the investigated TEP-related variables on the group-level.

**Table 1:** Summary of linear relationships between cTBS dose and N100 amplitude

| | Session | Channel | Slope (mean ± SD) | t-value | p-value |
|---|---|---|---|---|---|
| **Whole group (N=21)** | **cTBS** | C3 | -2.61 ± 48.45 | -0.241 | 0.812 |
| | | Cz | -33.11 ± 116.96 | -1.266 | 0.220 |
| | | C4 | 26.80 ± 196.73 | 0.609 | 0.549 |
| | **sham** | C3 | -5.15 ± 20.80 | 1.108 | 0.281 |
| | | Cz | -3.45 ± 102.65 | -0.150 | 0.882 |
| | | C4 | -2.85 ± 50.08 | -0.255 | 0.802 |
| **Inhibitory (N=9)** | **cTBS** | C3 | 7.97± 53.19 | 0.424 | 0.683 |
| | | Cz | -64.7 ± 104.19 | -1.756 | 0.117 |
| | | C4 | -1.28 ± 84.1 | -0.043 | 0.967 |
| | **sham** | C3 | -11.0 ± 18.05 | -1.725 | 0.123 |
| | | Cz | 24.28 ± 143.04 | 0.480 | 0.644 |
| | | C4 | -4.99 ± 27.32 | -0.516 | 0.62 |
| **Faciltatory (N=12)** | **cTBS** | C3 | -10.55 ± 42.92 | -0.816 | 0.432 |
| | | Cz | -9.41 ± 120.36 | -0.259 | 0.8 |
| | | C4 | 47.85 ± 247.77 | 0.640 | 0.535 |
| | **sham** | C3 | -0.76 ± 21.63 | -0.117 | 0.909 |
| | | Cz | -24.25 ± 45.68 | -1.761 | 0.106 |
| | | C4 | -1.25 ± 61.80 | -0.067 | 0.948 |

### 3.8 Direct comparison of TEPs between responder subgroups

The direct comparison of TEPs in the temporal domain revealed no significant differences between the two responder subgroups at baseline (TEP 0, Figure 10A). A qualitative comparison suggested that the amplitude of the TEP around 200 ms post stimulus was considerably larger and more variable in the inhibitory subgroup compared to the facilitatory subgroup. This ob-

servation was also evident when comparing the topographical representations at the P200 component (Figure 10B), even though this difference did not reach statistical significance. Higher variability was also observed in the GMFP of the inhibitory subgroup, even though this effect was not statistically significant from the facilitatory subgroup.

The TEP peaks revealed only minor differences regarding the scalp topographies between subgroups (Figure 10B, row 1 and 2). Both subgroups showed the characteristic bilateral negativity of the N100 component, as well as the predominantly ipsilateral negativity of the N45 component. Statistical comparison of these topographical maps only resulted in a single significant cluster of differences at the P60 component. This difference was characterized by a reduced P60 amplitude in the inhibitory subgroup, spatially organized at parietal, parieto-occipital and occipital channels with a tendency towards the contralateral hemisphere (P2, P4, P6, Pz, PO3, PO4, POz, O1, O2, Oz, $p = 0.0044$). For all other peak components, none of the clusters reached the cluster threshold for statistical significance ($p < 0.05$).

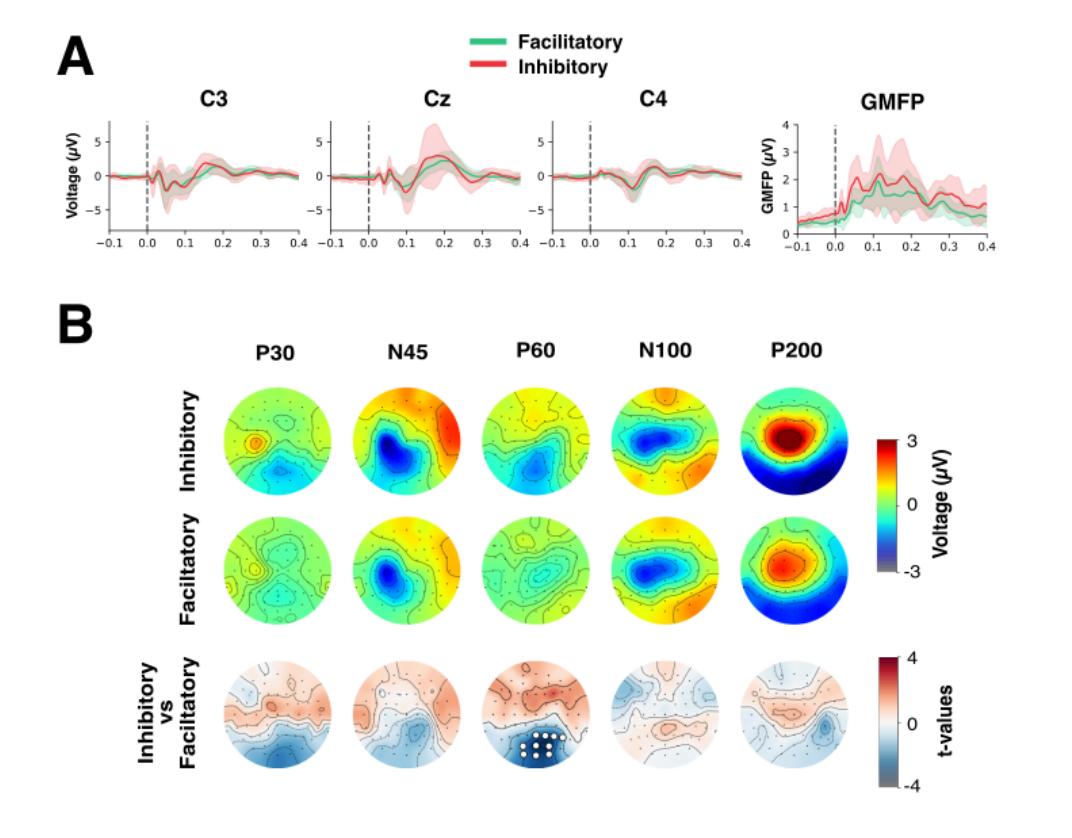


**Figure 10: Comparison of TEP between the two responder subgroups.** **(A)** Direct comparison of the TEPs between the two responder subgroups in the temporal domain, as average of the pre-interventional TEPs of both sessions (TEP 0). Shaded areas around the voltages indicate the SD. **(B)** Topographical scalp maps of the five TEP peaks for both subgroups, as well as the statistical comparison using a cluster based permutation test. White circles indicate channels belonging to clusters that were significantly different between the two groups ($p < 0.05$).

### 3.9 Relationship between MEP and TEP

Regarding the motor related channels (C3, Cz and C4), none of the correlations between MEPs and TEPs were statistically significant within the whole group after correcting for multiple comparisons (adjusted $\alpha$ = 0.00833). However, prior to correction, there was a statistically significant relationship between Δ TEP 1 and Δ MEP 2 in channel C3 (r = 0.518, p = 0.0161) and channel C4 (r = -0.479, p = 0.0279) after the first dose of cTBS. A similar negative correlation between Δ TEP 1 and Δ MEP 2 around channel C4 was also present within the facilitatory

subgroup (r = -0.685, p = 0.0139). Another correlation appeared after the second dose of cTBS between Δ TEP 2 and Δ MEP 3 in channel C3 (r = -0.650, p = 0.02203). In contrast, none of the correlations within the motor related EEG channels reached the threshold for statistical significance prior to Bonferroni correction within the inhibitory subgroup. Regarding the remaining 58 EEG channels, none of the correlations remained significant after the Bonferroni correction (adjusted $\alpha$ = 0.00086 (0.05/58)).

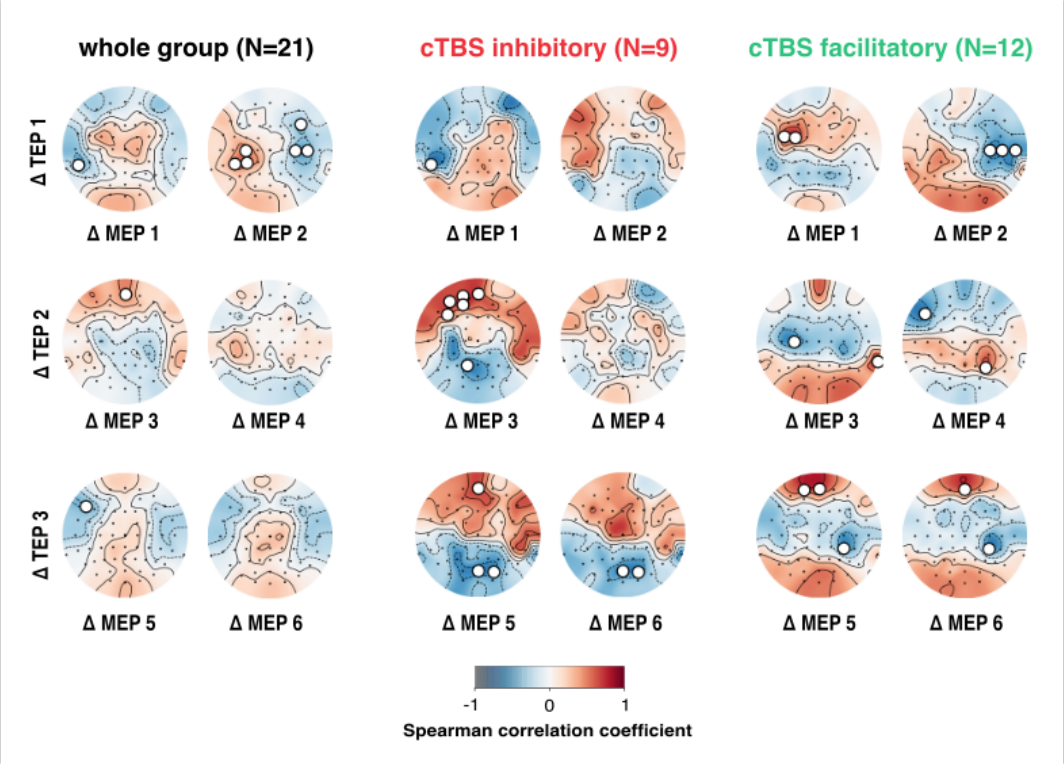


**Figure 11: Correlation between MEPs and TEPs.** Scalp maps depicting the Spearman's rank correlation coefficient between the N100 component of the TEP (indicated as Δ TEP) and the Δ MEP amplitude for the whole group and the two responder subgroups within the cTBS session. White circles indicate channels showing a statistically significant correlation between the Δ N100 and Δ MEP amplitude prior to Bonferroni correction ($p < 0.05$).

# 4 Discussion

## 4.1 Summary of results

In this single-blinded sham-controlled study, three doses of cTBS were applied over the left primary motor cortex of young and healthy individuals to investigate the neuromodulatory effects of cTBS on cortical (TEP) and corticospinal (MEP) excitability. Replicating previous findings, cTBS-induced neuroplastic effects were characterized by high degree of interindividual variability when measuring MEPs, resulting in the absence of significant after-effects on the group-level. Despite this lack of group-level effects, cTBS significantly modulated indices of excitability at the cortical level immediately after application of the first dose, showing the most differentiated cortical response at times when modulations of corticospinal excitability were most pronounced (after second dose). Furthermore, changes appeared not only around the ipsilateral M1 but also involved changes in the parietal regions and contralateral hemisphere. One novelty of the current study was the description and comparison of cortical responses within the responder subgroups, which were defined based on their overall change in corticospinal excitability following cTBS. This analysis provided additional insights into how cTBS-induced plasticity is represented in terms of the TEP, suggesting that inhibitory and facilitatory response characteristics are associated with different modulations of the TEP. Interestingly, there was a divergence between measures of excitability within the whole group and within subgroups, as cortical responses within the whole group seemed to be dominated by pattern occurring within the cTBS inhibitory subgroup, whereas whole group measures of corticospinal excitability were clearly driven by the responses of the cTBS facilitatory group. These findings will be discussed in more detail in the following sections of the discussion.

## 4.2 Effects of cTBS on RMT

Several studies have applied rTMS protocols and investigated the changes in the RMT afterwards, yielding mixed results. For example, low-frequency rTMS (LF-rTMS) has been shown

to effectively reduce corticospinal excitability when applied over the primary motor cortex (Chen et al., 1997; Maeda et al., 2000) in similar fashion as cTBS. In a review of Fitzgerald et al. (2006), the authors identified that out of 10 studies, only three observed an increase in RMT, whereas seven studies did not observe any changes following LF- rTMS. Regarding TBS, Klírová et al. (2020) observed a reduction in RMT after prolonged cTBS and prolonged iTBS (two doses applied consecutively without break). In the current study, RMT was not affected differently by the interventions over time (indicated by a non-significant interaction). Nevertheless, there was a significant difference in RMT between the two sessions of approximately 0.9% MSO at the end of the experimental protocol. However, the size of this difference is very likely negligible, since the calculation of individual stimulation intensities already involved some rounding inaccuracies, as the stimulator output could only be adjusted to integers but not decimals. As consequence, a difference of up to 0.5% MSO is implicitly included simply through technical restrictions and does not necessarily imply meaningful physiological differences in the threshold for cortical excitation.

### 4.3 Effects of cTBS on motor task performance

The performance in the PPT and the FTT was evaluated to investigate if cTBS-induced changes in corticospinal excitability were accompanied by meaningful behavioral changes that are of particular interest for TBS applications in the clinical environment. However, neither the PPT nor the FTT revealed any significant differences in performance between the cTBS and the sham session (Figure 2). Instead, there was a reappearing pattern, i.e. a main effect of the factor Time, showing that the execution of the experimental protocol itself was linked to a decrease in performance, irrespectively of whether participants received the cTBS or sham stimulation. This was in part unexpected, as a repetition of the tasks may have initiated motor learning processes, effectively leading to an increased performance (Karni et al., 1998).

This reduction in performance over time appeared in all three behavioral measurements when participants where using their right hand and could potentially be explained in two ways. First,

several hundred TMS pulses were applied over M1, ignoring the pulses delivered through cTBS. Even though single pulses with sufficient ISI are not supposed to interact with cortical excitability, they might still have affected cortical excitability to some degree. On the other hand, such changes were at least not evident when investigating corticospinal excitability directly. Second, there might have been differences in physical activity between the two hands during the experiment. While movements of the right hand were monitored by the observer (e.g. through spurious activity in the EMG signal), this was not the case for the left hand. Thus, subjects might have moved their left hand more frequently during the experiment (against the experimenter's instructions), thereby leading to less difficulties in reperforming the task with the left hand after the long period in which movements had to be actively suppressed.

There are again mixed results in the literature regarding changes in motor task performance and their relationship to changes in corticospinal excitability following application of rTMS. For example, Iezzi et al. (2008), observed reductions in MEP amplitude following cTBS, accompanied by reductions in peak velocity and peak acceleration during tests of motor retention. Furthermore, Bashir et al. (2011) applied LF-rTMS over the right motor cortex and observed an improvement in tapping frequency as well as reaction time of the hand ipsilateral to the rTMS-receiving hemisphere. Interestingly, these improvements in performance were associated with increases in corticospinal excitability over the left hemisphere, providing additional evidence for a relationship between corticospinal excitability and motor task performance. For example, Jelić et al. (2015) reported a significant slowing in PPT learning following cTBS in the hand contralateral to the stimulation site, showing that a reduction of cortical excitability following TBS protocols is associated with a reduction in PPT performance.

Overall, the current findings suggest that fatigue effects had a stronger impact on performance than potential learning effects. The absence of cTBS-related effects on task performance could also be explained by the timing at which the motor tasks were conducted. While group-level changes in corticospinal excitability were most pronounced around 20 minutes after the sec-

ond dose of cTBS, changes were comparably small at the last measurement of MEPs (MEP 6). Thus, performance of the motor tasks was reassessed at a point in time in which corticospinal excitability was already strongly declining. However, this can be contrasted by findings from Jäncke et al. (2004), who observed an effect on tapping frequency following LF-rTMS applied to M1 without any significant changes in MEP amplitude. Interestingly, the effect was only visible if individuals performed finger tapping at their maximum possible speed, as it was performed in the current study.

## 4.4 Effects of cTBS on MEPs

The current study replicates the high interindividual variability in corticospinal excitability following TBS that has been described by other researchers (Hamada et al., 2013; López-Alonso et al., 2014). As consequence, the comparison of corticospinal excitability between cTBS and sham did not reveal any significant differences when investigating the after-effects on a group-level, although cTBS showed an overall strong tendency to increase MEP amplitudes (Figure 3B). While this directional effect was opposite to the expected modulation of corticospinal excitability described by Huang et al. (2005) following cTBS, such deviations from the canonical response are possible, and rather indicating that the study sample consists more individuals showing cTBS facilitatory response rather than an inhibitory response. Indeed, the analysis of responder subgroups revealed a distribution of individuals that was highly comparable to the distributions of previous studies investigating the response characteristics following TBS-induced cortical plasticity (Hamada et al., 2013; Heidegger et al., 2017; Jannati et al., 2017). In the current study, 57% (12/21) of individuals showed a facilitatory response following cTBS whereas the remaining 43% (9/21) exhibited an inhibitory response. According to Hamada et al. (2013), who investigated a sample of 56 healthy volunteers, around 58% of all individuals responded with a facilitation in MEP amplitude to cTBS, whereas 42% responded with inhibition. Even though the number of participants was significantly smaller in this study, the actual

relationship between individuals responding with facilitation (12/21, 57%) and inhibition (9/21, 43%) was surprisingly similarly. A study from Jannati et al. (2017) administered a single dose of cTBS and found 12 individuals with a facilitatory response and 9 with an inhibitory response, i.e. an equal distribution of response characteristics as in this study. Heidegger et al. (2017) reported 7 facilitatory responders, 6 inhibitory responders after a single dose of cTBS, however they used a different approach to categorize responders, involving a gaussian mixture model. Furthermore, Rocchi et al. (2018) did not find a significant group-level effect of cTBS on corticospinal excitability when MEPs were acquired with an intensity that usually evokes MEPs of around 1mV, but observed an increase if MEPs were acquired with weaker stimulation intensities. It should be noted that there is also a considerable number of studies that observed very different ratios of response characteristics, which might be explained in part by how responder subgroups were defined (see Pellegrini et al. (2018)), but also very likely reflect true differences in response characteristics within the investigated population. Thus, the predominantly facilitatory after-effects observed in the current study therefore likely reflect some genuine responder characteristics that were present with a certain proportion in the study sample, leading to the observed ratio of facilitatory and inhibitory responses.

This is also particularly evident when comparing the effects of cTBS within the responder subgroups. A large portion of the group-level after-effects were driven by the larger induced plasticity within the facilitatory subgroup, observed especially after the second dose of cTBS (section 3.4). This peak of excitability changes after the second dose was followed by a reduction of corticospinal excitability after the third dose, which was also visible in the facilitatory responder subgroup. A qualitative comparison of the dose dependent effects between the two subgroups suggested that cTBS leads to an immediate reduction of corticospinal excitability within the inhibitory subgroup, which then recovers slowly towards the pre-interventional level within the next 20 minutes (Figure 4B), except after the third dose. In contrast, corticospinal excitability nearly increased monotonically within the facilitatory subgroups up to the third dose,

after which a reversal of the effect was observed (Figure 4C). At the last assessment (MEP 6), corticospinal excitability was also significantly different between cTBS and sham within the cTBS facilitatory group, even though the overall difference between the interventions was smaller. This suggests a reduction of variability in corticospinal excitability after the third dose of cTBS at group-level.

A sudden reversal of response direction or an abolishment of response characteristics after repeated applications of TBS has also been observed in other studies, revealing a complex relationship of repeated TBS applications to individual response characteristics (Gamboa et al., 2011; Murakami et al., 2012). Importantly, such reversal can occur if motor cortical excitability is altered intrinsically through voluntary motor activation Gentner et al. (2008), but also through extrinsically induced-changes in cortical excitability, e.g. through a priming stimulation. It has been suggested that these dose-dependent reversals in corticospinal excitability are likely mediated by processes of homeostatic metaplasticity in the cortical and corticospinal pathway (Gentner et al., 2008; Gamboa et al., 2011; Murakami et al., 2012). For example Gamboa et al. (2011) reported that two doses of cTBS, applied with a break of 2 or 5 minutes, resulted in a reversal of cTBS after-effects. However, this was not the case if the doses were applied with a break of 20 minutes, comparable to the break within this study. Nevertheless, the results of the current study may suggest that similar mechanisms of homeostatic plasticity were at play, as the cTBS-induced plasticity was reversed on the group-level as well as in the facilitatory subgroup, after the second dose of cTBS.

Regulatory homeostatic processes are extremely important in maintaining a balance between excitatory and inhibitory synaptic transmission in cortical circuits, effectively stabilizing the neuronal system (Turrigiano & Nelson, 2004; Yger & Gilson, 2015). In absence of such homeostatic plasticity, excitatory or inhibitory synaptic activity could be increased or decreased uncontrollably, potentially resulting in a loss of function of the neuronal networks involved (Tur-

rigiano & Nelson, 2004; Abraham, 2008; Cassidy et al., 2014). The absence of a reversal of induced plasticity in the inhibitory subgroup could be explained by the significantly lower induced plasticity in the inhibitory compared to the facilitatory subgroup (Figure 4 & section 3.4). Even after the third dose of cTBS, induced plasticity was smaller in the inhibitory subgroup (MEP 5 and 6) than the induced plasticity in the facilitatory subgroup (MEP 4 and 5) after the second dose of cTBS. Thus, assuming that the compensatory homeostatic mechanisms in the human motor system function similarly, irrespectively of the direction of effect, the induced plasticity in the inhibitory subgroup might have been too weak to initiate the compensatory mechanisms. Overall, the current results fit into the theoretical framework of homeostatic plasticity following repeated application of plasticity-inducing protocols. However, it is important to emphasize that the dose-dependent changes were not statistically different from sham after correction for multiple corrections. Thus, the interpretations can therefore not be considered as direct evidence, but rather serve as a possible explanation for the mechanism behind the observed changes in corticospinal excitability.

Interestingly, group-level changes in corticospinal excitability showed qualitatively dissimilar pattern when tested with 90% RMT and 110% RMT in the current study (Figure 3). For example, after the third dose of cTBS, group-level MEP amplitudes decreased (MEP 5) and then increased (MEP6) when tested with 90% RMT but showed a monotic decrease when probed with 110% RMT. While this might seem counterintuitive at first, it likely indicates intensity-related differences in the recruitment of neuronal populations by the TMS pulses. Epidural recordings have shown that the current direction, as well as the stimulation intensity have significant impact on the generation of corticospinal volleys, suggesting that different neuronal populations are depolarized depending on the interaction of these parameters (Burke et al., 1993; Werhahn et al., 1994; Nakamura et al., 1996; Di Lazzaro et al., 2004). In particular, near-threshold intensities are likely recruiting pyramidal tract neurons (PTN) transsynaptically through the activation of interneurons (indirect activation, I-waves), whereas higher stimula-

tion intensities additionally activate the pyramidal PTNs directly (D-waves) (Di Lazzaro et al., 2004). Importantly, the D-waves, resulting from direct stimulation of PTNs, were unaffected by cTBS whereas the early I-waves were suppressed, indicating that cTBS specifically acts on the excitatory circuits that activate the PTN transsynaptically (Di Lazzaro et al. 2005). These differences in neural recruitment provide a plausible mechanism behind the observed differences in response pattern of cTBS-induced after-effects following the probing at subthreshold and suprathreshold stimulation intensities. Additional support is provided by studies showing that the strongest cTBS-induced MEP suppressions can be observed when MEPs are probed with high stimulation intensities (150% RMT and higher) (Vallence et al., 2015; Goldsworthy et al., 2016). Especially when pulses with lower intensity where used to probe corticospinal excitability, cTBS after-effects were small or even absent. Due to these factors, the analysis and interpretation of MEPs was primarily based on the cTBS after-effects observed at MEPs acquired with 110% RMT.

Last, the present results also highlight the importance for appropriate sham conditions when investigating the effects of NIBS-induced changes in corticospinal or cortical excitability. The subgroup analysis contains several examples where MEP amplitudes were significantly different from the baseline of the session (Figure 3, MEP 1) but not significantly different from the sham session. In the absence of a sham condition, these differences would be interpreted as true modulation of cortical excitability, even though the effects represent a mixture of true modulation as well as natural variability of corticospinal excitability over time.

## 4.5 Effects of cTBS on TEPs

The results of the current study provide evidence for local and remote changes in cortical excitability following cTBS over M1. A direct comparison to sham revealed a differentiated pattern of changes in amplitude of the TEP peaks, with a prominent reduction of the N45 component primarily localized around the centro-parietal region of the ipsilateral hemisphere. This

reduction was present after each of the cTBS doses, even though the spatial arrangement was shifted towards a more bilateral centro-parietal pattern after the third dose. The amplitude of the N100 was only modulated after the second dose, characterized by significant increases in the ipsilateral motor and temporal regions and significant reductions around the centro-parietal region of the contralateral hemisphere, distant from the stimulation site. Importantly, all of these modulation of the TEP were statistically significant on a group-level, even though the changes in corticospinal excitability were not. Furthermore, the most differentiated modulations of the TEP, involving the P30, N45 and N100 component, were observed after the second dose of cTBS, which also corresponded to the time at which the most pronounced cTBS effects on corticospinal excitability were observed. Modulations of the P200 component were absent throughout all analyses. A direct comparison of TEPs in the temporal domain only revealed minor differences between cTBS and sham, whereas differences in the GMFP were absent. Furthermore, there was no evidence for a relationship between cTBS dose and the amplitude of the N100 component.

In the current study, decreases in N45 amplitude were spatially localized around the centro-parietal regions of the ipsilateral hemisphere adjacent to the stimulation site, but extended later also towards the contralateral hemisphere (Figure 8). This was especially evident after the third dose of cTBS, where the reductions showed a nearly equal involvement of the contralateral parietal regions. A similar observation has been made by Van Der Werf and Paus (2006), who reported a significant reduction of the N45 component around the vertex (Cz) following LF-rTMS over M1, even though group-level reductions in MEP amplitude were absent. Although they used a different stimulation protocol to modulate M1 excitability, the general direction of excitability modulation was replicable on the cortical level. In contrast, Vernet et al. (2013) investigated the influence of cTBS on MEP amplitude and TEP peaks after a single dose of cTBS. They observed an increase in N45 amplitude approximately 10 minutes after the application of cTBS, but a decrease at all other measurement times (5, 20, 30 and 40 min). Here,

TEPs were always acquired within a time window of approximately 7-22 min after cTBS in the current study and are therefore not necessarily incompatible with the observation from Vernet et al. (2013). Furthermore, the authors did not perform a statistical evaluation for this amplitude change over time, making it difficult to estimate the actual significance of their finding.

The predominance of excitability changes around the parietal region, posterior to the stimulation site, possibly indicates remote effects of cTBS around the posterior parietal cortex (PPC) mediated through cortico-cortical connections. Indeed, the PPC is closely interconnected to the primary motor and sensory regions of the cortex, acting as an important hub for sensorimotor integrations used in the planning and the realization of movements (Culham & Valyear, 2006; Lindner et al., 2010). The importance of this structural and functional relationship between PPC and motor regions has been exposed in numerous studies investigating monkeys (Bremmer et al., 2001; Mulliken et al., 2008; Gharbawie et al., 2011) and humans (Koch et al., 2010; Vesia & Crawford, 2012; Goldenkoff et al., 2021). In line with this, Koch et al. (2007) demonstrated that a conditioning pulse over the right PPC facilitated MEPs recorded from M1 of the contralateral hemisphere, providing plausible neurophysiological mechanisms behind remote changes in PPC excitability following cTBS over M1. Other remote excitability changes were also observed at the N100 within the inhibitory subgroup and the facilitatory subgroup (Figure 9, TEP 2 & 3), even though it is unclear through which cortical pathways these were mediated.

In line with previous studies, the N100 component appeared predominantly as spatially confined negativity, peaking over the central motor regions (Paus et al., 2001; Bonato et al., 2006; Premoli, Castellanos, et al., 2014) (Figure 8). After the second dose of cTBS, the N100 component was significantly increased around the stimulation site with additional involvement of fronto-lateral and temporal regions. In contrast, a significant reduction of the N100 component was observed in the contralateral hemisphere, with primary involvement of centro-parietal and parietal regions. In a study of Casula et al. (2014), a single dose of LF-rTMS was associated

with group-level reductions in MEP amplitude as well as increases of the P60 and the N100 amplitude. However, the authors did not find significant differences in amplitude between the two motor regions of the two hemispheres (around C3 and C4). While this was not explicitly tested, the two significant clusters with opposite polarity strongly suggest that such differences exist here after the second dose. Vernet et al. (2013) applied cTBS over M1 and observed an overall reduction in MEP amplitudes as well as an overall reduction in N100 amplitude. Although the direction of effects were opposite in the aforementioned study, the results are in consistence with the current study, where corticospinal excitability was increased on a group-level and the N100 component was also increased around the ipsilateral hemisphere.

The P30 component was characterized by a focal positivity around the ipsilateral hemisphere and centered around the stimulation site. There is some inconsistency regarding the localization of the component in previous studies. For example, Paus et al. (2001) described the appearance of the P30 more centrally, peaking over the vertex. Bonato et al. (2006) observed the component centrally and in the frontal region of the unstimulated hemisphere. However, several other studies observed a more lateralized occurrence of the P30 component (Mäki & Ilmoniemi, 2010; Opie et al., 2017). It has been demonstrated in five individuals that the peak to peak amplitude of the N15-P30 complex is correlated to the size of the MEP at the single trial level (Mäki & Ilmoniemi, 2010), suggesting an involvement of the components in the generation of corticospinal output. Vernet et al. (2013) investigated the relationship between TEP peaks and the MEP amplitude following cTBS and suggested that a reduction of the P30 component might be associated with a reduction in MEP amplitude. Gedankien et al. (2017) applied iTBS over M1 and found that the N15-P30 complex of the TEP was correlated to the MEP amplitudes. In the present study, P30 amplitude was significantly increased after the second dose of cTBS. These changes were primarily occurring around the bilateral parietal to occipital regions, with a slight predominance over the ipsilateral hemisphere, rather than the stimulation site. These changes show large spatial overlap with the changes observed around the N45 component, even

though the N45 component was characterized by a reduction in amplitude and not an increase. It could be speculated that this overlap is in part related to the adjacent temporal windows that were used for peak extraction.

Pharmacological studies have provided some insights into the mechanisms of neurotransmission related to the cortical propagation of TMS pulses (Premoli, Castellanos, et al., 2014; Premoli, Rivolta, et al., 2014; Premoli et al., 2017; Belardinelli et al., 2021). The N45 component is thought to reflect early $GABA_A$-mediated inhibitory neurotransmission within the human motor cortex (Premoli, Castellanos, et al., 2014; Darmani et al., 2016). Furthermore, it has been shown that several $GABA_A$-receptor agonists lead to a reduction of MEP amplitude, also pointing towards an increase in cortical inhibition (Paulus et al., 2008). In contrast, the N100 component is thought to reflect late $GABA_B$-mediated inhibitory neurotransmission within the human motor cortex (Premoli, Castellanos, et al., 2014).

Therefore, the observed reduction in amplitude of the N45 component suggests a reduction of inhibitory neurotransmission within the ipsilateral hemisphere. Indeed, this interpretation would be in accordance with the observed group-level facilitation in corticospinal excitability (Figure 3B). However, it is not necessarily supported by the observed modulation of TEPs within the responder subgroups. In particular, subgroup analysis suggested that reductions in N45 amplitude were primarily driven by the cTBS inhibitory subgroup, as statistical differences after the third dose appeared with nearly the same spatial configuration within the inhibitory subgroup and the whole group, but not the facilitatory subgroup (Figure 8 and Figure 9, TEP 3). This divergence could potentially suggest that the observed changes in excitability around the parietal region are caused by a remote after-effect, but are not necessarily themselves influencing the corticospinal output when probed with single pulses. Alternatively, the lack of effects of cTBS on the TEPs within responder subgroups could also result from a considerable amount interindividual variability in TEP responses. As consequence, more individuals might

be required to properly identify the significant changes on a group-level. In future, changes could be potentially investigated within individuals and not on a group-level, but this would likely require an even larger number of TEPs to be measured to obtain proper estimates of cortical excitability.

A similar divergence between cortical and corticospinal measures was also observed within the N100 component, where increases in inhibition on the cortical level (Figure 8, TEP 2) where contrasted by a pronounced facilitation of corticospinal excitability around the same time (Figure 3, MEP 3 and MEP 4). However, these increases in inhibitory neurotransmission were accompanied by a reduction of inhibitory neurotransmission around the motor and centro-parietal regions of the contralateral hemisphere. Such a modified balance in excitability between the two hemispheres might have an important impact on the generation of corticospinal outputs. It is known that the balance of inhibitory and excitatory function is crucial for the maintenance of physiological interhemispheric interactions, especially within the motor system (Grefkes & Fink, 2011; Takeuchi et al., 2012). Thus, the largely reduced inhibition of the contralateral hemisphere might indicate reduced maintenance of interhemispheric inhibition, thereby resulting in a net positive effect on corticospinal excitability within the ipsilateral hemisphere. As consequence, corticospinal output could to be facilitated whereas the N100 component suggested an increase in ipsilateral cortical inhibition. Again, this notion is somewhat contradicted by the analysis of responder subgroups, as the N100 component showed a similar significant reduction around the contralateral hemisphere within the inhibitory subgroup (Figure 8 and Figure 9, TEP 2). Interestingly, this reduction was also present in the faciliatory subgroup, but not statistically significant. Within the inhibitory subgroup, a net increase in inhibition around the contralateral hemisphere should have also resulted in an increased corticospinal output of the ipsilateral hemisphere, which was not the case.

It seems possible that TEP components (e.g. N45, N100) not necessarily reflect only inhibition or excitation, but are potentially indicating an interaction or balance between these two complementary mechanisms of cortical regulation (Du et al., 2018; Belardinelli et al., 2021). In addition, some of these inconsistency in neuroplastic effects on TEP peaks might be again attributable to differences in recruitment of neuronal populations in relation to different stimulation intensities used in the experiment. While cTBS might have primarily modulated interneurons that generate inputs to the PTNs, the higher stimulation intensities used during measurement of MEPs might have activated the PTNs directly, thereby superimposing the reduction of cortical excitability that is indicated by the increase of N100 component. Overall, the current results suggest that neither the N45 nor the N100 component are indexing the same properties of cortical excitability as the MEPs but instead represent different indices of excitability that may be in part independent. Thus, a reduction in N45 component might be general property of cTBS-induced cortical plasticity, irrespective of the observed changes in corticospinal excitability.

The direct comparison of TEP peaks between the two subgroups only revealed a significantly lower P60 amplitude within the inhibitory subgroup around the parietal and occipital region. It has been suggested recently that P60 component is linked to glutamate-mediated neurotransmission (Belardinelli et al., 2021). Thus, the reduction in amplitude could suggest reduced levels of glutamatergic neurotransmission in the occipital cortex. The existence of such difference seems possible, given the evidence for interactions between motor and visual cortex, which has also been demonstrated using TMS (Strigaro et al., 2015). Admittedly, it remains unclear whether this is truly a meaningful difference regarding the individuals susceptibility to modulations of M1 excitability or the generation of corticospinal outputs.

Overall, the current findings demonstrate that the combination of TEPs are able to detect a wide range of changes in cortical excitability following cTBS. This emphasizes the importance of

combining the conventional assessment of corticospinal excitability through measurement of MEP amplitudes with functional neuroimaging approaches, such as TMS-EEG. Otherwise, it will be difficult to identify the potentially remote after-effects in cortical excitability that appeared distant from the stimulation site (e.g. P30, N45, N100). Indeed, remote changes could still detected without TMS-EEG if they appear in connected regions within the motor network, e.g. through paired-pulse paradigms (Fiori et al., 2017). For instance, it has been demonstrated that that M1 excitability can be modulated via the cerebellothalamocortical pathways by applying TBS to the cerebellum (Harrington & Hammond-Tooke, 2015). However, such an investigation of remote after effects always requires a clear hypothesis about which distant regions are affected. If TBS is applied to regions without efferent connections to the motor system, it becomes impossible to measure such changes in cortical excitability without the help of neuroimaging.

## 4.6 Relationship between MEPs and TEPs

Even though many studies have recorded MEPs and TEPs in a variety of experimental settings, the relationship between those measures is still not fully understood and represented by a rather heterogenous body of results. In the current study, correlations were assessed between the peak of the N100 component and the corresponding MEPs, acquired before or after the measurement of the TEP. There is some evidence that the early components of the TEP, in particular the N15-P30 complex, are correlated to the amplitude of the MEP when both electrophysiological responses are acquired simultaneously (Mäki & Ilmoniemi, 2010). This relationship was also replicable to some degree by Gedankien et al. (2017), even if the averaged MEPs and TEPs were correlated on a group-level, rather than on a single-trials basis. On the other hand, Bonato et al. (2006) did not observe comparable significant relationships when correlating the mean MEP amplitude with the N15 (referred to as N18 in the original manuscript) or the P30 peak of the TEP.

In the current study, the relationship between Δ MEP amplitude and the Δ N100 peak was not assessed under the assumption of a direct temporal relationship on a single-trial basis. Here, the results from the correlations do not provide very strong evidence for or against the existence of a relationship between the N100 amplitude and the MEP amplitude within the whole group or any of the subgroups. Even though a positive relationship appeared between the ipsilateral M1 (C3) and a negative relationship between the contralateral M1 (C4) and Δ MEP 2 after the first dose of cTBS, neither of these relationships remained significant after correction for multiple comparisons. Three channels around the contralateral M1 also revealed a similar negative relationship with MEP 2 within the facilitatory subgroup but again, relationships did not remain significant after Bonferroni correction. This tendency towards an absence of a relationship is supported by other studies which investigated the relationship between the MEP amplitude and the N100 component of the TEP (Paus et al., 2001; Bender et al., 2005; Roos et al., 2021).

There are many reasons why such relationship might be absent. First, MEPs were acquired within a short interval of approximately 3 minutes but the TEP itself was acquired over a period of around at least 12 minutes. This period is already long enough for considerable changes in corticospinal excitability. As consequence, it might be difficult to establish a meaningful correlation between both measures as they probe cortical excitability at different points in time. Potential relationships might be easier to detect if TEPs are split in half, correlating the first half of TEPs with the early assessment of the MEPs and the second half with MEPs acquired at the later stage. Another issue might arise from the different stimulation intensities that were used to probe cortical excitability (80% RMT) and corticospinal excitability (90% RMT and 110% RMT). The neuronal substrates that are activated by the TMS pulse have different activation thresholds, and lower stimulation intensities have been shown to activate the corticospinal tract neurons indirectly through synaptic input from excitatory and inhibitory interneurons (Di Lazzaro et al., 2004; Di Lazzaro & Ziemann, 2013). Furthermore, cTBS likely alters cortical

plasticity by reducing the the excitatory inputs to the pyramidal tract neurons (Di Lazzaro et al., 2005). Thus, cTBS-induced changes of MEPs and TEPs might simply represent the activity of different cortical circuits. In addition, it has to be considered that the TEP represents cortical activity after several and complex modifications in the preprocessing, involving crucial steps like a (semi-automatic) separation of artificial signal distortions from components representing genuine TMS-induced cortical activity. In contrast, MEPs are derived from a single signal, require few steps of preprocessing and have a standardized way of quantification. Hence, a discrepancy between the assessment of cortical excitability using MEPs and TEPs might be attributable to signal distortions that appear during preprocessing, potentially altering or potentially breaking the relationships in an unpredictable manner. Overall, the current results suggest that MEPs and TEPs index in part different properties of cortical excitability and as consequence, no strong correlations may be expected.

In summary, the current findings demonstrate that repeated applications of cTBS alter corticospinal excitability in a complex manner, possibly involving mechanisms of homeostatic metaplasticity. The cortical response, measured through the TEP, revealed a statistically significant and differentiated pattern of changes following cTBS, even though group-level changes in corticospinal excitability were not significantly different from sham. This highlights the increased sensitivity of TMS-EEG to probe cTBS-induced changes in cortical plasticity, including network effects that appear distant from the stimulation site. The significant modulation of N45 component suggests that cTBS affects $GABA_A$-mediated inhibition within the centro-parietal regions of the cortex. However, it was not possible to establish any convincing relationship between the TEP and MEP amplitude. The present findings support the interpretation that TEPs and MEPs probe activity of different neuronal substrates that are not necessarily affected similarly by neuromodulatory protocols. The absence of a relationship is not completely unexpected, as findings already suggested that MEP and TEP are related in a rather complex manner (Vernet et al., 2013).

## 4.7 Limitations

The current study contains several limitations that need to be addressed in order to properly evaluate the findings with regards to their significance. First, the study contained a relatively small sample size of 21 individuals, as 8 of the subjects had to be excluded due to insufficient data quality. This is especially relevant for the analysis of responder subgroups, where only 9 cTBS inhibitory and 12 cTBS facilitatory subjects were included as consequence. Given the large interindividual variability of TEPs, this sample size might have been too small to detect meaningful changes in cortical responses between the two subgroups.

Second, the actual experimental paradigm was comparably long and took up to three hours to complete, depending on how fast a sufficiently low impedance was reached during application of the EEG electrodes. This long duration of the experimental protocol and the absence of any meaningful task for the participants lead to considerable problems in staying awake. Many participants had to be instructed repeatedly to keep their eyes open in order to stay awake. There is evidence that properties of TMS-evoked activity can be severely altered during sleep (Massimini et al., 2005). While the sham session can in part help to account for these vigilance-related changes in cortical activity, this nevertheless constitutes a serious confounding for the current investigation.

Third, the data analysis in the current study was only performed a single time with one particular preprocessing pipeline. A recent investigation by (Bertazzoli et al., 2021) suggested that even the several TMS-EEG preprocessing tools and pipelines available (Atluri et al., 2016; Mutanen et al., 2016; Rogasch et al., 2017), only recover in part the same neural activity. Especially the early components of the TEP (< 100 ms) were only correlated weakly when compared between the different preprocessing pipelines. Thus, the results reported here might rely heavily on the choices made during preprocessing.

Fourth, the TMS pulse can create various types of peripheral co-stimulations, including the activation of facial motor and sensory nerve fibers or auditory responses that in turn appear as evoked responses, superimposed onto the measured TEP response (Conde et al., 2019). Especially the loud clicking noise of the TMS coil during application of pulse has been shown to trigger auditory evoked potentials (AEP), which show similar spatiotemporal patterns, matching especially with the later components of the TEP (e.g. N100, P180/P200). While earplugs were used to reduce these contributions of AEPs, the state of the art technique utilizes white noise masking to further eliminate possible contribution of the AEP to the TEP (ter Braack et al., 2015).

Last, it is unclear to which extent the current findings are reproducible as cTBS was only applied in one session to each individual. For instance, a recent investigation of Ozdemir et al. (2021) found that the cTBS-induced changes in cortical responses were not reproducible on a second visit.

# 5 Conclusion

The current study largely replicated previous findings of high interindividual variability in response characteristics following TBS. The combination of TMS-EEG made it possible to measure cTBS after effects directly at the level of the cortex without contributions of the corticospinal pathways. The modulation of TEP peaks provided direct evidence for local and remote changes in cortical excitability. This existence of excitability changes distant from M1 corroborate the significance of combined TMS-EEG to measure TBS after-effects in remote regions interconnected to the stimulation site. The prominent reduction of the N45 component suggests that cTBS might be a suitable approach to alter $GABA_A$-mediated inhibition within the motor system. However, the relationship between changes in cortical and corticospinal excitability remains less clear. A divergence between the measures was especially noticeable when investi-

gating responder subgroups, where TEP peaks partly indicated opposite effects on excitability from what was actually deduced from the MEPs. Overall, the present findings suggest that MEPs and TEPs reflect separate, but not necessarily completely independent indices of cortical excitability. As consequence, it might be necessary to combine both measures to fully understand the extent of cTBS-induced plasticity on an individual level.

## Acknowledgements

We thank Dr. Rouhollah Abdollahi and Alexandra Kurganova for their valuable assistance during data acquisition.

## References

Abraham, W. C. (2008). Metaplasticity: Tuning synapses and networks for plasticity. *Nature Reviews Neuroscience*, *9*(5), 387–399. https://doi.org/10.1038/nrn2356

Ah Sen, C. B., Fassett, H. J., El-Sayes, J., Turco, C. V., Hameer, M. M., & Nelson, A. J. (2017). Active and resting motor threshold are efficiently obtained with adaptive threshold hunting. *PLoS ONE*, *12*(10), 1–9. https://doi.org/10.1371/journal.pone.0186007

Atluri, S., Frehlich, M., Mei, Y., Dominguez, L. G., Rogasch, N. C., Wong, W., Daskalakis, Z. J., & Farzan, F. (2016). TMSEEG: A MATLAB-based graphical user interface for processing electrophysiological signals during transcranial magnetic stimulation. *Frontiers in Neural Circuits*, *10*(OCT), 1–20. https://doi.org/10.3389/fncir.2016.00078

Bashir, S., Edwards, D., & Pascual-Leone, A. (2011). Neuronavigation increases the physiologic and behavioral effects of low-frequency rTMS of primary motor cortex in healthy subjects. *Brain Topography*, *24*(1), 54–64. https://doi.org/10.1007/s10548-010-0165-7

Belardinelli, P., König, F., Liang, C., Premoli, I., Desideri, D., Müller-Dahlhaus, F., Gordon, P. C., Zipser, C., Zrenner, C., & Ziemann, U. (2021). TMS-EEG signatures of glu-

tamatergic neurotransmission in human cortex. *Scientific Reports*, *11*(1), 1–14. https://doi.org/10.1038/s41598-021-87533-z

Bell, A. J., & Sejnowski, T. J. (1997). The "independent components" of natural scenes are edge filters. *Vision Research*, *37*(23), 3327–3338. https://doi.org/https://doi.org/10.1016/S0042-6989(97)00121-1

Bender, S., Basseler, K., Sebastian, I., Resch, F., Kammer, T., Oelkers-Ax, R., & Weisbrod, M. (2005). Electroencephalographic response to transcranial magnetic stimulation in children: Evidence for giant inhibitory potentials. *Annals of Neurology*, *58*(1), 58–67. https://doi.org/https://doi.org/10.1002/ana.20521

Bertazzoli, G., Esposito, R., Mutanen, T. P., Ferrari, C., Ilmoniemi, R. J., Miniussi, C., & Bortoletto, M. (2021). The impact of artifact removal approaches on TMS–EEG signal. *NeuroImage*, *239*, 118272. https://doi.org/10.1016/j.neuroimage.2021.118272

Bonato, C., Miniussi, C., & Rossini, P. M. (2006). Transcranial magnetic stimulation and cortical evoked potentials: A TMS/EEG co-registration study. *Clinical Neurophysiology*, *117*(8), 1699–1707. https://doi.org/10.1016/j.clinph.2006.05.006

Bonnard, M., Spieser, L., Meziane, H. B., De Graaf, J. B., & Pailhous, J. (2009). Prior intention can locally tune inhibitory processes in the primary motor cortex: Direct evidence from combined TMS-EEG. *European Journal of Neuroscience*, *30*(5), 913–923. https://doi.org/10.1111/j.1460-9568.2009.06864.x

Bremmer, F., Schlack, A., Duhamel, J. R., Graf, W., & Fink, G. R. (2001). Space coding in primate posterior parietal cortex. *NeuroImage*, *14*(1 Pt 2), S46–51. https://doi.org/10.1006/nimg.2001.0817

Burke, D., Hicks, R., Gandevia, S. C., Stephen, J., Woodforth, I., & Crawford, M. (1993). Direct comparison of corticospinal volleys in human subjects to transcranial magnetic and electrical stimulation. *The Journal of physiology*, *470*, 383–393. https://doi.org/10.1113/jphysiol.1993.sp019864

Casarotto, S., Lauro, L. J., Bellina, V., Casali, A. G., Rosanova, M., Pigorini, A., Defendi, S., Mariotti, M., & Massimini, M. (2010). EEG responses to TMS are sensitive to changes in the perturbation parameters and repeatable over time. *PLoS ONE*, *5*(4). https://doi.org/10.1371/journal.pone.0010281

Cassidy, J. M., Gillick, B. T., & Carey, J. R. (2014). Priming the brain to capitalize on metaplasticity in stroke rehabilitation. *Physical Therapy*, *94*(1), 139–150. https://doi.org/10.2522/ptj.20130027

Casula, E. P., Tarantino, V., Basso, D., Arcara, G., Marino, G., Toffolo, G. M., Rothwell, J. C., & Bisiacchi, P. S. (2014). Low-frequency rTMS inhibitory effects in the primary motor cortex: Insights from TMS-evoked potentials. *NeuroImage*, *98*, 225–232. https://doi.org/10.1016/j.neuroimage.2014.04.065

Cazzoli, D., Müri, R. M., Hess, C. W., & Nyffeler, T. (2009). Horizontal and vertical dimensions of visual extinction: a theta burst stimulation study. *Neuroscience*, *164*(4), 1609–1614. https://doi.org/10.1016/j.neuroscience.2009.09.044

Chen, R., Classen, J., Gerloff, C., Celnik, P., Wassermann, E. M., Hallett, M., & Cohen, L. G. (1997). Depression of motor cortex excitability by low-frequency transcranial magnetic stimulation. *Neurology*, *48*(5), 1398–1403. https://doi.org/10.1212/WNL.48.5.1398

Chen, R., & Seitz, R. J. (2001). Changing cortical excitability with low-frequency magnetic stimulation. *Neurology*, *57*(3), 379–380. https://doi.org/10.1212/WNL.57.3.379

Cho, S. S., Ko, J. H., Pellecchia, G., Van Eimeren, T., Cilia, R., & Strafella, A. P. (2010). Continuous theta burst stimulation of right dorsolateral prefrontal cortex induces changes in impulsivity level. *Brain Stimulation*, *3*(3), 170–176. https://doi.org/10.1016/j.brs.2009.10.002

Chung, S. W., Hill, A. T., Rogasch, N. C., Hoy, K. E., & Fitzgerald, P. B. (2016). Use of theta-burst stimulation in changing excitability of motor cortex: A systematic review and meta-analysis. *Neuroscience and Biobehavioral Reviews*, *63*, 43–64. https://doi.org/10.1016/j.neubiorev.2016.01.008

Chung, S. W., Rogasch, N. C., Hoy, K. E., & Fitzgerald, P. B. (2018). The effect of single and repeated prefrontal intermittent theta burst stimulation on cortical reactivity and working memory. *Brain Stimulation*, *11*(3), 566–574. https://doi.org/10.1016/j.brs.2018.01.002

Conde, V., Tomasevic, L., Akopian, I., Stanek, K., Saturnino, G. B., Thielscher, A., Bergmann, T. O., & Siebner, H. R. (2019). The non-transcranial TMS-evoked potential is an inherent source of ambiguity in TMS-EEG studies. *NeuroImage*, *185*(June 2018), 300–312. https://doi.org/10.1016/j.neuroimage.2018.10.052

Culham, J. C., & Valyear, K. F. (2006). Human parietal cortex in action. *Current Opinion in Neurobiology*, *16*(2), 205–212. https://doi.org/10.1016/j.conb.2006.03.005

Darmani, G., Zipser, C. M., Böhmer, G. M., Deschet, K., Müller-Dahlhaus, F., Belardinelli, P., Schwab, M., & Ziemann, U. (2016). Effects of the selective $\alpha$5-GABAAR antagonist S44819 on excitability in the human brain: A TMS–EMG and TMS–EEG phase I study. *Journal of Neuroscience*, *36*(49), 12312–12320. https://doi.org/10.1523/JNEUROSCI.1689-16.2016

Daskalakis, Z. J., Christensen, B. K., Chen, R., Fitzgerald, P. B., Zipursky, R. B., & Kapur, S. (2002). Evidence for impaired cortical inhibition in schizophrenia using transcranial magnetic stimulation. *Archives of general psychiatry*, *59*(4), 347–354. https://doi.org/10.1001/archpsyc.59.4.347

Delorme, A., & Makeig, S. (2004). EEGLAB: An open source toolbox for analysis of single-trial EEG dynamics including independent component analysis. *Journal of Neuroscience Methods*, *134*(1), 9–21. https://doi.org/10.1016/j.jneumeth.2003.10.009

Di Lazzaro, V., Oliviero, A., Pilato, F., Saturno, E., Dileone, M., Mazzone, P., Insola, A., Tonali, P. A., & Rothwell, J. C. (2004). The physiological basis of transcranial motor cortex stimulation in conscious humans. *Clinical Neurophysiology*, *115*(2), 255–266. https://doi.org/10.1016/j.clinph.2003.10.009

Di Lazzaro, V., Pilato, F., Dileone, M., Profice, P., Oliviero, A., Mazzone, P., Insola, A., Ranieri, F., Meglio, M., Tonali, P. A., & Rothwell, J. C. (2008). The physiological basis of the effects of intermittent theta burst stimulation of the human motor cortex. *The Journal of physiology*, *586*(16), 3871–3879. https://doi.org/10.1113/jphysiol.2008.152736

Di Lazzaro, V., Pilato, F., Saturno, E., Oliviero, A., Dileone, M., Mazzone, P., Insola, A., Tonali, P. A., Ranieri, F., Huang, Y. Z., & Rothwell, J. C. (2005). Theta-burst repetitive transcranial magnetic stimulation suppresses specific excitatory circuits in the human motor cortex. *The Journal of physiology*, *565*(Pt 3), 945–950. https://doi.org/10.1113/jphysiol.2005.087288

Di Lazzaro, V., & Ziemann, U. (2013). The contribution of transcranial magnetic stimulation in the functional evaluation of microcircuits in human motor cortex. *Frontiers in Neural Circuits*, *7*(JAN), 1–9. https://doi.org/10.3389/fncir.2013.00018

Du, X., Rowland, L. M., Summerfelt, A., Wijtenburg, A., Chiappelli, J., Wisner, K., Kochunov, P., Choa, F.-S., & Hong, L. E. (2018). TMS evoked N100 reflects local GABA and glutamate balance. *Brain stimulation*, *11*(5), 1071–1079. https://doi.org/10.1016/j.brs.2018.05.002

Fiori, F., Chiappini, E., Candidi, M., Romei, V., Borgomaneri, S., & Avenanti, A. (2017). Long-latency interhemispheric interactions between motor-related areas and the primary motor cortex: A dual site TMS study. *Scientific Reports*, *7*(1), 1–10. https://doi.org/10.1038/s41598-017-13708-2

Fitzgerald, P. B., Fountain, S., & Daskalakis, Z. J. (2006). A comprehensive review of the effects of rTMS on motor cortical excitability and inhibition. *Clinical Neurophysiology*, *117*(12), 2584–2596. https://doi.org/10.1016/j.clinph.2006.06.712

Gamboa, O. L., Antal, A., Laczo, B., Moliadze, V., Nitsche, M. A., & Paulus, W. (2011). Impact of repetitive theta burst stimulation on motor cortex excitability. *Brain Stimulation*, *4*(3), 145–151. https://doi.org/10.1016/j.brs.2010.09.008

Gedankien, T., Fried, P. J., Pascual-Leone, A., & Shafi, M. M. (2017). Intermittent theta-burst stimulation induces correlated changes in cortical and corticospinal excitability in healthy older subjects. *Clinical neurophysiology : official journal of the International Federation of Clinical Neurophysiology*, *128*(12), 2419–2427. https://doi.org/10.1016/j.clinph.2017.08.034

Gentner, R., Wankerl, K., Reinsberger, C., Zeller, D., & Classen, J. (2008). Depression of human corticospinal excitability induced by magnetic theta-burst stimulation: Evidence of rapid polarity-reversing metaplasticity. *Cerebral Cortex*, *18*(9), 2046–2053. https://doi.org/10.1093/cercor/bhm239

Gharbawie, O. A., Stepniewska, I., Qi, H., & Kaas, J. H. (2011). Multiple Parietal–Frontal Pathways Mediate Grasping in Macaque Monkeys. *Journal of Neuroscience*, *31*(32), 11660–11677. https://doi.org/10.1523/JNEUROSCI.1777-11.2011

Goldenkoff, E. R., Logue, R. N., Brown, S. H., & Vesia, M. (2021). Reduced Facilitation of Parietal-Motor Functional Connections in Older Adults. *Frontiers in Aging Neuroscience*, *13*(February). https://doi.org/10.3389/fnagi.2021.595288

Goldsworthy, M. R., Vallence, A. M., Hodyl, N. A., Semmler, J. G., Pitcher, J. B., & Ridding, M. C. (2016). Probing changes in corticospinal excitability following theta burst stimulation of the human primary motor cortex. *Clinical Neurophysiology*, *127*(1), 740–747. https://doi.org/10.1016/j.clinph.2015.06.014

Grefkes, C., & Fink, G. R. (2011). Reorganization of cerebral networks after stroke: New insights from neuroimaging with connectivity approaches. *Brain*, *134*(5), 1264–1276. https://doi.org/10.1093/brain/awr033

Groppa, S., Oliviero, A., Eisen, A., Quartarone, A., Cohen, L. G., Mall, V., Kaelin-Lang, A., Mima, T., Rossi, S., Thickbroom, G. W., Rossini, P. M., Ziemann, U., Valls-Solé, J., & Siebner, H. R. (2012). A practical guide to diagnostic transcranial magnetic stimulation: report of an IFCN committee. *Clinical neurophysiology : official journal of the*

*International Federation of Clinical Neurophysiology*, *123*(5), 858–882. https://doi.org/10.1016/j.clinph.2012.01.010

Hallett, M. (2007). Transcranial Magnetic Stimulation: A Primer. *Neuron*, *55*(2), 187–199. https://doi.org/10.1016/j.neuron.2007.06.026

Hamada, M., Murase, N., Hasan, A., Balaratnam, M., & Rothwell, J. C. (2013). The role of interneuron networks in driving human motor cortical plasticity. *Cerebral Cortex*, *23*(7), 1593–1605. https://doi.org/10.1093/cercor/bhs147

Harrington, A., & Hammond-Tooke, G. D. (2015). Theta burst stimulation of the cerebellum modifies the TMS-evoked N100 potential, a marker of GABA inhibition. *PLoS ONE*, *10*(11), 1–15. https://doi.org/10.1371/journal.pone.0141284

Heidegger, T., Hansen-Goos, O., Batlaeva, O., Annak, O., Ziemann, U., & Lötsch, J. (2017). A Data-Driven Approach to Responder Subgroup Identification after Paired Continuous Theta Burst Stimulation. *Frontiers in human neuroscience*, *11*, 382. https://doi.org/10.3389/fnhum.2017.00382

Hordacre, B., Goldsworthy, M. R., Graetz, L., & Ridding, M. C. (2021). Motor network connectivity predicts neuroplastic response following theta burst stimulation in healthy adults. *Brain Structure and Function*, *226*(6), 1893–1907. https://doi.org/10.1007/s00429-021-02299-4

Hoy, K. E., Bailey, N., Michael, M., Fitzgibbon, B., Rogasch, N. C., Saeki, T., & Fitzgerald, P. B. (2016). Enhancement of working memory and task-related oscillatory activity following intermittent theta burst stimulation in healthy controls. *Cerebral Cortex*, *26*(12), 4563–4573. https://doi.org/10.1093/cercor/bhv193

Huang, Y.-Z., Edwards, M. J., Rounis, E., Bhatia, K. P., & Rothwell, J. C. (2005). Theta burst stimulation of the human motor cortex. *Neuron*, *45*(2), 201–206. https://doi.org/10.1016/j.neuron.2004.12.033

Iezzi, E., Conte, A., Suppa, A., Agostino, R., Dinapoli, L., Scontrini, A., & Berardelli, A. (2008). Phasic voluntary movements reverse the aftereffects of subsequent theta-burst

stimulation in humans. *Journal of Neurophysiology*, *100*(4), 2070–2076. https://doi.org/10.1152/jn.90521.2008

Ilmoniemi, R. J., & Kičić, D. (2010). Methodology for combined TMS and EEG. *Brain Topography*, *22*(4), 233–248. https://doi.org/10.1007/s10548-009-0123-4

Ilmoniemi, R. J., Virtanen, J., Ruohonen, J., Karhu, J., Aronen, H. J., Näätänen, R., & Katila, T. (1997). Neuronal responses to magnetic stimulation reveal cortical reactivity and connectivity. *NeuroReport*, *8*(16), 3537–3540. https://doi.org/10.1097/00001756-199711100-00024

Jäncke, L., Steinmetz, H., Benilow, S., & Ziemann, U. (2004). Slowing fastest finger movements of the dominant hand with low-frequency rTMS of the hand area of the primary motor cortex. *Experimental Brain Research*, *155*(2), 196–203. https://doi.org/10.1007/s00221-003-1719-7

Jannati, A., Block, G., Oberman, L. M., Rotenberg, A., & Pascual-Leone, A. (2017). Interindividual variability in response to continuous theta-burst stimulation in healthy adults. *Clinical neurophysiology : official journal of the International Federation of Clinical Neurophysiology*, *128*(11), 2268–2278. https://doi.org/10.1016/j.clinph.2017.08.023

Jelić, M. B., Milanović, S. D., & Filipović, S. R. (2015). Differential effects of facilitatory and inhibitory theta burst stimulation of the primary motor cortex on motor learning. *Clinical Neurophysiology*, *126*(5), 1016–1023. https://doi.org/10.1016/j.clinph.2014.09.003

Jennum, P., Winkel, H., & Fuglsang-Frederiksen, A. (1995). Repetitive magnetic stimulation and motor evoked potentials. *Electroencephalography and clinical neurophysiology*, *97*(2), 96–101. https://doi.org/10.1016/0924-980x(94)00293-g

Kaneko, K., Kawai, S., Fuchigami, Y., Morita, H., & Ofuji, A. (1996). The effect of current direction induced by transcranial magnetic stimulation on the corticospinal excitability in human brain. *Electroencephalography and Clinical Neurophysiology - Electromyo-*

*graphy and Motor Control*, *101*(6), 478–482. https://doi.org/10.1016/S0921-884X(96)96021-X

Karni, A., Meyer, G., Rey-Hipolito, C., Jezzard, P., Adams, M. M., Turner, R., & Ungerleider, L. G. (1998). The acquisition of skilled motor performance: Fast and slow experience-driven changes in primary motor cortex. *Proceedings of the National Academy of Sciences of the United States of America*, *95*(3), 861–868. https://doi.org/10.1073/pnas.95.3.861

Katagiri, N., Yoshida, S., Koseki, T., Kudo, D., Namba, S., Tanabe, S., Huang, Y. Z., & Yamaguchi, T. (2020). Interindividual Variability of Lower-Limb Motor Cortical Plasticity Induced by Theta Burst Stimulation. *Frontiers in Neuroscience*, *14*(November), 1–10. https://doi.org/10.3389/fnins.2020.563293

Kerwin, L. J., Keller, C. J., Wu, W., Narayan, M., & Etkin, A. (2018). Test-retest reliability of transcranial magnetic stimulation EEG evoked potentials. *Brain Stimulation*, *11*(3), 536–544. https://doi.org/10.1016/j.brs.2017.12.010

Klírová, M., Hejzlar, M., Kostýlková, L., Mohr, P., Rokyta, R., & Novák, T. (2020). Prolonged Continuous Theta Burst Stimulation of the Motor Cortex Modulates Cortical Excitability But not Pain Perception. *Frontiers in systems neuroscience*, *14*, 27. https://doi.org/10.3389/fnsys.2020.00027

Klomjai, W., Katz, R., & Lackmy-Vallée, A. (2015). Basic principles of transcranial magnetic stimulation (TMS) and repetitive TMS (rTMS). *Annals of Physical and Rehabilitation Medicine*, *58*(4), 208–213. https://doi.org/10.1016/j.rehab.2015.05.005

Koch, G., Cercignani, M., Pecchioli, C., Versace, V., Oliveri, M., Caltagirone, C., Rothwell, J., & Bozzali, M. (2010). In vivo definition of parieto-motor connections involved in planning of grasping movements. *NeuroImage*, *51*(1), 300–312. https://doi.org/10.1016/j.neuroimage.2010.02.022

Koch, G., Fernandez Del Olmo, M., Cheeran, B., Ruge, D., Schippling, S., Caltagirone, C., & Rothwell, J. C. (2007). Focal Stimulation of the Posterior Parietal Cortex Increases the

Excitability of the Ipsilateral Motor Cortex. *Journal of Neuroscience*, *27*(25), 6815–6822. https://doi.org/10.1523/JNEUROSCI.0598-07.2007

Komssi, S., Aronen, H. J., Huttunen, J., Kesäniemi, M., Soinne, L., Nikouline, V. V., Ollikainen, M., Roine, R. O., Karhu, J., Savolainen, S., & Ilmoniemi, R. J. (2002). Ipsi- and contralateral EEG reactions to transcranial magnetic stimulation. *Clinical Neurophysiology*, *113*(2), 175–184. https://doi.org/10.1016/S1388-2457(01)00721-0

Lakhani, B., Bolton, D. A., Miyasike-daSilva, V., Vette, A. H., & McIlroy, W. E. (2014). Speed of processing in the primary motor cortex: A continuous theta burst stimulation study. *Behavioural Brain Research*, *261*, 177–184. https://doi.org/10.1016/j.bbr.2013.12.022

Larson, J., & Lynch, G. (1989). Theta pattern stimulation and the induction of LTP: the sequence in which synapses are stimulated determines the degree to which they potentiate. *Brain Research*, *489*(1), 49–58. https://doi.org/10.1016/0006-8993(89)90007-3

Larson, J., Wong, D., & Lynch, G. (1986). Patterned stimulation at the theta frequency is optimal for the induction of hippocampal long-term potentiation. *Brain Research*, *368*(2), 347–350. https://doi.org/10.1016/0006-8993(86)90579-2

Lehmann, D., & Skrandies, W. (1980). Reference-free identification of components of checkerboard-evoked multichannel potential fields. *Electroencephalography and Clinical Neurophysiology*, *48*(6), 609–621. https://doi.org/10.1016/0013-4694(80)90419-8

Lindner, A., Iyer, A., Kagan, I., & Andersen, R. A. (2010). Human posterior parietal cortex plans where to reach and what to avoid. *Journal of Neuroscience*, *30*(35), 11715–11725. https://doi.org/10.1523/JNEUROSCI.2849-09.2010

Lioumis, P., Kičić, D., Savolainen, P., Mäkelä, J. P., & Kähkönen, S. (2009). Reproducibility of TMS - Evoked EEG responses. *Human Brain Mapping*, *30*(4), 1387–1396. https://doi.org/10.1002/hbm.20608

López-Alonso, V., Cheeran, B., Río-Rodríguez, D., & Fernández-Del-Olmo, M. (2014). Inter-individual variability in response to non-invasive brain stimulation paradigms. *Brain Stimulation*, *7*(3), 372–380. https://doi.org/10.1016/j.brs.2014.02.004

Maeda, F., Keenan, J. P., Tormos, J. M., Topka, H., & Pascual-Leone, A. (2000). Interindividual variability of the modulatory effects of repetitive transcranial magnetic stimulation on cortical excitability. *Experimental Brain Research*, *133*(4), 425–430. https://doi.org/10.1007/s002210000432

Mäki, H., & Ilmoniemi, R. J. (2010). The relationship between peripheral and early cortical activation induced by transcranial magnetic stimulation. *Neuroscience Letters*, *478*(1), 24–28. https://doi.org/10.1016/j.neulet.2010.04.059

Maris, E., & Oostenveld, R. (2007). Nonparametric statistical testing of EEG- and MEG-data. *Journal of neuroscience methods*, *164*(1), 177–190. https://doi.org/10.1016/j.jneumeth.2007.03.024

Martin, P. G., Gandevia, S. C., & Taylor, J. L. (2006). Theta burst stimulation does not reliably depress all regions of the human motor cortex. *Clinical Neurophysiology*, *117*(12), 2684–2690. https://doi.org/10.1016/j.clinph.2006.08.008

Massimini, M., Ferrarelli, F., Huber, R., Esser, S. K., Singh, H., & Tononi, G. (2005). Neuroscience: Breakdown of cortical effective connectivity during sleep. *Science*, *309*(5744), 2228–2232. https://doi.org/10.1126/science.1117256

Meehan, S. K., Dao, E., Linsdell, M. A., & Boyd, L. A. (2011). Continuous theta burst stimulation over the contralesional sensory and motor cortex enhances motor learning post-stroke. *Neuroscience Letters*, *500*(1), 26–30. https://doi.org/10.1016/j.neulet.2011.05.237

Mulliken, G. H., Musallam, S., & Andersen, R. A. (2008). Forward estimation of movement state in posterior parietal cortex. *Proceedings of the National Academy of Sciences*, *105*(24), 8170–8177. https://doi.org/10.1073/pnas.0802602105

Murakami, T., Müller-Dahlhaus, F., Lu, M.-K., & Ziemann, U. (2012). Homeostatic metaplasticity of corticospinal excitatory and intracortical inhibitory neural circuits in human motor cortex (2012/08/28). *The Journal of physiology*, *590*(22), 5765–5781. https://doi.org/10.1113/jphysiol.2012.238519

Mutanen, T. P., Kukkonen, M., Nieminen, J. O., Stenroos, M., Sarvas, J., & Ilmoniemi, R. J. (2016). Recovering TMS-evoked EEG responses masked by muscle artifacts. *NeuroImage*, *139*, 157–166. https://doi.org/10.1016/j.neuroimage.2016.05.028

Mutanen, T. P., Mäki, H., & Ilmoniemi, R. J. (2013). The effect of stimulus parameters on TMS-EEG muscle artifacts. *Brain Stimulation*, *6*(3), 371–376. https://doi.org/10.1016/j.brs.2012.07.005

Nakamura, H., Kitagawa, H., Kawaguchi, Y., & Tsuji, H. (1996). Direct and indirect activation of human corticospinal neurons by transcranial magnetic and electrical stimulation. *Neuroscience Letters*, *210*(1), 45–48. https://doi.org/10.1016/0304-3940(96)12659-8

Nettekoven, C., Volz, L. J., Kutscha, M., Pool, E. M., Rehme, A. K., Eickhoff, S. B., Fink, G. R., & Grefkes, C. (2014). Dose-dependent effects of theta burst rTMS on cortical excitability and resting-state connectivity of the human motor system. *Journal of Neuroscience*, *34*(20), 6849–6859. https://doi.org/10.1523/JNEUROSCI.4993-13.2014

Nikulin, V. V., Kičić, D., Kähkönen, S., & Ilmoniemi, R. J. (2003). Modulation of electroencephalographic responses to transcranial magnetic stimulation: Evidence for changes in cortical excitability related to movement. *European Journal of Neuroscience*, *18*(5), 1206–1212. https://doi.org/10.1046/j.1460-9568.2003.02858.x

O'Brien, F. O., & Cousineau, D. (2014). Representing Error bars in within-subject designs in typical software packages. *Quant Methods Psychol*, (10), 56–67.

Oldfield, R. C. (1971). The assessment and analysis of handedness: The Edinburgh inventory. *Neuropsychologia*, *9*(1), 97–113. https://doi.org/https://doi.org/10.1016/0028-3932(71)90067-4

Opie, G. M., Rogasch, N. C., Goldsworthy, M. R., Ridding, M. C., & Semmler, J. G. (2017). Investigating TMS–EEG Indices of Long-Interval Intracortical Inhibition at Different Interstimulus Intervals. *Brain Stimulation*, *10*(1), 65–74. https://doi.org/10.1016/j.brs.2016.08.004

Ozdemir, R. A., Boucher, P., Fried, P. J., Momi, D., Jannati, A., Pascual-Leone, A., Santarnecchi, E., & Shafi, M. M. (2021). Reproducibility of cortical response modulation induced by intermittent and continuous theta-burst stimulation of the human motor cortex. *Brain Stimulation*, *14*(4), 949–964. https://doi.org/https://doi.org/10.1016/j.brs.2021.05.013

Pascual-Leone, A., Valls-Solé, J., Wassermann, E. M., & Hallett, M. (1994). Responses to rapid-rate transcranial magnetic stimulation of the human motor cortex. *Brain*, *117*(4), 847–858. https://doi.org/10.1093/brain/117.4.847

Paulus, W., Classen, J., Cohen, L. G., Large, C. H., Di Lazzaro, V., Nitsche, M., Pascual-Leone, A., Rosenow, F., Rothwell, J. C., & Ziemann, U. (2008). State of the art: Pharmacologic effects on cortical excitability measures tested by transcranial magnetic stimulation. *Brain Stimulation*, *1*(3), 151–163. https://doi.org/10.1016/j.brs.2008.06.002

Paus, T., Sipila, P. K., & Strafella, A. P. (2001). Synchronization of neuronal activity in the human primary motor cortex by transcranial magnetic stimulation: an EEG study. *Journal of neurophysiology*, *86*(4), 1983–1990. https://doi.org/10.1152/jn.2001.86.4.1983

Pellegrini, M., Zoghi, M., & Jaberzadeh, S. (2018). Cluster analysis and subgrouping to investigate inter-individual variability to non-invasive brain stimulation: A systematic review. *Reviews in the Neurosciences*, *29*(6), 675–697. https://doi.org/10.1515/revneuro-2017-0083

Petrichella, S., Johnson, N., & He, B. (2017). The influence of corticospinal activity on TMS-evoked activity and connectivity in healthy subjects: A TMS-EEG study. *PLoS ONE*, *12*(4), 1–18. https://doi.org/10.1371/journal.pone.0174879

Premoli, I., Bergmann, T. O., Fecchio, M., Rosanova, M., Biondi, A., Belardinelli, P., & Ziemann, U. (2017). The impact of GABAergic drugs on TMS-induced brain oscillations in human motor cortex. *NeuroImage*, *163*(September), 1–12. https://doi.org/10.1016/j.neuroimage.2017.09.023

Premoli, I., Castellanos, N., Rivolta, D., Belardinelli, P., Bajo, R., Zipser, C., Espenhahn, S., Heidegger, T., Müller-Dahlhaus, F., & Ziemann, U. (2014). TMS-EEG signatures of

GABAergic neurotransmission in the human cortex. *The Journal of neuroscience : the official journal of the Society for Neuroscience*, *34*(16), 5603–5612. https://doi.org/10.1523/JNEUROSCI.5089-13.2014

Premoli, I., Rivolta, D., Espenhahn, S., Castellanos, N., Belardinelli, P., Ziemann, U., & Müller-Dahlhaus, F. (2014). Characterization of GABAB-receptor mediated neurotransmission in the human cortex by paired-pulse TMS-EEG. *NeuroImage*, *103*, 152–162. https://doi.org/10.1016/j.neuroimage.2014.09.028

Ridding, M. C., & Ziemann, U. (2010). Determinants of the induction of cortical plasticity by non-invasive brain stimulation in healthy subjects. *Journal of Physiology*, *588*(13), 2291–2304. https://doi.org/10.1113/jphysiol.2010.190314

Rocchi, L., Ibáñez, J., Benussi, A., Hannah, R., Rawji, V., Casula, E., & Rothwell, J. (2018). Variability and predictors of response to continuous theta burst stimulation: A TMS-EEG study. *Frontiers in Neuroscience*, *12*(JUN), 1–11. https://doi.org/10.3389/fnins.2018.00400

Rogasch, N. C., & Fitzgerald, P. B. (2013). Assessing cortical network properties using TMS-EEG. *Human brain mapping*, *34*(7), 1652–1669. https://doi.org/10.1002/hbm.22016

Rogasch, N. C., Sullivan, C., Thomson, R. H., Rose, N. S., Bailey, N. W., Fitzgerald, P. B., Farzan, F., & Hernandez-Pavon, J. C. (2017). Analysing concurrent transcranial magnetic stimulation and electroencephalographic data: A review and introduction to the open-source TESA software. *NeuroImage*, *147*(October 2016), 934–951. https://doi.org/10.1016/j.neuroimage.2016.10.031

Roos, D., Biermann, L., Jarczok, T. A., & Bender, S. (2021). Local Differences in Cortical Excitability – A Systematic Mapping Study of the TMS-Evoked N100 Component. *Frontiers in Neuroscience*, *15*(February), 1–17. https://doi.org/10.3389/fnins.2021.623692

Rossini, P. M., Barker, A. T., Berardelli, A., Caramia, M. D., Caruso, G., Cracco, R. Q., Dimitrijević, M. R., Hallett, M., Katayama, Y., & Lücking, C. H. (1994). Non-invasive

electrical and magnetic stimulation of the brain, spinal cord and roots: basic principles and procedures for routine clinical application. Report of an IFCN committee. *Electroencephalography and clinical neurophysiology*, *91*(2), 79–92. https://doi.org/10.1016/0013-4694(94)90029-9

Sekiguchi, H., Takeuchi, S., Kadota, H., Kohno, Y., & Nakajima, Y. (2011). TMS-induced artifacts on EEG can be reduced by rearrangement of the electrode's lead wire before recording. *Clinical Neurophysiology*, *122*(5), 984–990. https://doi.org/10.1016/j.clinph.2010.09.004

Shammi, P., Bosman, E., & Stuss, D. T. (1998). Aging and variability in performance. *Aging, Neuropsychology, and Cognition*, *5*(1), 1–13. https://doi.org/10.1076/anec.5.1.1.23

Sommervoll, Y., Ettema, G., & Vereijken, B. (2011). Effects of age, task, and frequency on variability of finger tapping. *Perceptual and Motor Skills*, *113*(2), 647–661. https://doi.org/10.2466/10.25.PMS.113.5.647-661

Strigaro, G., Ruge, D., Chen, J. C., Marshall, L., Desikan, M., Cantello, R., & Rothwell, J. C. (2015). Interaction between visual and motor cortex: A transcranial magnetic stimulation study. *Journal of Physiology*, *593*(10), 2365–2377. https://doi.org/10.1113/JP270135

Suppa, A., Ortu, E., Zafar, N., Deriu, F., Paulus, W., Berardelli, A., & Rothwell, J. C. (2008). Theta burst stimulation induces after-effects on contralateral primary motor cortex excitability in humans. *The Journal of physiology*, *586*(18), 4489–4500. https://doi.org/10.1113/jphysiol.2008.156596

Takeuchi, N., Oouchida, Y., & Izumi, S. I. (2012). Motor control and neural plasticity through interhemispheric interactions. *Neural Plasticity*, *2012*. https://doi.org/10.1155/2012/823285

Teo, J. T., Swayne, O. B., Cheeran, B., Greenwood, R. J., & Rothwell, J. C. (2011). Human theta burst stimulation enhances subsequent motor learning and increases performance variability. *Cerebral Cortex*, *21*(7), 1627–1638. https://doi.org/10.1093/cercor/bhq231

ter Braack, E. M., de Goede, A. A., & van Putten, M. J. (2019). Resting Motor Threshold, MEP and TEP Variability During Daytime. *Brain Topography*, *32*(1), 17–27. https://doi.org/10.1007/s10548-018-0662-7

ter Braack, E. M., de Vos, C. C., & van Putten, M. J. (2015). Masking the Auditory Evoked Potential in TMS–EEG: A Comparison of Various Methods. *Brain Topography*, *28*(3), 520–528. https://doi.org/10.1007/s10548-013-0312-z

Tiffin, J., & Asher, E. J. (1948). The Purdue Pegboard: norms and studies of reliability and validity. *Journal of Applied Psychology*, *32*(3), 234–247. https://doi.org/10.1037/h0061266

Turrigiano, G. G., & Nelson, S. B. (2004). Homeostatic plasticity in the developing nervous system. *Nature Reviews Neuroscience*, *5*(2), 97–107. https://doi.org/10.1038/nrn1327

Vallence, A. M., Goldsworthy, M. R., Hodyl, N. A., Semmler, J. G., Pitcher, J. B., & Ridding, M. C. (2015). Inter- and intra-subject variability of motor cortex plasticity following continuous theta-burst stimulation. *Neuroscience*, *304*, 266–278. https://doi.org/10.1016/j.neuroscience.2015.07.043

Van Der Werf, Y. D., & Paus, T. (2006). The neural response to transcranial magnetic stimulation of the human motor cortex. I. Intracortical and cortico-cortical contributions. *Experimental Brain Research*, *175*(2), 231–245. https://doi.org/10.1007/s00221-006-0551-2

Verbruggen, F., Aron, A. R., Stevens, M. A., & Chambers, C. D. (2010). Theta burst stimulation dissociates attention and action updating in human inferior frontal cortex. *Proceedings of the National Academy of Sciences of the United States of America*, *107*(31), 13966–13971. https://doi.org/10.1073/pnas.1001957107

Vernet, M., Bashir, S., Yoo, W. K., Perez, J. M., Najib, U., & Pascual-Leone, A. (2013). Insights on the neural basis of motor plasticity induced by theta burst stimulation from TMS-EEG. *European Journal of Neuroscience*, *37*(4), 598–606. https://doi.org/10.1111/ejn.12069

Vesia, M., & Crawford, J. D. (2012). Specialization of reach function in human posterior parietal cortex. *Experimental brain research*, *221*(1), 1–18. https://doi.org/10.1007/s00221-012-3158-9

Werhahn, K. J., Fong, J. K., Meyer, B. U., Priori, A., Rothwell, J. C., Day, B. L., & Thompson, P. D. (1994). The effect of magnetic coil orientation on the latency of surface EMG and single motor unit responses in the first dorsal interosseous muscle. *Electroencephalography and Clinical Neurophysiology/ Evoked Potentials*, *93*(2), 138–146. https://doi.org/10.1016/0168-5597(94)90077-9

Yger, P., & Gilson, M. (2015). Models of metaplasticity: A review of concepts. *Frontiers in Computational Neuroscience*, *9*(November), 1–14. https://doi.org/10.3389/fncom.2015.00138

# 3 Study 2: Robustness of individualized inferences from longitudinal resting state dynamics

Preprint availabe at bioRxiv: https://doi.org/10.1101/2020.09.15.297572

Author Contributions

Conceived the research

**Shivakumar Viswanathan, Silvia Daun**

Performed the experiments

**Maximilian Hommelsen**

Data Preprocessing

**Maximilian Hommelsen, Shivakumar Viswanathan**

Data analysis

**Maximilian Hommelsen, Shivakumar Viswanathan**

Wrote the manuscript

**Maximilian Hommelsen, Shivakumar Viswanathan, Silvia Daun**

# Robustness of individualized inferences from longitudinal resting state dynamics

Maximilian HOMMELSEN[1], Shivakumar VISWANATHAN[1], Silvia DAUN[1,2*]

* Corresponding author

Running title: Individualized inference for longitudinal RS

Affiliations:

1. Cognitive Neuroscience, Institute of Neuroscience and Medicine (INM-3), Forschungszentrum Jülich, Jülich, Germany

2. Institute of Zoology, University of Cologne, Cologne, Germany

Corresponding author:

Silvia Daun, PhD

Cognitive Neuroscience, Institute of Neuroscience and Medicine (INM-3), Forschungszentrum Jülich, 52425, Jülich, Germany

*Email*: s.daun@fz-juelich.de, *Tel*: +49-2461-61 8638, *Fax*: +49-2461-61 1518

## ABSTRACT

Tracking how individual human brains change over extended timescales is crucial in scenarios ranging from healthy aging to stroke recovery. Tracking these neuroplastic changes with resting state (RS) activity is a promising but poorly understood possibility. It remains unresolved whether a person's RS activity over time can be reliably decoded to distinguish neurophysiological changes from confounding differences in cognitive state during rest. Here, we assessed whether this confounding can be minimized by tracking the configuration of an individual's RS activity that is shaped by their distinctive neurophysiology rather than cognitive state. Using EEG, individual RS activity was acquired over five consecutive days along with activity in tasks that were devised to simulate the confounding effects of inter-day cognitive variation. As inter-individual differences are shaped by neurophysiological differences, the inter-individual differences in RS activity on one day were analyzed (using machine learning) to identify a distinctive configuration in each individual's RS activity. Using this configuration as a classifier-rule, an individual could be re-identified with high accuracy from 2-second samples of the instantaneous oscillatory power acquired on a different day both from RS and confounded-RS. Importantly, the high accuracy of cross-day classification was achieved only with classifiers that combined information from multiple frequency bands at channels across the scalp (with a concentration at characteristic fronto-central and occipital zones). These findings support the suitability of longitudinal RS to support robust individualized inferences about neurophysiological change in health and disease.

## KEYWORDS

Neural plasticity, Individual differences, Individual identification, Electroencephalography (EEG), Power Spectrum, Frequency analysis, Machine learning, Multiclass classification

## 1. INTRODUCTION

Tracking how individual human brains change over extended time-scales (e.g., days to years) is crucial to monitor and modify neural plasticity processes in scenarios ranging from healthy aging (Boersma et al. 2011; Cabeza et al. 2018; Cassani et al. 2018) to stroke recovery (Giaquinto et al. 1994; Rehme et al. 2011; Wu et al. 2016; Bonkhoff et al. 2020; Saes et al. 2020; van der Vliet et al. 2020). A promising strategy to track an individual's changing neurophysiology is with repeated measurements of resting state (RS) activity, i.e., the ongoing neural oscillatory dynamics over a few minutes of wakeful rest (Vecchio et al. 2013; Carino-Escobar et al. 2019; Newbold et al. 2020; Pritschet et al. 2020; Saes et al. 2020). RS-activity has been shown to provide reliable indicators of neurobiological organization and integrity (Biswal et al. 1995; Damoiseaux and Greicius 2009; Van Den Heuvel et al. 2009; Hermundstad et al. 2013; Miŝic et al. 2016; Hoenig et al. 2018; Buckner and DiNicola 2019). The apparent informativeness of RS-activity as well as its convenient acquisition at relatively low cost (for example, with electroencephalography (EEG)) supports its relevance for long-term tracking. However, the relationship between RS changes over repeated measurements to neurophysiological change is poorly understood. Decoding this relationship is crucial to draw inferences about a person's changing brain using longitudinal RS.

A basic inference required from longitudinal RS is about the origin of inter-day RS differences. Suppose a person's RS-activity patterns $A_p$ and $A_q$ (on days $p$ and $q$) are different. Is this difference attributable to (i) a possible neurophysiological change (abbreviated as *NP+*), or (ii) an incidental difference in inter-day activity (i.e., *NP-*)? Although an *NP+/NP-* decision involves many considerations, a key question is whether this decision is decodable from the relationship between $A_p$ and $A_q$.

A major difficulty in decoding an *NP+/NP-* decision from RS-activity is the unconstrained format of the rest task. The rest task is defined by: (i) a *behavioral* state specified by instructions to stay still and keep eyes open (or closed) (Barry et al. 2007); and (ii) a *cognitive* state typically specified by instructions to relax and avoiding thinking of anything specific. Unlike the behavioral

state, the criteria to objectively verify the cognitive state are ill defined (Benjamin et al. 2010; Duncan and Northoff 2013; Kawagoe et al. 2018). Due to this ambiguity, inter-day RS changes do not have a simple correspondence to neuroplastic change. For instance, a person's incidental cognitive state during the rest-task could vary between days (e.g., session 1: free mind-wandering, session 2: struggling to stay awake, session 3: replaying emotional memories) (Diaz et al. 2013; Gonzalez-Castillo et al. 2021). The neural processing related to these differing cognitive states could in turn modify RS-activity *without* any changes to underlying neurophysiology. Therefore, large inter-day changes in RS-activity might not imply *NP+* and small changes might not imply *NP-*. Given this confounding potential built into the rest task, in the current study, we investigated whether RS-activity has other properties to support *NP+/NP-* classification.

Although inter-day RS *differences* are vulnerable to confounding by variable cognitive states, this might not be so for inter-day RS *commonalities*. We pursued this possibility by adopting a simple model of how inter-day RS commonalities might be structured. An individual's neurophysiology on a particular day is assumed to impose constraints on how RS-activity is configured irrespective of cognitive state. This constraint-defined configuration would be shared by RS-activity across days only if these unique constraints are also shared. Such a configuration, if it indeed exists, provides a decision-rule for *NP+/NP-* classification as follows.

Suppose $\mathbf{C}_p$ denotes the constraint-defined configuration in the activity pattern $A_p$. If activity $A_q$ on a different day is consistent with $\mathbf{C}_p$ then it supports an *NP-* classification, as inter-day consistency is assumed to require shared neurophysiological constraints. Conversely, if $A_q$ is not consistent with $\mathbf{C}_p$ then it suggests a change in these constraints and supports an *NP+* classification. As this constraint-defined configuration is assumed to be independent of cognitive state, the *NP+/NP-* decisions with such a decision-rule should presumably escape confounding by inter-day cognitive variability. Thus, according to this model, *NP+* and *NP-* are hypothesized to have distinctive, decodable signatures in RS-activity. Here, we sought to empirically test this predicted decodability of longitudinal RS.

Using EEG, longitudinal RS-activity was acquired on five consecutive days from a group of healthy, young participants. For these data, we sought to obtain decision-rules capable of *NP+/NP-* classification from the power spectrum of brief two-second samples of oscillatory activity at channels across the scalp. Testing the decision-rule's robustness to confounding needed suitable samples known to be (i) free of neurophysiological change (*NP-*) and (ii) samples containing such changes (*NP+*).

Testing *NP-* decisions posed an experimental challenge. Our participants were assumed to be neurophysiologically stable across the five-day measurement period. However, the variation in their inter-day cognitive states during the rest-task was unverifiable. Therefore, the measurement protocol included two additional tasks to produce *pseudo*-rest states that were matched to rest in behavior but not in cognitive state (Figure 1A). These pseudo-rest states served to simulate confounding RS differences of varying sizes and complexity and allowed a rigorous test of the robustness of *NP-* decisions.

Testing *NP+* decisions presented a methodological conundrum. Over long time-scales, an individual's neurobiology could change in variety of possible ways (Cabeza et al. 2018; Grefkes and Fink 2020), with very different associated consequences for RS-activity (Figure 1B). These hypothetically possible RS-activity patterns were, by definition, experimentally inaccessible and limited the options for an individual-specific test of *NP+* classification. As a pragmatic alternative, we used a cross-sectional approach where RS-activity from *other* individuals served as simulated examples of RS-activity requiring an *NP+* classification. We assume that an individual *S*'s neurophysiology differed from other individuals in the tested population to variable extents. Therefore, relative to each individual *S,* the RS-activity of others provided a diverse range of examples of RS-activity with an origin in true neurophysiological differences.

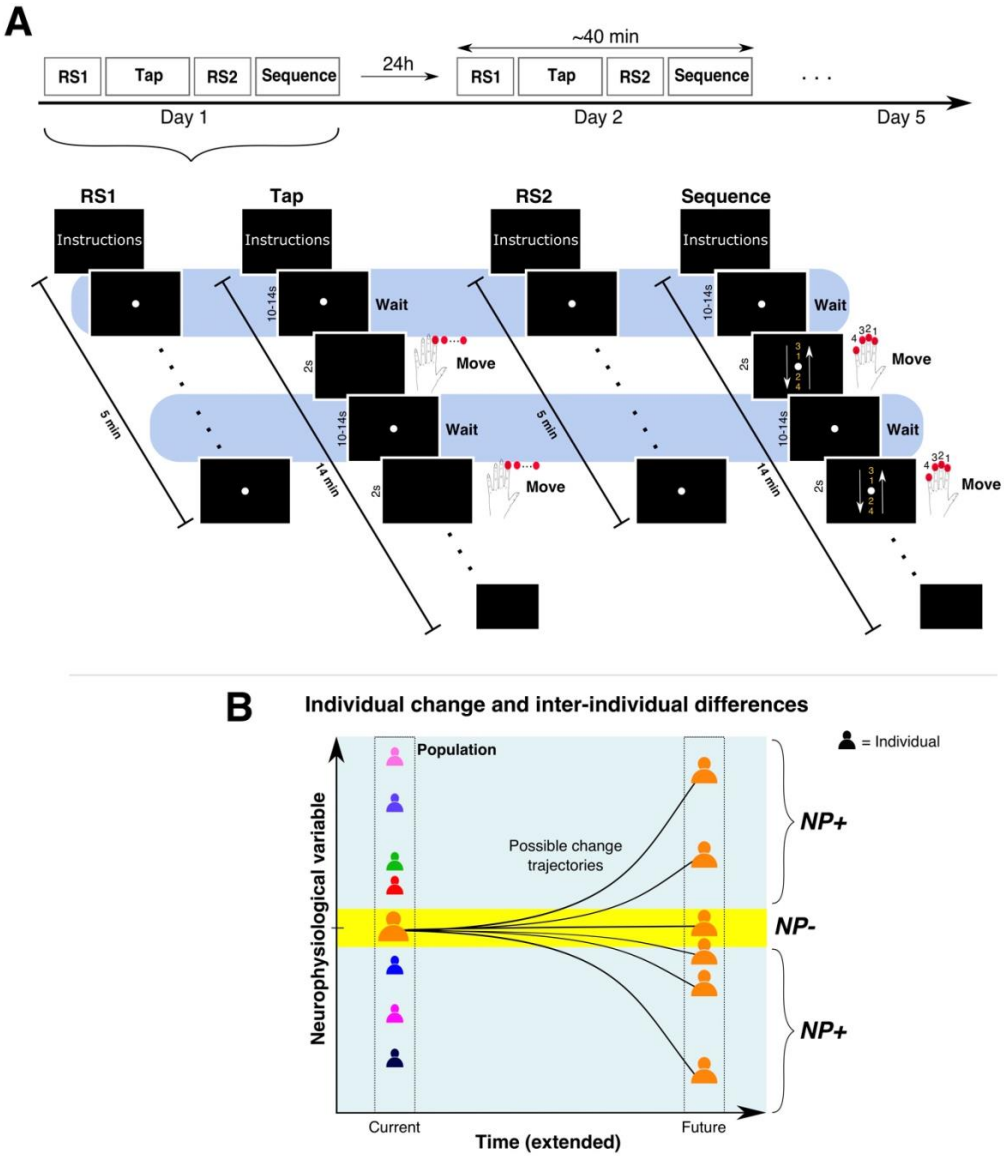


**Figure 1: Experiment rationale (A)** Four tasks (*RS1, Tap, RS2, Sequence*) were performed in the same fixed order daily on five consecutive days. Task details for one day are schematically illustrated. A white fixation point was continuously displayed during the *RS1* and *RS2* task periods, and during "waiting" periods in the *Tap* and *Sequence* tasks (highlighted in blue). In the *Tap* task, a blank screen cued a 2s movement interval requiring left index-finger movements to repeatedly press a button (shown as red dots). In the *Sequence* task, the movement cue was an image depicting four numbers between two arrows (not drawn to scale) indicating the sequence of buttons to be pressed in a continuous cyclical manner, e.g., 3-1-2-4-4-2-1-3-3-1-2-4, etc. Number-to-finger mapping is shown on cartoon hand. **(B)** Schematic of longitudinal changes to a single hypothetical neurophysiological variable for one selected individual (orange). The current value of this variable (yellow area; *NP-*) can change in a variety of possible ways over long time-scales (gray area; *NP+*). The values of this variable in other individuals in a population cross-section (colored icons) provide proxies for these unknown individual-specific change trajectories.

By adopting the above strategy to obtain suitable *NP-* and *NP+* examples, the demands for *NP+/NP-* classification shared similarities to the demands for *person* identification, namely, obtaining a decision-rule to distinguish *S* from other individuals based on RS-activity (Figure 1B). Numerous prior studies demonstrate that RS-activity can serve as a "fingerprint" for person identification (Huang et al. 2012; Campisi and Rocca 2014; Finn et al. 2015; Valizadeh et al. 2019; Pani et al. 2020). Although our focus was not on the neural basis of individual differences and trait-identification (Smit et al. 2005, 2006; Demuru et al. 2017; Finn et al. 2017; Gratton et al. 2018), this person identification approach provided a convenient technical platform for our test of individual-specific longitudinal inference. Therefore, we mapped our test of robust cross-day *NP+/NP-* classification into the terminology of a person identification problem and adopted a machine-learning approach to address this problem.

Decision-rules (i.e., classifiers) were trained to distinguish a person *S* from all others in the tested population using samples from a single day. The samples from *S* putatively share a constraint-defined configuration that is not shared by samples from other individuals. Therefore, the outcome of training should be a decision-rule that represents information about individual S's unique configuration. If this is indeed true, *S*'s decision-rule from one day should enable *S* to be re-identified from samples acquired on a different day as well as from samples of pseudo-RS activity despite cognitive state variability (*NP-*). Conversely, *S*'s decision-rule should classify samples from other individuals as not-*S*, consistent with a difference in neurophysiology co-mingled with cognitive state differences (*NP+*).

## 2. MATERIALS & METHODS

### 2.1. Participants

Twenty seven healthy volunteers (11 female, age (mean ± sd): 27.9 years ± 3.4, range: 22-34 years) participated in the study and received monetary compensation. Participants had normal or corrected-to-normal vision; no history of neurological or psychiatric disease; were not under

medication at that time; and had no cranial metallic implants (including cochlear implants). Handedness was not an inclusion criterion. Based on the Edinburgh Handedness Inventory (Oldfield 1971), 22 participants were right handed (score > 50), 2 were left handed (score < -50) and 3 had intermediate scores. The study was approved by the Ethics Commission of the Faculty of Medicine, University of Cologne (Zeichen: 14-006). All participants provided their written informed consent before the start of the experiment.

Datasets from 24 (of the 27) participants were used for statistical analyses (see section 2.6).

### 2.2. Apparatus and EEG data acquisition

Stimuli were displayed using the software Presentation (v. 20.2 Build 07.25.18, Neurobehehavioral Systems, Inc.) on an LCD screen (Hanns-G HS233H3B, 23-inch, resolution: 1920 x 1080 pixels). Behavioral responses were recorded with the fMRI Button Pad (1-Hand) System (LXPAD-1x5-10M, NAtA Technologies, Canada).

Scalp-EEG was acquired with a 64-channel active Ag/AgCl electrode system (actiCap, Brain Products, Germany) having a standard 10-20 spherical array layout (ground electrode at AFz, reference electrode on the left mastoid). Three electrodes (FT9, FT10, TP10) were used to record electrooculographic (EOG) activity: one below the left eye to record vertical movements and the other two near the left and right lateral canthi to record horizontal movements. During acquisition, measured voltages (0.1µV resolution) were amplified by a BrainAmp DC amplifier (BrainProducts GmbH, Germany) at a sampling rate of 2.5 kHz and filtered (low cutoff: DC, high cutoff: 250 Hz).

To ensure reliable positioning of the EEG cap across sessions, a stereotactic neuronavigation system (Brainsight v. 2.3, Rogue Research Inc, Canada) was used on each session to co-register the spatial coordinates of five selected electrodes (AFz, Cz, POz, C5, C6) to their coordinates on the first session (see section 2.4 for details).

### 2.3. Experiment protocol and paradigm

Participant completed five sessions of approximately 40 minutes each (Figure 1A, upper panel) scheduled at the same time on consecutive days (Monday to Friday). Sessions took place at three possible times: morning (6 x 9AM), noon (9 x 12PM) and afternoon (12 x 3PM). Due to technical problems during the scheduled recording, for one participant, the fifth session was re-acquired after a gap of three days. For all participants, every session consisted of two resting state recordings (*RS1* and *RS2*) interleaved with two non-rest tasks (referred to as *Tap* and *Sequence*) in the same order (namely, *RS1*, *Tap, RS2, Sequence*).

The *Tap* and *Sequence* tasks (Figure 1A, lower panel) involved some special design considerations. Both tasks required participants to press buttons in response to visual cues. However, these tasks had relatively long and variable inter-stimulus-intervals (10-14s) where participants fixated on the screen as they "waited" for the visual cue that required the instructed response. The cognitive states during these waiting periods (referred to as *TapWait* and *SeqWait*) were the primary focus of these tasks. The behavioral demands of the *Tap* and *Sequence* tasks were designed to modulate the cognitive states during these pre-movement wait periods, for example, covert movement preparation during *TapWait* and covert rehearsal of a movement sequence during *SeqWait.* With this covert modulation, the *TapWait* and *SeqWait* could be considered pseudo-rest states as they were matched to *RS1* and *RS2* in behavioral state but not in cognitive state. Furthermore, the *Tap* task was intended to produce cognitive states that were similar within and between days while the *Sequence* task was designed to elicit cognitive states that could systematically change across days. This was implemented by inducing participants to learn a difficult motor sequence where performance could improve with increasing practice across days. We now describe the different task periods in detail.

Each task period began with an instruction screen describing the task to be performed and ended with another instruction screen that instructed participants to take a short break and press a button to initiate the next part when they were ready.

*1: Resting State (RS1).* During this period lasting ~5minutes, a small white dot was continuously displayed at the center of the screen. Participants were instructed to keep their eyes open, fixate on the displayed white dot, relax and avoid movements (also see section: Procedure).

*2: Tap task.* In this task-period, a small white dot was centrally displayed on the screen (as in *RS1*). However, after variable intervals of 10-14 seconds, this dot disappeared for a 2 second period before reappearing. The offset of the dot was the cue for participants to repeatedly and rapidly press a button with their left index finger until the dot reappeared on the screen. The total task (duration ~14 minutes) consisted of 60 movement periods (dot absent) interleaved with 60 waiting periods (dot present). These waiting periods are referred to as *TapWait* and the response execution periods are referred to as *TapMov*.

*3: Resting State (RS2).* A second resting state recording was acquired with all task parameters being identical to *RS1*. This recording is referred to as *RS2*.

*4: Sequence task.* As with the *Tap* task, the sequence task consisted of 60 waiting periods of 10-14s each (i.e., *SeqWait*) where a small white dot was centrally displayed on the screen interleaved with 60 movement periods of 2s duration (i.e., *SeqMov*). Unlike the *Tap* task, each movement period was cued by a centrally displayed visual stimulus consisting of four vertically displayed digits (3-1-2-4) between two vertical arrows. Each number was mapped to a different button on the response pad. The vertical ordering of the numbers indicated the sequence in which the indicated buttons had to be pressed using fingers of the left hand. The arrows indicated that this sequence had to be executed rapidly and repeatedly in a cyclical manner starting from top to bottom and back. For example, following stimulus onset, the required sequence of button-presses was 3-1-2-4-4-2-1-3-3-1-2-4-… and so on. This continuing sequence had to be executed until the offset of the stimulus. No performance feedback was provided during the task. This particular sequence of digits was selected

as it was challenging to execute rapidly. To promote learning of this sequence across trials and days, the same sequence of numbers and number-to-finger-mapping was used on all sessions. The same sequence and number-to-finger mapping was also used for all participants.

Handedness was not an inclusion criterion in our experiment. However, for uniformity in task-related neural activity, all participants used fingers of their left hand to execute the button-press responses in the *Tap* and *Sequence* tasks.

### 2.4. Procedure

Prior to the start of the recordings on each of the five days, participants completed the Positive and Negative Affect Schedule (PANAS) (Watson et al. 1988) and completed brief questionnaires to report the caffeine consumption on that day and the amount and quality of sleep on the previous night.

On the first day, participants received detailed instructions about the experiment. For the resting state periods, participants were instructed to keep their eyes open, fixate on the displayed white dot and to avoid movements. Additionally, they were also asked to relax, stay awake and not think of anything in particular. For the *Tap* task, participants were instructed to press the buttons as rapidly as possible without causing discomfort. For the *Sequence* task, participants were familiarized with the task and the mapping of the number to finger. They practiced performing the task using a different digit sequence from the one used in the main experiment. Furthermore, they were explicitly instructed on each session to try to improve their performance particularly the number of buttons pressed during each response period. Finally, on all sessions, we repeatedly emphasized the importance of minimizing eye-blinks, maintaining fixation at all times during the recording, and the avoidance of all unnecessary movements of the fingers, head and body.

As the study's objective was to relate the spatio-temporal organization of neural activity across days, minimizing inter-day variation in the EEG cap's position was an important priority. We therefore implemented an additional spatial registration procedure on each day after the EEG cap

was secured to the participant's head. Using a stereotactic neuronavigation system, the participant's head was registered to the Montreal Neurological Institute (MNI) space using standard cranial landmarks. The positions of five selected electrodes along the midline and lateral axis (AFz, Cz, POz, C5, C6) were then localized using the neuronavigation software. The electrode locations obtained on the first day were used as the reference for the remaining sessions. On each subsequent session, the positioning of the cap was interactively adjusted so that each electrode's coordinates closely matched its reference location. Due to scheduling constraints, this spatial registration procedure was not performed for 7 participants.

The application of electrode gel followed after cap positioning. Skin-electrode impedance was brought below 10kΩ before starting the recording. Recordings were acquired in a light-dimmed and acoustically shielded EEG chamber. Participants were seated in a comfortable chair with their heads stabilized with a chinrest in front of the computer screen at a viewing distance of ~65cm. The response pad was placed in a recess under the table so that participants could not see their hands during the task-periods especially while pressing the buttons. During the recording, participants were monitored via a video camera to ensure that they maintained fixation, minimized eye-blinks, and stayed awake.

### 2.5. EEG preprocessing

The EEG data were preprocessed using the EEGLAB software (Delorme and Makeig 2004) and custom scripts in a MATLAB environment (R2016b, MathWorks, Inc., Natick, MA).

The continuous recordings were down-sampled to 128Hz, and then band-pass filtered to the range 1Hz-40Hz with a Hamming windowed sinc FIR filter (high pass followed by low pass). The continuous recordings then underwent an artifact correction process to remove oculomotor activity related to eye-blinks and saccades.

Eye blink removal was performed separately for each day's dataset (including all task periods) using the procedure described by Winkler et al. (2015). Following this procedure, a copy of

a dataset was first created which was then filtered with a high-pass 2 Hz filter. This duplicate dataset was visually inspected to remove data segments and EEG channels with artifacts related to repeated paroxysmal amplitudes changes (> 50μV), electromyographic contamination, electrical noise and signal loss. Next, the artifact-free data from all task-periods were segmented into 2s epochs. These epochs were then submitted to an Independent Components Analysis (ICA) decomposition using the infomax-ICA algorithm (implemented as *runica* in EEGLAB). To minimize inter-condition biases, ICA was performed on a balanced mixture of epochs from *RS1, TapWait, RS2* and *SeqWai*t. Epochs from the *TapMov* and *SeqMov* periods were excluded from this step to avoid movement-specific biases. The ICA weights obtained with the duplicate dataset were then transferred and applied to the original, non-filtered dataset. ICA components related to eye-blinks and saccades were then identified and removed using an automatic detection algorithm ADJUST (Mognon et al. 2011).

Following eye-blink correction, the original dataset was then again visually inspected to remove time periods and channels with artifacts. The signals in rejected channels were replaced with signals interpolated from other channels using spherical spline interpolation. All channels were then re-referenced to the Common Average Reference. Finally, the visually inspected continuous data were segmented into 2s epochs according to the six different experimental states: *RS1*, *RS2*, *TapWait*, *TapMov*, *SeqWait* and *SeqMov*. The epoch duration of 2s was heuristically selected to meet the tradeoff of (i) being short enough to obtain a sufficient number of samples for the machine-learning analysis (see section 2.6) while (ii) being long enough to obtain a suitable estimate of the power spectrum. Furthermore, this allowed epochs from the non-movement periods to match the 2s duration of the task-defined movement period.

For the two movement-related states (*TapMov* and *SeqMov),* epochs were defined from +0.25s to +2.25s following the visual cue to exclude initial transients and response-time delays following cue onset and to include residual movements in the period immediately following the cue offset. To avoid any carry-over effects from movement into the *TapWait* and *SeqWait* epochs, a

time interval of 500ms immediately prior to cue onset and 1000ms immediately following cue offset were excluded before segmenting the *TapWait* and *SeqWait* epochs. Furthermore, all *TapWait* and *SeqWait* epochs that contained button presses were excluded.

To establish face-validity of the task states based on their time-courses, we created a separate set of epochs from -1 to +3s relative to the onset of the visual cue. The signals were band-pass filtered in the $\beta$ frequency band (14-30Hz) and the signal amplitude was extracted using the Hilbert transform. After removing edge artifacts, the signal was normalized by calculating the percentage change in the signal relative to the mean amplitude in the pre-stimulus period [-898ms, 0ms]. After normalization, the signals were averaged across epochs, days and individuals.

### 2.6. Data quality assessment

Preprocessing resulted in 135 datasets (27 participants x 5 days). To be included in our analysis, each subject had to have completed the first three of the four tasks on all sessions and have at least 4 (out of 5) session-datasets that met the following data-quality criteria for analysis. We required a preprocessed dataset to have (i) less than seven rejected channels, (ii) $\geq$ 90 artifact-free epochs from both resting state periods (i.e., *RS1* and *RS2*), and (iii) $\geq$ 90 artifact-free epochs from the available resting-matched conditions (i.e., *TapWait, SeqWait*). Note that the number of epochs for *TapMov* and *SeqMov* were necessarily $\leq$ 60 as each task only had 60 response periods of 2s duration.

Datasets from 24 out of 27 participants met these data-quality criteria: 18 (of 24) had completed all 4 task-periods on each session and the remaining 6 (of the 24) participants had completed only the first 3 (of the 4 parts). To maintain uniformity in the statistical analyses, final analyses were performed only on the best 4 of the 5 session-datasets. For participants where all 5 datasets were of high quality, we excluded the first day's dataset as it might involve effects of initial familiarization. To maximize the use of the available data after these exclusions, analyses involving only *RS1* and *RS2* included data from 24 participants, while analyses involving any of the non-rest

tasks used data from 18 participants. For these 18 participants, the mean number of epochs per day in *TapMov* was 52.7 (min: 45.3, max: 57.7; SD = 2.9; minimum/day = 36) and in *SeqMov* was 53.4 (min: 49.2, max: 57.7; SD = 2.5; minimum/day = 42).

### 2.7. Feature specification: Oscillatory power spectrum

All classification analyses were based on a description of the oscillatory power spectrum on each 2-second epoch. Each epoch's power spectrum was described using 305 features that specified the power in five canonical frequency bands (δ: 1-3.5 Hz; θ: 4-7.5 Hz; α: 8-13.5 Hz; $\beta_1$ (low β): 14-22.5; $\beta_2$ (high β): 23-30 Hz) at each of the 61 channels.

These features were extracted with the procedure schematically displayed in Figure 2A. For each 2s epoch of EEG activity, the oscillatory power spectrum at each channel over the range of 1 to 30 Hz (0.5Hz resolution) was computed using the Fast Fourier Transform (FFT). The power at all frequencies within each band's frequency range was averaged to obtain the mean power per frequency band. The mean power per band was then logarithmically transformed (base 10) so that the resulting distribution across epochs had an approximate normal distribution. These five features (one per band) provided a minimal description of each channel's power spectrum. Finally, these five features from each channel were concatenated to obtain a single vector with 305 feature values (5 frequency bands x 61 channels). This extended feature set describing an epoch's power spectrum across the scalp was used for the classification analyses.

For detailed analyses, we defined subsets of the full feature set referred to here as the (i) mono-band and (ii) mono-location feature sets. Each *mono-band* feature set ($B_f$) consisted of features belonging to only one frequency band *f*. The five mono-band feature sets (each with 61 features) were $B_\delta$, $B_\theta$, $B_\alpha$, $B_{\beta 1}$ and $B_{\beta 2}$. Each *mono-location* feature set ($L_z$) (Figure 2A, top panel) consisted of features from 10 bilaterally symmetric channels in the spatial zone *z* on the scalp along the anterior-posterior axis. The four mono-location sets were defined at the frontal ($L_F$); fronto-central ($L_{FC}$), centro-parietal ($L_{CP}$) and parieto-occipital ($L_{PO}$) zones respectively.

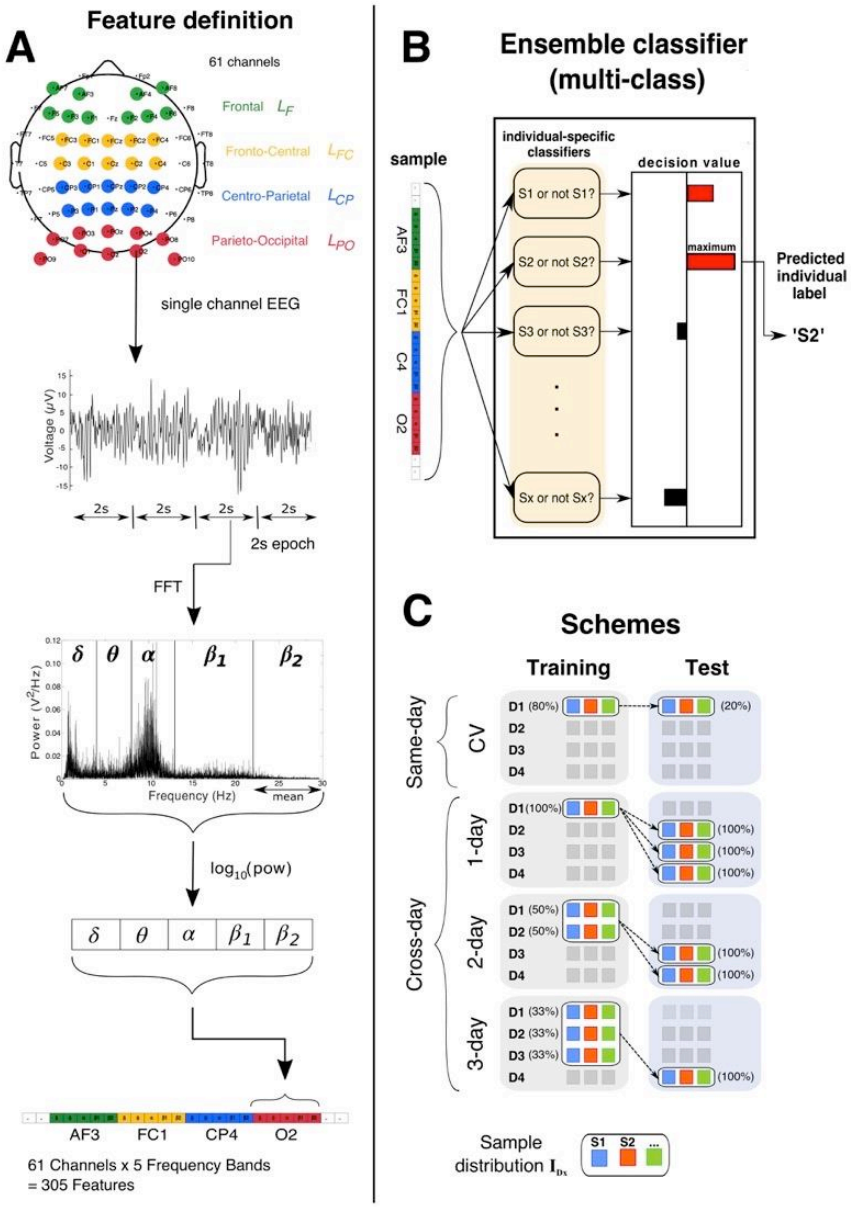


**Figure 2: Classification procedure. (A)** Feature definition pipeline**.** Channels in each mono-location subset are identified by color (green: $L_F$, yellow: $L_{FC}$, blue: $L_{CP}$, red: $L_{PO}$). The continuous signal from each channel was segmented into 2s epochs followed by an estimation of the frequency spectrum with the Fast Fourier Transform (FFT). The mean power within each of the five bands was log transformed (base 10) and concatenated with corresponding values from all other channels to obtain a feature vector. **(B)** Schematic of a multiclass decision with an ensemble of individual-specific binary classifiers. Each classifier evaluates the sample (*Sx* or not-*Sx*) to output a decision-value (red bars > 0, black bars < 0) and the classifier with the maximum decision value was the predicted label (here, S2). **(C)** Classification schemes ${}^{A}\mathbf{I}_{Dx} \rightarrow {}^{A}\mathbf{I}_{Dy}$ (rows) were defined by the configuration of training (left column) and test sets (right column) (where **Di** denotes samples from day *i*). The sample distribution ($\mathbf{I}_{Dx}$) had samples from all individuals (multi-colored boxes). Percentages indicate the proportion of each day's samples used for training/testing. Same-day identification was estimated with 5-fold cross-validation (CV). The training set for cross-day aggregation had an equal proportion of samples from each day and the total number of training samples was the same across aggregation levels.

## 2.8. Multi-class classification

### *2.8.1. Definition*

All classification models were numerically estimated using a soft-margin linear Support Vector Machine (SVM, with *L2* regularization) algorithm as implemented by the *LinearSVC* package in the *scikit-learn* library (Pedregosa et al. 2011) implemented in Python 3.6. SVM learning was initialized with parameters (tolerance = $10^{-5}$, max iterations =$10^4$, hinge loss, balanced class weighting). The hyper-parameter *C* had a value of 1, which has been shown to be a reasonable default for M/EEG classification (Varoquaux et al. 2017). For our data, tuning *C*'s value seemed to produce only marginal changes to the classification accuracies (results not shown).

As defined above, each epoch was a 2-second sample of the ongoing oscillatory activity from one person (of 24) on one specific day (of 4) engaged in a particular task state (of 6 possible states: true rest {*RS1*, *RS2*}, pseudo-rest {*TapWait, SeqWait*}, non-rest {*TapMov, SeqMov*}). The classification analyses involved predicting an epoch's origin either by (i) a person's identity or (ii) task-state. Multi-class classifiers (using an ensemble of binary classifiers) were used for person identification as described below. Standalone binary classifiers were used to distinguish alternative task-states within the same person.

The input to a multi-class classifier (see Figure 2B) was a single sample (i.e., epoch) from an unspecified person $S_x$ in the studied group and the required output was the predicted identity of that person (e.g., $S_2$). The multi-class classifiers used here employed a *one-vs-all* scheme (as implemented by *scikit-learn*). Specifically, an *N*-class classifier ($N \geq 2$) consisted of an ensemble of *N* binary-classifiers. Each of these binary classifiers was independently trained to distinguish whether a sample was from one specific person (e.g., $S_2$) or from any of the other *N-1* persons (i.e., not $S_2$). Therefore, each individual was associated with a unique classifier in the ensemble. To obtain a classification with such an ensemble, each sample was separately evaluated by each of the *N* binary-classifiers to obtain a decision value from each classifier (i.e., the signed distance to the separation hyperplane (Rifkin and Klautau 2004)). These decision values were compared and the

final classification was assigned to the binary classifier with the maximum decision value.

### *2.8.2. Accuracy scoring*

Even though an ensemble was used for multi-class classification, our interest was in the accuracy of each individual-specific binary classifier in the ensemble. To obtain a measure of classification accuracy of each individual classifier from the ensemble classification accuracy, we defined the accuracy $a_i$ of the classifier for person $S_i$ as

$$a_i = \frac{1}{2}(H_i + CR_i)$$

where $H_i$ denotes the hit rate (i.e., positive identification rate) of the classifier and $CR_i$ denotes the correct rejection rate. The hit rate $H_i$ was the proportion of instances where samples from $S_i$ were correctly predicted as being from $S_i$ by the ensemble (i.e., a true positive where the classifier $S_i$ had a larger decision value than the competing classifiers). Correct rejection was defined based on the pair-wise relationship of $S_i$ to each of the other classifiers $S_j$. If the ensemble (incorrectly) predicts $S_i$ for a sample from a different person $S_j$ then it implies that the classifier $S_i$ (incorrectly) had a larger decision value than the competing classifiers, i.e., a false positive. The false positive rate $FP_{i,j}$ denotes the proportion of instances where samples from $S_j$ were incorrectly predicted as being from $S_i$ by the ensemble. The correct rejection $CR_{i,j}$ was defined as $CR_{i,j} = 1 - FP_{i,j}$. Based on this rationale, the overall correct rejection $CR_i$ for $S_i$ was defined as the mean of the pair-wise correct rejection rates

$$CR_i = \frac{1}{N-1}\sum_{j=1}^{N} CR_{i,j} \text{ where j} \neq i$$

With this formulation, random chance for each classifier was 50% even though random chance for the entire ensemble was $(100/N)\%$.

To identify individuals who were frequently misclassified (i.e., confused) with each other, we report confusion matrices for cross-day classification. In this confusion matrix, the rows

represent the true label of a sample and the columns indicate the predicted label for that sample by the ensemble. The value for the row corresponding to individual $S_i$ and column corresponding to individual $S_j$ indicated the proportion of samples from $S_i$ that were classified as $S_j$. The rows/columns of the matrices were re-organized to cluster together individuals who were confused with each other. This was implemented with the so-called Louvain method to maximize modularity (Blondel et al. 2008), implemented in the Community Detection Toolbox (Kehagias 2021).

The accuracy score can have different contributions from the hit-rate (e.g., high false negatives) and the correct rejection rate (e.g., high false positives). To disentangle these contributions, we estimated the *recall* and *precision* scores from the confusion matrix (Davis and Goadrich 2006). The *recall* score for individual $S_i$ is the ratio (True Positives)/(True Positives + False negatives). The recall score for $S_i$ would be low if samples from $S_i$ are misclassified as belonging to another individual (i.e., false negatives). The precision score for individual $S_i$ is the ratio (True Positives)/(True positives + False positives). The precision score for $S_i$ would be low if samples from other individuals are misclassified as belonging to $S_i$ (i.e., false positives).

### *2.8.3. Training and testing schemes*

Classification was defined by the samples used for training and testing. Irrespective of classifier type (multi-class or standalone binary classifier), the training data were always balanced, (i.e., having an equal number of samples per class) to avoid biases arising from imbalanced classes (Abraham and Elrahman 2013).

Person (multi-class) identification was organized into two schemes based on whether the training and test samples belonged to the (i) same day (namely, same-day vs cross-day identification) and the (ii) same task (namely, same-task vs cross-task identification). A schematic of the same-day/cross-day schemes are shown in (Figure 2C). For convenience, we use the following notational convention to describe these classification schemes. As multi-class classification involves an ensemble decision, it involves the conjoint influence of the sample

distributions from multiple persons. This combined distribution on a particular state (e.g., *RS1*) on day *d* is denoted as ${}^{RS1}\mathbf{I}_d$. A classification scheme where a decision-rule is trained on samples from ${}^{A}\mathbf{I}_p$ (i.e., from task state *A* on day *p*) and tested on samples from ${}^{B}\mathbf{I}_q$ (i.e., from state *B* on day *q*) is denoted as ${}^{A}\mathbf{I}_p \rightarrow {}^{B}\mathbf{I}_q$. Similarly, a classification scheme where a decision-rule was trained on samples aggregated from different days (e.g., ${}^{A}\mathbf{I}_p$ and ${}^{A}\mathbf{I}_q$) and tested on ${}^{B}\mathbf{I}_r$. is denoted as ${}^{A}\mathbf{I}_p \circ {}^{A}\mathbf{I}_q \rightarrow {}^{B}\mathbf{I}_r$. (see below).

*Same-day/same-task identification:* The accuracy of same-day person identification in task state *A* (${}^{A}\mathbf{I}_p \rightarrow {}^{A}\mathbf{I}_p$) was estimated using a 5-fold cross-validation (CV) procedure (Blum et al. 1999). Specifically, the set of samples from state *A* on one day (for example, day D1 in Figure 2C, upper row), were partitioned into 5 equal folds. Training was performed on four folds (80% of the sample set) and tested on the left-out fifth fold (the remaining 20%). This training-testing procedure was repeated so that each fold was used as a test-set once. The mean classification accuracy across folds was defined as the same-day identification accuracy for that day. In this manner, the CV accuracy was estimated separately for each of the four days and the mean CV accuracy across days was denoted as the same-day accuracy for task state *A*.

*Cross-day/same-task identification:* For cross-day identification in task state *A* (${}^{A}\mathbf{I}_p \rightarrow {}^{A}\mathbf{I}_q$), samples in the test set were from a different day than the samples in the training set. We modulated the training set's day-specificity by aggregating samples from different days in a stratified manner. In an *n*-day training set, the *k* training samples per person consisted of *k*/*n* samples from each of *n* different days. Here, *n* could take three possible values, namely, 1, 2 or 3 (see Figure 2C, first column). The number of samples per person, *k*, was held constant to enable comparison of classification accuracy across all values of *n*. Irrespective of the extent of aggregation in the training set, samples in the test-set were never aggregated from different days. Mean identification accuracy for a particular *n*-day aggregation scheme (e.g., ${}^{A}\mathbf{I}_{d1} \circ {}^{A}\mathbf{I}_{d2} \ldots {}^{A}\mathbf{I}_{dn} \rightarrow {}^{A}\mathbf{I}_r$.) was obtained by (i) independently estimating the accuracy for each possible training/test-set combination that satisfied the day constraints (e.g., day $p \neq$ day $q \neq$ day $r$) and then (ii) averaging these accuracy values.

*Cross-task identification:* This was treated as a special instance of cross-day identification. For example, the accuracy for the configuration ${}^{A}\mathbf{I}_p \rightarrow {}^{B}\mathbf{I}_q$ was estimated by replacing the test set with samples from state *B* while retaining all other day-related constraints as in cross-day/same-task identification. Unless specified otherwise, cross-task identification was always tested across days, that is, the training and test sets were always from different days. This was done to exclude potential inter-state similarities that might be present due to the joint preprocessing of data from all states within the same day (see section 2.5).

### *2.8.4. Classification schemes: Interpretation of accuracy relationships*

The same-day accuracy for a particular state was treated as a pre-condition to estimate the cross-day identification accuracy for that state. If same-day accuracy were greater than random chance, it would confirm that the distribution from which the training set was drawn contained sufficient information to allow identification in the absence of potential inter-day changes. Cross-day accuracy is reported and interpreted here only if this pre-condition was satisfied.

Based on this pre-condition, a reduction in cross-day (1-day) accuracy (e.g., ${}^{A}\mathbf{I}_p \rightarrow {}^{A}\mathbf{I}_q$) relative to same-day accuracy (e.g., ${}^{A}\mathbf{I}_p \rightarrow {}^{A}\mathbf{I}_p$) can be attributed to a systematic difference in the distributions ${}^{A}\mathbf{I}_p$ and ${}^{A}\mathbf{I}_q$ between days (red arrow, Figure 3A). Aggregation was used to evaluate the source of this cross-day accuracy reduction by varying the statistical properties of the training set (i.e., by aggregating samples across days) while holding the properties of the test set constant. Specifically, we assumed aggregation would lead to decision-rules that discount day-specific properties in favor of day-general properties. Therefore, depending on the relative roles of day-specific/general properties in the classification decision, the cross-day accuracy might stay constant, increase or decrease with increasing aggregation (Figure 3A).

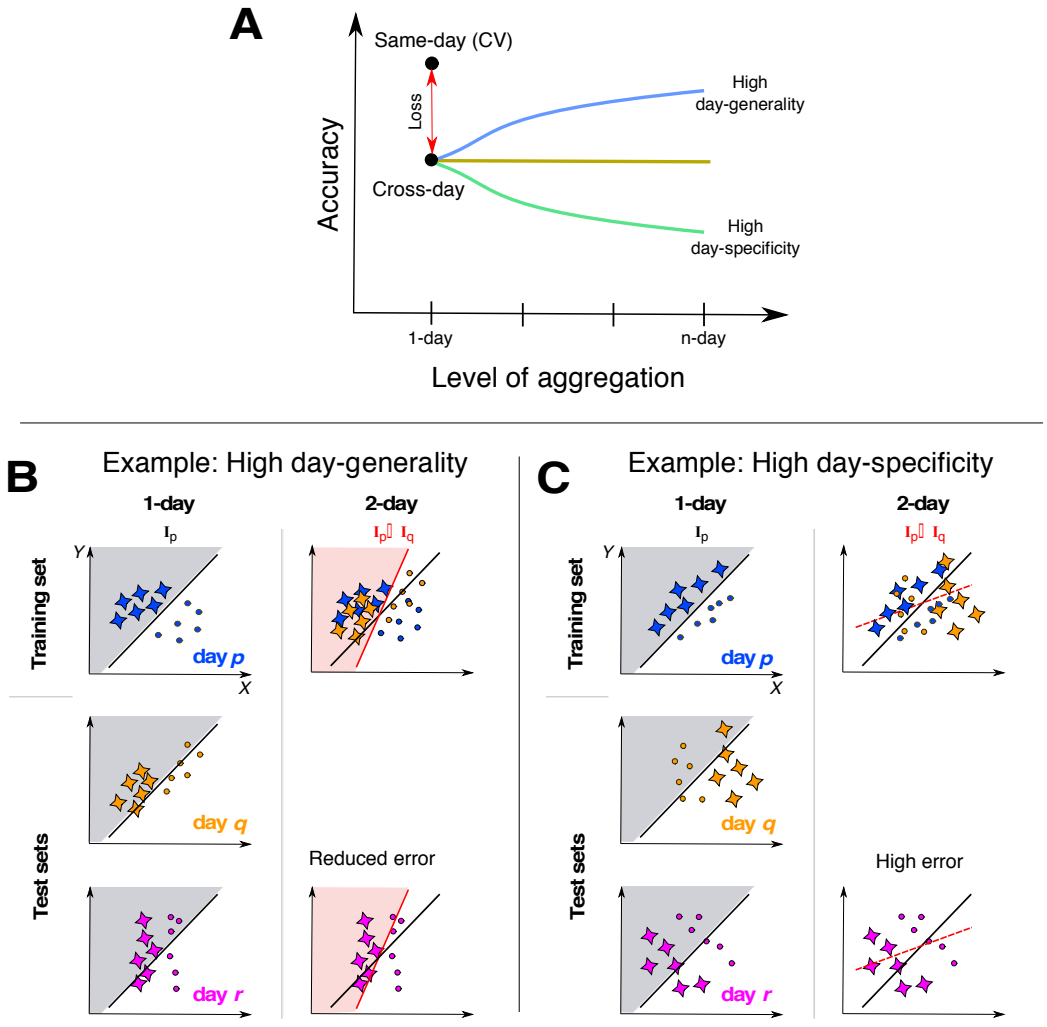


**Figure 3: Effect of aggregation. (A)** Schematic of relationship between same-day and cross-day identification accuracy. Cross-day (1-day) accuracy can be lower than same-day accuracy (red-arrow) due to day-specificity of the decision-rule. Training decision-rules on aggregated samples (y-axis) can change cross-day accuracy, which could increase (blue, see panel **B**), or stay constant (dark green), or even decrease (light green, see panel **C**). **(B)** Idealized example of how cross-day accuracy (column 1) can increase with aggregation (column 2) due to day-general information. Samples from two classes (stars, circles) are shown along two features (day-general: *X*, day-specific: *Y*) with each day's samples shown in different colors (*p*: blue, *q*: orange, *r:* purple). The 1-day decision-rule ($\mathbf{I}_p$) (top left panel) is depicted with thick black line and shaded areas. This decision-rule can successfully classify samples from days *q* and *r* but with some errors. However, a decision-rule trained on data from days *p* and *q* ($\mathbf{I}_p \circ \mathbf{I}_q$) (thick red line, red shaded area) reduces cross-day classification errors (lower right). **(C)** Idealized example of high day-specificity. Even though the classes are separable within each day, the 1-day decision-rule ($\mathbf{I}_p$) has a poor cross-day accuracy (column 1). 2-day training (column 2) produces a decision-rule with worse classification both on the training set itself (dotted red line) as well as across days (lower right).

Figures 3B and 3C show idealized examples of how aggregation could both increase as well as decrease cross-day accuracy. In the example shown in Figure 3B, the two classes systematically differ on feature *X* (x-axis) but with an inconsistent role for feature *Y* (y-axis). Due to incidental day-specific variation, feature *Y* has a role in distinguishing the classes on day *p* but not on other days. Consequently, a decision-rule trained on day *p* does not effectively separate the classes on other days (column 1). However, training on aggregation samples from day *p* and *q* (column 2) reduces *Y*'s role in the aggregated decision-rule leading to an improved separation of the classes across days. Figure 3C illustrates an extreme example of day-specificity where the two features have a conjoint relationship allowing classification within each day but with low generality across days. Therefore, training on samples aggregated from day *p* and *q* leads to an overall reduction in accuracy on the training set itself as well across days.

### *2.8.5. Weights and normalized weights*

The characteristic weights for a particular classification scheme (e.g., ${}^{A}\mathbf{I}_p \rightarrow {}^{A}\mathbf{I}_q$) were obtained by averaging the weights across all training sets. In a multiclass classifier, the decision-rules are organized in a winner-take-all competition to label each sample (Figure 2B). Therefore, for each sample to be uniquely assigned to only one person, the person-specific classifiers in the ensemble necessarily require different decision-rules. This difference in decision-rules might only be in the sign (positive/negative) assigned to the weights. Therefore, for all weight-related analyses, the absolute values of the weights were used in order to allow inter-individual comparisons.

To identify the high-consistency weights, the absolute weights were z-scored across all features for each subject to retain information about inter-feature weight differences in the statistical tests. However, this "raw" weight measure does not account for power differences. For features *i* and *j,* the weight $|w_i|$ might be greater than $|w_j|$ while the power $|P_i|$ might be less than $|P_j|$. Consequently, neither the relationship between the weights nor the power are reliable indicators of the relative influence of *i* and *j* on the eventual classification decision. Therefore, we defined a

feature $i$'s unit weight $\overline{w}_i$ as the idealized weight value such that $\overline{w}_i P_i = 1$. The normalized weight was thus defined as the ratio $w_i/\overline{w}_i$, which was effectively equal to $w_i P_i$. Due to the characteristic differences in power between bands, for statistical comparisons, the absolute normalized weights (i.e., |w*P|) were z-scored within each band for each subject.

### 2.9. Statistical Analysis

The relative differences in the accuracy of different classification schemes were assessed by performing paired t-tests, repeated measures one-way or two-way analysis of variance (ANOVA) implemented by the pingouin python package (version 0.3.2) (Vallat 2018).

The random chance accuracy for the multi-class and standalone binary classifier was 50% and accuracy deviations from random chance were evaluated with one-sample t-tests. The Bonferroni threshold was used to correct for multiple comparisons. Due to the sequential relationship between the different multiclass classification schemes, following Figure 3A, the tests for same-day accuracy (CV) and cross-day accuracy were planned tests that were considered significant at a threshold of $p < 0.05$. The tests for 2-day and 3-day aggregation were evaluated at a threshold of $p < (0.05/2)$. For tests for the mono-band and mono-location sets, the thresholds were further corrected for the number of feature sets. Correlations between individual accuracy values were evaluated using Spearman's rank correlation due to the focus on relative ordering rather than a strict cardinal relationship.

Two kinds of error-bars are used in the plots. For plots depicting variable changes due to a single-factor, error bars indicate the standard deviation (SD). Plots depicting multi-factor changes use error bars displaying the within-subject standard error (s.e.m.) (O'Brien and Cousineau 2014). The type of error-bar used is explicitly noted in the figure caption.

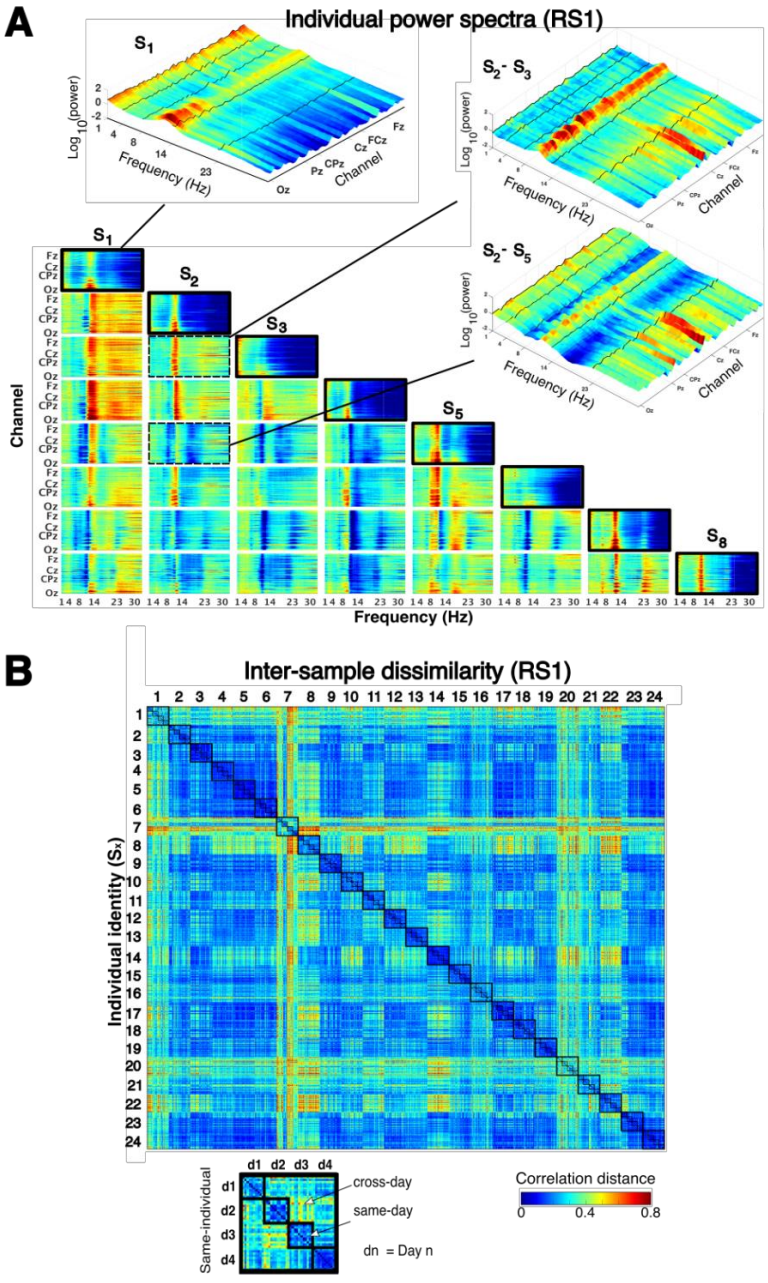


**Figure 4: Inter-individual and inter-day differences. (A)** Matrix showing the oscillatory (full) power spectra in *RS1* at all channels (averaged across samples and days) for 8 selected individuals ($S_i$, diagonal, thick black boundary) and their pair-wise differences. The difference in power spectra for each pair of individuals $S_i$ and $S_j$ (i.e., $S_i - S_j$) is shown at row $i$, column $j$ of matrix. In each spectrogram, channels have a posterior-to-anterior ordering. Insets show magnified view of the power spectrum for $S_1$ (left upper) and differences for $S_2 - S_3$ (right upper) and $S_2 - S_5$ (right lower), with frequency band boundaries marked with black lines. **(B)** Inter-sample dissimilarity matrix for *RS1* (90 samples per individual per day, each sample was defined by 305 features = 61 channels x 5 bands). The dissimilarity of two samples was defined by their correlation distance (= 1 - $r$, where $r$ is the Pearson's correlation coefficient). Large black squares on diagonal contain values from the same individual, and the four smaller squares each contain same-day values.

## 3. RESULTS

### 3.1. Face-validity of individual power spectra

Our investigation assumed that an individual's power spectrum at rest can systematically (i) differ between days, and also (ii) differ from the spectra of other individuals. We first confirmed the face-validity of these assumptions in our data.

The structured inter-individual differences during *RS1* were qualitatively evident from the mean (full) power spectrum at different channels (Figure 4A) before its reduction to the minimal description used for the classification analyses. As shown for one example individual $S_1$, individual power spectra had a similar form across channels with a higher power in the δ and α bands and a higher overall power in the posterior and anterior channels relative to the central channels. These individual spectra also showed prominent pair-wise differences as illustrated for a few selected individuals. The diverse varieties of inter-individual differences highlight the difficulty of representing an individual's unique properties as illustrated for individual $S_2$. The combination of channels and frequencies (i.e., features) at which $S_2$ and $S_3$ showed prominent differences were not the same features at which $S_2$ differed from $S_5$. However, the required decision-rule to identify $S_2$ was a single feature configuration capable of distinguishing $S_2$ from *all* others while allowing $S_2$ to be re-identified across days, despite inter-day variations.

The systematic inter-day differences were evident from the dissimilarity between samples from all participants and all days (90 samples per participant per day) (Figure 4B). The dissimilarity between any two samples was described by their correlation distance (= 1 - $r$, where $r$ is the Pearson's correlation coefficient)(Diedrichsen and Kriegeskorte 2017; Dimsdale-Zucker and Ranganath 2019; Pani et al. 2020). For all 24 participants, the mean dissimilarity between samples from the *same day* was lower than between samples from different days (*cross-day*) [$t_{23} = -6.74$, $p < 0.0001$]. However, the dissimilarity between same-day and cross-day samples varied from person to person suggesting their possible confusability with samples from other individuals. This was the

critical issue to be resolved with an appropriate decision-rule, to be identified using machine-learning.

### 3.2. Identification of individuals from RS activity within and across days

#### *3.2.1. High same-day accuracy but reduced cross-day accuracy of individual decision-rules*

To identify a person from a 2s sample of RS activity with an ensemble classifier, a decision-rule was numerically estimated to represent each person's unique RS characteristics. The decision-rules estimated for each day could identify each person (of 24) from a sample acquired on the same day (i.e., according to the scheme ${}^{RS1}\mathbf{I}_p \rightarrow {}^{RS1}\mathbf{I}_p$) with a mean cross-validated (CV) accuracy of 99.98 ± 0.04% (mean ± sd) that was significantly larger than the theoretically expected accuracy for random guessing [> 50%: $t_{23}$ = 5596.13, p < 0.00001] (Figure 5A, Table A.1). However, for longitudinal tracking, a key demand is that decision-rules from one day should identify a person from samples acquired on a different day (i.e., ${}^{RS1}\mathbf{I}_p \rightarrow {}^{RS1}\mathbf{I}_q$). The same-day decision-rules identified individuals across days with a mean accuracy of 92.10% ± 6.8% that was higher than random chance [$t_{23}$ = 30.14, $p$ < 0.00001] but less accurate than same-day identification by ~8% [paired $t_{23}$ = 5.64, $p$ = 0.00001].

The confusion matrix (Figure 5B) of how individuals were misclassified during cross-day (1-day) identification revealed four clusters of individuals who were confused with each other. Notably, the individuals with the lowest cross-day accuracies (namely, $S_2$, $S_{11}$, $S_{15}$, $S_{24}$) belonged to different clusters rather than being solely confused with each other. The clustering of misclassified individuals suggested that errors in identifying an individual $S_X$ were due to a combination of (i) changes to $S_X$'s RS-activity between days (i.e., false negatives) and (ii) changes to other individuals who were then misclassified as $S_X$ (i.e., false positives). Nevertheless, the increased errors in individual identification illustrate the challenge of *NP+/NP-* decisions. Errors in identifying a person $S_X$ across days seemingly imply that $S_X$*'s* unique identifying characteristics had changed

across days even though the individuals here were unlikely to have changed in their underlying neurophysiology over the 5-day testing period.

### *3.2.2. Aggregated training increases cross-day accuracy*

In numerical terms, the cross-day loss in accuracy implies that certain properties of each day's decision-rules were of predictive relevance to same-day samples but of limited generality to other days. To discount the role of these day-specific properties in favor of day-general properties, the decision-rules were trained using samples aggregated from *multiple* days (i.e., ${}^{RS1}\mathbf{I}_p \circ {}^{RS1}\mathbf{I}_q \ldots \rightarrow {}^{RS1}\mathbf{I}_s$) (Figure 5A). The mean cross-day accuracy *increased* from 92.10% ± 6.8% without aggregation (1-day) to 95.93 ± 3.63% with 2-day aggregation, with an additional increase to 97.39% ± 2.65% with 3-day aggregation [one-way ANOVA, $F_{2,46} = 28.83$, $p < 0.00001$]. Following aggregation, the cross-day accuracy was a mere ~2% lower than the same-day accuracy. The effects of aggregated training on individual-specific identification errors are shown in Figure 5C. The decision-rules obtained with 3-day aggregation were associated with fewer false negatives (indexed by the higher recall score) especially for individuals with the lowest 1-day accuracies, i.e., $S_2$, $S_{11}$, $S_{15}$ and $S_{24}$. This was associated with interrelated changes in errors in individuals who belonged to the same cluster. For example, there was a prominent reduction in false positives (indexed by the higher precision score) for $S_{17}$ who was in the same cluster $S_{24}$ and $S_{23}$ (highlighted in green). The increased accuracy with aggregation despite the true inter-day differences in RS-activity was consistent with the presence of *day-general* properties (section 2.8.4, Figure 3).

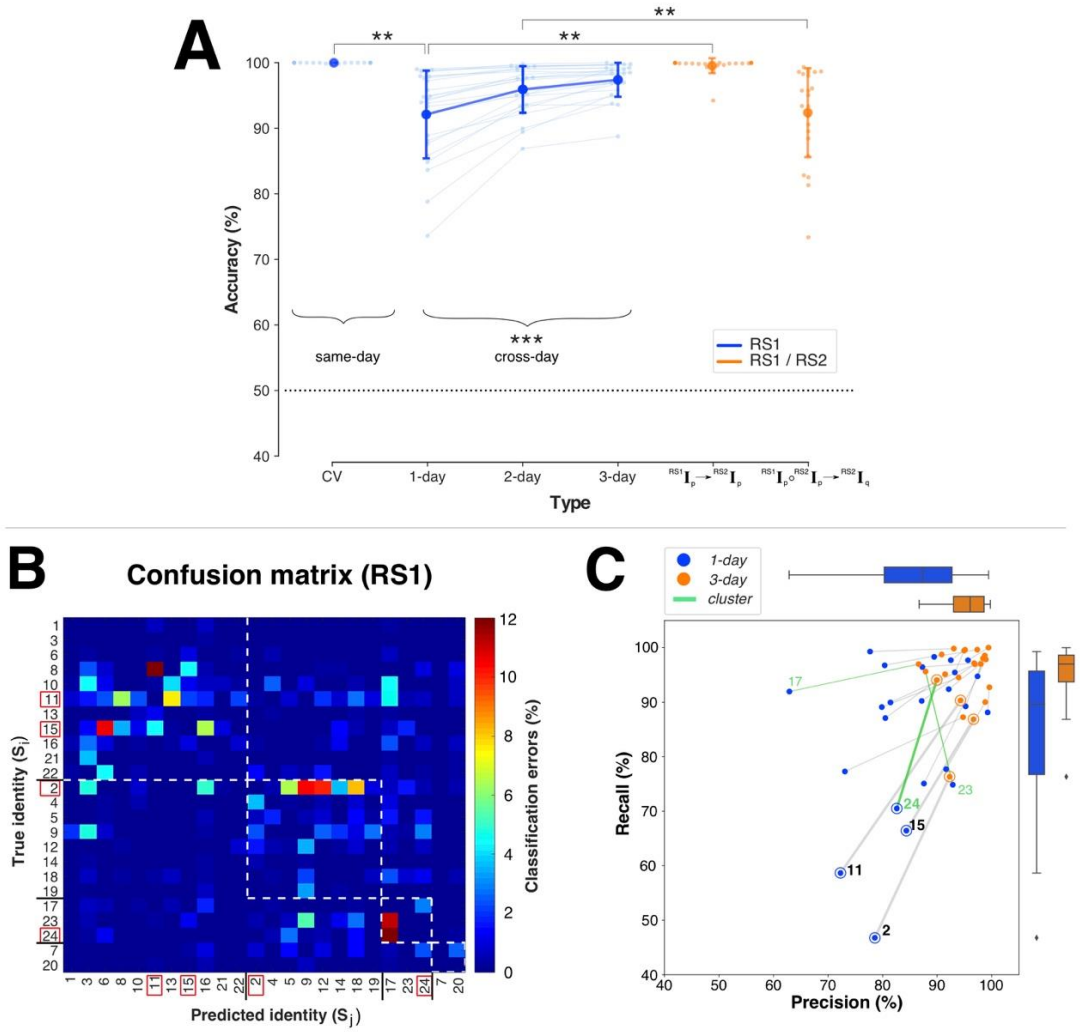


**Figure 5: Identification accuracy at rest. (A)** Mean identification accuracy with *RS1* (blue) on same-day (CV), across days (1-day, 2-day, 3-day), and schemes relating *RS1* and *RS2* (orange). Light colored dots/lines depict individual accuracies (*N*=24). Horizontal dotted line depicts random chance accuracy (50%). Error bars: SD (** = 0.00001 ≤ $p$ < 0.001; *** = $p$ < 0.00001). **(B)** Confusion matrix for cross-day (1-day) identification (only errors are shown). Dotted squares indicate clusters of individuals who are more confused with each other. Identities of individuals with the lowest cross-day accuracies are highlighted with red squares. **(C)** Changes to precision and recall scores with aggregation for the whole group (shown with boxplots) and for individuals (1-day: blue dots, 3-day: orange dots). Individuals with lowest 1-day accuracy are indicated with rings and thick gray lines. Green lines highlight $S_{24}$, $S_{23}$ and $S_{17}$ who belong to the same cluster, shown in **(B).**

### *3.2.3. Cross-day versus cross-measurement identification are not equivalent*

We next assessed whether the above accuracy relationships across days (with and without aggregation) was related to a difference in *days* rather than simply a difference in *measurements*.

In our experimental protocol (Figure 1A), *RS2* was the second RS measurement on each day. The effects of aggregation on cross-day identification with *RS1* were successfully replicated on *RS2* without statistically detectable differences (Table A.1) [two-way ANOVA, Condition {*RS1, RS2*} x Type {1-day, 2-day, 3-day}, Type*Condition: $F_{2, 46} = 0.56$, $p = 0.57$; Type: $F_{2, 46} = 31.31$, $p < 0.00001$; Condition: $F_{1, 23} = 0.38$, $p = 0.54$]. Importantly, *RS2* validated the *day-specific* properties of the decision-rules (Figure 5A). Same-day decision-rules from *RS1* classified samples of *RS2* from the same day (${}^{RS1}\mathbf{I}_p \rightarrow {}^{RS2}\mathbf{I}_p$) with a mean accuracy of 99.55 ± 1.15% that was significantly greater than the accuracy in classifying *RS1* across days (${}^{RS1}\mathbf{I}_p \rightarrow {}^{RS1}\mathbf{I}_q$) (92.10 ± 6.84%) [paired $t_{23} = 5.19$, $p = 0.00003$]. Furthermore, *RS2* validated the importance of aggregating samples from different days (rather than different measurements) to reduce day-specificity. Decision-rules trained on aggregated same-day samples from *RS1* and *RS2* (${}^{RS1}\mathbf{I}_p \circ {}^{RS2}\mathbf{I}_p \rightarrow {}^{RS1}\mathbf{I}_r$) had a *lower* cross-day accuracy (92.38 ± 6.92%) than decision-rules trained on aggregated *RS1* samples from two different days (${}^{RS1}\mathbf{I}_p \circ {}^{RS1}\mathbf{I}_q \rightarrow {}^{RS1}\mathbf{I}_r$) (95.93 ± 3.63 %) [paired $t_{23}=-4.83$, $p = 0.00007$].

In summary, the reduction in cross-day accuracy without aggregation was indicative of *inter-day* (rather than inter-measurement) variations in RS activity. Despite this inter-day variation in RS activity, the cross-day accuracy increased with aggregation and further revealed the existence of *day-general* properties in RS-activity that were unchanged across days. These properties were consistent with an activity configuration that was putatively defined by individual-specific neurophysiological constraints.

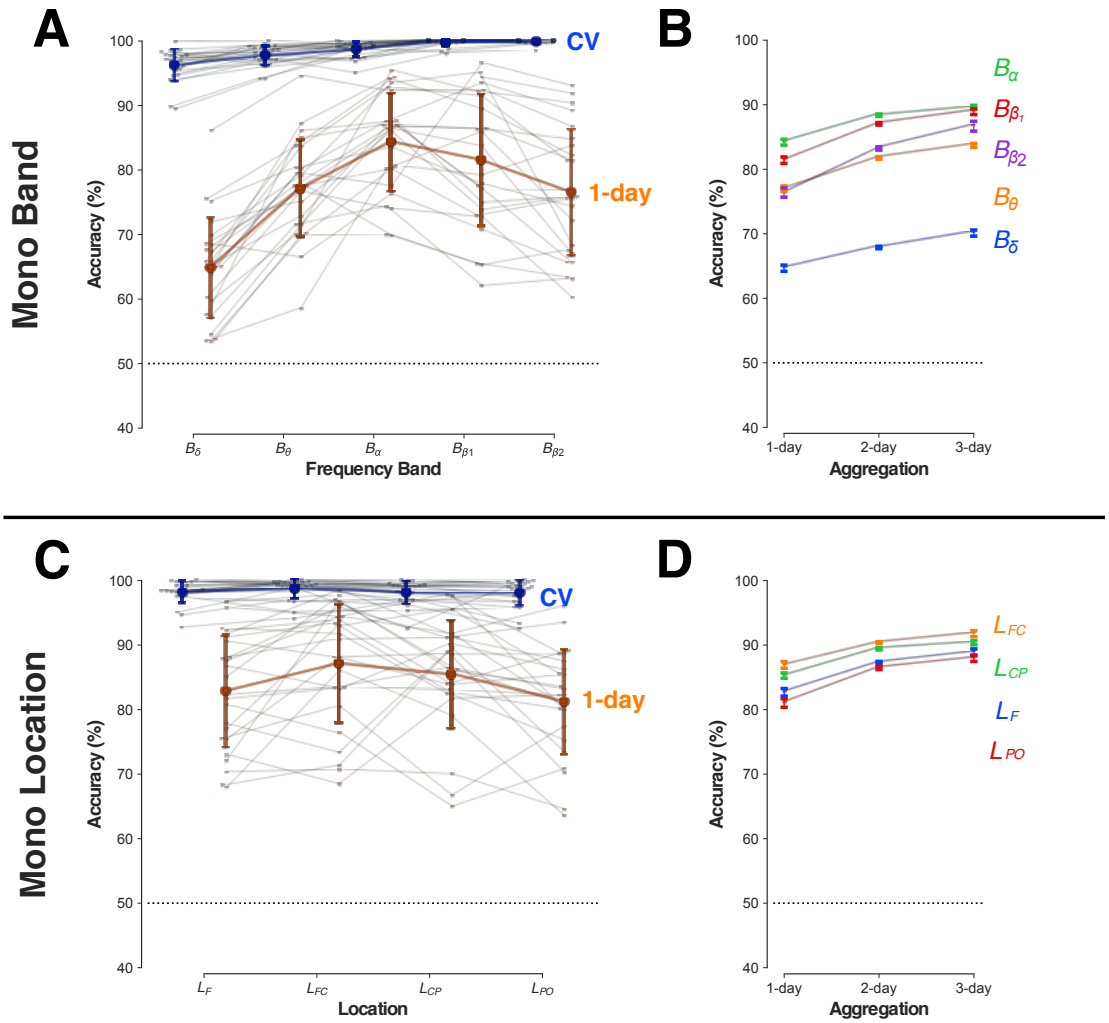


**Figure 6: Identification at rest with mono-band/location feature subsets. (A)** Mean identification accuracy for *RS1* with mono-band feature sets of increasing frequency (x-axis) on the same-day (blue, CV) and across-days (orange, 1-day). Light-colored dots/lines depict individual accuracies (*N*=24*)*. Error bars: SD. **(B)** Change in cross-day identification with increasing aggregation (x-axis) for different mono-band feature subsets (colored lines). Error bars: Within-subject s.e.m. (O'Brien and Cousineau 2014). **(C)** Mean identification accuracy for mono-location feature sets (x-axis, from anterior to posterior) with graphical representation and error bars as in panel **A**. **(D)** Change in cross-day identification with increasing aggregation (x-axis) for different mono-location feature subsets (colored lines). Error bars: Within-subject s.e.m. Horizontal dotted lines depicts the random chance accuracy (50%) in all panels.

### 3.3. Information organization in resting activity enabling individual identification

The hypothesized configuration in RS-activity was suggestive of a multivariate relationship between distributed features. However, the accuracy relationships described above do not indicate whether such a distributed configuration was necessary to enable individual identification. Therefore, we evaluated the information organization required for individual identification.

#### *3.3.1. Low cross-day identification with information from only one frequency or one location*

Each sample was a snapshot of RS activity described by 305 informational features (5 bands x 61 channels). To test the informational role of these different features, we evaluated whether identification comparable to the full feature-set was possible with subsets of features that were defined either by frequency band (i.e., mono-band sets) or spatial location (i.e., mono-location sets).

Each *mono-band* feature set ($B_f$) consisted of features from one frequency band $f$ at all 61 channels. For all five mono-band sets (Figure 6A, Table A.2), same-day identification had a mean accuracy greater than 95%. However, the size of the cross-day loss in accuracy was band-dependent and ranged from ~14% for $B_\alpha$ to nearly ~32% for $B_\delta$ [ANOVA, Type {CV, 1-day} x Band {$B_\delta$, $B_\theta$, $B_\alpha$, $B_{\beta 1}$, $B_{\beta 2}$}, Type*Band: $F_{4,92} = 24.83$, $p < 0.00001$; Type: $F_{1,23} = 232.11$, $p < 0.00001$; Band: $F_{4,92} = 40.30$, $p < 0.00001$]. The divergence in cross-day losses for $B_\alpha$ and $B_\delta$ was striking as these two bands have a characteristically higher power relative to the other bands (Figure 4). Training with multi-day aggregation (Figure 6B) increased cross-day accuracy by differing amounts for each band by, for example, +10% for $B_{\beta 2}$ but only +6% for $B_\delta$ [ANOVA, Band {$B_\delta$, $B_\theta$, $B_\alpha$, $B_{\beta 1}$, $B_{\beta 2}$}x Type {*1-day, 2-day, 3-day*}, Type*Band: $F_{8,184} = 9.19$, $p < 0.00001$; Type: $F_{2,46} = 146.02$, $p < 0.00001$; Band: $F_{4,92} = 43.13$, $p < 0.00001$]. However, even with 3-day aggregation, the residual difference between cross-day and same-day accuracy (minimum: ~7% for $B_\alpha$, maximum: ~26% for $B_\delta$) was larger than the ~2% difference with the full feature-set.

Each *mono-location* feature set ($L_z$) consisted of 50 features (5 bands x 10 channels) in the spatial zone $z$ (Figure 2A). The mean same-day accuracy was greater than 95% for all mono-

location feature sets (Figure 6C, Table A.2). However, the mean cross-day (1-day) accuracy showed reductions of ~12%-16% for all locations [ANOVA, Type {CV, 1-day} x Location {$L_F$, $L_{FC}$, $L_{CP}$, $L_{PO}$}, Type*Location: $F_{3,69} = 3.77$, $p = 0.015$; Type: $F_{1,23} = 108.91$, $p < 0.00001$; Location: $F_{3,69} = 5.45$, $p = 0.0020$]. The mean cross-day accuracy for the fronto-central ($L_{FC}$) and centro-parietal ($L_{CP}$) sets were marginally higher than for the parieto-occipital ($L_{PO}$) and frontal ($L_F$) sets. This zonal accuracy difference was notable as the mean power for all bands was typically higher over the posterior and anterior channels than the centrally located channels (Figure 4A). Aggregation increased cross-day accuracy by ~6% for all four location sets (Figure 6D) [ANOVA, Location: {$L_F$, $L_{FC}$, $L_{CP}$, $L_{PO}$} x Type {*1-day, 2-day, 3-day*} [Type*Location: $F_{6,138} = 2.07$, $p = 0.06$; Type: $F_{2,46} = 115.38$, $p < 0.00001$; Location: $F_{3,69} = 4.79$, $p = 0.0043$]. Nevertheless, the residual ~7%-10% loss in cross-day accuracy was larger than with the full feature-set.

In summary, all the mono-band and mono-location sets contained sufficient information to enable same-day identification with nearly error-free accuracy. However, this information had a low day-generality. Even with aggregation, these feature sets had a much lower cross-day accuracy than the full feature-set that combined these feature sets together. This is notable with regard to machine learning algorithms. Generalization accuracy can reduce with an increase in the number of features (the so called Hughes effect (Campenhout 1978; Sima and Dougherty 2008)). However, here, a feature set of 305 features showed greater cross-day generalization than small feature-sets of 50/60 features that have comparable same-day cross-validated accuracy. This divergence suggests that the higher cross-day robustness with the full feature-set involves a role for multivariate relationships between different frequency bands (i.e., unlike the mono-band subsets) at spatially distributed channels (i.e., unlike the mono-location subsets). To assess how this multi-feature configuration was organized, we evaluated the pattern of weights associated with the different features of the full feature-set.

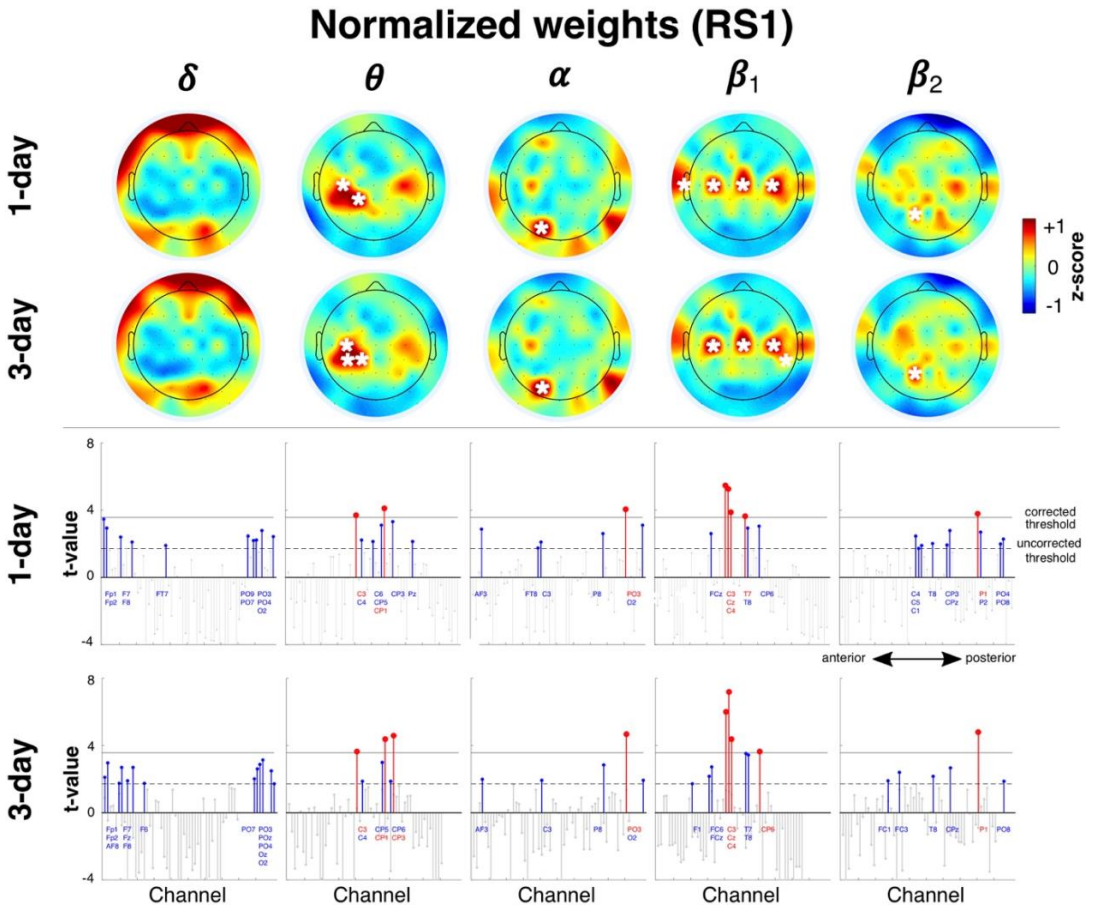


**Figure 7: High-consistency features.** Spatial distribution of high-consistency normalized weights for frequency bands of full feature set (z-scored per band) and their changes with aggregation (1-day, 3-day). Mean weights in each scalp map that were significantly greater than zero are indicated with a white asterisk ($p < 0.05/61$). Lower two rows show *t*-values for the features corresponding to the upper rows. Channels have an anterior-to-posterior ordering (x-axis). Red stems indicate channels with t-values higher than the corrected threshold ($p < 0.05/61$, horizontal black line) while blue stems show channels that only pass uncorrected thresholds ($p < 0.05$, dotted horizontal line). Colored channel labels are grouped from top-to-bottom for visibility and correspond to stems from left to right.

### *3.3.2. Concentration of high-consistency features at fronto-central and occipital zones*

Each individual's linear decision-rule was defined by the configuration of weights assigned to the different features, where weights with a larger magnitude (irrespective of sign) have a larger role in the classification decision even if in an indirect manner (Haufe et al. 2014; Schrouff and Mourao-Miranda 2018). However, individual-specific weight configurations might differ from each other in an idiosyncratic manner with little consistency between individuals since, for example, a high-weighted feature in $S_X$'s decision-rule might be of limited relevance to individual $S_Y$'s decision-rule.

Figure 7 shows the topographic distribution of high-consistency features in the full feature-set after normalization for power differences (see Suppl. Figure 1 for high-consistency non-normalized (raw) weights). At corrected thresholds (see *t*-values in Figure 7, lower panels), the features associated with all frequency bands except the $\delta$ band contained at least one high-consistency feature. Rather than having an idiosyncratic organization, the high-consistency features were concentrated at distinctive zones in each frequency band.

In $B_\theta$, there was a concentration of high consistency features at CP1 and C3, with the addition of CP3 with aggregation. There was a similar, although weaker, concentration of consistent features at corresponding channels over the right hemisphere. Showing a similar spatial organization, the high-consistency features in $B_{\beta 1}$ showed a striking bilaterally symmetric configuration along the transverse midline at channels C3, Cz and C4 with an aggregation-modulated role for CP6 and T7 (and possibly T8). This similarity in organization was notable since the frequency ranges of the $\theta$ band (4-7.5 Hz) and $\beta_1$ (14-22.5 Hz) were not contiguous and were separated by the $\alpha$ band.

Unlike this central concentration of features in $B_{\beta 1}$ and $B_\theta$, the features in $B_\alpha$ contained a single, strongly consistent feature in the occipital zone at PO3. At uncorrected thresholds, there were other distributed features across the scalp that were weakly consistent for both 1-day and 3-day identification, namely, at AF3, C3, P8 and O2. Similarly, the features of the high-frequency $\beta_2$

band (i.e., $B_{\beta 2}$) only had a single consistent feature at P1 with a diffuse distribution of consistent features at uncorrected thresholds.

In general, the distribution of high-consistency features was by itself not a simple indicator of their contribution to cross-day accuracy. For example, the relative number of high-valued weights in the different bands and spatial locations had a low correspondence to relative accuracy of cross-day identification based solely on the mono-band/location subsets (see Supplementary Figure 2). Nevertheless, the organized distribution of high-consistency features at channels over the sensorimotor cortex and the occipital cortex was prima facie support for an individual-specific configuration with a basis in neurophysiological constraints. The relevance of the high-consistency zones was of particular interest to the relationship of *RS1* to the non-rest task states where the power over the sensorimotor and occipital zones was expected to differ from *RS1*.

### 3.4. Relationship of rest to non-rest states

The behavioral demands during *TapMov* and *SeqMov* were designed to modulate the cognitive states during the *TapWait* and *SeqWait* periods and produce neural activity deviations from *RS1* in the absence of behavioral differences. Furthermore, the *Tap* and *Sequence* tasks were designed to elicit neural states that varied between days for *Sequence* (low cross-day similarity) but remained constant for *Tap* (high cross-day similarity). We sought to first explicitly verify that such deviations from *RS1* were indeed present. Note that all analyses of *Tap* and *Seq* states were performed in a subgroup of $N$=18 participants (see section 2.6).

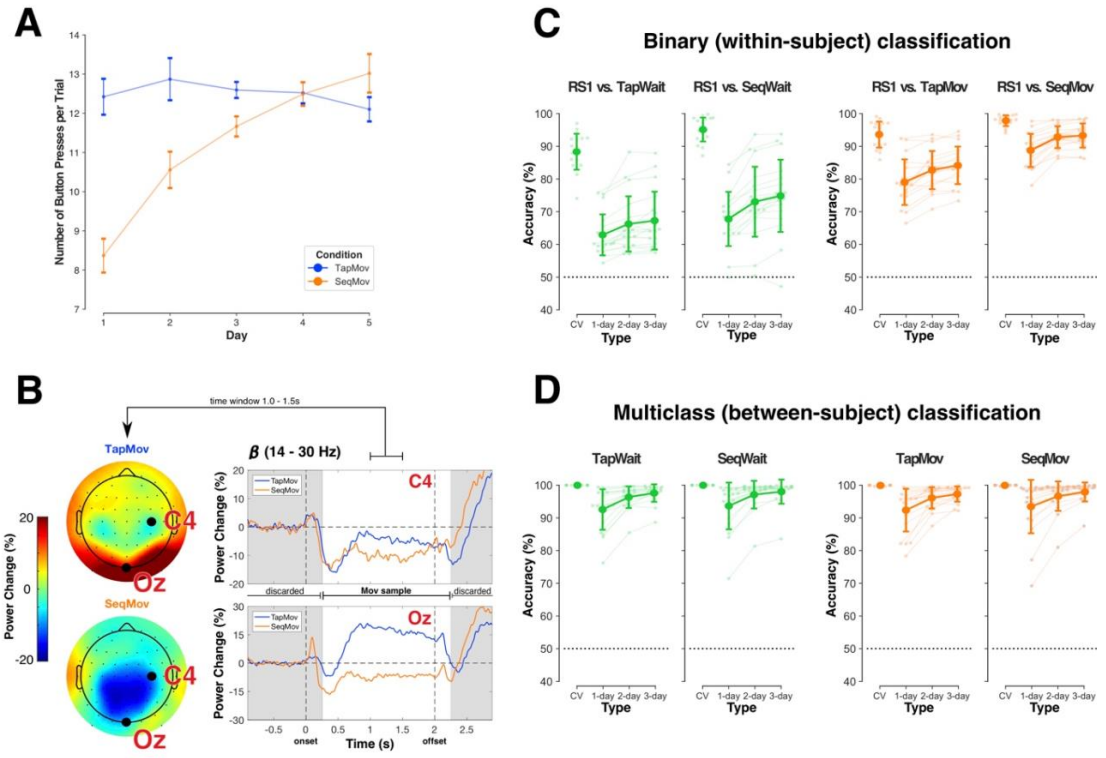


**Figure 8: Difference between *RS1* and task-states. (A)** Change in behavior indexed by mean number of button-presses across days (x-axis) during *TapMov* (blue) and *SeqMov* (orange). Error bars: Within-subject s.e.m. **(B)** Movement-related power dynamics in the $\beta$ band (14-30 Hz) in *TapMov* (blue) and *SeqMov* (orange) at channels C4 (upper right) and Oz (lower right) averaged across participants and days. Intervals marked in gray were discarded from the *TapWait* and *SeqWait* samples used for classification to avoid movement-related carry over effects into the waiting periods. Scalp plots (left panel) show the mean power distribution over the period [+1s, +1.5s] following onset of the movement cue. **(C)** Same-day/cross-day accuracy in distinguishing *RS1* vs pseudo-rest states (green) and *RS1* vs movement states (orange) using within-subject binary classifiers. Cross-day differences to *RS1* were lowest for *TapWait* (far left) and highest for *SeqMov* (far right). Error bars: SD. (**D**) Person identification accuracy (multiclass) when the training/test sets were from the same task state (green: pseudo-rest states, orange: movement states). Error bars: SD.

### *3.4.1. Neural activity during Tap and Sequence verifiably deviate from RS1*

The inter-day changes in behavior during the *TapMov* and *SeqMov* periods were consistent with the experimental assumptions (Figure 8A). During *TapMov*, the mean number of button presses per trial (~12-13) remained effectively constant across days [one-way ANOVA, $F_{4, 68} = 0.55$, $p = 0.70$]. In contrast, during *SeqMov*, the mean number of button-presses increased from ~8 on the first day to ~13 on the fifth day [one-way ANOVA, $F_{4, 68} = 21.36$, $p < 0.00001$]. This inter-day change in motor performance in *SeqMov* was systematically different from *TapMov* as confirmed by the statistically significant interaction in an ANOVA with factors Condition {*TapMov*, *SeqMov*} x Days {D1,..,D5} [Condition*Days: $F_{4, 68} = 12.38$, $p < 0.00001$; Condition: $F_{1, 17} = 3.13$, $p = 0.095$; Days: $F_{4, 68} = 10.71$, $p < 0.00001$].

The neural state during the movement-period (*TapMov, SeqMov)* showed typically expected dynamic states (Figure 8B). Changes in the mean $\beta$ power at channel C4 (contralateral to the moved fingers) were in line with the Event-Related De-synchronization/Synchronization (ERD/ERS) phenomenon for repetitive movements (Pfurtscheller and Lopes da Silva 1999; Cassim et al. 2000; Alegre et al. 2004; Erbil and Ungan 2007), namely, a power reduction at the onset of movement execution (i.e., ERD) with an increase after the termination of all movements (i.e., ERS). Furthermore, the $\beta$ power changes at Oz showed a task-dependent neural response consistent with differing visual stimulation, that is, an increase for *TapMov* (blank screen) but a decrease for *SeqMov* (image depicting the sequence). These movement-vs-wait differences were validated in the samples used for classification. A within-subject binary classification of *TapWait* vs *TapMov* had a mean cross-validated accuracy of 85.91 ± 7.23% [> 50%: $t_{17} = 21.06$, $p < 0.00001$]*;* and *SeqWait* vs *SeqMov* had a mean CV accuracy of 94.58 ± 3.20% [> 50%: $t_{17} = 59.02$, $p < 0.00001$].

The critical verification for our study was the relationship between *RS1* and the pseudo-rest states (*TapWait*, *SeqWait*). Samples from *TapWait* and *SeqWait* were distinguishable from *RS1* on the same day with high cross-validated accuracy (*RS1* vs *TapWait*: 88.28 ± 5.70%; *RS1* vs *SeqWait*: 95.12 ± 3.74%) (Figure 8C left panels, Table A.3). However, the cross-day accuracy (without

aggregation) for both *RS1* vs *TapWait* (62.91 ± 6.44% ) and *RS1* vs *SeqWait* (67.79 ± 8.53%) was substantially lower than the same-day accuracy by more than ~25%. Nevertheless, the cross-day accuracy for *RS1* vs *SeqWait* was marginally higher than for *RS1* vs *TapWait* with increasing aggregation [ANOVA: Condition {*RS1* vs *TapWait*, *RS1* vs *SeqWait*} x Type {1-day, 2-day, 3-day}, Condition*Type: $F_{2, 34} = 6.22$, $p = 0.005$; Condition: $F_{1, 17} = 8.37$, $p = 0.01009$; Type: $F_{2, 34} = 38.89$, $p < 0.00001$].

*TapMov* and *SeqMov* were also distinguishable from *RS1* on the same-day with high (cross-validated) accuracy (*RS1* vs *TapMov:* 93.56 ± 4.12%; *RS1* vs *SeqMov*: 97.81 ± 1.76%) (Figure 8C, right panel, Table A.3). Similar to the wait periods, the cross-day accuracy for *RS1* vs *SeqMov* was higher than for *RS1* vs *TapMov* across aggregation levels [ANOVA: Condition {RS vs *TapMov*, RS1 vs *SeqMov*} x Type {1-day, 2-day, 3-day}, Condition*Type: $F_{2, 34} = 0.61$, $p = 0.55$; Condition: $F_{1, 17} = 30.91$, $p = 0.00003$; Type: $F_{2, 34} = 69.47$, $p < 0.00001$].

The above findings verified the neural activity differences in the task-states in *Tap* and *Sequence* to each other and to *RS1*. Crucially, the structure of the same-day differences had a low cross-day generality.

### *3.4.2. Robust identification of individuals from Tap and Sequence activity within and across days*

The above differences between task-states and *RS1* raised the issue of whether the task-related functional states also disrupt the information that enables individual identification with *RS1*. To assess this possibility, we evaluated whether the different *Tap* and *Sequence* task-states contained sufficient information for person identification in a same-task classification scheme (i.e., with the scheme ${}^{X}\mathbf{I}_p \rightarrow {}^{X}\mathbf{I}_q$ for task *X*) (Figure 8D).

The same-day accuracy for both *TapWait* and *SeqWait* was ~99% (Figure 8D left panels, Table A.1). The mean cross-day accuracy (without aggregation) for *TapWait* (92.58 ± 6.39%) was lower than its corresponding same-day accuracy by only ~7% [$t_{17} = 4.92$, $p = 0.00013$]. Similarly, for *SeqWait*, the mean cross-day (1-day) (93.67 ± 7.35%) accuracy was lower than the same-day

accuracy by ~6% [$t_{17}$ = 3.65, p = 0.00197]. Furthermore, the effect of aggregation on mean cross-day accuracy for *TapWait* and for *SeqWait* were statistically indistinguishable [ANOVA: Condition {*TapWait*, *SeqWait*} x Type {1-day, 2-day, 3-day} [Condition*Type: $F_{2, 34}$ = 0.88, p = 0.42; Condition: $F_{1,17}$ = 1.35, p = 0.26; Type: $F_{2, 34}$ = 21.30, p < 0.00001].

Despite the deviations of *TapMov* and *SeqMov* along both the behavioral and cognitive dimensions of rest and their differences with each other, the accuracies of individual identification across days for *TapMov* and *SeqMov* were greater than 90% for all levels of aggregation and were not statistically distinguishable from each other (Table A.1, Figure 8D right panels) [ANOVA: Condition {*TapMov*, *SeqMov*} x Type {1-day, 2-day, 3-day} [Condition*Type: $F_{2, 34}$ = 0.86, p = 0.43; Condition: $F_{1, 17}$ = 1.26, p = 0.28; Type: $F_{2, 34}$ = 14.50, p = 0.00003].

Thus, individual identification was robustly possible in the task states despite their differences to *RS1*. Furthermore, the identification accuracy was similar between the *Tap* and *Seq* states despite their functional differences. Two further lines of evidence supported the possibility that these similarities were based on common task-independent properties. The spatial distribution of high-consistency features for these states (Figure 9A, Suppl. Figure 3) exhibited a striking qualitative similarity to each other as well as to the corresponding distribution for *RS1* (Figure 7). Additionally, the individual cross-day (1-day) accuracy in these task states showed a striking correlation to the corresponding cross-day accuracy in *RS1* (Figure 9B)[threshold: $p < 0.05/4$; *TapWait*: $r(17)=0.882$, $p < 0.00001$; *SeqWait*: $r(17)=0.635$, $p = 0.00466$; *TapMov*: $r(17)=0.75$, $p = 0.00034$; *SeqMov*: $r(17)=0.653$, $p = 0.00329$]. Thus, the inter-individual relationships revealed by the errors in cross-day classification during *RS1* (Figure 5B) seemingly extended to these non-rest states as well. We next turned to a formal assessment of this cross-task relationship.

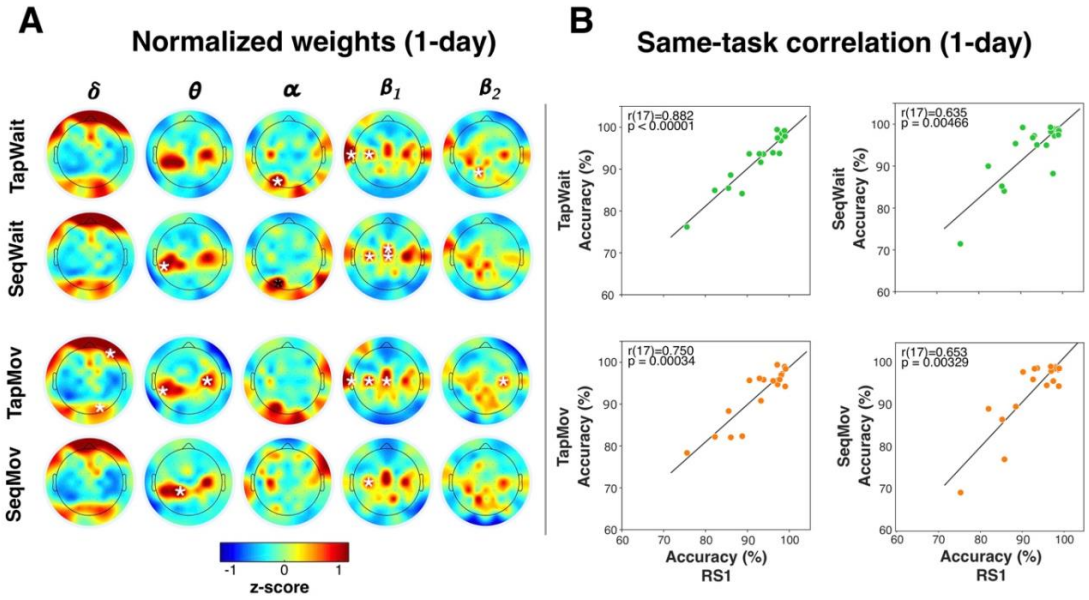


**Figure 9: Inter-task relationships**. **(A)** Spatial distribution of high-consistency features in different task-states (absolute, z-scored) for 1-day decision-rules (without aggregation). Weights in each scalp map that were significantly greater than zero are indicated with a white asterisk ($p < 0.05/61$, see Supplementary Figure 3). Each frequency band (column) had a characteristic spatial distribution of high weighted channels that was qualitatively similar across task-states and also to *RS1* (Figure 7). **(B)** Scatter plots of cross-day (1-day) identification accuracy in *RS1* to the corresponding same-task accuracy in the pseudo-rest states (upper row) and movement states (lower row). Each dot represents one individual. Correlations were assessed with Spearman's rank order correlation (threshold: $p < 0.05/4$).

### 3.5. Generalization of rest-based decision to cross-task individual identification

If person identification with *RS1* was based on a neural configuration related to an individual's neurophysiological state then identification should be possible despite cognitive state variations. Therefore, decision-rules trained on *RS1* should be capable of accurate person identification with samples acquired from the pseudo-rest states (*TapWait* and *SeqWait*) and the movement states (*TapMov* and *SeqMov*).

#### *3.5.1. Robust cross-task identification with RS1 with full feature-set*

We used the cross-task scheme ${}^{RS1}\mathbf{I}_p \rightarrow {}^{X}\mathbf{I}_q$ to test the invariance of *RS1*-based identification to inter-day cognitive state variations (i.e., task states *X*) (Figure 10A, Table A.4**)**. Increasing deviations from *RS1* solely due to cognitive state differences (*X = {RS1, TapWait, SeqWait}*) did not produce comparable, statistically distinguishable reductions in mean identification accuracy (*RS1*: 92.79 ± 6.76%, *TapWait*: 91.90 ± 6.46%; *SeqWait*: 90.81 ± 7.09%) [one-way ANOVA, $F_{2, 34} = 2.06$, $p = 0.14$]. However, increasing deviations from *RS1* due to cognitive and behavioral state differences (*X = {RS1, TapMov, SeqMov}*) produced significant reductions in identification accuracy most notably for *SeqMov* (*TapMov*: 88.79 ± 7.57%; *SeqMov*: 83.85 ± 10.35%)[one-way ANOVA, $F_{2, 34} = 14.07$, $p = 0.00004$].

To disentangle the role of cross-task from cross-day effects, we compared cross-task (${}^{RS1}\mathbf{I}_p \rightarrow {}^{X}\mathbf{I}_q$) and same-task identification (${}^{X}\mathbf{I}_p \rightarrow {}^{X}\mathbf{I}_q$) across days (Table A.1, 4**)**. For the pseudo-rest states (*X = {TapWait, SeqWait}*), cross-task accuracy with *RS1* decision-rules produced a small but statistically significant reduction relative to same-task identification [ANOVA, Train {*RS1*, *Same*} x Condition {*TapWait*, *SeqWait*}, Train*Condition: $F_{1,17} = 4.14$, $p = 0.06$; Train: $F_{1,17} = 10.02$, $p = 0.00566$; Condition: $F_{1, 17} = 0.00001$, $p = 1.00$]. The cross-task accuracy reduction was significantly larger for the movement-states (*X = {TapMov, SeqMov}*) with a larger loss for *SeqMov* [ANOVA, Train{*RS*,*Same*} x Condition {*TapMov*, *SeqMov*}, Train*Condition: $F_{1,17} = 9.15$, $p = 0.00764$; Train: $F_{1,17} = 43.94$, $p < 0.00001$; Condition: $F_{1, 17} = 2.51$, $p = 0.13$].

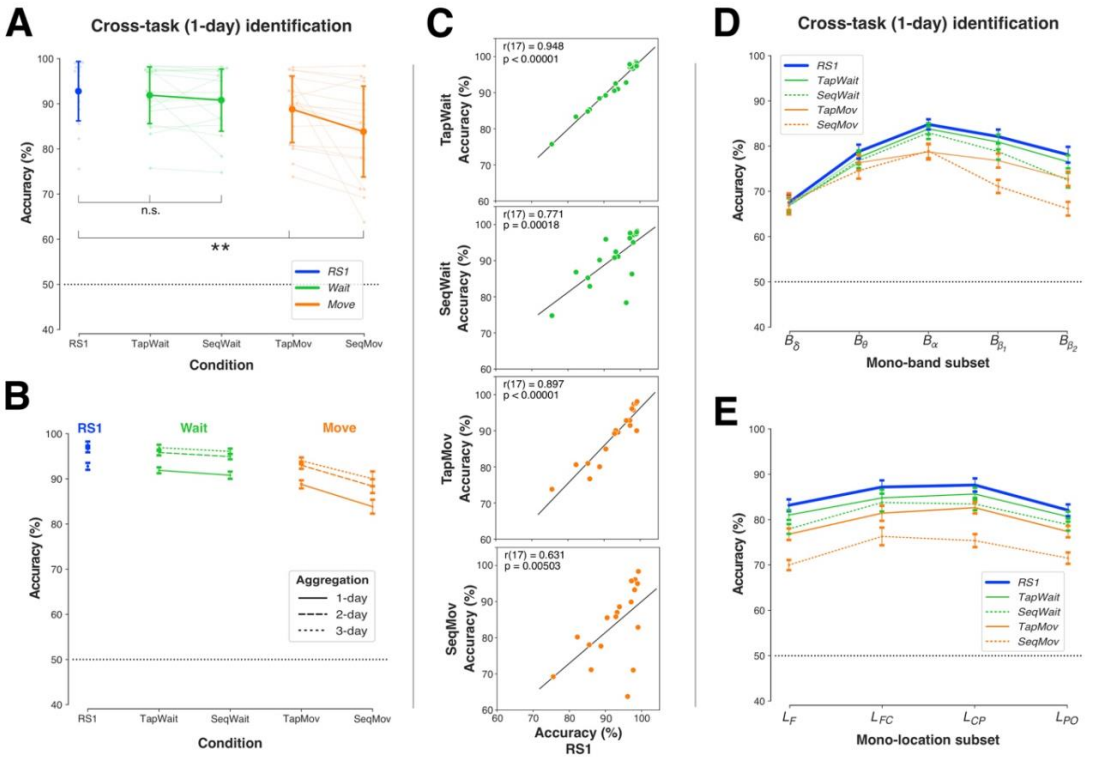


**Figure 10: Cross-task identification with RS1. (A)** Mean accuracy of decision-rules trained on *RS1* (1-day) and tested across days on *RS1* (blue), pseudo-rest states (green) and movement states (orange). Light colored dots/lines indicate individual accuracies. Error bars: SD. Accuracy differences between *RS1* and pseudo-rest states were not statistically significant (n.s.), but were between *RS1* and movement states (** = $0.00001 \leq p < 0.001$). (**B**) Decision-rules trained on *RS1* with different levels with aggregation (dotted lines) increased cross-day accuracy for all task-states. Error bars: Within-subject s.e.m. (**C**) Scatter plots of cross-day (1-day) accuracy in *RS1* to the corresponding cross-task accuracy in all non-rest tasks. Each dot represents one individual. Correlations were assessed with Spearman's rank order correlation (threshold: $p < 0.05/4$). **(D)** Cross-task/day accuracy of *RS1* with mono-band subsets. Deviations from cross-day accuracy for *RS1* were larger for the movement states (orange) than the pseudo-rest states (green) and deviations increased with the frequency (lowest for $B_{\delta}$, highest for $B_{\beta 2}$). Error bars: Within-subject s.e.m. **(E)** Cross-task/day accuracy of *RS1* with mono-location subsets. Deviations from *RS1* were larger for movement states (orange) than pseudo-rest states (green). Error bars: Within-subject s.e.m.

To disentangle the role of day-specificity in ${}^{RS1}\mathbf{I}_p \rightarrow {}^{X}\mathbf{I}_q$, we used multi-day aggregation (${}^{RS1}\mathbf{I}_p \circ {}^{RS1}\mathbf{I}_q \ \ldots \rightarrow {}^{X}\mathbf{I}_r$). Although aggregation reduced day-specificity with *RS1* (Figure 5), it could nevertheless increase specificity to the properties of *RS1*. If so, aggregation might lower the accuracy of cross-task identification. Contrary to this possibility, aggregation *increased* cross-task accuracy to the pseudo-rest states (*TapWait*, *SeqWait*) in a comparable manner to same-task accuracy (Figure 10B) [ANOVA: Condition {*RS1, TapWait, SeqWait*} x Type {1-day, 2-day, 3-day} [Condition*Type: $F_{4, 68} = 0.52$, $p = 0.72$; Condition: $F_{2, 34} = 2.44$, $p = 0.10$; Type: $F_{2, 34} = 21.63$, $p < 0.00001$]. This was particularly striking because aggregation (i.e., related to day-specificity) produced a relatively larger increase in cross-task accuracy than a change in task-specificity. Following aggregation, the mean residual cross-task/day accuracy loss relative to same-task/day identification with *RS1* was only ~3%. Aggregation also *increased* cross-task accuracy to the movement states (*TapMov, SeqMov*) [ANOVA: Condition {*RS1, TapMov*, *SeqMov*} x Type {1-day, 2-day, 3-day} [Condition*Type: $F_{4, 68} = 1.35$, $p = 0.26$; Condition: $F_{2, 34} = 13.04$, $p = 0.00006$; Type: $F_{2, 34} = 29.33$, $p < 0.00001$]. Following aggregation, the mean residual cross-task/day difference was less than ~10% for the movement states.

Similar to the same-task correlations described above (section 3.4.2, Figure 9B), the individual *cross-task* (1-day) accuracy in each of these task states showed a statistical significant correlation to the corresponding cross-day accuracy in *RS1* (Figure 10C)[threshold: $p < 0.05/4$; *TapWait*: $r(17)=0.948$, $p < 0.00001$; *SeqWait*: $r(17)=0.771$, $p = 0.00018$; *TapMov*: $r(17)=0.897$, $p<0.00001$; *SeqMov*: $r(17)=0.631$, $p = 0.00503$]. The correlation coefficients were particularly high for both *Tap* states *(TapWait* and *TapMov*) as compared to the *Seq* states (*SeqWait* and *SeqMov),* Furthermore, the scatter plots suggested that the relatively lower cross-task/day accuracy for *SeqMov* was driven by the low generalization of a few individuals.

In summary, decision-rules trained on *RS1* on a single day could identify individuals from samples from states that verifiably differed from *RS1* to differing extents. Importantly, aggregated

training solely on *RS1* lead to *increases* in identification accuracy on samples from these non-rest task states.

### *3.5.2. Low cross-task identification with feature subsets*

The full-feature set has a crucial role in limiting the cross-day loss in accuracy in *RS1* (Figure 6). Appling the cross-task scheme ${}^{RS1}\mathbf{I}_p \rightarrow {}^{X}\mathbf{I}_q$ to the mono-band (Figure 10D) and mono-location (Figure 10E) feature sets provided further evidence of the importance of the full feature-set to enable robust cross-task identification.

For the mono-band feature sets (Figure 10D), increasing deviations from *RS1* in cognitive state ($X$ = *{RS1, TapWait, SeqWait}*) lead to state-related accuracy reductions that were also larger for the higher frequency bands [ANOVA: Condition {*RS1, TapWait, SeqWait*} x Band {$B_\delta$, $B_\theta$, $B_\alpha$, $B_{\beta 1}$, $B_{\beta 2}$} [Condition*Band: $F_{8, 136} = 2.60$, $p = 0.01136$; Condition: $F_{2, 34} = 6.44$, $p = 0.00426$; Band: $F_{4, 68} = 18.36$, $p < 0.00001$]. In a similar manner, increasing deviations from *RS1* for the movement states ($X$ = *{RS1, TapMov, SeqMov}*) produced state-related accuracy reductions that were greater for *SeqMov* than for *TapMov* particularly at the higher frequencies [ANOVA: Condition {*RS1, TapMov, SeqMov*} x Band {$B_\delta$, $B_\theta$, $B_\alpha$, $B_{\beta 1}$, $B_{\beta 2}$} [Condition*Band: $F_{8, 136} = 8.95$, $p < 0.00001$; Condition: $F_{2, 34} = 20.59$, $p < 0.00001$; Band: $F_{4, 68} = 12.16$, $p < 0.00001$]. These task-linked accuracy reductions were notably absent at $B_\delta$.

The pattern of cross-task accuracy deviation from *RS1* took a different form for the mono-location feature sets (Figure 10E). For the pseudo-rest states ($X$ = *{RS1, TapWait, SeqWait}*), increasing deviations from *RS1* lead to increasing accuracy reductions (largest for *SeqWait*) that were relatively uniform at all the locations [ANOVA: Condition {*RS1, TapWait, SeqWait*} x Location {$L_F$, $L_{FC}$, $L_{CP}$, $L_{PO}$} [Condition*Location: $F_{6, 102} = 0.98$, $p = 0.45$; Condition: $F_{2, 34} = 8.99$, $p = 0.00073$; Location: $F_{3, 51} = 4.34$, $p = 0.00849$]. This pattern of reduction was similar for the movement states ($X$ = *{RS1, TapMov, SeqMov}*), where deviations from *RS1* lead to accuracy reductions that were largest for *SeqMov* and relatively uniform at all locations [ANOVA: Condition

{*RS1, TapMov, SeqMov*} x Location {$L_F$, $L_{FC}$, $L_{CP}$, $L_{PO}$} [Condition*Location: $F_{6, 102} = 0.99$, $p = 0.44$; Condition: $F_{2, 34} = 32.92$, $p < 0.00001$; Location: $F_{3, 51} = 4.95$, $p = 0.00432$].

Thus, the large accuracy reductions with band/location-defined feature subsets confirmed that the full feature-set was crucial to high cross-task identification accuracy. Taken together, the cross-task/cross-day robustness of person identification with the full feature-set was consistent with the hypothesized properties of a configuration constrained by individual neurophysiology.

## 4. DISCUSSION

The central motivation for the current study was whether RS-activity could support a critical demand for individualized longitudinal tracking, namely, decoding the origin of inter-day RS differences (i.e., *NP+* or *NP-*) from the relationship between the resting state activity patterns. A major obstacle to *NP+/NP-* decoding was the ill-defined rest task itself and its potential to confound the interpretation of RS-activity *differences*. To evaluate a *commonality*-based alternative, we hypothesized that the existence of an activity configuration defined by neurophysiological constraints would afford an escape from the confounding effects of the rest task. Our findings support the existence of such a configuration in the longitudinal characteristics of the EEG oscillatory power spectrum at rest. Formulated in terms of individual identification, inter-day differences in individual RS-activity were classified with high accuracy across a diverse range of confounding inter-day differences, with day-generality confirmed using aggregation. Consistent with a configuration based in whole-brain neurophysiology, accurate identification was higher with a full feature-set that enabled the integration of information from multiple frequency bands at channels distributed across the scalp.

### 4.1. Empirical simulations of cognitive and neurophysiological variation

A methodological novelty here was our use of empirical "simulations". Although ad hoc, they provided a means to obtain verifiable instances of cognitive state variation and neurophysiological change relative to RS.

As previous studies have demonstrated (Duncan and Northoff 2013; Kawagoe et al. 2018), the potential for arbitrary cognitive state variation during the rest task is related to experimental context and instructions. However, beyond the assumption that participants were awake, we did not model the participant's cognitive state, for example, using participant's self-reported subjective assessments of their cognitive state during the RS measurement (Diaz et al. 2013). Since the cognitive state and the extent of its fluctuation during rest are difficult to establish for each individual, the high identification accuracy with *RS1* might have been attributable to highly motivated and instruction-compliant participants rather than the neural characteristics of the rest state. Therefore, the *Tap* and *Sequence* tasks provided verifiable within-subject examples of states that deviated from rest in order to assess the generality of RS-based inferences.

In a longitudinal setting, the classification problem of interest requires a decision between *NP+* and *NP-* within the same individual. However, here *NP+* was defined based on samples of RS activity from *other* individuals. This use of inter-individual differences provided a pragmatic means to simulate a diverse range of possible changes to an individual's neurophysiology (Figure 1B) with the assumption that detecting true within-subject neurophysiological change would possibly be far more challenging. For example, in the *Sequence* task, the motor learning across the five days in our experiment involved neuroplastic changes (Wymbs et al. 2012; Wymbs and Grafton 2014; Bassett et al. 2015) and the accompanying changes in *SeqWait* and *SeqMov* over the duration of the experiment (Figure 8) could be considered as consequence of this learning-induced neuroplasticity. However, due to the unclear carryover effects of these plastic changes on *RS1* over this five day period, we instead used the *SeqWait* and *SeqMov* to simulate incidental cognitive-state variations

(*NP*-) with high inter-day variance, where the neural dynamics on each day was a poor model of the dynamics on other days.

### 4.2. Reliability of identity inferences versus reliability of features

Numerous prior studies have investigated the inter-day similarity in RS activity within a test-retest framework (Bijsterbosch et al. 2017; Cox et al. 2018; Noble et al. 2019; Postema et al. 2019). In that framework, the focus is on evaluating whether a particular measure of RS activity on day *p* was reliably reproduced for RS activity on day *q* in the assumed absence of a true change. However, our focus is on the reliability of inferences in the assumed presence of true inter-day activity changes. This focus required differing considerations about how an individual's unique identity was defined and represented as illustrated with an analogy to object recognition.

Consider images of the same object *X* from day 1 (test) and day 2 (retest) (Figure 11**)** represented by a list of filled pixel locations (i.e., features). With this representation, a simple measure of test-retest reliability is whether a pixel's filled state on day 1 is a reliable predictor of its state on day 2. The scenario in Figure 11A is consistent with a *high* feature-level reliability as the majority of filled pixels on day 1 are also filled on day 2. However, this high reliability is misleading about the object's unique identity. On day 1, object *X* can be readily distinguished from object *Y* based on a few critical pixels (circled). These critical pixels on object *X* are, however, unfilled on day 2. Thus, object *X* is not uniquely identifiable on day 2 as it is now confusable with object *Y*. Conversely, in the scenario shown in Figure 11B, a pixel-based test of reliability would indicate a *low* reliability due to the large number of filled pixels from day 1 that are unfilled on day 2. However, this low reliability is a limitation of how the object was represented (i.e., as a list of filled pixel locations relative to the main axes). If this representation included information about the relationships between the filled locations, then the object's defining characteristics would be deemed as being reliably conserved on day 2, e.g., a rotation of the object *X* on day 2 would bring it into correspondence with its form on day 1.

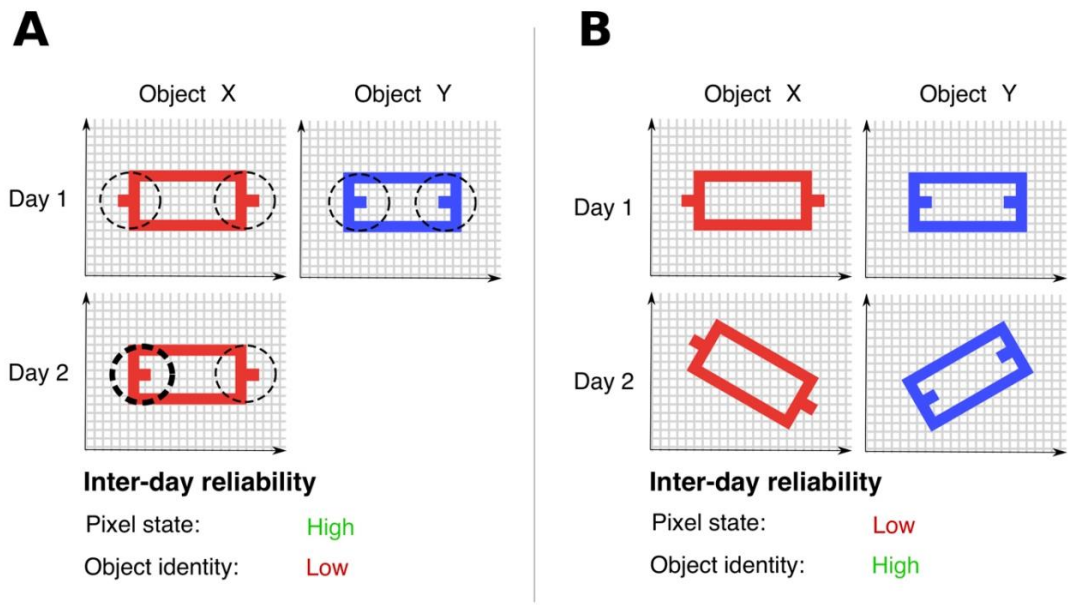


**Figure 11: Test-retest reliability versus individual re-identification. (A)** Objects *X* (red) and *Y* (blue) are uniquely defined by the configuration of filled and unfilled pixels. On day 1, (top row), the dotted circles indicates the critical pixels that distinguish *X* and *Y*. Most pixels of object *X* from day 1 are also filled on day 2 (lower row). However, pixels in the left dotted circle on day 2 differ in their state from day 1. Due to this difference on day 2, object *X* cannot be uniquely re-identified as being object *X* based on its form as it is now confusable with object *Y*. High inter-day reliability in pixel state does not imply the same for object identity. (**B**) The orientation of objects *X* on day 2 is rotated relative to its orientations on day 1. If this orientation is accounted for, then object *X* can be uniquely re-identified on day 2. However, when considering individual pixels, most of the filled pixels on day 1 are not on day 2. Low inter-day reliability in pixel state does not imply the same for object identity.

As demonstrated by this analogy, high test-retest reliability of individual features does not imply the reliability of the configuration of these features to enable individual identification and vice versa. This relationship between reliability and how an individual's identity is defined and represented was a central consideration here.

Despite using an analogy of an individual's configuration to a static object in the above example, the core variance model in our analysis involved an assumption about time and time-scales. Each same-day measurement was segmented into 2s non-overlapping epochs where each epoch was treated as a sample drawn from an underlying individual-specific distribution. The dynamic variability between samples was assumed to be an important characteristic of this individual-specific distribution. Cross-day/cross-task identification was predicated on whether training classifiers based on the inter-sample variability on short time-scales (i.e., between the samples acquired within seconds/minutes of each other on the same day) was a viable model for samples obtained on long time-scales, i.e., days apart (Figure 1).

Even though we do not use an explicit model of functional connectivity, the multivariate representations used to represent an individual's decision-rule assumes a coupling between power values across distributed locations. A distinction is often drawn between static and dynamic connectivity based on how the neural time-series over the resting task is interpreted (Hutchison et al. 2013; Calhoun et al. 2014). Static connectivity refers to the extraction of a single measure (e.g., a graph) from the time-series. In contrast, dynamic connectivity is based on the view that resting state refers to a collection of states that dynamically vary at different time points. However, our approach and findings here are agnostic as to whether the inter-sample differences indicate variability around a characteristic mean value (i.e., static connectivity) or characteristic transitions between distinct states (i.e., dynamic connectivity). The relationship between the classifier-based multivariate representations to connectivity and distances measures (e.g., Valizadeh et al. 2019; Pani et al. 2020) is a key issue to be resolved by future studies.

### 4.3. Individual identification and longitudinal tracking

By using individual differences as a source of neurophysiological information, here the problem of distinguishing between *NP*+ and *NP*- was equivalent to the problem of individual identification with similarities to numerous studies that have, for example, sought to use RS-EEG as an individual-specific signature for biometric identification (Campisi and Rocca 2014; Gui et al. 2015; Valizadeh et al. 2019). However, our focus was not biometric identification or the important issues related to the neural basis of individual differences and trait-identification (Smit et al. 2005, 2006; Demuru et al. 2017; Finn et al. 2017; Gratton et al. 2018). Nevertheless, our findings are consistent with these prior studies in demonstrating the high distinctiveness of individual differences and its robust detectability even across days and tasks from two-second snapshots of the oscillatory power spectra at rest.

However, the inter-individual differences in cross-day identification with *RS1* both with and without aggregation (Figure 5, 6A, 6C) also demonstrated that resting activity was not the strict equivalent of a "fingerprint", i.e., in being entirely immune to cognitive state or even whether a person is alive (Campisi and Rocca 2014). Even though individual identification was possible across tasks with high accuracy, the RS-based individual signatures were not completely independent of cognitive state. Large deviations from rest during *TapMov* and *SeqMov* reduced cross-task identification accuracy even though identification was above random chance. These accuracy reductions were due to cognitive state differences with *RS1* and not merely because *TapMov* and *SeqMov* conditions lacked identifiable signatures or had more movement-related artifacts (Figure 8D).

The use of an individual identification strategy involved certain tradeoffs. An individual's identity was defined by analyzing differences to other individuals in the studied group. Therefore, the characteristics represented by an individual $S_X$'s decision-rule could vary depending on the properties of the other individuals in the group. Rather than the number of individuals in the group, the key determinants of how $S_X$ is represented would be the diversity and properties of the most-

similar individuals (as illustrated by the confusion matrix and inter-individual clustering in Figure 5). Furthermore, identifying features that distinguish an individual from others would lead to the exclusion of features *shared* by all individuals. For example, in a study of the heritability of individual RS-connectivity properties with magnetoencephalography (MEG) (Demuru et al. 2017), the explicit removal of connectivity characteristics shared by all individuals in the group was found to significantly improve individual identification. However, down-weighting the role of shared features (explicitly or implicitly) has a tradeoff for tracking neural plasticity since changes to an individual's neurophysiology on these shared features might go undetected.

### 4.4. What makes an individual configuration robust to changes in cognitive state?

Our primary findings are based on black-box statistical inferences, namely, the pattern of classification accuracies obtained with different training/test sets that were selected based on experimental variables (e.g., the effect of day, the conditions defining the cognitive state, and the feature set). Therefore, an important issue is whether these statistical regularities are consistent with a neurophysiological signature in RS-activity rather than a byproduct of other factors specific to our implementation.

The shape of the power spectrum in the frequency domain at rest has long been suggested as an important individual characteristic (Näpflin et al. 2007; Chiang et al. 2011; Bazanova and Vernon 2014). This shape has multiple peaks over an aperiodic background of 1/f noise. The specific frequencies at which these peaks occur, particularly in the α band and in the β band have been the topic of considerable investigation (van Albada and Robinson 2013; Voytek et al. 2015). Importantly, in different cognitive states, the changes to this spectrum are not arbitrary and primarily involve changes to the power at the peaks (as well as small shifts in the peak frequency) but without large changes to the 1/f background (Buzsáki et al. 2012; Haegens et al. 2014; Cole and Voytek 2017). Furthermore, Demuru and Fraschini (2020) found that this aperiodic background was

highly individual-specific and allowed individuals to be identified with higher accuracy than the power in canonical frequency bands.

Therefore one possibility to explain our results is that an individual's decision-rule implicitly represents the shape of their unique power spectrum. If this were the case then it would provide a plausible explanation for the observed high specificity despite cognitive state variation. In our feature representation, the power over the full power spectrum was averaged into five canonical bands. Therefore, capturing the individual shape of the spectrum and, for example, the approximate location of the α power peak would require a role for features representing the power in the θ, α and $\beta_1$ bands. Indeed, it was these three bands that also showed the main consistencies in term of a few, high valued weights. The classical depiction of the power spectrum is from a particular channel. Our finding suggests that representation of the individual-specific power in the different bands were distributed over the scalp with a concentration in the fronto-central and occipital zones. Although the power spectra are similar across channels, any one channel is an incomplete representation of that individual's characteristic power distribution. Consequently, it might lack the robustness to represent individual variability across days. By contrast, a decision-rule that combines each band's best representation might have a greater robustness.

### 4.4. Outlook

In the current study, we assumed that individuals in the studied group did not undergo extensive plastic changes. If individual identification was not possible with longitudinal RS even with such a group of healthy individuals over a period of five days, then the merits of using RS as a tracking indicator would seem to require critical re-evaluation especially for tracking over longer periods of time and with populations where such neuroplastic changes would be expected. Prior studies have found changes to the power spectrum with aging (van Albada et al. 2010; Chiang et al. 2011; Voytek et al. 2015; Knyazeva et al. 2018), for example, age-related reductions in the frequencies of the alpha and beta band peaks. Voytek et al. (2015) suggest that such changes might

indicate a change in the 1/f baseline possibly due to increased physiological noise with aging. Furthermore, systematic longitudinal changes in the power spectrum have been observed following stroke (Giaquinto et al. 1994; Saes et al. 2020). Thus, the application of this physiological signature to monitor longitudinal RS in clinical populations is an important future priority.

## Acknowledgments

This work was funded by the University of Cologne Emerging Groups Initiative (CONNECT group) implemented into the Institutional Strategy of the University of Cologne and the German Excellence Initiative; and by the Deutsche Forschungsgemeinschaft (DFG, German Research Foundation) – Project-ID 431549029 – SFB 1451. SD gratefully acknowledges support from the German Research Foundation (DA 1953/5-2). We thank Hannah Kirsten, Alexandra Kurganova, and members of the INM-3 for their valuable assistance in data acquisition.

## CRediT author statement

**Maximilian Hommelsen**: Conceptualization, Methodology, Software, Validation, Formal analysis, Investigation, Writing: Original Draft, Visualization. **Shivakumar Viswanathan**: Conceptualization, Methodology, Software, Validation, Formal analysis, Writing: Review & Editing, Visualization. **Silvia Daun:** Conceptualization, Writing: Review & Editing, Visualization, Supervision, Project administration, Funding acquisition.

## Conflict of interest

None

## APPENDIX

**Table A.1**: Identification accuracies in different experimental states reported as Mean % (SD). All values were significantly above random chance (50%) (see Suppl. Table 1**).**

| States | Type | | | |
|---|---|---|---|---|
| | **CV** | **1-day** | **2-day** | **3-day** |
| ***RS1*** (*N*=24) | 99.98 (0.04) | 92.10 (6.84) | 95.93 (3.63) | 97.39 (2.65) |
| ***RS1*** (*N*=18) | 99.98 (0.06) | 92.79 (6.76) | 96.61 (3.30) | 97.53 (2.51) |
| ***RS2*** (*N*=24) | 99.99 (0.04) | 91.58 (7.49) | 95.86 (4.18) | 96.99 (3.50) |
| ***TapWait*** (*N*=18) | 99.99 (0.02) | 92.58 (6.39) | 96.36 (3.42) | 97.60 (2.77) |
| ***SeqWait*** (*N*=18) | 99.99 (0.02) | 93.67 (7.35) | 97.12 (4.36) | 98.03 (3.80) |
| ***TapMov*** (*N*=18) | 99.94 (0.12) | 92.39 (6.72) | 96.12 (3.34) | 97.29 (2.41) |
| ***SeqMov*** (*N*=18) | 100.00 (0.00) | 93.47 (8.41) | 96.67 (4.64) | 97.95 (2.99) |

**Table A.2**: Identification accuracies for *RS1* with mono-band and mono-location feature subsets reported as Mean % (SD). All values were significantly above random chance (50%) (see Suppl. Table 2).

| **Subset** (*N*=24) | **Type** | | | |
|---|---|---|---|---|
| | **CV** | **1-day** | **2-day** | **3-day** |
| $\boldsymbol{B_{\delta}}$ | 96.10 (2.54) | 64.66 (7.92) | 67.87 (8.12) | 70.12 (8.01) |
| $\boldsymbol{B_{\theta}}$ | 97.63 (1.52) | 76.99 (7.69) | 81.76 (7.11) | 83.70 (6.94) |
| $\boldsymbol{B_{\alpha}}$ | 98.51 (1.17) | 84.20 (7.74) | 88.38 (6.34) | 89.59 (5.67) |
| $\boldsymbol{B_{\beta 1}}$ | 99.65 (0.57) | 81.41 (10.44) | 87.03 (9.03) | 88.92 (8.14) |
| $\boldsymbol{B_{\beta 2}}$ | 99.74 (0.30) | 76.37 (9.98) | 83.22 (9.00) | 86.66 (7.96) |
| $\boldsymbol{L_{F}}$ | 98.01 (1.80) | 82.68 (8.89) | 87.30 (7.45) | 88.87 (6.56) |
| $\boldsymbol{L_{FC}}$ | 98.54 (1.55) | 86.93 (9.38) | 90.39 (7.45) | 91.76 (6.12) |
| $\boldsymbol{L_{CP}}$ | 97.94 (1.78) | 85.28 (8.57) | 89.43 (7.30) | 90.37 (6.52) |
| $\boldsymbol{L_{PO}}$ | 97.96 (2.02) | 81.02 (8.32) | 86.47 (7.35) | 87.97 (7.06) |

| **Table A.3**: Classification accuracy of *RS1* vs task state (binary, within-subject) reported as Mean % (SD). All values were significantly above random chance (50%) (see Suppl. Table 3). | | | | |
|---|---|---|---|---|
| ***RS1* vs** (*N*=18) | **Type** | | | |
| | **CV** | **1-day** | **2-day** | **3-day** |
| ***TapWait*** | 88.35 (5.66) | 62.91 (6.44) | 66.26 (8.69) | 67.28 (9.11) |
| ***SeqWait*** | 95.12 (3.74) | 67.79 (8.53) | 73.05 (11.01) | 74.86 (11.37) |
| ***TapMov*** | 93.56 (4.12) | 79.04 (7.17) | 82.75 (5.99) | 84.18 (5.92) |
| ***SeqMov*** | 97.81 (1.76) | 88.77 (5.21) | 92.81 (3.43) | 93.32 (3.77) |

| **Table A.4**: Accuracy of cross-task ${}^{RS1}\mathbf{I}_p \rightarrow {}^{X}\mathbf{I}_q$ identification reported as Mean % (SD). All values were significantly above random chance (50%) (see Suppl. Table 4). | | | |
|---|---|---|---|
| **Test states** (*N = 18*) | **Type** | | |
| | **1-day** | **2-day** | **3-day** |
| ***TapWait*** | 91.90 (6.46) | 95.84 (3.30) | 96.90 (2.44) |
| ***SeqWait*** | 90.81 (7.09) | 94.95 (4.39) | 96.09 (3.40) |
| ***TapMov*** | 88.79 (7.57) | 93.02 (5.49) | 94.01 (4.51) |
| ***SeqMov*** | 83.85 (10.35) | 88.39 (9.28) | 90.03 (8.87) |

## REFERENCES


Abraham A, Elrahman SMA. 2013. A Review of Class Imbalance Problem. J Netw Innov Comput. 1:332–340.

Alegre M, De Gurtubay IG, Labarga A, Iriarte J, Malanda A, Artieda J. 2004. Alpha and beta oscillatory activity during a sequence of two movements. Clin Neurophysiol. 115:124–130.

Barry RJ, Clarke AR, Johnstone SJ, Magee CA, Rushby JA. 2007. EEG differences between eyes-closed and eyes-open resting conditions. Clin Neurophysiol. 118:2765–2773.

Bassett DS, Yang M, Wymbs NF, Grafton ST. 2015. Learning-induced autonomy of sensorimotor systems. Nat Neurosci. 18:744–751.

Bazanova OM, Vernon D. 2014. Interpreting EEG alpha activity. Neurosci Biobehav Rev. 44:94–110.

Benjamin C, Lieberman DA, Changl M, Ofen N, Whitfield-Gabrieli S, Gabrieli JDE, Gaab N. 2010. The influence of rest period instructions on the default mode network. Front Hum Neurosci. 4:1–9.

Bijsterbosch J, Harrison S, Duff E, Alfaro-Almagro F, Woolrich M, Smith S. 2017. Investigations into within- and between-subject resting-state amplitude variations. Neuroimage. 159:57–69.

Biswal B, Zerrin Yetkin F, Haughton VM, Hyde JS. 1995. Functional connectivity in the motor cortex of resting human brain using echo-planar mri. Magn Reson Med. 34:537–541.

Blondel VD, Guillaume JL, Lambiotte R, Lefebvre E. 2008. Fast unfolding of communities in large networks. J Stat Mech Theory Exp. 2008.

Blum A, Kalai A, Langford J. 1999. Beating the hold-out: bounds for K-fold and progressive cross-validation. Proc Annu ACM Conf Comput Learn Theory. 203–208.

Boersma M, Smit DJA, De Bie HMA, Van Baal GCM, Boomsma DI, De Geus EJC, Delemarre-Van De Waal HA, Stam CJ. 2011. Network analysis of resting state EEG in the developing young brain: Structure comes with maturation. Hum Brain Mapp. 32:413–425.

Bonkhoff AK, Hope T, Bzdok D, Guggisberg AG, Hawe RL, Dukelow SP, Rehme AK, Fink GR. 2020. Bringing proportional recovery into proportion : Bayesian modelling of post-stroke motor impairment. 1–18.

Buckner RL, DiNicola LM. 2019. The brain's default network: updated anatomy, physiology and evolving insights. Nat Rev Neurosci. 20:593–608.

Buzsáki G, Anastassiou C a., Koch C. 2012. The origin of extracellular fields and currents — EEG, ECoG, LFP and spikes. Nat Rev Neurosci. 13:407–420.

Cabeza R, Albert M, Belleville S, Craik FIM, Duarte A, Grady CL, Lindenberger U, Nyberg L, Park DC, Reuter-Lorenz PA, Rugg MD, Steffener J, Rajah MN. 2018. Maintenance, reserve and compensation: the cognitive neuroscience of healthy ageing. Nat Rev Neurosci. 19:701–710.

Calhoun VD, Miller R, Pearlson G, Adali T. 2014. The Chronnectome: Time-Varying Connectivity Networks as the Next Frontier in fMRI Data Discovery. Neuron. 84:262–274.

Campenhout JM Van. 1978. On the Peaking of the Hughes Mean Recognition Accuracy - the Resolution of an Apparent Paradox. IEEE Trans Syst Man Cybern. SMC-8:390–395.

Campisi P, Rocca D La. 2014. Brain waves for automatic biometric-based user recognition. IEEE Trans Inf Forensics Secur. 9:782–800.

Carino-Escobar RI, Carrillo-Mora P, Valdés-Cristerna R, Rodriguez-Barragan MA, Hernandez-Arenas C, Quinzaños-Fresnedo J, Galicia-Alvarado MA, Cantillo-Negrete J. 2019. Longitudinal analysis of stroke patients' brain rhythms during an intervention with a brain-computer interface. Neural Plast. 2019.

Cassani R, Estarellas M, San-Martin R, Fraga FJ, Falk TH. 2018. Systematic review on resting-state EEG for Alzheimer's disease diagnosis and progression assessment. Dis Markers. 2018.

Cassim F, Szurhaj W, Sediri H, Devos D, Bourriez JL, Poirot I, Derambure P, Defebvre L, Guieu JD. 2000. Brief and sustained movements: Differences in event-related (de)synchronization (ERD/ERS) patterns. Clin Neurophysiol. 111:2032–2039.

Chiang AKI, Rennie CJ, Robinson PA, van Albada SJ, Kerr CC. 2011. Age trends and sex differences of alpha rhythms including split alpha peaks. Clin Neurophysiol. 122:1505–1517.

Cole SR, Voytek B. 2017. Brain Oscillations and the Importance of Waveform Shape. Trends Cogn Sci. 21:137–149.

Cox R, Schapiro AC, Stickgold R. 2018. Variability and stability of large-scale cortical oscillation patterns. Netw Neurosci. 2:481–512.

Damoiseaux JS, Greicius ÆMD. 2009. Greater than the sum of its parts : a review of studies combining structural connectivity and resting-state functional connectivity. 525–533.

Davis J, Goadrich M. 2006. The relationship between Precision-Recall and ROC curves. In: ACM International Conference Proceeding Series. p. 233–240.

Delorme A, Makeig S. 2004. EEGLAB: An open source toolbox for analysis of single-trial EEG dynamics including independent component analysis. J Neurosci Methods. 134:9–21.

Demuru M, Fraschini M. 2020. EEG fingerprinting: Subject-specific signature based on the aperiodic component of power spectrum. Comput Biol Med. 120:103748.

Demuru M, Gouw AA, Hillebrand A, Stam CJ, Van Dijk BW, Scheltens P, Tijms BM, Konijnenberg E, Ten Kate M, Den Braber A, Smit DJA, Boomsma DI, Visser PJ. 2017. Functional and effective whole brain connectivity using magnetoencephalography to identify monozygotic twin pairs. Sci Rep. 7:1–11.

Diaz BA, van der Sluis S, Moens S, Benjamins JS, Migliorati F, Stoffers D, den Braber A, Poil SS, Hardstone R, Van't Ent D V., Boomsma DI, de Geus E, Mansvelder HD, Van Someren EJW, Linkenkaer-Hansen K. 2013. The Amsterdam Resting-state Questionnaire reveals multiple phenotypes of resting-state cognition. Front Hum Neurosci. 7:1–15.

Diedrichsen J, Kriegeskorte N. 2017. Representational models: A common framework for understanding encoding, pattern-component, and representational-similarity analysis, PLoS Computational Biology.

Dimsdale-Zucker HR, Ranganath C. 2019. Representational Similarity Analyses: A Practical Guide

for Functional MRI Applications. Handb Behav Neurosci. 28:509–525.

Duncan NW, Northoff G. 2013. Overview of potential procedural and participant-related confounds for neuroimaging of the resting state. J Psychiatry Neurosci. 38:84–96.

Erbil N, Ungan P. 2007. Changes in the alpha and beta amplitudes of the central EEG during the onset, continuation, and offset of long-duration repetitive hand movements. Brain Res. 1169:44–56.

Finn ES, Scheinost D, Finn DM, Shen X, Papademetris X, Constable RT. 2017. Can brain state be manipulated to emphasize individual differences in functional connectivity? Neuroimage. 160:140–151.

Finn ES, Shen X, Scheinost D, Rosenberg MD, Huang J, Chun MM, Papademetris X, Constable RT. 2015. Functional connectome fingerprinting: Identifying individuals using patterns of brain connectivity. Nat Neurosci. 18:1664–1671.

Giaquinto S, Cobianchi A, Macera F, Nolfe G. 1994. EEG Recordings in the course of recovery from stroke. Stroke. 25:2204–2209.

Gonzalez-Castillo J, Kam JWY, Colin HW, Bandettini PA. 2021. How to interpret resting-state fMRI : ask your participants . 41:1–19.

Gratton C, Laumann TO, Nielsen AN, Greene DJ, Gordon EM, Gilmore AW, Nelson SM, Coalson RS, Snyder AZ, Schlaggar BL, Dosenbach NUF, Petersen SE. 2018. Functional Brain Networks Are Dominated by Stable Group and Individual Factors, Not Cognitive or Daily Variation. Neuron. 98:439-452.e5.

Grefkes C, Fink GR. 2020. Recovery from stroke : current concepts and future perspectives. 6.

Gui Q, Jin Z, Xu W. 2015. Exploring EEG-based biometrics for user identification and authentication. 2014 IEEE Signal Process Med Biol Symp IEEE SPMB 2014 - Proc. 1–6.

Haegens S, Cousijn H, Wallis G, Harrison PJ, Nobre AC. 2014. Inter- and intra-individual variability in alpha peak frequency. Neuroimage. 92:46–55.

Haufe S, Meinecke F, Görgen K, Dähne S, Haynes JD, Blankertz B, Bießmann F. 2014. On the

interpretation of weight vectors of linear models in multivariate neuroimaging. Neuroimage. 87:96–110.

Hermundstad AM, Bassett DS, Brown KS, Aminoff EM, Clewett D, Freeman S, Frithsen A, Johnson A, Tipper CM, Miller MB, Grafton ST, Carlson JM. 2013. Structural foundations of resting-state and task-based functional connectivity in the human brain. Proc Natl Acad Sci U S A.

Hoenig MC, Bischof GN, Seemiller J, Hammes J, Kukolja J, Onur ÖA, Jessen F, Fliessbach K, Neumaier B, Fink GR, van Eimeren T, Drzezga A. 2018. Networks of tau distribution in Alzheimer's disease. Brain.

Huang X, Altahat S, Tran D, Sharma D. 2012. Human identification with electroencephalogram (EEG) signal processing. 2012 Int Symp Commun Inf Technol Isc 2012. 1021–1026.

Hutchison RM, Womelsdorf T, Allen EA, Bandettini PA, Calhoun VD, Corbetta M, Della Penna S, Duyn JH, Glover GH, Gonzalez-Castillo J, Handwerker DA, Keilholz S, Kiviniemi V, Leopold DA, de Pasquale F, Sporns O, Walter M, Chang C. 2013. Dynamic functional connectivity: Promise, issues, and interpretations. Neuroimage. 80:360–378.

Kawagoe T, Onoda K, Yamaguchi S. 2018. Different pre-scanning instructions induce distinct psychological and resting brain states during functional magnetic resonance imaging. Eur J Neurosci. 47:77–82.

Kehagias A. 2021. Community Detection Toolbox (https://www.mathworks.com/matlabcentral/fileexchange/45867-community-detection-toolbox), MATLAB Central File Exchange.

Knyazeva MG, Barzegaran E, Vildavski VY, Demonet J-F. 2018. Aging of human alpha rhythm. Neurobiol Aging. 69:261–273.

Miŝic B, Betzel RF, De Reus MA, Van Den Heuvel MP, Berman MG, McIntosh AR, Sporns O. 2016. Network-level structure-function relationships in human neocortex. Cereb Cortex. 26:3285–3296.

Mognon A, Jovicich J, Bruzzone L, Buiatti M. 2011. ADJUST: An automatic EEG artifact detector based on the joint use of spatial and temporal features. Psychophysiology. 48:229–240.

Näpflin M, Wildi M, Sarnthein J. 2007. Test-retest reliability of resting EEG spectra validates a statistical signature of persons. Clin Neurophysiol. 118:2519–2524.

Newbold DJ, Laumann TO, Hoyt CR, Hampton JM, Montez DF, Raut R V., Ortega M, Mitra A, Nielsen AN, Miller DB, Adeyemo B, Nguyen AL, Scheidter KM, Tanenbaum AB, Van AN, Marek S, Schlaggar BL, Carter AR, Greene DJ, Gordon EM, Raichle ME, Petersen SE, Snyder AZ, Dosenbach NUF. 2020. Plasticity and Spontaneous Activity Pulses in Disused Human Brain Circuits. Neuron. 0:1–10.

Noble S, Scheinost D, Constable RT. 2019. A decade of test-retest reliability of functional connectivity: A systematic review and meta-analysis. Neuroimage. 203:116157.

O'Brien F, Cousineau D. 2014. Representing Error bars in within-subject designs in typical software packages. Quant Methods Psychol. 10:56–67.

Oldfield RC. 1971. The assessment and analysis of handedness: The Edinburgh inventory. Neuropsychologia. 9:97–113.

Pani SM, Ciuffi M, Demuru M, La Cava SM, Bazzano G, D'Aloja E, Fraschini M. 2020. Subject, session and task effects on power, connectivity and network centrality: A source-based EEG study. Biomed Signal Process Control. 59.

Pedregosa F, Weiss R, Brucher M, Varoquaux G, Gramfort A, Michel V, Thirion B, Grisel O, Blondel M, Prettenhofer P, Weiss R, Dubourg V, Vanderplas J, Passos A, Cournapeau D, Brucher M, Perrot M, Duchesnay É. 2011. Scikit-learn: Machine Learning in Python. J Mach Learn Res. 12:2825–2830.

Pfurtscheller G, Lopes da Silva FH. 1999. Event-related EEG/MEG synchronization and desynchronization: basic principles. Clin Neurophysiol. 110:1842–1857.

Postema MC, De Marco M, Colato E, Venneri A. 2019. A study of within-subject reliability of the brain's default-mode network. Magn Reson Mater Physics, Biol Med. 32:391–405.

Pritschet L, Santander T, Taylor CM, Layher E, Yu S, Miller MB, Grafton ST, Jacobs EG. 2020. Functional reorganization of brain networks across the human menstrual cycle. Neuroimage. 220:117091.

Rehme AK, Fink GR, Cramon DY Von, Grefkes C. 2011. The Role of the Contralesional Motor Cortex for Motor Recovery in the Early Days after Stroke Assessed with Longitudinal fMRI.

Rifkin R, Klautau A. 2004. In Defense of One-Vs-All Classification. J Mach Learn Res. 5:2–6.

Saes M, Zandvliet SB, Andringa AS, Daffertshofer A, Twisk JWR, Meskers CGM, van Wegen EEH, Kwakkel G. 2020. Is Resting-State EEG Longitudinally Associated With Recovery of Clinical Neurological Impairments Early Poststroke? A Prospective Cohort Study. Neurorehabil Neural Repair. 34:389–402.

Schrouff J, Mourao-Miranda J. 2018. Interpreting weight maps in terms of cognitive or clinical neuroscience: Nonsense? 2018 Int Work Pattern Recognit Neuroimaging, PRNI 2018.

Sima C, Dougherty ER. 2008. The peaking phenomenon in the presence of feature-selection. Pattern Recognit Lett. 29:1667–1674.

Smit CM, Wright MJ, Hansell NK, Geffen GM, Martin NG. 2006. Genetic variation of individual alpha frequency (IAF) and alpha power in a large adolescent twin sample. Int J Psychophysiol. 61:235–243.

Smit DJA, Posthuma D, Boomsma DI, De Geus EJC. 2005. Heritability of background EEG across the power spectrum. Psychophysiology. 42:691–697.

Valizadeh SA, Riener R, Elmer S, Jäncke L. 2019. Decrypting the electrophysiological individuality of the human brain: Identification of individuals based on resting-state EEG activity. Neuroimage. 197:470–481.

Vallat R. 2018. Pingouin: statistics in Python. J Open Source Softw. 3:1026.

van Albada SJ, Kerr CC, Chiang AKI, Rennie CJ, Robinson PA. 2010. Neurophysiological changes with age probed by inverse modeling of EEG spectra. Clin Neurophysiol. 121:21–38.

van Albada SJ, Robinson PA. 2013. Relationships between electroencephalographic spectral peaks

across frequency bands. Front Hum Neurosci. 7:1–18.

Van Den Heuvel MP, Mandl RCW, Kahn RS, Hulshoff Pol HE. 2009. Functionally linked resting-state networks reflect the underlying structural connectivity architecture of the human brain. Hum Brain Mapp. 30:3127–3141.

van der Vliet R, Selles RW, Andrinopoulou ER, Nijland R, Ribbers GM, Frens MA, Meskers C, Kwakkel G. 2020. Predicting Upper Limb Motor Impairment Recovery after Stroke: A Mixture Model. Ann Neurol. 87:383–393.

Varoquaux G, Raamana PR, Engemann DA, Hoyos-Idrobo A, Schwartz Y, Thirion B. 2017. Assessing and tuning brain decoders: Cross-validation, caveats, and guidelines. Neuroimage. 145:166–179.

Vecchio F, Babiloni C, Lizio R, De Vico Fallani F, Blinowska K, Verrienti G, Frisoni G, Rossini PM. 2013. Resting state cortical EEG rhythms in Alzheimer's disease: Toward EEG markers for clinical applications: A review. 1st ed, Supplements to Clinical Neurophysiology. Elsevier B.V.

Voytek B, Kramer MA, Case J, Lepage KQ, Tempesta ZR, Knight RT, Gazzaley A. 2015. Age-Related Changes in 1/f Neural Electrophysiological Noise. J Neurosci. 35:13257–13265.

Watson D, Clark LA, Tellegen A. 1988. Development and validation of brief measures of positive and negative affect: The PANAS scales. J Pers Soc Psychol. 54:1063–1070.

Winkler I, Debener S, Muller KR, Tangermann M. 2015. On the influence of high-pass filtering on ICA-based artifact reduction in EEG-ERP. Proc Annu Int Conf IEEE Eng Med Biol Soc EMBS. 2015-Novem:4101–4105.

Wu J, Srinivasan R, Quinlan EB, Solodkin A, Small SL, Cramer SC. 2016. Utility of EEG measures of brain function in patients with acute stroke. J Neurophysiol. 115:2399–2405.

Wymbs NF, Bassett DS, Mucha PJ, Porter M a., Grafton ST. 2012. Differential Recruitment of the Sensorimotor Putamen and Frontoparietal Cortex during Motor Chunking in Humans. Neuron. 74:936–946.

Wymbs NF, Grafton ST. 2014. The Human Motor System Supports Sequence-Specific Representations over Multiple Training-Dependent Timescales. Cereb Cortex. 25:4213–4225.

# 4 Discussion

The main of this goal this thesis was to provide a better understanding about the modulation and measurement of neuroplasticity using the different methodological frameworks from Study 1 and Study 2. The discussion of this thesis will primarily focus on the question to what extend the current findings about the measurement and induction of neuroplasticity may be used to improve the individual therapeutic strategies in stroke recovery and what additional challenges might be encountered when translating the approaches into stroke populations.

In Study 1, cTBS was applied over M1 in a dose-dependent manner and changes in cortical and corticospinal excitability were quantified through TEPs and MEPs. The results provided evidence that the combination of TMS-EEG is a suitable technique to measure cTBS-induced plasticity in local and remote regions of the brain. Especially the N45 component, a marker of $GABA_A$-mediated neurotransmission, was significantly modulated after each dose around the centro-parietal regions (Study 1, Figure 8). The N100 component, a marker of $GABA_B$-mediated cortical inhibition, was altered within ipsilateral and contralateral hemisphere around and in proximity of the motor regions, potentially suggesting a shift in interhemispheric balance of $GABA_B$-mediated inhibition (Study 1, Figure 8). The findings provide novel insights into cTBS-induced plasticity, suggesting that changes in the $GABA_A$-mediated neurotransmission around centro-parietal sites are a characteristic of cTBS over M1. However, the results also demonstrated that the mechanisms that mediate responses to rTMS are complex, and conclusions about the cTBS response directions based on the unmodulated TEP seem to be limited, according to the responder subgroup comparison (Figure 10). Nevertheless, TMS-EEG provides a promising framework to measure and study cTBS-induced changes in cortical excitability in healthy individuals.

The results provided preliminary evidence that cTBS might be a suitable tool to modify $GABA_A$-mediated neurotransmission within the human motor system and adjacent regions. This finding is especially relevant for stroke rehabilitation strategies, as $GABA_A$-mediated cortical inhibition is heavily increased around the lesion site after stroke (Carmichael, 2012; Clarkson et al., 2010). This increase of inhibitory $GABA_A$ results in a reduction of excitability within the lesioned hemisphere. Measures of this inhibition also serve as an important prognostic marker for the potential functional recovery stroke patients might experience in the following weeks to month (Bembenek et al., 2012; Stinear et al., 2012). It has been hypothesized that this increase in $GABA_A$ around the perilesional region acts as initial protective mechanism to prevent excitotoxicity (Cassidy et al., 2014) caused by an abundance of excitatory glutamate neurotransmitter (Armada-Moreira et al., 2020). Transcallosal inhibition from the contralateral M1 is frequently increased following stroke, constituting another mechanism that leads to additional inhibition of ipsilesional M1 (Cassidy et al., 2014; Nowak et al., 2009). This severe upregulation of inhibitory mechanisms can reduce other efforts to normalize cortical excitability within the lesioned hemisphere and thereby impair the process of recovery (Murase et al., 2004). Administration of drugs that counteract this inhibition have been shown to promote functional recovery in mice (Clarkson et al., 2010). While delivering drugs selectively to one particular region of the brain is challenging, cTBS might allow to normalize levels of $GABA_A$-mediated inhibition in a more localized fashion, involving the target site and possibly some of the connected regions.

It remains to be clarified if the observed after-effects can be induced within larger populations and represent a genuine mode of action of cTBS. In Study 1, the N45 amplitude indicated that $GABA_A$-mediated inhibition was reduced around the motor and parietal regions. Interestingly, this reduction appeared within the whole group, the inhibitory subgroup and to some weaker extent also within the facilitatory subgroup (Study 1, Figure 8 & 9). Thus, there was a general tendency of cTBS to reduce $GABA_A$-mediated inhibition, even though after-effects on corticospinal excitability indicated modulations in opposite direction within subgroups (Study 1, Figure 4). While it is unclear what exactly caused this divergence, it could be hypothesized cTBS-induced $GABA_A$-mediated inhibition primarily affects cortical circuits that are not involved or only marginally affecting the generation of corticospinal output.

Reliability studies are of high importance to validate the cTBS-induced after-effects and its modulation of the N45 component. Here, cTBS was only applied in a single session, but a study from Schilberg et al. (2017) suggests that TBS after-effects on corticospinal excitability show high interindividual and interindividual variability. As consequence, the after-effects were rather largely inconsistent when investigated in separate sessions. This also seems to be the case of the TEP itself, as a recent study from Ozdemir et al. (2021), who investigated the reliability of cTBS after-effects on the TEP, observed that cTBS after-effects were indistinguishable from sham when measured at separate visits. Unfortunately, the authors did not specifically report effects on the N45 peak and it remains to be clarified if this lack of reliability also applies to measures of $GABA_A$-mediated inhibition. Thus, further reliability measurements are necessary to validate if this predominant reduction of $GABA_A$-mediated inhibition is a genuine mode of action of cTBS, or if it may reflect a coincidental effect related to some peculiarity of the study sample. If cTBS-induced changes in N45 component are for the greater part uncoupled from the cTBS-induced changes in corticospinal excitability, the current observation might simply reflect that the study sample consisted of many individuals that are prone to respond with a reduction of $GABA_A$-mediated inhibition to cTBS, rather than an increase.

Regarding the translation into clinical populations, it should be expected that variability of after-effects is even more pronounced in a sample of individuals suffering from stroke, as the lesions will affect how pulses can spread through cortico-cortical connections, resulting in more heterogeneous activation of cortical networks. For example, an fMRI study by Diekhoff-Krebs et al. (2017) demonstrated that interindividual differences in iTBS response characteristics in stroke patients are influenced by the coupling strength within the motor network of the lesion hemisphere. Thus, replicating studies are required within healthy and stroke individuals to validate the findings of Study 1. If reductions in $GABA_A$-mediated inhibition consistently appear in a large proportion of individuals, this would certainly increase the suitability of cTBS to induce neuroplasticity in the framework of rTMS-based rehabilitation for stroke recovery. It would be valuable to assess in future studies if those seemingly unidirectional changes in cortical excitability appear consistently across larger groups of individuals or if there are responder subgroups, comparable to those that can be defined when measuring MEPs measurements.

Another important consideration is related to the existence of local and remote changes in cortical excitability. In Study 1, cTBS altered cortical responses to a considerable amount in parietal and occipital regions or even on the contralateral hemisphere, rather than locally around ipsilateral M1. For example, cTBS resulted in bilateral and distant changes of the N45 (Study 1, Figure 8, TEP 3) and the N100 component (Study 1, Figure 8, TEP 2) of the TEP. Interestingly, those distant changes were in part characterized by increases at one cortical region and reductions in another. This raises the question to what extend a localized and unilateral modulation of M1 might be achievable in clinical practice. The model of interhemispheric competition after stroke suggests that the contralesional hemisphere exerts increased transcallosal inhibition over the ipsilesional hemisphere (Hoyer & Celnik, 2011; Nowak et al., 2009). The existence of significant alterations in cortical excitability distant from the stimulation site suggests that it may be rather challenging to increase or decrease excitability locally within one hemisphere without affecting projections to the contralateral hemisphere or adjacent regions in an undesired way. Optimizing stimulation intensities could potentially improve selective activation of target regions while reducing the spread to other regions. However, increasing the focality of stimulation is at least in part limited by the physical principles behind TMS. The electrical current in the stimulation coil has to be strong enough to generate a magnetic field that can pass through the skull, consequently generating a stronger but less focal electrical field within the brain (Gomez et al., 2018; Wagner et al., 2009). Thus, even the smallest possible activation of the target region might still be strong enough to enable propagation of the pulse to connected regions.

Regarding the measurement of cTBS-induced plasticity through the TEP, it is only poorly understood to which degree a TEP response can be evoked within stroke individuals. So far, it is unknown whether the mechanisms of neurotransmission can be indexed in a similar fashion in stroke individuals as it has been demonstrated in healthy individuals. Not only structural integrity of the brain, but also ongoing oscillatory dynamics influence how the cortical response to a TMS pulse will propagate through the brain. For example, complexity and spread of TEP response were significantly reduced after participants entered the non-rem sleep phase compared to wakefulness (Massimini et al., 2005). In vegetative patients, a simple and focal response could be measured, whereas TEPs in minimally conscious patients were more complex and also spread to more distant cortical regions (Rosanova et al., 2012). Future studies might attempt to control for differences in

vigilance to avoid such potential confounding factors. RS-EEG measurements could be included between TMS measurements as a way to track EEG markers of fatigue and wakefulness (De Gennaro et al., 2007; Jap et al., 2009). TEP responses acquired from M1 stimulation in acute stroke patients have been shown to demonstrate similar reductions in complexity as during non-rem sleep (Tscherpel et al., 2020), indicating that stroke related lesions can disrupt connectivity and prevent the TMS-induced electric field to spread from the stimulation site to distant brain regions. In the study by Tscherpel et al. (2020), TEPs were so heavily reduced in complexity, that the N45 peak was not even detectable in some of the individuals. Such modifications of the TEP might drastically reduce its capabilities to track neuroplasticity in clinical populations. In contrast, Pellicciari et al. (2018) investigated TEPs in patients affected by subcortical stroke. While the authors did not investigate individual TEP peaks, cortical responses were differentiated and more complex than the ones reported by Tscherpel et al. (2020). Additional support for the usability of TMS-EEG in stroke patients is provided by Hordacre et al. (2019), who reported a relationship between amplitude of the N45 component and the hold ratio in stroke patients. Thus, extent of the lesion and remaining integrity of the cortico-cortical connections might play an important role in determining whether TEPs are able to measure TBS-induced changes in $GABA_A$-mediated neurotransmission in individuals affected by stroke.

In Study 2, EEG was acquired on five subsequent days to test the suitability of RS for longitudinal tracking of individual neuroplastic changes. It was investigated if individual-specific signatures obtained from RS-EEG would allow to distinguish changes in neurophysiological organization from unintentional variations in cognitive state that are likely to occur between measurements. The ability to make such distinction is a crucial prerequisite to use RS-EEG for longitudinal tracking in scenarios of increased neuroplasticity, as differences in cognitive state between measurements might lead to wrong inferences, erroneously interpreting variations in cognitive state as ongoing process of cortical reorganization. Assuming that healthy individuals do not undergo significant neuroplastic changes within this five day period, activity pattern of other individuals were used as proxy to simulate a wide range of potential neurophysiological changes. The results extend previous findings about high interindividual and low intraindividual variability of EEG oscillatory dynamics at rest (Gasser et al., 1985; Näpflin et al., 2007), and thereby strongly supports the usage of RS-EEG for individualized longitudinal tracking. Moreover, it was demonstrated that RS-EEG

contains configurations of oscillatory activity that are highly specific to individual neurophysiological organization and very stable across time. Distinguishing inter-day variations in cognitive state from the simulated changes in neurophysiological organization was therefore possible with very high accuracy. These results emphasize the high specificity of oscillatory dynamics at rest with respect to individual neurophysiological brain organization. They furthermore provide a proof of concept for the potential of longitudinal RS-EEG to track individual trajectories of neuroplastic reorganization, even in the presence of inter-day variability in cognitive state.

The translation of this approach towards individualized tracking in individuals affected by stroke requires additional important considerations and raises several questions. For example, how does oscillatory power change after stroke and in the following period of cortical reorganization? Would the approach from Study 2 be able to recognize such changes over time? One of the fundamental assumptions of Study 2 was that the oscillatory power during rest is highly structured, reflecting the individual neurophysiological organization of underlying large-scale brain networks. If these networks are reorganized, as consequence of neuroplastic processes or neurodegenerative diseases, this should lead to distinctive changes in the oscillatory signature recorded from the scalp. Previous studies have already demonstrated that RS-EEG can reveal similar information about integrity and functional state of large-scale brain networks as the fMRI-based RS measurements (Deligianni et al., 2014; Mantini et al., 2007).
An asymmetry in activity between hemispheres is a common observation in stroke patients when investigating them with techniques such as TMS or fMRI (Cunningham et al., 2015; Traversa et al., 1998). Similar observations also exist from RS-EEG studies, showing that the measurement of oscillatory power can also serve as indicator of interhemispheric imbalances after stroke (Agius Anastasi et al., 2017; Sebastián-Romagosa et al., 2020; Trujillo et al., 2017; Van Putten & Tavy, 2004). Another important EEG marker of stroke is the delta and alpha power ratio (DAR), which reflects the relationship of oscillations in the delta and the alpha frequency band. The DAR has been shown to have a prognostic value in predicting the recovery perspectives of patients after stroke (Fanciullacci et al., 2017; Leon-Carrion et al., 2009). Thus, there is sufficient evidence showing that EEG dynamics are considerably altered as consequence of the stroke related lesions.

The classification framework in Study 2 did not make any explicit assumptions made about how exactly oscillatory signatures are required to change to allow a differentation of neuroplastic reorganization from cognitive state variations. Instead, individual-specific signatures were extracted from cortical dynamics and represented in a high dimensional feature space, containing all channels and covering frequencies from 1-40 Hz. Such large-scale changes in asymmetry of oscillatory power between hemispheres or changes in the DAR likely fall into the category of changes that could potentially be recognized using the classification approach of Study 2. However, it has to be considered that those significant changes are often based on group-level inferences and in comparison to healthy populations. Distinguishing changes in DAR or changes in interhemispheric imbalance over time from cognitive state variations within individuals will be considerably more challenging. There is also only little evidence about how these EEG markers of stroke change over time during the process of recovery. A longitudinal study by Saes et al. (2020) reported that the DAR of the affected hemisphere gradually returned to normal levels after stroke within the first months, whereas the BSI remained lateralized. Thus, more studies are required to assess to what extend such EEG markers of stroke also track the progress of ongoing neuroplastic processes, rather than simply reflecting damage of the networks compared to a healthy population.

The usage of interindividual differences to simulate neuroplastic changes was a novel and practical implementation to generate possible examples of significant changes in individual neurophysiological brain organization for the classification. However, it has to be considered that these were undoubtedly extreme examples of neurophysiological change. In reality, EEG correlates of cortical reorganization will likely be more subtle and therefore certainly more difficult to distinguish from incidental changes in cognitive state. Furthermore, Study 2 demonstrated that individual-specific RS pattern show a high degree of stability across days. It is unclear to what extend those findings translate to individuals suffering from stroke. Evidence from stroke individuals in the chronic stage suggested that EEG power is in general reliable, with some exception regarding the delta band (Dalton et al., 2021). However, the delta band (in form of the DAR) is a critical feature of stroke related changes in EEG dynamics and a lack of reliability might prevent adequate tracking of such changes within individuals. Interestingly, the delta band was also the frequency band with the lowest cross-day classification accuracy (Study 2, Figure 6A), indicating a certain lack of robustness across time within healthy individuals.

The extraction of individual-specific signatures in Study 2 was realized through a classification model. A core assumption behind this strategy was that oscillatory EEG dynamics at rest show a considerable degree of interindividual variability, which are mainly governed by individual differences in the underlying neurophysiological organization. By finding combinations of characteristic features that were robust across time and maximize these interindividual differences, it was hypothesized to identify signatures of brain activity that primarily represent the individual underlying neurophysiological organization rather than day-specific characteristics of the prevalent brain state. Conversely, this implies that individual-specific signatures always depend on the composition of the group that was used to extract the signature (see Study 2, section 4.3). This raises the question how the other group should be defined regarding the application of this strategy in stroke individuals. A homogeneous group of stroke patients with very similar lesions might actually have a lower interindividual variability than a group of individuals with heterogenous lesions, or a mixture of healthy individuals and patients. In addition, the study sample was relatively small with 27 subjects in Study 2 and it was not not investigated how individual-specific pattern would change in relation to the composition of the group. It should be investigated if robust signatures can also be obtained from smaller or larger study samples. These are critical questions that need to be addressed when translating this approach into stroke populations for the longitudinal tracking of neuroplasticity.

Future studies might also combine the two methodological approaches from Study 1 and Study 2 to improve experimental designs, possibly providing deeper insights into the induction and tracking of neuroplastic changes using TMS and EEG. For example, as demonstrated in Study 1, rTMS protocols can induce neuroplasticity in a target brain region and connected networks. The significance of Study 2 was limited due to the inability to systematically induce cortical plasticity within healthy individuals. As consequence, brain activity pattern of other individuals had to be used to test the robustness of individual- specific signatures. By using rTMS to induce cortical plasticity within those healthy and young individuals, it could be explicitly tested if such neuroplastic changes would be recognizable and distinguishable from inter-day variations in cognitive state or not. This induction of cortical plasticity would certainly constitute a more realistic and neurophysiologically plausible representation of neuroplastic changes compared to the extreme examples that were used for classification in Study 2.

On the other hand, RS-EEG could be used to inform the experimenter in real-time about the strength and frequencies of brain oscillations, and thereby potentially improve the way of how neuroplasticity can be induced via rTMS. There are indications that the individual oscillatory dynamics play an important role in mediating the effects of rTMS, and might therefore help to reduce variability of TBS after-effects. For example, the bursts of TBS are usually applied with a fixed frequency of 5 Hz, which approximately corresponds to the frequency of the human theta rhythm (4-7 Hz). However, it has been suggested that an adaptation of the burst frequency to the individual frequency of theta oscillations measured by EEG could potentially reduce response variability and improve TBS after-effects (Brownjohn et al., 2014; Chung et al., 2019).

Another promising approach to reduce outcome variability of neuromodulatory brain stimulation is based on the approach to apply the rTMS pulses in phase with the ongoing oscillatory rhythm of the human motor system. Zrenner et al. (2018) hypothesized that the phase of the dominant oscillatory activity around the motor cortex, the μ-rhythm, represents states of low and high cortical excitability. By recording EEG activity in real-time and triggering TMS pulses at either the positive or negative phase of the rhythm, they were able to demonstrate that rTMS pulses applied around the negative phase of the human μ-rhythm induces neuroplasticity, but not at the positive phase of the rhythm (Zrenner et al., 2018). In contrast, this assumption was challenged by (Madsen et al., 2019) who did not find any indications of such phase-based relationship between stimulation effects and cortical excitability states.

Since Study 1 already required the setup of EEG recordings, it would have been possible to implement the techniques described above to potentially reduce the variability of cTBS-induced neuroplasticity. Especially the tuning to individual theta frequency rhythms can be realized without any major obstacles, as it simply requires an estimation of the thet rhythm peak frequency, which can be easily obtained from a short period of RS-EEG measurements prior to the application of cTBS. In contrast, real-time and phase-based triggering of rTMS pulses is technically very challenging as it requires a forward estimation of the phase from the ongoing oscillatory activity. Only recently, a toolbox for this real-time phase estimation was published by Zrenner et al. (2020). However, due to the complexity of this method, it is unlikely that it can be translated into clinical practice in near future.

# 5 Conclusion

This thesis was motivated by the difficult challenges that are encountered in clinical practice in the realms of stroke recovery. First, therapeutic interventions, such as rTMS, require a profound understanding about the direction and extent of induced plasticity to achieve the best possible therapy outcome. Second, it is necessary to measure neuroplastic processes on an individual basis to optimize the timing of interventions to support ongoing beneficial cortical reorganization while inhibiting changes that might turn out maladaptive. The goal of this thesis was therefore to provide a better understanding about the induction and measurement of cortical plasticity within the human brain, using a combination of rTMS, TMS-EEG and RS-EEG in two different experimental frameworks.

The studies yield experimental evidence for the suitability of TMS-EEG and RS-EEG to measure processes of cortical plasticity in healthy and young individuals. Study 1 demonstrated that TMS-EEG could be a viable strategy to characterize the degree and spatial extent of cTBS-induced plasticity as complementary measure of MEPs. It was shown that cTBS-induced plasticity affects markers of $GABA_A$- and $GABA_B$-mediated inhibition, suggesting that cTBS could be a useful therapeutic approach to normalize abnormal levels of $GABA_A$-mediated inhibition after stroke. The relationship between measures of cortical and corticospinal excitability require further investigation. While strong relationships between both measures were absent, cTBS altered excitability in remote but connected regions and it is unlikely that MEPs are able to indicate such remote excitability changes accurately. Interestingly, a recent investigation by Ozdemir et al. (2021) raised significant doubts about the ability of TMS-EEG to measure cTBS-induced plasticity in a reliable manner. This problem needs to be addressed in future studies, to find out if reliability is

limited by the measurement of plasticity via TMS-EEG or the induction of plasticity via cTBS. Improvements of the preprocessing pipelines could help to standardize the still complex analysis of TMS-EEG measurements and help to translate the approach into clinical practice.

The results of Study 2 support the suitability of RS-EEG to realize individualized longitudinal tracking of neuroplastic changes. Measurements of RS power were very stable across time. In addition, it was possible to extract signatures of brain activity that were present in other cognitive states but were at the same time, highly specific to the individual neurophysiological organization. The results demonstrate that distinguishing inter-day variations in cognitive state from changes in the neurophysiological organization are possible with very high accuracy. While the study did not directly induce neuroplasticity within the healthy participants, it still provides preliminary evidence that such distinctions are possible, eliminating one important confounding factor that might limit the usability of RS in repeated measurements. Importantly, the applied classification approach is not restricted to measurements of RS power or EEG, but could be translated to other neuroimaging modalities to explore other possibilities to track neuroplasticity within individuals over time. Further studies are required to investigate if such tracking would be possible in stroke patients and are sensitive enough to detect neuroplastic reorganization during the critical period of stroke recovery.

In conclusion, TMS-EEG and RS-EEG have desirable properties to measure intrinsic or cTBS-induced plasticity. While both studies had an explorative character regarding the methodologies and the analytical approaches, they provide an important basis for future studies to improve and extend the measurement and induction of neuroplasticity using TMS and EEG.

# Bibliography


Aeschbach, D., & Borbély, A. A. (1993). All-night dynamics of the human sleep EEG. *Journal of sleep research*, *2*(2), 70–81. https://doi.org/10.1111/j.1365-2869.1993.tb00065.x

Agius Anastasi, A., Falzon, O., Camilleri, K., Vella, M., & Muscat, R. (2017). Brain symmetry index in healthy and stroke patients for assessment and prognosis. *Stroke Research and Treatment*, *2017*. https://doi.org/10.1155/2017/8276136

Armada-Moreira, A., Gomes, J. I., Pina, C. C., Savchak, O. K., Gonçalves-Ribeiro, J., Rei, N., Pinto, S., Morais, T. P., Martins, R. S., Ribeiro, F. F., Sebastião, A. M., Crunelli, V., & Vaz, S. H. (2020). Going the Extra (Synaptic) Mile: Excitotoxicity as the Road Toward Neurodegenerative Diseases. *Frontiers in Cellular Neuroscience*, *14*(April), 1–27. https://doi.org/10.3389/fncel.2020.00090

Barker, A. T., Jalinous, R., & Freeston, I. L. (1985). Non-invasive magnetic stimulation of human motor cortex. https://doi.org/10.1016/s0140-6736(85)92413-4

Barry, R. J., Clarke, A. R., Johnstone, S. J., Magee, C. A., & Rushby, J. A. (2007). EEG differences between eyes-closed and eyes-open resting conditions. *Clinical Neurophysiology*, *118*, 2765–2773. https://doi.org/10.1016/j.clinph.2007.07.028

Başar-Eroglu, C., Strüber, D., Schürmann, M., Stadler, M., & Başar, E. (1996). Gamma-band responses in the brain: A short review of psychophysiological correlates and functional significance. *International Journal of Psychophysiology*, *24*(1-2), 101–112. https://doi.org/10.1016/S0167-8760(96)00051-7

Belardinelli, P., König, F., Liang, C., Premoli, I., Desideri, D., Müller-Dahlhaus, F., Gordon, P. C., Zipser, C., Zrenner, C., & Ziemann, U. (2021). TMS-EEG signatures of glutamatergic neurotransmission in human cortex. *Scientific Reports*, *11*(1), 1–14. https://doi.org/10.1038/s41598-021-87533-z

Bembenek, J. P., Kurczych, K., Karliński, M., & Członkowska, A. (2012). The prognostic value of motor-evoked potentials in motor recovery and functional outcome after stroke - A systematic review of the literature. *Functional Neurology*, *27*(2), 79–84. https://doi.org/10.1016/j.clinph.2013.04.156

Berger, H. (1929). Über das Elektrenkephalogramm des Menschen. *Archiv für Psychiatrie und Nervenkrankheiten*, *87*(1), 527–570. https://doi.org/10.1007/BF01797193

Bestmann, S., & Krakauer, J. W. (2015). The uses and interpretations of the motor-evoked potential for understanding behaviour. *Experimental Brain Research*, *233*(3), 679–689. https://doi.org/10.1007/s00221-014-4183-7

Bijsterbosch, J. D., Barker, A. T., Lee, K. H., & Woodruff, P. W. (2012). Where does transcranial magnetic stimulation (TMS) stimulate? Modelling of induced field maps for some common cortical and cerebellar targets. *Medical and Biological Engineering and Computing*, *50*(7), 671–681. https://doi.org/10.1007/s11517-012-0922-8

Biswal, B., Zerrin Yetkin, F., Haughton, V. M., & Hyde, J. S. (1995). Functional connectivity in the motor cortex of resting human brain using echo-planar mri. *Magnetic Resonance in Medicine*, *34*(4), 537–541. https://doi.org/https://doi.org/10.1002/mrm.1910340409

Bonnard, M., Spieser, L., Meziane, H. B., De Graaf, J. B., & Pailhous, J. (2009). Prior intention can locally tune inhibitory processes in the primary motor cortex: Direct evidence from combined TMS-EEG. *European Journal of Neuroscience*, *30*(5), 913–923. https://doi.org/10.1111/j.1460-9568.2009.06864.x

Bonnard, M., Camus, M., De Graaf, J., & Pailhous, J. (2003). Direct Evidence for a Binding between Cognitive and Motor Functions in Humans: A TMS Study. *Jour-*

*nal of Cognitive Neuroscience*, *15*(8), 1207–1216. https://doi.org/10.1162/089892903322598157

Brownjohn, P. W., Reynolds, J. N., Matheson, N., Fox, J., & Shemmell, J. B. (2014). The effects of individualized theta burst stimulation on the excitability of the human motor system. *Brain Stimulation*, *7*(2), 260–268. https://doi.org/10.1016/j.brs.2013.12.007

Buzsáki, G. (2006). *Rhythms of the brain.* Oxford University Press. https://doi.org/10.1093/acprof:oso/9780195301069.001.0001

Buzsáki, G., Anastassiou, C. a., & Koch, C. (2012). The origin of extracellular fields and currents — EEG, ECoG, LFP and spikes. *Nature Reviews Neuroscience*, *13*(6), 407–420. https://doi.org/10.1038/nrn3241

Carmichael, S. T. (2012). Brain excitability in stroke: the yin and yang of stroke progression. *Archives of neurology*, *69*(2), 161–167. https://doi.org/10.1001/archneurol.2011.1175

Carod-Artal, F. J., & Egido, J. A. (2009). Quality of life after stroke: The importance of a good recovery. *Cerebrovascular Diseases*, *27*(SUPPL. 1), 204–214. https://doi.org/10.1159/000200461

Casarotto, S., Lauro, L. J., Bellina, V., Casali, A. G., Rosanova, M., Pigorini, A., Defendi, S., Mariotti, M., & Massimini, M. (2010). EEG responses to TMS are sensitive to changes in the perturbation parameters and repeatable over time. *PLoS ONE*, *5*(4). https://doi.org/10.1371/journal.pone.0010281

Cassidy, J. M., Gillick, B. T., & Carey, J. R. (2014). Priming the brain to capitalize on metaplasticity in stroke rehabilitation. *Physical Therapy*, *94*(1), 139–150. https://doi.org/10.2522/ptj.20130027

Chen, H., Epstein, J., & Stern, E. (2010). Neural plasticity after acquired brain injury: Evidence from functional neuroimaging. *PM and R*, *2*(12 SUPPL), S306–S312. https://doi.org/10.1016/j.pmrj.2010.10.006

Chen, R., Classen, J., Gerloff, C., Celnik, P., Wassermann, E. M., Hallett, M., & Cohen, L. G. (1997). Depression of motor cortex excitability by low-frequency transcra-

nial magnetic stimulation. *Neurology*, *48*(5), 1398–1403. https://doi.org/10.1212/WNL.48.5.1398

Chung, S. W., Sullivan, C. M., Rogasch, N. C., Hoy, K. E., Bailey, N. W., Cash, R. F. H., & Fitzgerald, P. B. (2019). The effects of individualised intermittent theta burst stimulation in the prefrontal cortex: A TMS-EEG study. *Human brain mapping*, *40*(2), 608–627. https://doi.org/10.1002/hbm.24398

Clarkson, A. N., Huang, B. S., MacIsaac, S. E., Mody, I., & Carmichael, S. T. (2010). Reducing excessive GABA-mediated tonic inhibition promotes functional recovery after stroke. *Nature*, *468*(7321), 305–309. https://doi.org/10.1038/nature09511

Coleman, E. R., Moudgal, R., Lang, K., Hyacinth, H. I., Awosika, O. O., Kissela, B. M., & Feng, W. (2017). Early Rehabilitation After Stroke: a Narrative Review. *Current atherosclerosis reports*, *19*(12), 59. https://doi.org/10.1007/s11883-017-0686-6

Cortes, J. C., Goldsmith, J., Harran, M. D., Xu, J., Kim, N., Schambra, H. M., Luft, A. R., Celnik, P., Krakauer, J. W., & Kitago, T. (2017). A Short and Distinct Time Window for Recovery of Arm Motor Control Early After Stroke Revealed With a Global Measure of Trajectory Kinematics. *Neurorehabilitation and neural repair*, *31*(6), 552–560. https://doi.org/10.1177/1545968317697034

Cramer, S. C. (2008). Repairing the human brain after stroke: I. Mechanisms of spontaneous recovery. *Annals of Neurology*, *63*(3), 272–287. https://doi.org/10.1002/ana.21393

Creel, D. J. (2019). *Visually evoked potentials* (1st ed., Vol. 160). Elsevier B.V. https://doi.org/10.1016/B978-0-444-64032-1.00034-5

Cunningham, D. A., Machado, A., Janini, D., Varnerin, N., Bonnett, C., Yue, G., Jones, S., Lowe, M., Beall, E., Sakaie, K., & Plow, E. B. (2015). Assessment of inter-hemispheric imbalance using imaging and noninvasive brain stimulation in patients with chronic stroke. *Archives of Physical Medicine and Rehabilitation*, *96*(4), S94–S103. https://doi.org/10.1016/j.apmr.2014.07.419

Dafotakis, M., Grefkes, C., Eickhoff, S. B., Karbe, H., Fink, G. R., & Nowak, D. A. (2008). Effects of rTMS on grip force control following subcortical stroke. *Exper-*

*imental Neurology*, *211*(2), 407–412. https://doi.org/10.1016/j.expneurol.2008.02.018

Dalton, S. G., Cavanagh, J. F., & Richardson, J. D. (2021). Spectral Resting-State EEG (rsEEG) in Chronic Aphasia Is Reliable, Sensitive, and Correlates With Functional Behavior. *Frontiers in Human Neuroscience*, *15*(March), 1–16. https://doi.org/10.3389/fnhum.2021.624660

Damoiseaux, J. S., Rombouts, S. A. R. B., Barkhof, F., Scheltens, P., Stam, C. J., Smith, S. M., & Beckmann, C. F. (2006). Consistent resting-state networks across healthy subjects. *Proceedings of the National Academy of Sciences*, *103*(37), 13848–13853. https://doi.org/10.1073/pnas.0601417103

Daskalakis, Z. J., Christensen, B. K., Chen, R., Fitzgerald, P. B., Zipursky, R. B., & Kapur, S. (2002). Evidence for impaired cortical inhibition in schizophrenia using transcranial magnetic stimulation. *Archives of general psychiatry*, *59*(4), 347–354. https://doi.org/10.1001/archpsyc.59.4.347

Davis, C. J., Clinton, J. M., Jewett, K. A., Zielinski, M. R., & Krueger, J. M. (2011). Delta wave power: An independent sleep phenotype or epiphenomenon? *Journal of Clinical Sleep Medicine*, *7*(5), 7–9. https://doi.org/10.5664/JCSM.1346

Dayan, E., & Cohen, L. G. (2011). Neuroplasticity subserving motor skill learning. *Neuron*, *72*(3), 443–454. https://doi.org/10.1016/j.neuron.2011.10.008

De Gennaro, L., Marzano, C., Veniero, D., Moroni, F., Fratello, F., Curcio, G., Ferrara, M., Ferlazzo, F., Novelli, L., Concetta Pellicciari, M., Bertini, M., & Rossini, P. M. (2007). Neurophysiological correlates of sleepiness: A combined TMS and EEG study. *NeuroImage*, *36*(4), 1277–1287. https://doi.org/10.1016/j.neuroimage.2007.04.013

Deligianni, F., Centeno, M., Carmichael, D. W., & Clayden, J. D. (2014). Relating resting-state fMRI and EEG whole-brain connectomes across frequency bands. *Frontiers in Neuroscience*, *8*(August), 1–16. https://doi.org/10.3389/fnins.2014.00258

Deng, Z.-D., Lisanby, S. H., & Peterchev, A. V. (2013). Electric field depth-focality tradeoff in transcranial magnetic stimulation: simulation comparison of 50 coil designs. *Brain stimulation*, *6*(1), 1–13. https://doi.org/10.1016/j.brs.2012.02.005

Deng, Z.-D., Lisanby, S. H., & Peterchev, A. V. (2014). Coil design considerations for deep transcranial magnetic stimulation. *Clinical neurophysiology : official journal of the International Federation of Clinical Neurophysiology*, *125*(6), 1202–1212. https://doi.org/10.1016/j.clinph.2013.11.038

de Vos, F., Koini, M., Schouten, T. M., Seiler, S., van der Grond, J., Lechner, A., Schmidt, R., de Rooij, M., & Rombouts, S. A. (2018). A comprehensive analysis of resting state fMRI measures to classify individual patients with Alzheimer's disease. *NeuroImage*, *167*(December 2016), 62–72. https://doi.org/10.1016/j.neuroimage.2017.11.025

Di, Y., An, X., He, F., Liu, S., Ke, Y., & Ming, D. (2019). Robustness Analysis of Identification Using Resting-State EEG Signals. *IEEE Access*, *7*, 42113–42122. https://doi.org/10.1109/ACCESS.2019.2907644

Di Lazzaro, V., & Ziemann, U. (2013). The contribution of transcranial magnetic stimulation in the functional evaluation of microcircuits in human motor cortex. *Frontiers in Neural Circuits*, *7*(JAN), 1–9. https://doi.org/10.3389/fncir.2013.00018

Diana, M., Raij, T., Melis, M., Nummenmaa, A., Leggio, L., & Bonci, A. (2017). Rehabilitating the addicted brain with transcranial magnetic stimulation. *Nature Reviews Neuroscience*, *18*(11), 685–693. https://doi.org/10.1038/nrn.2017.113

Diekhoff-Krebs, S., Pool, E. M., Sarfeld, A. S., Rehme, A. K., Eickhoff, S. B., Fink, G. R., & Grefkes, C. (2017). Interindividual differences in motor network connectivity and behavioral response to iTBS in stroke patients. *NeuroImage: Clinical*, *15*(January), 559–571. https://doi.org/10.1016/j.nicl.2017.06.006

Du, J., Yang, F., Hu, J., Hu, J., Xu, Q., Cong, N., Zhang, Q., Liu, L., Mantini, D., Zhang, Z., Lu, G., & Liu, X. (2019). Effects of high- and low-frequency repetitive transcranial magnetic stimulation on motor recovery in early stroke patients: Evidence from a randomized controlled trial with clinical, neurophysiological and

functional imaging assessments. *NeuroImage: Clinical*, *21*(August 2018), 101620. https://doi.org/10.1016/j.nicl.2018.101620

Duncan, P. W., & Sue Min Lai. (1997). Stroke recovery. *Topics in Stroke Rehabilitation*, *4*(3), 51–58. https://doi.org/10.1310/KYD7-HN2K-VGYG-8C98

Duque, J., Greenhouse, I., Labruna, L., & Ivry, R. B. (2017). Physiological Markers of Motor Inhibition during Human Behavior. *Trends in neurosciences*, *40*(4), 219–236. https://doi.org/10.1016/j.tins.2017.02.006

Engel, A. K., & Fries, P. (2010). Beta-band oscillations—signalling the status quo? *Current Opinion in Neurobiology*, *20*(2), 156–165. https://doi.org/https://doi.org/10.1016/j.conb.2010.02.015

Cognitive neuroscience

Ergenoglu, T., Demiralp, T., Bayraktaroglu, Z., Ergen, M., Beydagi, H., & Uresin, Y. (2004). Alpha rhythm of the EEG modulates visual detection performance in humans. *Cognitive Brain Research*, *20*(3), 376–383. https://doi.org/10.1016/j.cogbrainres.2004.03.009

Erickson, B., Truelove-Hill, M., Oh, Y., Anderson, J., Zhang, F. (, & Kounios, J. (2018). Resting-state brain oscillations predict trait-like cognitive styles. *Neuropsychologia*, *120*, 1–8. https://doi.org/https://doi.org/10.1016/j.neuropsychologia.2018.09.014

Fanciullacci, C., Bertolucci, F., Lamola, G., Panarese, A., Artoni, F., Micera, S., Rossi, B., & Chisari, C. (2017). Delta power is higher and more symmetrical in ischemic stroke patients with cortical involvement. *Frontiers in Human Neuroscience*, *11*(July), 1–10. https://doi.org/10.3389/fnhum.2017.00385

Ferbert, A., Priori, A., Rothwell, J. C., Day, B. L., Colebatch, J. G., & Marsden, C. D. (1992). Interhemispheric inhibition of the human motor cortex. *The Journal of physiology*, *453*, 525–546. https://doi.org/10.1113/jphysiol.1992.sp019243

Fitzgibbon, S. P., Pope, K. J., MacKenzie, L., Clark, C. R., & Willoughby, J. O. (2004). Cognitive tasks augment gamma EEG power. *Clinical Neurophysiology*, *115*(8), 1802–1809. https://doi.org/10.1016/j.clinph.2004.03.009

Foxe, J. J., & Snyder, A. C. (2011). The role of alpha-band brain oscillations as a sensory suppression mechanism during selective attention. *Frontiers in Psychology*, *2*(JUL), 1–13. https://doi.org/10.3389/fpsyg.2011.00154

Galván, A. (2010). Neural plasticity of development and learning. *Human Brain Mapping*, *31*(6), 879–890. https://doi.org/10.1002/hbm.21029

Gasser, T., Bächer, P., & Steinberg, H. (1985). Test-retest reliability of spectral parameters of the EEG. *Electroencephalography and Clinical Neurophysiology*, *60*(4), 312–319. https://doi.org/10.1016/0013-4694(85)90005-7

George, M. S., Taylor, J. J., & Short, E. B. (2013). The expanding evidence base for rTMS treatment of depression. *Current Opinion in Psychiatry*, *26*(1), 13–18. https://doi.org/10.1097/YCO.0b013e32835ab46d

Golestani, A. M., Tymchuk, S., Demchuk, A., & Goodyear, B. G. (2013). Longitudinal evaluation of resting-state fMRI after acute stroke with hemiparesis. *Neurorehabilitation and Neural Repair*, *27*(2), 153–163. https://doi.org/10.1177/1545968312457827

Gomez, L. J., Goetz, S. M., & Peterchev, A. V. (2018). Design of transcranial magnetic stimulation coils with optimal trade-off between depth, focality, and energy. *Journal of neural engineering*, *15*(4), 46033. https://doi.org/10.1088/1741-2552/aac967

Groppa, S., Oliviero, A., Eisen, A., Quartarone, A., Cohen, L. G., Mall, V., Kaelin-Lang, A., Mima, T., Rossi, S., Thickbroom, G. W., Rossini, P. M., Ziemann, U., Valls-Solé, J., & Siebner, H. R. (2012). A practical guide to diagnostic transcranial magnetic stimulation: report of an IFCN committee. *Clinical neurophysiology : official journal of the International Federation of Clinical Neurophysiology*, *123*(5), 858–882. https://doi.org/10.1016/j.clinph.2012.01.010

Hallett, M. (2001). Plasticity of the human motor cortex and recovery from stroke. *Brain research. Brain research reviews*, *36*(2-3), 169–174. https://doi.org/10.1016/s0165-0173(01)00092-3

Hallett, M. (2007). Transcranial Magnetic Stimulation: A Primer. *Neuron*, *55*(2), 187–199. https://doi.org/10.1016/j.neuron.2007.06.026

Hamada, M., Murase, N., Hasan, A., Balaratnam, M., & Rothwell, J. C. (2013). The role of interneuron networks in driving human motor cortical plasticity. *Cerebral Cortex*, *23*(7), 1593–1605. https://doi.org/10.1093/cercor/bhs147

Hannah, R., Rocchi, L., Tremblay, S., & Rothwell, J. C. (2016). Controllable pulse parameter TMS and TMS-EEG as novel approaches to improve neural targeting with rTMS in human cerebral cortex. *Frontiers in Neural Circuits*, *10*(NOV), 1–5. https://doi.org/10.3389/fncir.2016.00097

Hata, M., Kazui, H., Tanaka, T., Ishii, R., Canuet, L., Pascual-Marqui, R. D., Aoki, Y., Ikeda, S., Kanemoto, H., Yoshiyama, K., Iwase, M., & Takeda, M. (2016). Functional connectivity assessed by resting state EEG correlates with cognitive decline of Alzheimer's disease - An eLORETA study. *Clinical Neurophysiology*, *127*(2), 1269–1278. https://doi.org/10.1016/j.clinph.2015.10.030

Heller, A., Wade, D. T., Wood, V. A., Sunderland, A., Hewer, R. L., & Ward, E. (1987). Heller $1987_{a}rmfunctionafterstrokeNHPT$. *Journal of neurology, neurosurgery, and psychiatry*, *50*(March 1986), 714–719.

Herculano-Houzel, S. (2012). The remarkable, yet not extraordinary, human brain as a scaled-up primate brain and its associated cost. *Proceedings of the National Academy of Sciences*, *109*(Supplement 1), 10661–10668. https://doi.org/10.1073/pnas.1201895109

Hordacre, B., Ghosh, R., Goldsworthy, M. R., & Ridding, M. C. (2019). Transcranial Magnetic Stimulation-EEG Biomarkers of Poststroke Upper-Limb Motor Function. *Journal of Stroke and Cerebrovascular Diseases*, *28*(12), 104452. https://doi.org/10.1016/j.jstrokecerebrovasdis.2019.104452

Hosp, J. A., & Luft, A. R. (2011). Cortical plasticity during motor learning and recovery after ischemic stroke. *Neural Plasticity*, *2011*. https://doi.org/10.1155/2011/871296

Hoyer, E. H., & Celnik, P. A. (2011). Understanding and enhancing motor recovery after stroke using transcranial magnetic stimulation. *Restorative neurology and neuroscience*, *29*(6), 395–409. https://doi.org/10.3233/RNN-2011-0611

Huang, Y.-Z., Edwards, M. J., Rounis, E., Bhatia, K. P., & Rothwell, J. C. (2005). Theta burst stimulation of the human motor cortex. *Neuron*, *45*(2), 201–206. https://doi.org/10.1016/j.neuron.2004.12.033

Hummel, F. C., Steven, B., Hoppe, J., Heise, K., Thomalla, G., Cohen, L. G., & Gerloff, C. (2009). Deficient intracortical inhibition (SICI): During movement preparation after chronic stroke. *Neurology*, *72*(20), 1766–1772. https://doi.org/10.1212/WNL.0b013e3181a609c5

Ilmoniemi, R. J., & Kičić, D. (2010). Methodology for combined TMS and EEG. *Brain Topography*, *22*(4), 233–248. https://doi.org/10.1007/s10548-009-0123-4

Ilmoniemi, R. J., Virtanen, J., Ruohonen, J., Karhu, J., Aronen, H. J., Näätänen, R., & Katila, T. (1997). Neuronal responses to magnetic stimulation reveal cortical reactivity and connectivity. *NeuroReport*, *8*(16), 3537–3540. https://doi.org/10.1097/00001756-199711100-00024

Jackson, A. F., & Bolger, D. J. (2014). The neurophysiological bases of EEG and EEG measurement: A review for the rest of us. *Psychophysiology*, *51*(11), 1061–1071.

Jacobs, J., Hwang, G., Curran, T., & Kahana, M. J. (2006). EEG oscillations and recognition memory: Theta correlates of memory retrieval and decision making. *NeuroImage*, *32*(2), 978–987. https://doi.org/10.1016/j.neuroimage.2006.02.018

Jap, B. T., Lal, S., Fischer, P., & Bekiaris, E. (2009). Using EEG spectral components to assess algorithms for detecting fatigue. *Expert Systems with Applications*, *36*(2 PART 1), 2352–2359. https://doi.org/10.1016/j.eswa.2007.12.043

Jasper, H. H. (1958). The 10/20 international electrode system. *Electroencephalography and Clinical Neurophysiology*, *10*(2), 370–375.

Jennum, P., Winkel, H., & Fuglsang-Frederiksen, A. (1995). Repetitive magnetic stimulation and motor evoked potentials. *Electroencephalography and clinical neurophysiology*, *97*(2), 96–101. https://doi.org/10.1016/0924-980x(94)00293-g

Kasai, T., Kawai, S., Kawanishi, M., & Yahagi, S. (1997). Evidence for facilitation of motor evoked potentials (MEPs) induced by motor imagery. *Brain Research*, *744*(1), 147–150. https://doi.org/10.1016/S0006-8993(96)01101-8

King, R. B. (1996). Quality of life after stroke. *Stroke*, *27*(9), 1467–1472. https://doi.org/10.1161/01.str.27.9.1467

Kirschstein, T., & Köhling, R. (2009). What is the source of the EEG? *Clinical EEG and neuroscience*, *40*(3), 146–149. https://doi.org/10.1177/155005940904000305

Kleinjung, T., Eichhammer, P., Langguth, B., Jacob, P., Marienhagen, J., Hajak, G., Wolf, S. R., & Strutz, J. (2005). Long-term effects of repetitive transcranial magnetic stimulation (rTMS) in patients with chronic tinnitus. *Otolaryngology - Head and Neck Surgery*, *132*(4), 566–569. https://doi.org/10.1016/j.otohns.2004.09.134

Klimesch, W. (1999). EEG alpha and theta oscillations reflect cognitive and memory performance: a review and analysis. *Brain research. Brain research reviews*, *29*(2-3), 169–195. https://doi.org/10.1016/s0165-0173(98)00056-3

Klomjai, W., Katz, R., & Lackmy-Vallée, A. (2015). Basic principles of transcranial magnetic stimulation (TMS) and repetitive TMS (rTMS). *Annals of Physical and Rehabilitation Medicine*, *58*(4), 208–213. https://doi.org/10.1016/j.rehab.2015.05.005

Kolb, B., & Whishaw, I. Q. (1998). Brain plasticity and behavior. *Annual review of psychology*, *49*, 43–64. https://doi.org/10.1146/annurev.psych.49.1.43

Komssi, S., Aronen, H. J., Huttunen, J., Kesäniemi, M., Soinne, L., Nikouline, V. V., Ollikainen, M., Roine, R. O., Karhu, J., Savolainen, S., & Ilmoniemi, R. J. (2002). Ipsi- and contralateral EEG reactions to transcranial magnetic stimulation. *Clinical Neurophysiology*, *113*(2), 175–184. https://doi.org/10.1016/S1388-2457(01)00721-0

Kubicki, S., Herrmann, W. M., Fichte, K., & Freund, G. (1979). Reflections on the Topics: EEG Frequency Bands and Regulation of Vigilance TT - Überlegungen zu den Themen: EEG-Frequenzbandeinteilung und Regulierung der Vigilanz. *Pharmacopsychiatry*, *12*(02), 237–245.

Kwakkel, G., Kollen, B., & Twisk, J. (2006). Impact of time on improvement of outcome after stroke. *Stroke*, *37*(9), 2348–2353. https://doi.org/10.1161/01.STR.0000238594.91938.1e

La Rocca, D., Campisi, P., & Scarano, G. (2012). EEG biometrics for individual recognition in resting state with closed eyes. *Proceedings of the International Conference of the Biometrics Special Interest Group, BIOSIG 2012*, (Figure 1), 39–50.

Laakso, I., Hirata, A., & Ugawa, Y. (2013). Effects of coil orientation on the electric field induced by TMS over the hand motor area. *Physics in Medicine and Biology*, *59*(1), 203–218. https://doi.org/10.1088/0031-9155/59/1/203

Langhorne, P., Coupar, F., & Pollock, A. (2009). Motor recovery after stroke: a systematic review. *The Lancet Neurology*, *8*(8), 741–754. https://doi.org/10.1016/S1474-4422(09)70150-4

Lefaucheur, J. P. (2006). Stroke recovery can be enhanced by using repetitive transcranial magnetic stimulation (rTMS). *Neurophysiologie Clinique*, *36*(3), 105–115. https://doi.org/10.1016/j.neucli.2006.08.011

Leon-Carrion, J., Martin-Rodriguez, J. F., Damas-Lopez, J., Barroso y Martin, J. M., & Dominguez-Morales, M. R. (2009). Delta-alpha ratio correlates with level of recovery after neurorehabilitation in patients with acquired brain injury. *Clinical Neurophysiology*, *120*(6), 1039–1045. https://doi.org/10.1016/j.clinph.2009.01.021

Lin, Q., Rosenberg, M. D., Yoo, K., Hsu, T. W., O'Connell, T. P., & Chun, M. M. (2018). Resting-state functional connectivity predicts cognitive impairment related to Alzheimer's disease. *Frontiers in Aging Neuroscience*, *10*(APR), 1–10. https://doi.org/10.3389/fnagi.2018.00094

Lovinger, D. M. (2008). Communication networks in the brain: neurons, receptors, neurotransmitters, and alcohol. *Alcohol research health : the journal of the National Institute on Alcohol Abuse and Alcoholism*, *31*(3), 196–214. https://pubmed.ncbi.nlm.nih.gov/23584863%20https://www.ncbi.nlm.nih.gov/pmc/articles/PMC3860493/

Madsen, K. H., Karabanov, A. N., Krohne, L. G., Safeldt, M. G., Tomasevic, L., & Siebner, H. R. (2019). No trace of phase: Corticomotor excitability is not tuned by phase of pericentral mu-rhythm. *Brain Stimulation*, *12*(5), 1261–1270. https://doi.org/10.1016/j.brs.2019.05.005

Maeda, F., Keenan, J. P., Tormos, J. M., Topka, H., & Pascual-Leone, A. (2000). Interindividual variability of the modulatory effects of repetitive transcranial magnetic stimulation on cortical excitability. *Experimental Brain Research*, *133*(4), 425–430. https://doi.org/10.1007/s002210000432

Magistris, M. R., Rösler, K. M., Truffert, A., & Myers, J. P. (1998). Transcranial stimulation excites virtually all motor neurons supplying the target muscle: A demonstration and a method improving the study of motor evoked potentials. *Brain*, *121*(3), 437–450. https://doi.org/10.1093/brain/121.3.437

Mansur, C., Fregni, F., & Boggio, P. (2005). A sham controlled trial of rTMS of the unaffected hemisphere. *Neurology*, *64*(10), 1802–1804. https://doi.org/10.1212/01.WNL.0000161839.38079.92

Mantini, D., Perrucci, M. G., Del Gratta, C., Romani, G. L., & Corbetta, M. (2007). Electrophysiological signatures of resting state networks in the human brain. *Proceedings of the National Academy of Sciences of the United States of America*, *104*(32), 13170–13175. https://doi.org/10.1073/pnas.0700668104

Massimini, M., Ferrarelli, F., Huber, R., Esser, S. K., Singh, H., & Tononi, G. (2005). Neuroscience: Breakdown of cortical effective connectivity during sleep. *Science*, *309*(5744), 2228–2232. https://doi.org/10.1126/science.1117256

Münte, T. F., Altenmüller, E., & Jäncke, L. (2002). The musician's brain as a model of neuroplasticity. *Nature reviews. Neuroscience*, *3*(6), 473–478. https://doi.org/10.1038/nrn843

Murase, N., Duque, J., Mazzocchio, R., & Cohen, L. G. (2004). Influence of interhemispheric interactions on motor function in chronic stroke. *Annals of neurology*, *55*(3), 400–409. https://doi.org/10.1002/ana.10848

Murphy, T. H., & Corbett, D. (2009). Plasticity during stroke recovery: From synapse to behaviour. *Nature Reviews Neuroscience*, *10*(12), 861–872. https://doi.org/10.1038/nrn2735

Näpflin, M., Wildi, M., & Sarnthein, J. (2007). Test-retest reliability of resting EEG spectra validates a statistical signature of persons. *Clinical Neurophysiology*, *118*(11), 2519–2524. https://doi.org/10.1016/j.clinph.2007.07.022

Nettekoven, C., Volz, L. J., Leimbach, M., Pool, E. M., Rehme, A. K., Eickhoff, S. B., Fink, G. R., & Grefkes, C. (2015). Inter-individual variability in cortical excitability and motor network connectivity following multiple blocks of rTMS. *NeuroImage*, *118*, 209–218. https://doi.org/10.1016/j.neuroimage.2015.06.004

Noble, A. J., & Schenk, T. (2014). Psychological distress after subarachnoid hemorrhage: Patient support groups can help us better detect it. *Journal of the Neurological Sciences*, *343*(1-2), 125–131. https://doi.org/10.1016/j.jns.2014.05.053

Nowak, D. A., Grefkes, C., Ameli, M., & Fink, G. R. (2009). Interhemispheric Competition After Stroke: Brain Stimulation to Enhance Recovery of Function of the Affected Hand. *Neurorehabilitation and Neural Repair*, *23*(7), 641–656. https://doi.org/10.1177/1545968309336661
doi: 10.1177/1545968309336661

Oberman, L., Edwards, D., Eldaief, M., & Pascual-Leone, A. (2011). Safety of theta burst transcranial magnetic stimulation: A systematic review of the literature. *Journal of Clinical Neurophysiology*, *28*(1), 67–74. https://doi.org/10.1097/WNP.0b013e318205135f

Ozdemir, R. A., Boucher, P., Fried, P. J., Momi, D., Jannati, A., Pascual-Leone, A., Santarnecchi, E., & Shafi, M. M. (2021). Reproducibility of cortical response modulation induced by intermittent and continuous theta-burst stimulation of the human motor cortex. *Brain Stimulation*, *14*(4), 949–964. https://doi.org/https://doi.org/10.1016/j.brs.2021.05.013

Park, C. H., Chang, W. H., Ohn, S. H., Kim, S. T., Bang, O. Y., Pascual-Leone, A., & Kim, Y. H. (2011). Longitudinal changes of resting-state functional connectivity

during motor recovery after stroke. *Stroke*, *42*(5), 1357–1362. https://doi.org/10.1161/STROKEAHA.110.596155

Pascual-Leone, A., Peris, M., Tormos, J. M., Pascual, A. P., & Catalá, M. D. (1996). Reorganization of human cortical motor output maps following traumatic forearm amputation. *Neuroreport*, *7*(13), 2068–2070. https://doi.org/10.1097/00001756-199609020-00002

Pascual-Leone, A., Amedi, A., Fregni, F., & Merabet, L. B. (2005). The plastic human brain cortex. *Annual Review of Neuroscience*, *28*, 377–401. https://doi.org/10.1146/annurev.neuro.27.070203.144216

Pascual-Leone, A., Valls-Solé, J., Wassermann, E. M., & Hallett, M. (1994). Responses to rapid-rate transcranial magnetic stimulation of the human motor cortex. *Brain*, *117*(4), 847–858. https://doi.org/10.1093/brain/117.4.847

Pathania, A., Clark, M., Cowan, R., Euler, M., Duff, K., & Lohse, K. (2021). Relating resting EEG power spectra to age-related differences in cognitive performance: An observational pilot study. *medRxiv*, 2021.02.12.21251655. https://doi.org/10.1101/2021.02.12.21251655

Pellicciari, M. C., Bonnì, S., Ponzo, V., Cinnera, A. M., Mancini, M., Casula, E. P., Sallustio, F., Paolucci, S., Caltagirone, C., & Koch, G. (2018). Dynamic reorganization of TMS-evoked activity in subcortical stroke patients. *NeuroImage*, *175*(September 2017), 365–378. https://doi.org/10.1016/j.neuroimage.2018.04.011

Pfurtscheller, G., & Lopes da Silva, F. H. (1999). Event-related EEG/MEG synchronization and desynchronization: basic principles. *Clinical Neurophysiology*, *110*(11), 1842–1857. https://doi.org/https://doi.org/10.1016/S1388-2457(99)00141-8

Pisoni, A., Vergallito, A., Mattavelli, G., Varoli, E., Fecchio, M., Rosanova, M., Casali, A. G., & Romero Lauro, L. J. (2018). TMS orientation and pulse waveform manipulation activates different neural populations: Direct evidence from TMS-EEG. *bioRxiv*. https://doi.org/10.1101/308981

Pool, E.-M., Rehme, A. K., Eickhoff, S. B., Fink, G. R., & Grefkes, C. (2015). Functional resting-state connectivity of the human motor network: differences between right- and left-handers. *NeuroImage*, *109*, 298–306. https://doi.org/10.1016/j.neuroimage.2015.01.034

Premoli, I., Castellanos, N., Rivolta, D., Belardinelli, P., Bajo, R., Zipser, C., Espenhahn, S., Heidegger, T., Müller-Dahlhaus, F., & Ziemann, U. (2014). TMS-EEG signatures of GABAergic neurotransmission in the human cortex. *The Journal of neuroscience : the official journal of the Society for Neuroscience*, *34*(16), 5603–5612. https://doi.org/10.1523/JNEUROSCI.5089-13.2014

Quartarone, A., Siebner, H. R., & Rothwell, J. C. (2006). Task-specific hand dystonia: can too much plasticity be bad for you? *Trends in Neurosciences*, *29*(4), 192–199. https://doi.org/10.1016/j.tins.2006.02.007

Rabiller, G., He, J. W., Nishijima, Y., Wong, A., & Liu, J. (2015). Perturbation of brain oscillations after ischemic stroke: A potential biomarker for post-stroke function and therapy. *International Journal of Molecular Sciences*, *16*(10), 25605–25640. https://doi.org/10.3390/ijms161025605

Raichle, M. E. (2015). The Brain's Default Mode Network. *Annual Review of Neuroscience*, *38*(April), 433–447. https://doi.org/10.1146/annurev-neuro-071013-014030

Rehme, A. K., Fink, G. R., von Cramon, D. Y., & Grefkes, C. (2011). The Role of the Contralesional Motor Cortex for Motor Recovery in the Early Days after Stroke Assessed with Longitudinal fMRI. *Cerebral Cortex*, *21*(4), 756–768. https://doi.org/10.1093/cercor/bhq140

Reineberg, A. E., Andrews-Hanna, J. R., Depue, B. E., Friedman, N. P., & Banich, M. T. (2015). Resting-state networks predict individual differences in common and specific aspects of executive function. *NeuroImage*, *104*, 69–78. https://doi.org/10.1016/j.neuroimage.2014.09.045

Ridding, M. C., & Rothwell, J. C. (2007). Is there a future for therapeutic use of transcranial magnetic stimulation? *Nature reviews. Neuroscience*, *8*(7), 559–567. https://doi.org/10.1038/nrn2169

Robinson, R. G. (1997). Neuropsychiatric consequences of stroke. *Annual Review of Medicine*, *48*(1), 217–229. https://doi.org/10.1146/annurev.med.48.1.217

Rogasch, N. C., & Fitzgerald, P. B. (2013). Assessing cortical network properties using TMS-EEG. *Human brain mapping*, *34*(7), 1652–1669. https://doi.org/10.1002/hbm.22016

Roos, D., Biermann, L., Jarczok, T. A., & Bender, S. (2021). Local Differences in Cortical Excitability – A Systematic Mapping Study of the TMS-Evoked N100 Component. *Frontiers in Neuroscience*, *15*(February), 1–17. https://doi.org/10.3389/fnins.2021.623692

Rosanova, M., Gosseries, O., Casarotto, S., Boly, M., Casali, A. G., Bruno, M. A., Mariotti, M., Boveroux, P., Tononi, G., Laureys, S., & Massimini, M. (2012). Recovery of cortical effective connectivity and recovery of consciousness in vegetative patients. *Brain*, *135*(4), 1308–1320. https://doi.org/10.1093/brain/awr340

Rossi, S., Hallett, M., Rossini, P. M., & Pascual-Leone, A. (2009). Safety, ethical considerations, and application guidelines for the use of transcranial magnetic stimulation in clinical practice and research. *Clinical neurophysiology : official journal of the International Federation of Clinical Neurophysiology*, *120*(12), 2008–2039. https://doi.org/10.1016/j.clinph.2009.08.016

Rothwell, J. C. (1997). Techniques and mechanisms of action of transcranial stimulation of the human motor cortex. *Journal of Neuroscience Methods*, *74*(2), 113–122. https://doi.org/10.1016/S0165-0270(97)02242-5

Saes, M., Zandvliet, S. B., Andringa, A. S., Daffertshofer, A., Twisk, J. W. R., Meskers, C. G. M., van Wegen, E. E. H., & Kwakkel, G. (2020). Is Resting-State EEG Longitudinally Associated With Recovery of Clinical Neurological Impairments Early Poststroke? A Prospective Cohort Study. *Neurorehabilitation and neural repair*, *34*(5), 389–402. https://doi.org/10.1177/1545968320905797

Scally, B., Burke, M. R., Bunce, D., & Delvenne, J.-f. (2018). Neurobiology of Aging Resting-state EEG power and connectivity are associated with alpha peak frequency slowing in healthy aging. *Neurobiology of Aging*, *71*, 149–155. https://doi.org/10.1016/j.neurobiolaging.2018.07.004

Schacter, D. L. (1977). EEG theta waves and psychological phenomena: A review and analysis. *Biological Psychology*, *5*(1), 47–82. https://doi.org/10.1016/0301-0511(77)90028-X

Schilberg, L., Schuhmann, T., & Sack, A. T. (2017). Interindividual Variability and Intraindividual Reliability of Intermittent Theta Burst Stimulation-induced Neuroplasticity Mechanisms in the Healthy Brain. *Journal of cognitive neuroscience*, *29*(6), 1022–1032. https://doi.org/10.1162/jocn_a_01100

Sebastián-Romagosa, M., Udina, E., Ortner, R., Dinarès-Ferran, J., Cho, W., Murovec, N., Matencio-Peralba, C., Sieghartsleitner, S., Allison, B. Z., & Guger, C. (2020). EEG Biomarkers Related With the Functional State of Stroke Patients. *Frontiers in Neuroscience*, *14*(July), 1–16. https://doi.org/10.3389/fnins.2020.00582

Siebner, H. R., Hartwigsen, G., Kassuba, T., & Rothwell, J. C. (2009). How does transcranial magnetic stimulation modify neuronal activity in the brain? Implications for studies of cognition. *Cortex*, *45*(9), 1035–1042. https://doi.org/10.1016/j.cortex.2009.02.007

Srinivasan, R., Winter, W. R., & Nunez, P. L. (2006). Source analysis of EEG oscillations using high-resolution EEG and MEG. In C. Neuper & W. Klimesch (Eds.), *Event-related dynamics of brain oscillations* (pp. 29–42). Elsevier. https://doi.org/https://doi.org/10.1016/S0079-6123(06)59003-X

Stam, C. J., Montez, T., Jones, B. F., Rombouts, S. A., Van Der Made, Y., Pijnenburg, Y. A., & Scheltens, P. (2005). Disturbed fluctuations of resting state EEG synchronization in Alzheimer's disease. *Clinical Neurophysiology*, *116*(3), 708–715. https://doi.org/10.1016/j.clinph.2004.09.022

Stpień, M., Conradi, J., Waterstraat, G., Hohlefeld, F. U., Curio, G., & Nikulin, V. V. (2011). Event-related desynchronization of sensorimotor EEG rhythms in hemi-

paretic patients with acute stroke. *Neuroscience letters*, *488*(1), 17–21. https://doi.org/10.1016/j.neulet.2010.10.072

Stinear, C. M., Barber, P. A., Petoe, M., Anwar, S., & Byblow, W. D. (2012). The PREP algorithm predicts potential for upper limb recovery after stroke. *Brain*, *135*(8), 2527–2535. https://doi.org/10.1093/brain/aws146

Sugata, H., Yagi, K., Yazawa, S., Nagase, Y., Tsuruta, K., Ikeda, T., Nojima, I., Hara, M., Matsushita, K., Kawakami, K., & Kawakami, K. (2020). Role of beta-band resting-state functional connectivity as a predictor of motor learning ability. *NeuroImage*, *210*(July 2019), 116562. https://doi.org/10.1016/j.neuroimage.2020.116562

Takeuchi, N., & Izumi, S. I. (2012). Maladaptive plasticity for motor recovery after stroke: Mechanisms and approaches. *Neural Plasticity*, *2012*. https://doi.org/10.1155/2012/359728

Talelli, P., Greenwood, R. J., & Rothwell, J. C. (2007). Exploring Theta Burst Stimulation as an intervention to improve motor recovery in chronic stroke. *Clinical Neurophysiology*, *118*(2), 333–342. https://doi.org/10.1016/j.clinph.2006.10.014

Tandon, O. P. (1998). Average evoked potentials–clinical applications of short latency responses. *Indian journal of physiology and pharmacology*, *42*(2), 172–188.

Traversa, R., Cicinelli, P., Pasqualetti, P., Filippi, M., & Rossini, P. M. (1998). Follow-up of interhemispheric differences of motor evoked potentials from the 'affected' and 'unaffected' hemispheres in human stroke. *Brain Research*, *803*(1-2), 1–8. https://doi.org/10.1016/S0006-8993(98)00505-8

Trujillo, P., Mastropietro, A., Scano, A., Chiavenna, A., Mrakic-Sposta, S., Caimmi, M., Molteni, F., & Rizzo, G. (2017). Quantitative EEG for predicting upper limb motor recovery in chronic stroke robot-Assisted rehabilitation. *IEEE Transactions on Neural Systems and Rehabilitation Engineering*, *27*(5), 1058–1067. https://doi.org/10.1109/TNSRE.2017.2678161

Tscherpel, C., Dern, S., Hensel, L., Ziemann, U., Fink, G. R., & Grefkes, C. (2020). Brain responsivity provides an individual readout for motor recovery after stroke. *Brain*, *143*(6), 1873–1888. https://doi.org/10.1093/brain/awaa127

Van Putten, M. J., & Tavy, D. L. (2004). Continuous quantitative EEG monitoring in hemispheric stroke patients using the brain symmetry index. *Stroke*, *35*(11), 2489–2492. https://doi.org/10.1161/01.STR.0000144649.49861.1d

Verheyden, G., Nieuwboer, A., De Wit, L., Thijs, V., Dobbelaere, J., Devos, H., Severijns, D., Vanbeveren, S., & De Weerdt, W. (2008). Time course of trunk, arm, leg, and functional recovery after ischemic stroke. *Neurorehabilitation and neural repair*, *22*(2), 173–179. https://doi.org/10.1177/1545968307305456

Wagner, T., Rushmore, J., Eden, U., & Valero-Cabre, A. (2009). Biophysical foundations underlying TMS: Setting the stage for an effective use of neurostimulation in the cognitive neurosciences. *Cortex*, *45*(9), 1025–1034. https://doi.org/10.1016/j.cortex.2008.10.002

Walsh, P., Kane, N., & Butler, S. (2005). The clinical role of evoked potentials. *Neurology in Practice*, *76*(2), 16–22. https://doi.org/10.1136/jnnp.2005.068130

Ward, N. S., Brown, M. M., Thompson, A. J., & Frackowiak, R. S. (2003). Neural correlates of motor recovery after stroke: A longitudinal fMRI study. *Brain*, *126*(11), 2476–2496. https://doi.org/10.1093/brain/awg245

Wu, J., Srinivasan, R., Kaur, A., & Cramer, S. C. (2014). NeuroImage Resting-state cortical connectivity predicts motor skill acquisition. *NeuroImage*, *91*, 84–90. https://doi.org/10.1016/j.neuroimage.2014.01.026

Zrenner, C., Desideri, D., Belardinelli, P., & Ziemann, U. (2018). Real-time EEG-defined excitability states determine efficacy of TMS-induced plasticity in human motor cortex. *Brain Stimulation*, *11*(2), 374–389. https://doi.org/10.1016/j.brs.2017.11.016

Zrenner, C., Galevska, D., Nieminen, J. O., Baur, D., Stefanou, M.-I., & Ziemann, U. (2020). The shaky ground truth of real-time phase estimation. *NeuroImage*, *214*, 116761. https://doi.org/https://doi.org/10.1016/j.neuroimage.2020.116761

# Acknowledgements

I am very grateful for the immense help I have received from various people over the past years. First of all, I would like to thank my supervisor Prof. Silvia Daun, who was always present when I required guidance, enriched me with scientific discussions and supported me to the best of her abilities. I would also like to thank Prof. Christian Grefkes, who originally paved my way to the Forschungszentrum Jülich and always provided me with valuable feedback and advice. I also thank Prof. Gereon R. Fink and Prof. Weiss-Blankenhorn for giving me the opportunity to do this work at the Institute of Neuroscience and Medicine (INM-3).

I thank all members of the INM-3 and especially my colleagues from the Computational Neurology group. A big thank you goes to Dr. Rouhollah Abdollahi, Dr. Nils Rosjat, Dr. Shivakumar Viswanathan and Dr. Azamat Yeldesbay who always helped me with the difficult technical and scientific challenges I encountered throughout these years. I thank Dr. Eva Nießen and Dr. Paola Mengotti for helping me with my first steps in Jülich. A special thanks goes to all the other PhD students of the INM-3 and Dr. Simon Steinkamp for the pleasant discussions.

Moreover, I am thankful for the unconditional support of my parents and siblings. Thank you Marlies, Sayeed, Jonas and Marie. This is also true for all of my dearest friends, of whom there are too many to list them all here. Last, I want to thank Leslie for always being by my side, bringing joy to my life and supporting me throughout this difficult and challenging time.

**Erklärung zur Dissertation**
gemäß der Promotionsordnung vom 12. März 2020

Hiermit versichere ich an Eides statt, dass ich die vorliegende Dissertation selbstständig und ohne die Benutzung anderer als der angegebenen Hilfsmittel und Literatur angefertigt habe. Alle Stellen, die wörtlich oder sinngemäß aus veröffentlichten und nicht veröffentlichten Werken dem Wortlaut oder dem Sinn nach entnommen wurden, sind als solche kenntlich gemacht. Ich versichere an Eides statt, dass diese Dissertation noch keiner anderen Fakultät oder Universität zur Prüfung vorgelegen hat; dass sie - abgesehen von unten angegebenen Teilpublikationen und eingebundenen Artikeln und Manuskripten - noch nicht veröffentlicht worden ist sowie, dass ich eine Veröffentlichung der Dissertation vor Abschluss der Promotion nicht ohne Genehmigung des Promotionsausschusses vornehmen werde. Die Bestimmungen dieser Ordnung sind mir bekannt. Darüber hinaus erkläre ich hiermit, dass ich die Ordnung zur Sicherung guter wissenschaftlicher Praxis und zum Umgang mit wissenschaftlichem Fehlverhalten der Universität zu Köln gelesen und sie bei der Durchführung der Dissertation zugrundeliegenden Arbeiten und der schriftlich verfassten Dissertation beachtet habe und verpflichte mich hiermit, die dort genannten Vorgaben bei allen wissenschaftlichen Tätigkeiten zu beachten und umzusetzen. Ich versichere, dass die eingereichte elektronische Fassung der eingereichten Druckfassung vollständig entspricht.

**Teilpublikationen**:

**(1)** Robustness of individualized inferences from longitudinal resting state dynamics; Maximilian Hommelsen, Shivakumar Viswanathan, Silvia Daun. bioRxiv 2020.09.15.297572; doi: https://doi.org/10.1101/2020.09.15.297572

Köln, den 18. August 2021 Maximilian Hommelsen